

**MULTIFUNCTIONAL
CHROMATOGRAPHY
MATERIALS:
NEW DESIGNS & APPLICATIONS**

Author

Stephan Joseph

A thesis submitted to the University of Birmingham for
the degree of

DOCTOR OF PHILOSOPHY

School of Chemical Engineering

College of Engineering and Physical Sciences

2019

UNIVERSITY OF
BIRMINGHAM

University of Birmingham Research Archive

e-theses repository

This unpublished thesis/dissertation is copyright of the author and/or third parties. The intellectual property rights of the author or third parties in respect of this work are as defined by The Copyright Designs and Patents Act 1988 or as modified by any successor legislation.

Any use made of information contained in this thesis/dissertation must be in accordance with that legislation and must be properly acknowledged. Further distribution or reproduction in any format is prohibited without the permission of the copyright holder.

Abstract

Process chromatography proves to be a continual bottleneck in bioprocessing, especially when considered against constraints such as rocketing product titres, complexity and size of emerging bio-products and a drive to reduce cost of goods and waste generation. Incremental changes in mono-functional chromatography media do not appear to be sufficient in coping with these increased demands and opens the door for novel ‘multifunctional’ beaded media, designed from the ground up, to posit a solution.

This work will, in part, demonstrate the creation of bi-layered chromatography resins with size-exclusion and anion exchange functionality and subsequently assess their performance against benchmarked commercial beads of similar structure. Three size exclusion chromatography matrices, differing in agarose content, cross-linker chemistry, particle and pore size distributions, were transformed into bi-layered supports featuring anion exchange functionalised cores and exterior size excluding shells.

The media were evaluated with respect to loss of surface and core binding, utilising finite bath studies allied with confocal scanning laser microscopic imaging. Plasmid DNA, bovine serum albumin and bovine serum albumin nanoparticles were utilised as surface and core binding probes, and the binding selectivities of different bi-layered support materials were compared by means of a simple selectivity ratio (μg of pDNA (or NP) bound per mg of BSA bound); the lower the number the more selective the support. The best performing bi-layered matrix was Superose 6 Prep Grade, when challenged with both plasmid DNA and BSA nanoparticles. Results for other base matrices was dependent on the nanoplex challenge as well as the bi-layering technique employed.

A second challenge addressed in this thesis was the acquisition of representative virus feedstock to road-test chromatography media, which can pose several practical issues with respect to requirements of particle concentration, volume and methods for tracking the species through chromatography media. A major focus has been developing a reliable platform in characterising commercial and in-house manufactured mono-functional and multi-functional chromatography resins, especially in the context of purifying large nanoplexes.

Against this backdrop, this work details a method for the reproducible manufacture of protein nanoparticles using a modified desolvation method; the nanoparticles function as surrogate mimics of virus products with a view to characterising viral chromatographic media.

Initially, BSA nanoparticles were explored and their manufacture optimised to develop a robust and reproducible system for creating defined nanoparticles within a defined size range. The nanoparticles were subsequently characterised for efficiency of manufacture, their morphological appearance, and secondary protein structure composition as well as how well they represented a *bona fide* viral species, namely adenovirus type V. The approach was then translated to other readily available proteins (e.g. lysozyme, bovine haemoglobin and ovalbumin) to determine the flexibility of the desolvation/coacervation approach and to target a wider range of viral species in terms of their physiochemical properties. The concept here was to develop a “toolbox approach” to develop custom-made nanoparticles to target a variety of viral species. Similar characterisation techniques were applied to the newly formed nanoparticles, as well as novel strategies applied to develop “second-generation nanoparticles” using alternative cross-linking mechanisms to produce multi-component nanoparticles.

The final chapter brings the work full-circle and looks to road-test the chromatography materials manufactured in Chapter II, with a range of sizes of BSA nanoparticles described in Chapter III. The nanoparticles are qualitatively assessed using confocal microscopy alongside quantitative assessment to determine bead performance. As in Chapter II, BSA protein is utilised as a core-binding probe. The nanoparticles are also applied to commercial resins, Q-Sepharose Fast Flow and Capto™ Core 700, both in batch and column scenarios. Of the bi-layered materials, Superose 6 Prep Grade generally outperformed both Sepharose 6 Fast Flow and Superose 12 Prep Grade, revealing differences between the media not shown by the plasmid DNA binding studies. This was generally supported by the complimentary confocal data, which provided an insight into the spatial location and binding kinetics when challenged onto the beads.

It is envisioned that the chromatographic supports manufactured here may be utilised in large scale nanoplex purification, exploiting their utility derived from their bi-functional modality. Furthermore, it is hoped that the protein nanoparticle-viral mimic methodology may be employed in the characterisation of a wider range of purification materials, taking advantage of their low cost and rapid manufacture, as well as their ability to provide valuable purification data which may inform important bioprocessing decisions.

Dedication

I would like to dedicate this thesis to my parents.

Acknowledgements

First and foremost I would like to thank Professor Owen Thomas, for your guidance and support over the course of this PhD. I have learned so much under your supervision which will no doubt hold me in good stead for the future; for this, I am eternally grateful.

To Professors Daniel Bracewell & Paul Dalby, thank you for your support and for always making me feel welcome back at UCL. The CDT, with its training courses and financial support, has helped me to no end during this PhD and for that I am very thankful.

To my colleagues and all the members of Biochemical Engineering, thank you for your support during my research time at Birmingham. Particularly to Elaine and Ronnie, for turning a blind eye every time I took reagents from the Teaching Lab and generally for being an enormous help over the last four years. A special thank you to Theresa Morris and Paul Stanley for their help with the Electron Microscopy work in this thesis and for showing me for the first time what my nanoparticles looked like!

A particular mention to Hong Li, thank you for everything – you always ensured I had my daily dose of sugar and caffeine and were always there to listen. I will miss sharing an office and laboratory with you. To Charles, thank you for being a good friend, beverage partner and also for the help with the CD work in this thesis!

To the army of Masters' students I supervised over the course of the last four years, I can't name all of you, but thank you for your time in the laboratory with me, I hope you enjoyed your projects and time in Birmingham.

Finally thank you to my friends and family, particularly to my parents and to my partner Alexandra, for all your support behind the scenes. This would not have been possible without you all.

Table of Contents

CHAPTER I

INTRODUCTION.....	8
-------------------	---

CHAPTER II

MANUFACTURE & CHARACTERISATION OF MULTI-FUNCTIONALBI-LAYERED CHROMATOGRAPHY MATRICES.....	93
---	----

CHAPTER III

MANUFACTURE & CHARACTERISATION OF PROTEIN NANOPARTICLES AS SURROGATE VIRUS MIMICS.....	137
---	-----

CHAPTER IV

BUILDING & CHARACTERISING A LIBRARY OF VIRAL MIMICS VIA A TOOLBOX APPROACH.....	229
--	-----

CHAPTER V

SYNTHETIC PROTEIN NANOPARTICLES AS TOOLS INFORMING THE CHROMATOGRAPHY OF VIRUS PARTICLE PRODUCTS.....	263
---	-----

CHAPTER VI CONCLUDING REMARKS & FURTHER RECOMMENDATIONS	289
---	-----

CHAPTER VII APPENDICES.....	293
-----------------------------	-----

CHAPTER I

INTRODUCTION

Abbreviations

A/C/I-EX/C: An-/Cat-
/Ion Exchange
Chromatography

AAV: Adeno-Associated
Virus

ADA: Adenosine
Deaminase Deficiency

AdV: Adenovirus

AIDS: Acquired Immune
Deficiency Syndrome

ATPS: Aqueous Two
Phase Systems

BSA: Bovine Serum
Albumin

c DNA: Circular DNA

CAR-T: Chimeric Antigen
Receptor T Cells

Cas-9: CRISPR-associated
9 Protein

CRISPR: Clustered
Regularly Interspaced

PEI: Polyethylenimine

PHA: Polyhydroxyalkanoates

Short Palindromic Repeat
Nucleases

DEAE: Diethylaminoethyl

DNA: Deoxyribonucleic
Acid

ds DNA: Double Stranded
DNA

EU: Endotoxin Units

FDA: Food & Drug
Agency

GST: Glutathione S-
Transferase

HAC: Hydroxyapatite
Chromatography

HEPES: 4-(2-
hydroxyethyl)-1-
piperazineethanesulfonic
acid buffer

HIC: Hydrophobic
Interaction
Chromatography

HIV: Human
Immunodeficiency Virus

HPV: Human Papilloma
Virus

HSV: Herpes Simplex
Virus

IMAC: Immobilised Metal
Affinity Chromatography

mAbs: Monoclonal
Antibodies

MMC: Mixed-Mode
Chromatography

mRNA: Messenger RNA

NIH: National Institute of
Health

oc DNA: Open Circular
DNA

PAA: Polyacrylic Acid

pDNA: Plasmid DNA

PEG: Polyethylene Glycol

PIC: Pre-Initiation Complex

PLGA: Poly-(Lactic-co-Glycolic) Acid

qPCR: Quantitative Polymerase Chain Reaction

RNA: Ribonucleic Acid

RPC: Reverse Phase Chromatography

tDNA: Transfer DNA

sc DNA: Supercoiled DNA

THAC: Triple Helix Affinity Chromatography

SCID: Severe Combined Immunodeficiency Disease

TIL: Tumour Infiltrating Lymphocytes

SDS: Sodium Dodecyl Sulphate

VLP: Virus-Like Particle

SEC: Size Exclusion Chromatography

ZFN: Zinc Finger Nucleases

TALEN: Transcription Activator-like Effector Nucleases

Table of Contents

CHAPTER I.....	8
INTRODUCTION.....	8
Abbreviations.....	8
List of Figures.....	12
List of Tables.....	13
1.1 Project Overview.....	14
1.2 Gene Therapy.....	17
1.3 Gene & Cell Therapy.....	27
1.4 Gene Delivery Vectors.....	28
1.4.1 Viral Vectors.....	28
1.4.2 Non-Viral Vectors.....	35
1.5 Nanoplex Purification.....	41
1.6 Chromatographic Purification.....	49
1.6.1 Ion Exchange Chromatography.....	49
1.6.2 Affinity Chromatography.....	51
1.6.3 Hydrophobic Interaction Chromatography.....	54
1.6.4 Reverse Phase Chromatography.....	55
1.6.5 Size Exclusion Chromatography.....	56
1.7 Developments in Chromatographic Separation.....	57
1.7.1 Mixed Mode Chromatography.....	57
1.7.2 Membrane & Monolithic Chromatography.....	58
1.7.3 Tentacular Supports.....	58
1.7.4 Wide-Pore Matrices.....	59
1.7.5 Multi-Layer Chromatography Beads.....	59
1.8 Virus Mimics.....	60
1.8.1 Inclusion Bodies.....	60
1.8.2 Silica Nanoparticles.....	61
1.8.3 Gold Nanoparticles.....	61
1.8.4 Polymeric Nanoparticles.....	61
1.8.5 Virus-Like Particles.....	62
1.8.6 Protein Nanoparticles.....	62

1.9	Nanoplex Market Analysis.....	63
1.10	References	65

List of Figures

Fig. 1.1 The fundamental concepts behind gene therapy defining both allogeneic and autologous treatment routes (Collins and Thrasher, 2015).

Fig. 1.2 The progress of gene therapy from the late 1980s to date; **a)** The number of gene therapy clinical trials to November 2017. **b)** Proportion of target indications addressed by gene therapy clinical trials. **c)** Types of therapeutic genes transferred in clinical trials. (Data sourced from Ginn et al. 2018).

Fig. 1.3 Adenovirus-mediated gene transfer into the host cell (from Lee et al. 2017).

Fig. 1.4 Adeno-associated viral replication and infection with the aid of a helper virus (from Daya & Berns 2008).

Fig. 1.5 The structure, life-cycle and replication pathway for HSV-1 viral vectors (from Artusi et al. 2018).

Fig. 1.6 The life cycle of a generic retrovirus including the use of reverse transcriptase prior to transport to the host genome (adapted from Power 2001).

Fig. 1.7 Lentiviral vector cellular entry, reverse transcription and formation of the PIC complex prior to integration into the host nucleus (from (Nienhuis, 2008).

Fig. 1.8 Poxvirus replication completely contained within the cytoplasm of the host cell (from McFadden 2005).

Fig. 1.9 Gene delivery achieved by **a)** Lipofection (from Koirala et al. 2013) and **b)** Calcium phosphate precipitation (from Carter et al. 2015).

Fig. 1.10 Mechanism of the “gene gun” as a technique to deliver therapeutic DNA to host tissue (from Carter et al. 2015).

Fig. 1.11 Purification strategies for generic **a)** plasmid DNA and **b)** viral vector products (adapted from Prazeres et al. 1999; Ferreira et al. 2000; Fuerstenau-Sharp et al. 2003; Shi et al. 2009; Allay et al. 2011; Merten et al. 2014; Florencio et al. 2015; van der Loo & Wright 2016; Lloyd-Evans 2017; Terova et al. 2018).

Fig. 1.12 Theoretical schematic of the electrostatic interaction between a positively charged anion-exchange stationary phase (in this case a weak AEX matrix, DEAE) and the negatively charged phosphodiester functional groups of double stranded DNA (sourced from Huber 1998).

Fig. 1.13 A schematic detailing the principles of reverse-phase chromatography, whereby it is possible to elute species based by modulating the polarity of the mobile phase (from Salvato et al. 2012).

Fig. 1.14 A cartoon depiction of Fractogel’s tentacular arms interaction with target solute species in the mobile phase (courtesy of Aldridge 2009).

List of Tables.

Table 1.1 *Gene therapy products which have attained market approval to date (adapted from Dunbar et al. 2018).*

Table 1.2 *Clinical testing parameters and specifications for the manufacture of an example plasmid vector and adeno-associated vector (Diogo et al., 2000; Stadler, Lemmens and Nyhammar, 2004; Allay et al., 2011; Lloyd-Evans, 2017; Penaud-Budloo et al., 2018) .*

Table 1.3 *Characteristics pertinent to the purification of common gene therapy viral vectors (adapted from Kieff et al. 1971; Francis & Bradford 1976; Lankinen et al. 1991; Baxby 1996; Müller et al. 2000; Gray et al. 2010; Michen & Graule 2010; Segura et al. 2011a; Venkatakrishnan et al. 2013). Important to note here is that the characteristics may vary depending on virus serotype and buffer conditions.*

1.1 Project Overview

The bioprocessing landscape is continually evolving in an effort to meet the growing and ever more complex demands of global patient requirements. Biological therapeutics are at the forefront of a capricious battle to treat the ailments and issues of an ageing population; their utility stems from their inherent diversity, high specificity and the ability to produce large volumes of bulk product in a tightly-controlled fashion. There is therefore a persistent need to innovate and improve our approaches to developing and manufacturing therapeutics such that effective treatments can reach patients faster and are produced in an efficient and sustainable manner.

This doctoral research project is supported by the Engineering and Physical Sciences Research Council's Centre for Doctoral Training in Emergent Macromolecular Therapies who aim to "deliver new scientific advances into safely produced, more selective therapies for currently intractable conditions at affordable costs."

Chapter I sets the scene for the thesis through a literature review of gene therapy and its current applications. The literature then transitions to the need of vectors for delivery of gene therapy and how these vectors can be purified. The chapter ends with some literature on similar work in the field which this thesis falls within and highlights the need for a robust method for chromatography development and methods for characterisation.

The primary objective of this work is to develop novel chromatography strategies for the purification of macromolecular nanoplex products and focusses on the creation of a unique bi-layered bead architecture. The methodology looks to modify commercially available chromatographic base supports (un-functionalised agarose size-exclusion media) through an allyl glycidal ether / partial bromination route to create an inert shell around the bead.

Chapter II describes the manufacture and characterise a set of bi-layered chromatography matrices from a variety of starting base resin materials. The bi-layering is carried out through a partial bromination strategy, which is tightly controlled through temperature and viscosity mediated techniques. The materials are then road-tested using biological species, namely Bovine Serum Albumin to test core binding and plasmid DNA to assess residual shell binding.

The properties of the shell (i.e. its thickness and robustness) are strongly dependent on the manufacturing technique and the research looks at fine-tuning the viscosity and temperature conditions of the partial bromination step to enhance the characteristics of the shell that forms, playing on a reaction-diffusion balancing paradigm governed by the Stokes-Einstein principle. The characteristics of the base supports also play a role here, with different particle diameters and pore sizes impacting the success of manufacture and also the chromatographic performance of the modified resins.

Once manufactured, the resins are rigorously characterised to determine key performance metrics including binding capacity and chromatographic resolution (selectivity). Initially, Bovine Serum

Albumin and plasmid DNA were used to assess core and shell binding, respectively, whilst also coupled with orthogonal fluorescence studies to compliment the quantitative data.

In characterising these bi-layered materials, it is important to assess their performance when challenged with the separation of a variety of clinically applicable feed-streams. Given the renaissance of gene therapy, strategies to improve the purification of viral vectors become increasingly more relevant. However, the acquisition of sufficient viral material (as well as the techniques to assay them) to assess and optimise analytical scale chromatography materials is both financially and practically unfeasible in most downstream processing laboratory environments. As such, a secondary objective of the project arises; the development of a novel characterisation platform that utilises protein nanoparticles as surrogate analogues of viruses.

Consequently, **Chapter III** moves away from chromatographic materials and transitions into the manufacture of protein nanoparticles, namely from Bovine Serum Albumin, to mimic viral species, specifically the adenovirus type V. The protein nanoparticles mimic the physiochemical properties of *bona fide* viral particles such that they interact with chromatography species in a similar way; therefore affording an alternative approach to viral chromatography optimisation screening and optimisation.

The research details the ability to produce nanoparticles within a tightly controlled size range as well assessing a number of factors during the desolvation, coacervation and cross-linking process which can affect the quality of the final nanoparticle preparation. The nanoparticles are also characterised with respect to their size, shape, surface properties and composition and finally compared to the true adenoviral species to determine suitability as a mimic.

The platform is advantageous in that the nanoparticles can be produced safely and rapidly, using un-sophisticated manufacturing equipment at low cost and utilising commonly available reagents. Furthermore, the manufacturing conditions can be modified to tailor the mimic to a variety of viral physiochemical properties, including size and surface charge.

Chapter IV expands on the work of Chapter III, utilising a wider range of proteins as “building blocks” with the aim of creating nanoparticulates with adjustable properties; thus facilitating the production of a range of viral mimics. Ovalbumin, Bovine Haemoglobin and Lysozyme are tested for their suitability in the coacervation reaction and the final nanoparticles undergo similar characterisation. The work in the chapter develops further into the manufacture of “second generation nanoparticles” which look to produce multi-component protein nanoparticles using different cross-linking strategies which target various functional groups on the proteins. Two approaches emerge here, blended and core-shell nanoparticles, each with varying degrees of success.

Chapter V looks to tie up both sides of the thesis by applying a range of nanoparticles described in Chapter III with the chromatographic materials manufactured in Chapter II. The nanoparticles are also applied to commercial chromatography media, highlighting their utility as a tool for screening the purification potential of various chromatography resins. It is also interesting to see

how the bi-layered materials from Chapter II respond to a different nanoplex challenge aside from plasmid DNA.

Finally, **Chapter VI** highlights the conclusions from the work and any further recommendations for future work, both from the perspective of the chromatography media and the nanoparticle manufacture.

In summary, the research detailed herein aims to address one of the fundamental steps in purifying biological therapeutics; to ensure that product purity and yield are preserved and that patient safety is not compromised. This work looks at re-modelling the purification of an emergent type of therapeutic molecule, the nanoplex, adapting and tailoring its chromatographic separation strategy to suit its physiochemical characteristics and ultimately achieve higher yields, purity and bioprocessing throughput as a result. The thesis will address the development of new types of bi-layered chromatographic materials and subsequently assaying their performance using a novel protein nanoparticle-viral mimic developed in-house.

The literature review begins with gene therapy; the general literature detailing the general field of bioprocessing can be found in the appendices (Chapter VII, 7.1).

1.2 Gene Therapy

Gene therapy is defined as a treatment which “involves the insertion of a functioning gene into cells to correct a cellular dysfunction or to provide new cellular function” (Culver, 1994). The methodology relies upon the successful transfer of nucleic acids to the nucleus of patient’s cells, usually with the aid of a vector.

There are two classifications for gene therapy; 1. **Germ line gene therapy:** The integration of functional genes into the chromosomes of gametes to facilitate treatment of genetic diseases and counteract hereditary disorders. 2. **Somatic gene therapy:** In this case, functionality is restored in somatic cells of the patient and as such no hereditary implications can result from such a treatment. The focus of gene therapy has been on somatic treatment, due to both ethical and practical implications of treating human germ cells (Razi Soofiyan *et al.*, 2013).

The ethical implications of germ line gene therapy have become a topic of contentious debate in recent times as a consequence of the work by He Jiankui of the Southern University of Science & Technology, Shenzhen, China. He claims to have successfully edited the genetic make-up of two twin girls by knocking out the CCR5 gene, thus protecting the girls (and their future inheritance lineage) against HIV infection. His announcement was met with a great deal of controversy given its un-regulated approach and questionable ethics (Cyranoski and Ledford, 2018). The fundamental routes of gene therapy are described in Figure 1.1.

Two administration routes are possible with gene therapy, either ***ex vivo***, an autologous therapy where patient cells are harvested and transfected and usually amplified prior to re-administering into the patient’s body, or ***in vivo*** where transfection is targeted to post-mitotic cells in the patient. Both rely on the use of a **vector** for targeted gene transfer, through either viral or non-viral carriers (Mulligan, 1993; Kumar *et al.*, 2016).

The concept of gene therapy dates back, somewhat surprisingly, to the early 1960s where the geneticist Joshua Lederberg developed work on the bacterial transfer of genetic material and the method of transduction. He predicted “...the direct control of nucleotide sequences in human chromosomes...it will only be a matter of time...before polynucleotide sequences can be grafted by chemical procedures onto viral DNA” (Cotrim and Baum, 2008). Fast forward to 1989, where the first approved gene therapy clinical study was reported; the use of autologous human tumour infiltrating lymphocytes (TIL) plus interleukin-2, which had undergone retroviral-mediated gene transfer to facilitate neomycin resistance (essentially a genetic marker), to expedite metastatic melanoma regression in five patients. This proof of concept study demonstrated that retroviral

gene transduction of human cells (and re-introduction into patients) in gene therapy was both feasible and safe (Rosenberg *et al.*, 1990; Ginn *et al.*, 2018a).

On the back of this, in 1990 a successful gene therapy treatment was reported; a four year old infant by the name of Ashanti De Silva, born of a Sri Lankan migrant family (much like myself, in fact), was treated for severe combined immunodeficiency (SCID), more specifically adenosine deaminase (ADA) deficiency. The treatment comprised of 11 infusions of T Lymphocyte cells, transduced (by engineered oncoretroviral vectors) with the ADA gene *in vitro*, over the course of two years to the point of 20-25% circulation level of gene-corrected T cells, with evidence of transduced T cell persistence up to 20 years later (Blaese *et al.*, 1995; Mullen *et al.*, 1996; Anderson, 2000; Fischer, Hacein-Bey-Abina and Cavazzana-Calvo, 2010).

It should be noted here that two important breakthroughs precluded this ground-breaking work and without them gene therapy would simply not be possible. The first was the work by Wacław Szybalski, who demonstrated the ability to carry out DNA-mediated gene transfer in mammalian cell lines (Szybalska and Szybalski, 1962), whilst the second was the proof-of-concept work by Rogers and Pfunderer, who were the first to mediate gene transfer using a viral vector (Rogers and Pfunderer, 1968).

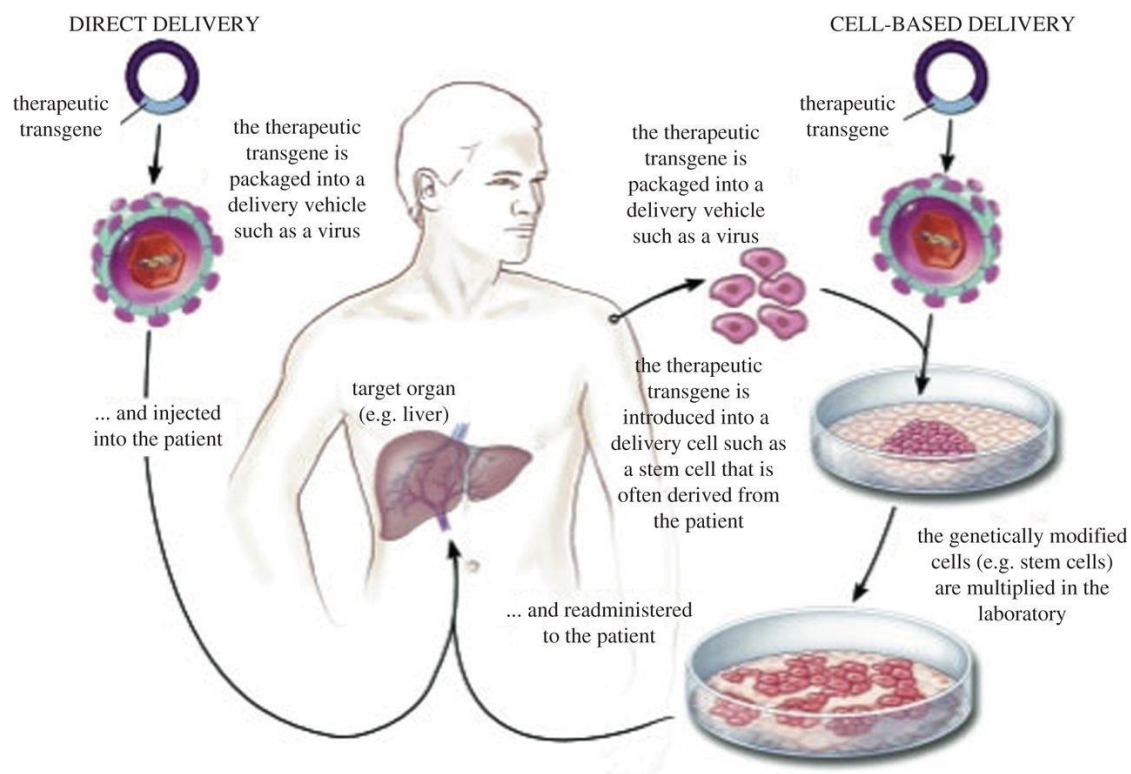


Fig. 1.1 The fundamental concepts behind gene therapy defining both allogeneic and autologous treatment routes (Collins and Thrasher, 2015).

There was consequently a great deal of enthusiasm surrounding gene therapy in the 1990s; a review in *Nature* in 1992 opened with “the treatment of human disease by gene transfer has now moved the theoretical to the practical realm” (Miller, 1992) – the TIL-neomycin marker research was heralded as a “landmark study” which evidenced the potential of gene therapy as a viable treatment option for a range of clinical applications including tissue damage, autoimmune, neurodegenerative and haematological diseases, protein deficiencies and a number of cancers. In many ways this work was the advent of gene therapy and paved the way for a number of gene therapy-based studies and clinical trials, which continue even today (Cotrim and Baum, 2008; Hanna *et al.*, 2017; Ginn *et al.*, 2018a).

Similar ADA-SCID trials were run in the same year in Italy and showed similar promising results in two patients with evidence of ADA gene expression after two years (Bordignon *et al.*, 1995). In 1998, a group in Finland then demonstrated successful transfer of the β -galactosidase gene in treating malignant brain tumours (Puumalainen *et al.*, 1998). However, it was not always plain sailing for gene therapy; there was fierce debate as to the efficacy of the gene therapy treatment given to Ashanti De Silva, as she was simultaneously receiving enzyme replacement therapy (PEG-ADA). On top of this, a second child in the same trial had a significantly reduced response to the treatment and naturally the trial, and gene therapy, was subject to some scrutiny (Wirth, Parker and Ylä-Herttuala, 2013). In 1995, the National Institute of Health (NIH) panel advised that a deeper understanding of the biology behind viral transfection, the target cells and the diseases that the therapy aimed to treat (Orkin, Motulsky and Varmus, 1995).

The main event which tarnished the reputation of gene therapy was the untimely death of teenager Jesse Gelsinger as a result of a trial in 1999. In an attempt to treat an ornithine transcarbamylase deficiency of the liver, an adenoviral vector was used to introduce corrective genes. Tragically, however, his immune system responded heavily to the high adenoviral dose and he unfortunately died four days later due to multi-organ failure (Stolberg, 1999; Jenks, 2000).

As a result, the late 1990s and early 2000s saw a gradual decline in optimism in gene therapy and although trials were carried out, early indications were disappointing with little to no clinical benefit observed. As per advice from the NIH, research was ongoing, however was hampered by worrying evidence of therapy-related toxicities, derived from unmodulated high gene transfer efficacy resulting in high immune responses (similar to that of the Gelsinger case), insertional genotoxicity and a compromising of the target cells immune response (Jenks, 2000; Nienhuis, Dunbar and Sorrentino, 2006; Mingozzi and High, 2011).

However the last decade has seen somewhat of a renaissance in gene therapy, fuelled by significant breakthroughs in vector development, genetic engineering and gene editing, geared towards improving the safety and efficacy of gene therapy (Kumar *et al.*, 2016; Dunbar *et al.*, 2018). One of the main driving forces was the continual improvement in retroviral technology (Mann, Mulligan and Baltimore, 1983; Watanabe and Temin, 1983), facilitating the production of vectors which could carry out reverse transcription coupled with DNA integration whilst also being replication-deficient (Danos and Mulligan, 1988; Miller *et al.*, 1991). The design of self-inactivating retroviral

vectors was also a step forward in the fight to reduce genotoxicity and drive gene therapy towards regular clinical application (Yu *et al.*, 1986; Baum *et al.*, 2011).

Table 1.1 Gene therapy products which have attained market approval to date (adapted from Dunbar *et al.* 2018).

Abbreviations: **FDA**: U.S. Food & Drug Administration, **EMA**: European Medicines Agency, **γRV**: murine-γ-retrovirus, **LV**: lentivirus, **HSPC**: haematopoietic stem and progenitor cells, **X-SCID**: X-linked severe combined immunodeficiency, **BCMA**: B cell maturation antigen, **ARSA**: arylsulfatase A, **ABCD1**: transporter gene mutated in adrenoleukodystrophy, **CNS**: Central Nervous System, **AAV**: Adeno-associated virus, **AADC**: amino acid decarboxylase, **IDA**: iduronate-2-sulfotase.

Cell type	Disease	Vector		Research Institution	Product Approval
T cells <i>Ex vivo</i>	Adult Acute Lymphoblastic Leukaemia	γRV (CD28) T	CD19 CAR-	Memorial Sloan Kettering Cancer Centre	FDA 2014
	Paediatric Acute Lymphoblastic Leukaemia	LV 1BB)	CD19 (4- CAR-T	University of Pennsylvania/Novartis	FDA Oncology Advisory Committee recommended approval 2017; EMA 2016
		γRV (CD28) T	CD19 CAR-	National Cancer Institute/Kite	
		LV CAR-T, TALEN knockout of TCR and CD52	CD19 of	Collectis/Servier/Pfizer	
	Diffuse large B cell lymphoma	γRV (CD28) T	CD19 CAR-	National Cancer Institute/Kite	FDA 2014

Cell type	Disease	Vector	Research Institution	Product Approval
		γ RV CD19 (CD28) CAR	Multiple academic sites/Kite	FDA 2015; EMA 2016
		LV CD19 (4-1BB) CAR-T	Multiple academic sites/Juno	FDA 2016; EMA 2016
		LV CD19 (4-1BB) CAR-T	Multiple academic sites/Novartis	FDA 2017
Chronic Lymphocytic Leukaemia/indolent lymphoma		LV CD19 (4-1BB) CAR-T	University of Pennsylvania/Novartis	
		γ RV CD19 (CD28) CAR-T	National Cancer Institute	
Multiple myeloma		γ RV BCMA (CD28) CAR-T	National Cancer Institute/Kite	
		γ RV BCMA (4-1BB) CAR-T	Memorial Sloan Kettering Cancer Center/Juno	
		LV-BCMA CAR-T	Nanjing Legend Biotech	
Synovial sarcoma		γ RV -NY-ESO-TCR	National Cancer Institute	
		LV-NY-ESO-TCR	Multiple academic sites/Adaptimmune	FDA 2016; EMA 2016

Cell type	Disease	Vector		Research Institution	Product Approval
	Human immunodeficiency virus	ZFN	CCR5 electroporation	University of Pennsylvania/Sangamo	
HSPC <i>Ex vivo</i>	β -Thalassemia	LV	anti-sickling β -haemoglobin	Hopitaux de Paris/academic centres worldwide/Bluebird Bio	FDA 2015; EMA 2016
		LV		San Raffaele Telethon Institute of Gene Therapy/	
			β -haemoglobin	GlaxoSmithKline	
		LV	β -haemoglobin	Memorial Sloan Kettering Cancer Centre	
	Sickle cell anaemia	LV	anti-sickling β -haemoglobin	Hopitaux de Paris/US academic sites/Bluebird Bio	
		LV	anti-sickling β -haemoglobin	UCLA/California Institute of Regenerative Medicine	
	Wiskott-Aldrich syndrome	LV WAS		San Raffaele Telethon Institute of Gene Therapy/GlaxoSmithKline	
		LV WAS		Hospital Necker-Enfants/University College/Genethon	
	Adenosine deaminase deficiency	γ RV ADA		San Raffaele Telethon Institute of Gene Therapy/	EMA 2016 approved "Strimvelis"
				GlaxoSmithKline	

Cell type	Disease	Vector		Research Institution	Product Approval
		LV ADA		University College/UCLA/ Orchard Therapeutics	FDA 2015
	IL2R γ -deficient X-SCID	γ RV IL2R γ	SIN	Hopital Necker-Enfants/ Great Ormond Street	
		LV IL2R γ		National Institute of Allergy and Infectious Diseases	
	Adreno-leukodystrophy	LV ABCD1		St. Vincent de Paul, Paris	
		LV ABCD1		Multiple academic sites/ Bluebird Bio	
	Metachromatic leukodystrophy	LV ARSA		San Raffaele Telethon Institute of Gene Therapy/ GlaxoSmithKline	EU Orphan Drug 2007
	Human Immunodeficiency virus	ZFN	CCR5 electroporation	City of Hope/Sangamo	
CNS <i>In vivo</i>	Parkinson's disease	AAV2-AADC		Jichi Medical University/ UCSF/Voyager	
	Aromatic l-amino acid decarboxylase deficiency	AAV2-AADC		Jichi Medical University/ National Taiwan University	
	Spinal muscular atrophy	AAV9-SMN		Nationwide Children's Hospital/ AveXis	FDA 2016; EMA 2017

Cell type	Disease		Vector	Research Institution	Product Approval
Liver <i>In vivo</i>	Haemophilia B		AAV8-Factor IX	Royal Free Hospital/ St. Jude	FDA 2014; EMA 2017
			AAV100-FIX Padua	Spark Therapeutics	FDA 2016; EMA 2017
			AAV5-Factor IX	uniQure	FDA 2017; EMA 2017
			AAV2/6-Factor IX and ZFNs	Sangamo Therapeutics	FDA 2017
	Haemophilia A		AAV5-Factor VIII	Multiple academic sites/ Biomarin	EMA 2017
			AAV200-Factor VIII	Spark Therapeutics	
			AAV2/6-B domain-deleted Factor VIII and ZFNs	Sangamo Therapeutics	
	Muco-polysaccharidosis type II (Hunter's syndrome)		AAV2/6-IDA and ZFNs	Sangamo Therapeutics	
Muscle <i>In vivo</i>	Lipoprotein lipase deficiency	lipase	AAV1-LPL	uniQure	EMA 2012 approval of "Glybera", company will not renew license as of 2017

Cell type	Disease	Vector	Research Institution	Product Approval
Retina <i>In vivo</i>	Inherited retinal dystrophy due to autosomal recessive mutations in <i>RPE65</i>	AAV2-RPE65	Children's Hospital of Philadelphia/Spark	FDA approval 2017
		AAV2-RPE65	University College London/ MeiraGTx	
		AAV2-RPE65	University of Florida	

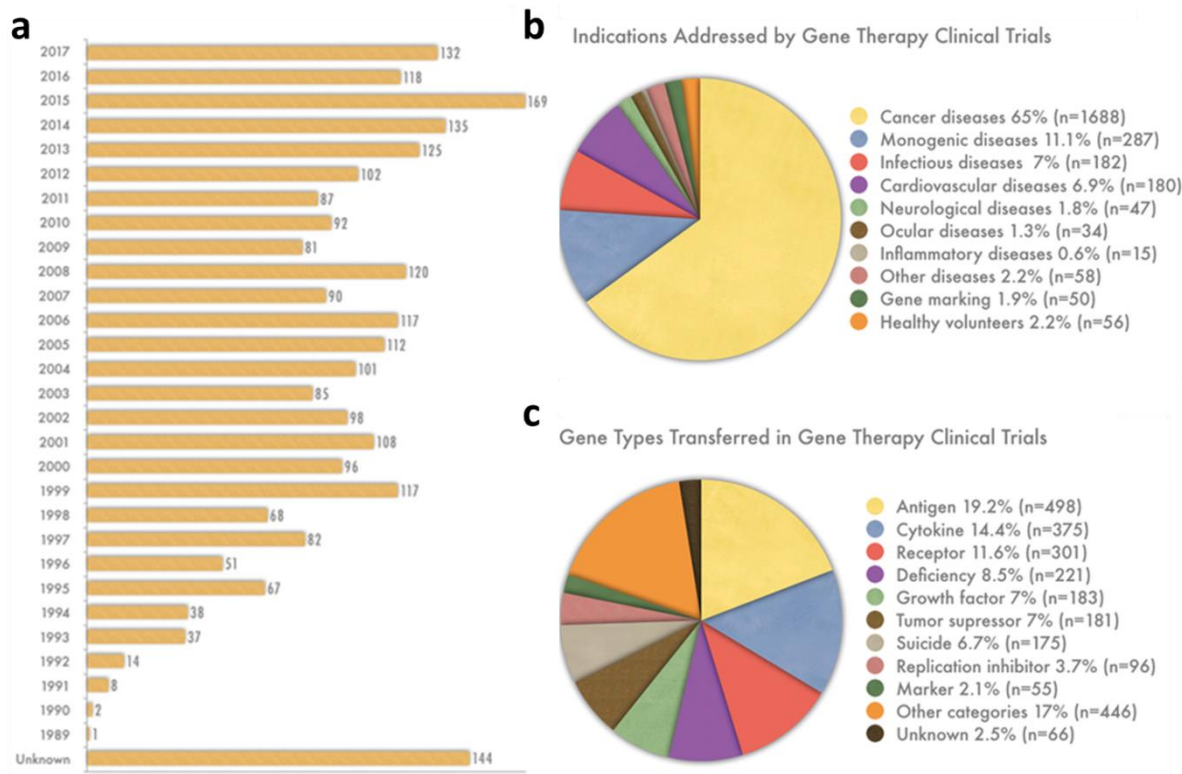


Fig. 1.2 The progress of gene therapy from the late 1980s to date; **a)** The number of gene therapy clinical trials to November 2017. **b)** Proportion of target indications addressed by gene therapy clinical trials. **c)** Types of therapeutic genes transferred in clinical trials. (Data sourced from Ginn et al. 2018).

The mid-1990s saw progress in the engineering of lentiviral (Naldini *et al.*, 1996) and spumaviral (Russell and Miller, 1996) vectors as well, offering advantages such as the incorporation of larger and highly complex gene cassettes as well as preferential integration into the coding regions of target genes, thus reducing the propensity of oncogenic insertional mutagenesis (Montini *et al.*, 2009). Adeno-associated viruses (AAVs) also slowly came to prominence, first in murine models (Kessler *et al.*, 1996; Xiao, Li and Samulski, 1996) and later in humans (Kay *et al.*, 2000; Manno *et al.*, 2006). Whilst having a relatively smaller packaging capacity compared to retroviral vectors, AAVs have the advantage of being non-integrating with the t-DNA packaged and stabilised within an episome within the host cell (Dunbar *et al.*, 2018).

Amidst global developments in genetic and vector engineering, gene therapy products were slowly gaining regulatory approval and emerging onto the market. The first regulatory approved gene therapy product arrived in China in 2004; Gendicine®, developed by Shenzhen SiBiono GeneTech Co. Ltd., is a treatment for head and neck squamous cell carcinoma which functions on the basis of a recombinant human adenovirus type V vector, engineered to carry a wild-type p53 gene responsible for tumour suppression (Peng, 2005). Designed to work in-tandem with radio/chemo therapy, Gendicine® has been administered to over 30,000 cancer patients in over 30 published clinical trials (Liu, Pestka and Shi, 2012; Zhang *et al.*, 2018). This has led to a plethora of gene therapy products entering the market, as summarised in Table 1.1 and Fig. 1.2.

Advances in genome editing have also complimented the resurgence of gene therapy in recent times. For more detail on genome editing, refer to the appendices (Chapter VII, 7.2). The early 2000s saw the birth of site-specific endonucleases; the first of these was the engineering of zinc finger nucleases (ZFN) which carry out DNA alteration through nuclease-induced double-stranded breaks followed by corrective host repair mediated by homing endonucleases (meganucleases) initiating homologous recombination using an introduced template (Urnov *et al.*, 2010; Collins and Thrasher, 2014). This was followed by significant developments in the alteration of transcription activator-like effectors (TALEs) on bacterial proteins to produce TALE nucleases (or TALENs) (Christian *et al.*, 2010; Li *et al.*, 2011); enzymes which have a broad applicability in specific cleaving of theoretically any DNA sequence (Reyon *et al.*, 2012) thus making it highly amenable for gene therapy.

A pivotal milestone occurred in 2012, when Charpentier demonstrated the efficacy of using closely clustered regularly interspaced short palindromic repeat (CRISPR) nucleases, guided by a complementary gRNA sequence (to the target site), to specifically cleave DNA. This, coupled with a CRISPR-associated 9 (Cas 9) protein, was demonstrated in mammalian cell lines for efficient and adaptable gene editing, whereby the nucleases can be programmed to theoretically cleave any specific DNA sequence, opening the door to a wide range of applications, including gene therapy (Jinek *et al.*, 2012; Mali *et al.*, 2013). This technique was a major stepping stone, providing a solution to simple viral vector-mediated gene transfer, such as reduced genotoxicity and better gene expression regulation as a result of high specificity and control using an endogenous promoter (Eyquem *et al.*, 2017; Dunbar *et al.*, 2018).

1.3 Gene & Cell Therapy

Recent developments have seen a marriage between gene and cell therapy for therapeutic application spurred by significant progress in genetic editing techniques to date; ZFNs have been used to develop HIV resistance in both T and haematopoietic stem cells through disruption of the C-C motif chemokine receptor type V (Perez *et al.*, 2008; Li *et al.*, 2013; Tebas *et al.*, 2014). One of the most promising ventures has stemmed from the treatment of B cell acute lymphoblastic leukaemia through use of TALENs to modify lentiviral-induced anti-CD19 chimeric antigen receptor T (CAR-T) cells by selective gene disruption of T cell receptor α -chain and CD52 gene loci. This methodology represented a transition away from autologous therapy to an “off-the-shelf” allogeneic approach, whereby a theoretical “universal T cell bank” can be developed (Qasim *et al.*, 2017).

The CAR-T approach offers simpler manufacture of T cells, increases the availability of the treatment to a wider patient base and avoids harvesting cells from the patient prior to gene editing, which can be tricky, especially in infant cases. As such, two CAR-T cell products, Yescarta (Kite Pharma) and Kymriah (Novartis), received FDA approval in 2017 (Salmikangas, Kinsella and Chamberlain, 2018), the latter gaining EMA approval earlier this year (August 2018) and an agreement between Novartis and the NHS in England to treat children with acute lymphoblastic leukaemia using the promising gene therapy product (Hawkes, 2018).

Recent advances have seen the CAR-T approach being applied to a number of indications, with pre- and clinical trials currently being run on haematological diseases such as multiple myeloma, targeting the B cell maturation antigen (BCMA) in B and plasma cells (de Larrea *et al.*, 2019). CAR-T cell therapies continue to make headway in treating many B cell malignancies, with 19 clinical trials currently under way (as of March 2019) for treating non-Hodgkin lymphoma, with early reports suggesting complete remission rates of between 40-60% (Hill, Lulla and Heslop, 2019).

Exciting animal studies have demonstrated the power of stem cell and gene therapy in other disease states too; one such example was the utilisation of neural progenitor cells (NPCs) in a transgenic murine model to treat Huntington’s disease (HD). In this study, NPCs were isolated from rhesus monkeys prior to genetic modification to allow for stable expression of small hairpin RNA and subsequent grafting back into HD mice. Immunohistochemistry illustrated both integration and differentiation of the grafted, engineered cells and the mice displayed both improved motor functions as well as prolonged lifespans (Cho *et al.*, 2019).

Another interesting clinical trial looked at the treatment of Wiskott-Aldrich syndrome (WAS) using genetically modified haemopoietic stem cells, mediated by lentiviral transduction of a corrected WAS gene, with favourable outcomes reported for all eight patients in the trial. Four of the patients were able to move away from a protected environment into normal society with no adverse effects reported after a follow up 3 years after the treatment (Ferrua *et al.*, 2019).

1.4 Gene Delivery Vectors

Naturally, developments in gene therapy have simultaneously seen a complimentary rise in interest in the use and development of suitable delivery vectors. It has now reached a stage where there is a diverse arsenal of gene delivery vehicle at the disposal of gene therapy clinicians, depending on the specific application. Therapeutic genes can be delivered in a number of different ways and can generally be classed into either viral or non-viral mediated delivery mechanisms; the relative popularity of each delivery mechanism is summarised in Chapter IV, Fig.4.1.

1.4.1 Viral Vectors

1.4.1.1 Adenovirus

Adenoviral vectors are ds linear DNA viruses which have a high delivery capacity of ~ 36 kb. There are over 100 serotypes of adenovirus and their popularity in gene therapy application originates from their broad tissue tropism and their ability to transfect both dividing and non-dividing cells. This wide ranging tropism stems from an adaptable viral fibre protein – cell surface interaction which can be enhanced with an integrin co-receptor (Kay, Glorioso and Naldini, 2001).

The vector fibre proteins are amenable to modification; the attachment of seven lysine residues to the fibre facilitates binding to the heparin sulphate moieties on the cell surface whilst the attachment of small binding epitopes has improved specific cell targeting. Even antibodies against specific proteins have been conjugated to fibre proteins to mediate better targeting properties with higher affinity to receptors (Nayerossadat, Maedeh and Ali, 2012).

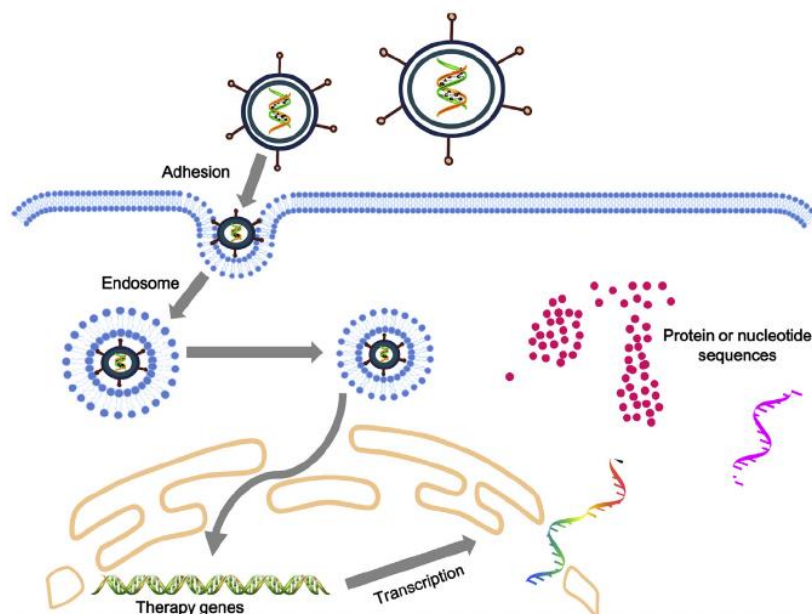


Fig. 1.3 Adenovirus-mediated gene transfer into the host cell (from Lee et al. 2017).

There are significant disadvantages to adenoviral-based gene therapy; a significant one is low levels of transient gene expression, which can limit its applicability in treating genetic disorders, which require long expression times. This is because a defective adenovirus is needed for gene therapy and as such, the E1 gene is removed, which limits both expression and replication. There is also a great deal of concern as to the safety of adenoviral vectors, which, at high infusion concentrations, can illicit both cell-mediated and humoral immune responses, leading to devastating effects, as in the case of Jesse Gelsinger.

There have been attempts to construct “second-generation, gutless vectors” through deletion of specific open reading frames of the E4 and E2 genes to reduce antigenicity, though this has further compounded the issue of low gene expression and as such, compromises the therapeutic modality of the vector. Research continues into adenoviral vector mediated gene therapy mainly due to their wide applicability to a range of tissue tropisms (Robbins and Ghivizzani, 1998).

1.4.1.2 Adeno-associated Virus

Adeno-associated viruses (AAVs) are small (~20-25 nm) non-enveloped, ssDNA viruses which are a member of the Parvoviridae family. AAVs require a helper virus to initiate gene expression and replication and as such are part of the *Dependovirus* genus; these ancillary viruses can range from adenovirus, herpes simplex, vaccinia, cytomegalo- and human papilloma viruses. These helper viruses allow the AAV ssDNA to be converted to replicative dsDNA to facilitate gene expression and replication (Merten and Al-Rubeai, 2011).

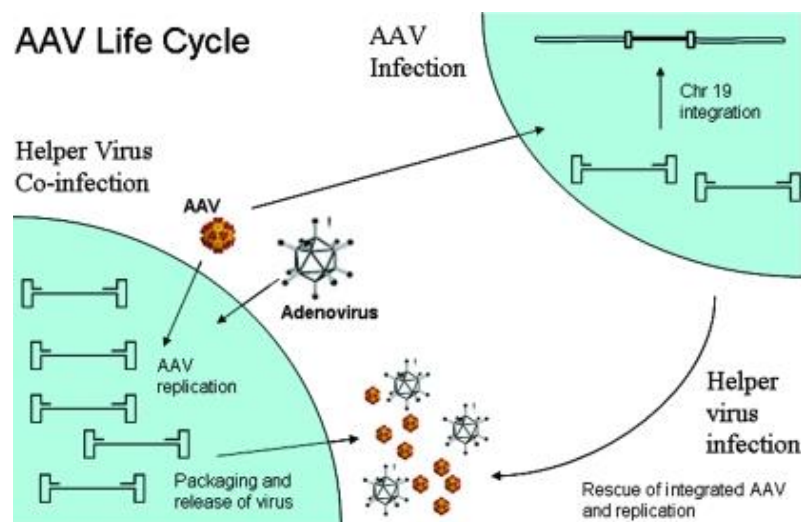


Fig. 1.4 Adeno-associated viral replication and infection with the aid of a helper virus (from Daya & Berns 2008).

Like adenovirus, wild-type AAVs are able to transfect non-dividing cells, however crucially they facilitate stable gene expression rather than transient; they are able to integrate specifically to a locus on chromosome 19 and as such avoid issues such as random insertional mutagenesis.

Recombinant AAV does not integrate into the host genome and remains episomal after gene transfer.

One of the main disadvantages of AAVs is their relatively small packaging capacity (~5.2 kb), as well as low production yields. However recent advances in scalable production methods have helped to mitigate this issue and opened the door for high dose-applications in *in vivo* gene therapy clinical trials (Robbins and Ghivizzani, 1998; Merten and Al-Rubeai, 2011).

1.4.1.3 Herpes Simplex Virus

The herpes simplex virus (HSV) is a large (~ 200 nm), enveloped human pathogenic virus. It is structured with four concentric layers, with its linear dsDNA encased in a icosahedral shaped capsid, which is further enshrouded by a tegument, a layer containing twenty viral proteins. The tegument is contained within a lipid envelope containing viral glycoproteins (Laine *et al.*, 2015). Glycoprotein D, H, L and B mediate host cellular entry by envelope fusion initiated by interaction with a surface receptor on the cell membrane.

Gene regulation is determined by first recognition of viral protein 16, which instigates an enhancer to express immediate early (IE) genes which are responsible for producing infected cell proteins (ICP); the IE gene also controls early (E) and late (L) genes which are responsible for controlling viral replication and producing virion structural proteins (Artusi *et al.*, 2018).

A relatively new entrant to the arena of gene therapy, HSV vectors have carried favour due to their significantly high delivery capacity (~150 kb), partially due to the size of the viral vector but also as there are ~ 40 non-essential genes which can be deleted from its genome while still preserving its replication capacity. This genome complexity can also be exploited to derive oncolytic potential, selectively targeting cancer cells for instance.

Like adenovirus and AAVs, HSV has a broad tissue tropism; importantly this includes neurons, which open this vector up to interesting applications. Further advantages include its lack of integration into host genomes, which lowers the risk of insertional mutagenesis (Fink *et al.*, 1996; Nayerossadat, Maedeh and Ali, 2012; Kanda *et al.*, 2017).

A significant risk of HSV vectors is the potential for recombination with latent HSV infected cells and thus reactivate and potentially spread to other individuals. Additionally, HSV transfection is mitigated by pre-existing immunity in ~ 70% of people and as such HSV vectors and transfected cells which present HSV cell surface markers are inactivated by a specific immune response (Vannucci *et al.*, 2013).

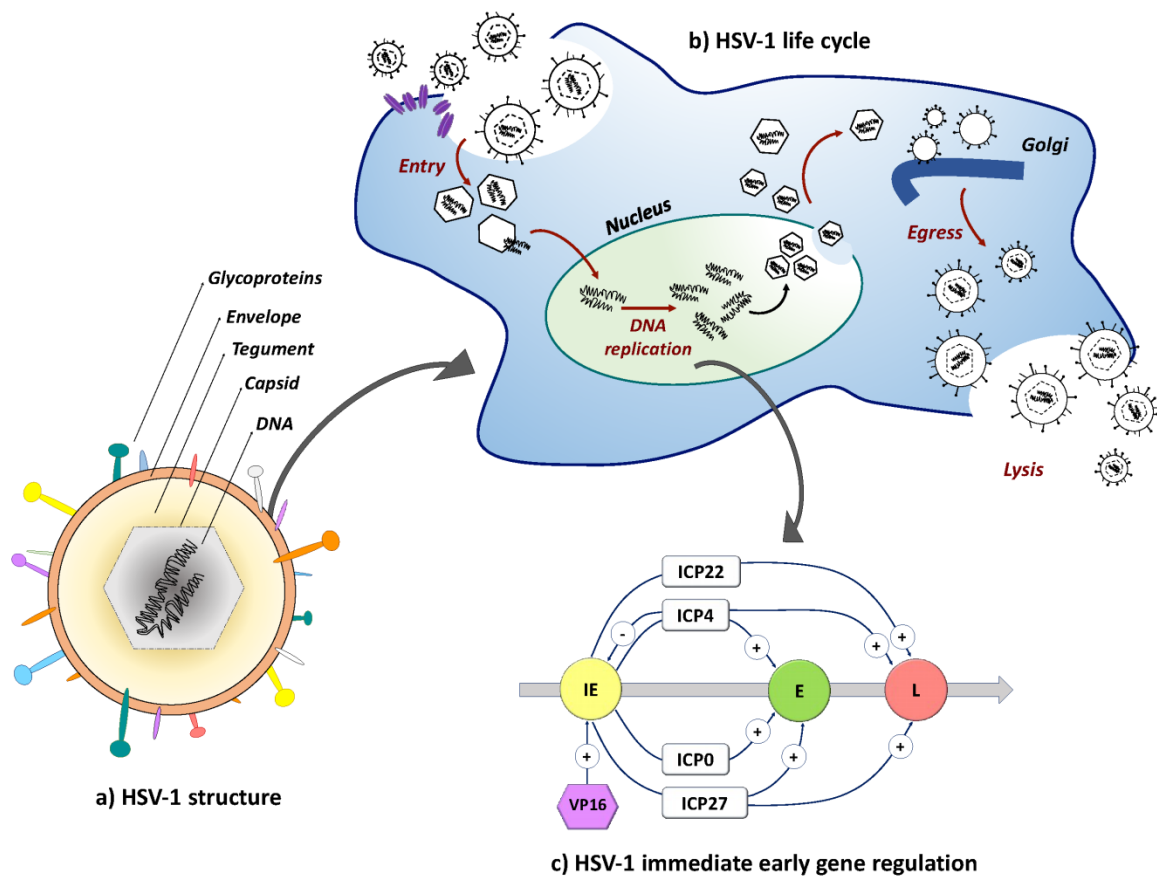


Fig. 1.5 The structure, life-cycle and replication pathway for HSV-1 viral vectors (from Artusi *et al.* 2018).

Another limitation of HSV is its potential cytotoxicity and high inflammatory risk, partially due to a trade-off concerning its ICP0 gene, which is required for both infection and sustained transgene expression. As such, gene expression tends to be transient, though recent work into activating a HSV-1 protein whilst deleting ICP0 has overcome issues of low expression levels (Thomas *et al.*, 2002; Thomas, Ehrhardt and Kay, 2003).

1.4.1.4 Retrovirus

One of the most popular choices for gene therapy delivery vectors during the advent of gene therapy (e.g. in X-SCID clinical trials), most retroviral vectors are based on the Moloney murine leukaemia virus (MMLV) which encodes three polyprotein genes, *gag* (which forms the viral core structure), *env* and *pol*. Retroviruses are RNA viruses which use a DNA intermediate to achieve replication and are spherical particles of ~ 80-100 nm, enveloped by a lipid bi-layer.

Transfection occurs through a specific interaction between a viral envelope protein (*env*) and a cell surface receptor. Once internalised, the retrovirus, mediated by its *pol* reverse transcriptase, is uncoated followed by reverse-transcription of its RNA into dsDNA. The dsDNA is then integrated into the host cell genome via an integrase enzyme, allowing for stable expression, compared to DNA viruses which tend to be transient (Anson, 2004).

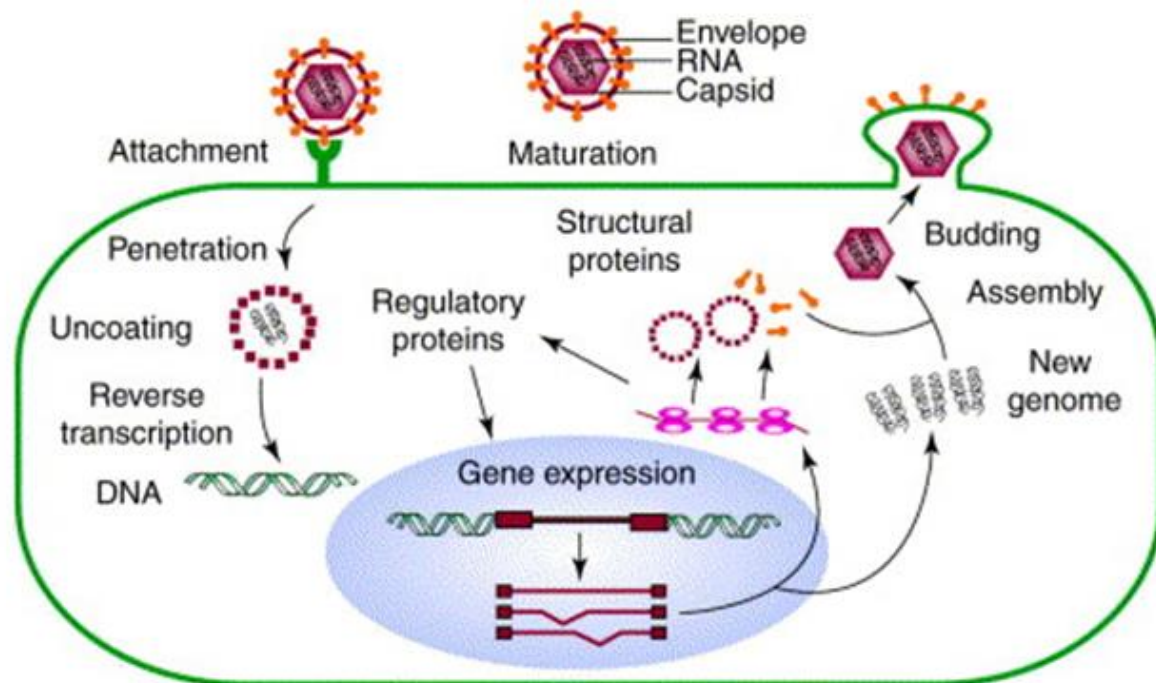


Fig. 1.6 The life cycle of a generic retrovirus including the use of reverse transcriptase prior to transport to the host genome (adapted from Power 2001).

As the provirus is maintained during mitotic division, the transduced cell population can be expanded through cloning. Retroviral vectors also have a limited impact on the growth properties of the cell, facilitating sustained viral production through stable producer lines, with titres of 10^7 cfu/ml now possible. As many of the source viral genes have been removed, the packaging capacity of retroviral vectors are also moderately high, ~ 8 kb (Nayerossadat, Maedeh and Ali, 2012).

The main drawback of retroviral vectors is that they require mitosis to instigate breakdown of the nuclear envelope to integrate the viral genome into the host and thus can only infect dividing cells. There are a few exceptions, for instance lentivirus (e.g. HIV), which have both *cis*- (viral genome sequences localised to the same DNA molecule) and *trans*- (viral elements which can achieve gene regulation in isolation) acting factors, which can mediate active transport of DNA to the nucleus of non-mitotic cells. Consequently, this feature allows for *in vivo* gene therapy and broadens the range of treatment of non-dividing cells (Robbins and Ghivizzani, 1998).

1.4.1.5 Lentivirus

Lentiviral vectors are classed a genus of the *Retroviridae* family and are spherical, enveloped viruses with a diameter of $\sim 80 - 100$ nm. As is common within the retroviral family, the lentiviral genome contains the 5'-gag-pol-env-3' viral proteins, though lentiviruses also have *tat* and *rev* regulatory genes, as well as regulatory genes, depending on the strain (e.g. for HIV-1 they are *vif*, *vpr*, *vpu* and *nef*) – these genes mediate viral RNA synthesis and replication (Buchsacher, 2003).

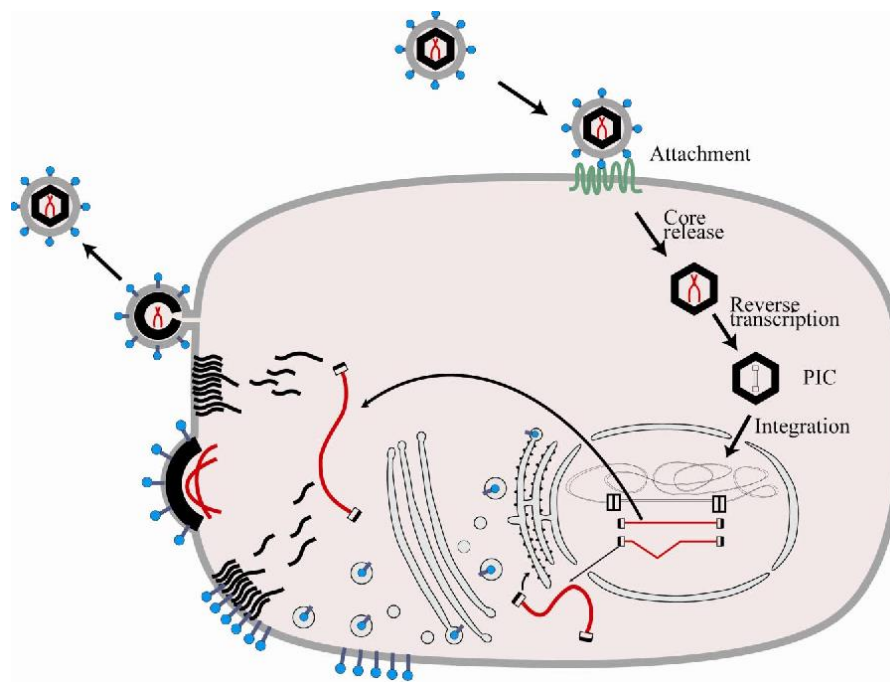


Fig. 1.7 Lentiviral vector cellular entry, reverse transcription and formation of the PIC complex prior to integration into the host nucleus (from Nienhuis 2008).

One of the fundamental discrepancies between conventional c-type retroviruses and lentiviral vectors is that the latter viral cDNA forms a pre-initiation complex (PIC) with other viral factors. This facilitates translocation across the nuclear membrane, mediated by a central polypurine tract within the cDNA and a valine residue at position 165 in the PIC. Crucially, this means that, unlike other retroviruses, lentiviral vectors can transfect non-dividing cells, with a broad tissue tropism including neurons, hematopoietic precursor and lymphoid cells, which makes them amenable to treating a wide range of indications, including neurological diseases (Thomas, Ehrhardt and Kay, 2003; Anson, 2004).

Packaging capacity is usually the same as with other retroviruses (~ 8 kb) and as the vector genome is integrated gene expression is stable and persistent, which makes the vector suitable for long-term treatments. Despite integration, there is low risk of insertional mutagenesis or oncogenesis as genome integration occurs away from cellular promoters (Vannucci *et al.*, 2013).

One disadvantage of lentiviral vectors is their relative complexity in engineering and manufacture, relative to other retroviruses, and this stems from a higher proportion of regulatory genes required for replication and function. These genes need to be provided within the vector or separate construct such as in a DNA plasmid (Vannucci *et al.*, 2013). A second disadvantage is concern over biosafety, particularly in the case of HIV, when one considers the pathogenic nature of the parental virus. A major worry is the creation of replication-competent recombinant viruses; however sequential generations of new viral vector construct engineering have aimed to mitigate this.

Initial work looked to delete virulence-linked genes (*Vpr*, *Vif*, *Vpu*, *Nef* and *Tat*), leaving only *gag*, *pol* and *rev* genes from the original parental virus. More recently, self-inactivating vectors have been

engineered by deletion of part of the U3 region of the 3'-long terminal repeat of the DNA prior to transcription to viral RNA. Both these measures improve the safety implications in using lentiviral vectors as they significantly reduce the risk of a replication-competent virus will form in the target cells also limiting the potential for recombination with wild-type virus in the host system (Zufferey *et al.*, 1998).

1.4.1.6 Pox Virus / Vaccinia Virus

Poxvirus or Vaccinia virus is part of the Poxviridae family and are large (~ 200 nm), enveloped viruses containing linear dsDNA. Poxviruses are characterised by their large and complex genome, with approximately 250 genes and replication that occurs completely within the cytoplasm. The genetic delivery capacity is significantly large (30 kb) as many of these genes are non-essential and therefore can be deleted (Moroziewicz & Kaufman 2005).

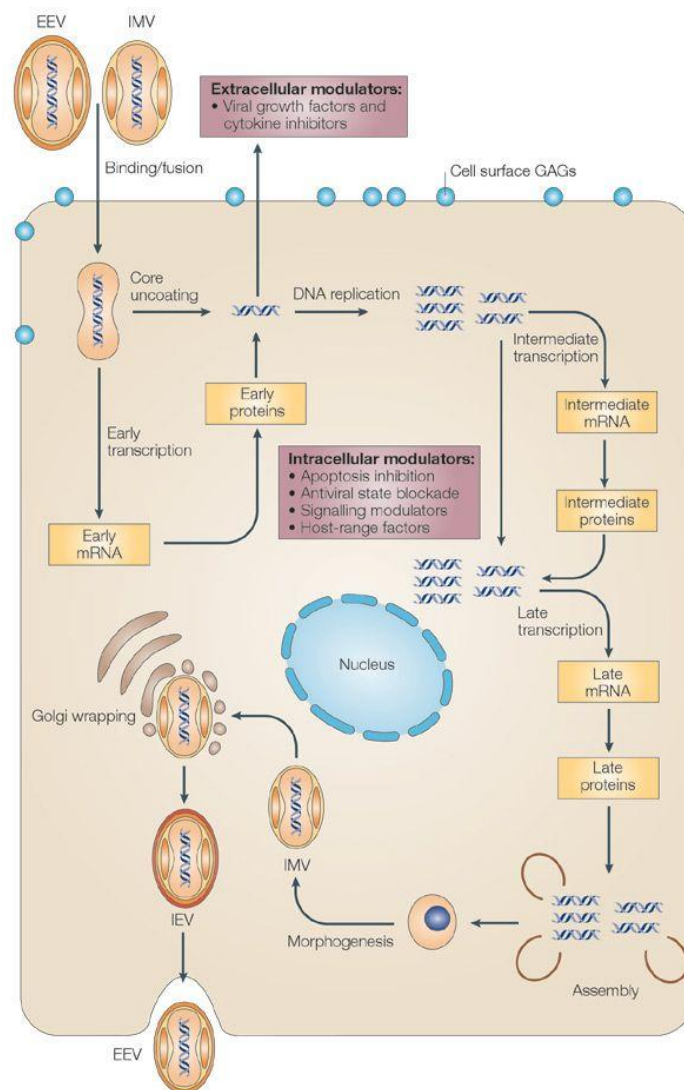


Fig. 1.8 Poxvirus replication completely contained within the cytoplasm of the host cell (from McFadden 2005).

Poxvirus also differs in that transgene insertion is achieved through homologous recombination or *in vitro* ligation and as such are characterised as recombinant viral vectors. Expression of the transgene is high but transient and thus poxvirus is commonly used for vaccination, cancer therapies and recombinant protein production; a recent example of this was the use of Orthopoxvirus modified vaccinia ankara (MVA) which was used en masse as a smallpox vaccination (Nayerossadat *et al.* 2012).

Poxvirus has a number of advantages as a gene therapy vector as it is flexible in offering numerous potential sites for insertion of the transgene, as well as having low levels of pre-existing immunity in patient populations. There are however issues; the complexity of engineering the recombinant viruses and the attenuated nature of the virus compromising the replication efficiency has limited the use of poxvirus. Further research is required to address issues of cytotoxicity and safety in order to justify their clinical use and utilise their high genetic transfection capacity (Nayerossadat *et al.* 2012; Vannucci *et al.* 2013).

1.4.2 Non-Viral Vectors

1.4.2.1 Chemical

1.4.2.1.1 Lipofection

The process of lipofection employs the use of a lipid-DNA complex to achieve effective gene transfer. A liposome forms around the therapeutic DNA, by way of a nucleic acid-poly-cationic complex, prior to delivery and enters the host cell by endocytosis or fusion with the plasma membrane. Liposomes are particularly useful as they circumvent the safety issues associated with viral vectors, with little to no immunogenic or pathogenic associated implications. Their manufacture is also significantly simpler and quicker to produce than a typical viral vector and can be scaled to large scale manufacture (Carter *et al.*, 2015).

A major issue with lipofection is its low efficiency, partially due to host endonucleases degrading the introduced DNA via the host reticuloendothelial system. This being said, recent developments in engineered, stimuli-sensitive liposomes have drastically increased the transfection efficiency from a miserly 1% to some reports of 60-70%. One possible rationale for this is the resistance to lysosomal DNA degradation through the enzymatic disruption of endosomes, as well as directed fusion between the DNA/liposome complex with the cell membrane, both of which either regresses or limits the endosome-mediate lysosomal pathway which leads to DNA degradation and ultimately loss of transfection efficiency (Young *et al.*, 2002).

In addition, the use of polycations such as polyethylenimine (PEI) in the liposome complex can serve two functions; the first is the high cationic charge increases its DNA complexing capacity and secondly the molecule instigates what is known as a “proton sponge” effect. Here, PEI exploits its high buffer capacity and “absorbs” the protons released by lysosomes, which consequently leads to an influx of chloride ions and water. This leads to lysosomal membrane disruption as a result of osmotic swelling and cationic charge repulsion, further limiting DNA degradation and improving transfection efficiency (Benjaminsen *et al.*, 2013).

Further improvements have been instigated through surface modification of the liposomes with hydrophilic polymers (e.g. PEG) or by modulating the pH and ionic strength of the formulation buffer to optimise gene transfection. Research into liposome-based delivery systems for gene therapy continues, driven by their ability to target a broad range of tissue tropisms, largely due to their modification potential with signal peptides, antibodies, carbohydrates etc., all of which aid in achieving directed genetic transfer to target cells (Son, Tkach and Hall, 2000; Nayerossadat, Maedeh and Ali, 2012).

1.4.2.1.2 Calcium Phosphate Precipitation

Therapeutic DNA can also be complexed with calcium phosphate precipitates, prior to cellular transfection. The methodology is relatively simple: DNA is mixed with a solution of calcium chloride, prior to addition of a source of phosphate ions, usually 4-(2-hydroxyethyl)-1-piperazineethanesulfonic acid (HEPES) buffered saline. A precipitate complex is formed between the calcium and phosphate ions, consequently causing a co-precipitating effect on the DNA in solution. These precipitates can then transfect cells through endocytosis and as such presents a relatively inexpensive, quick method of manufacturing a vector for gene therapy (Khan *et al.*, 2016).

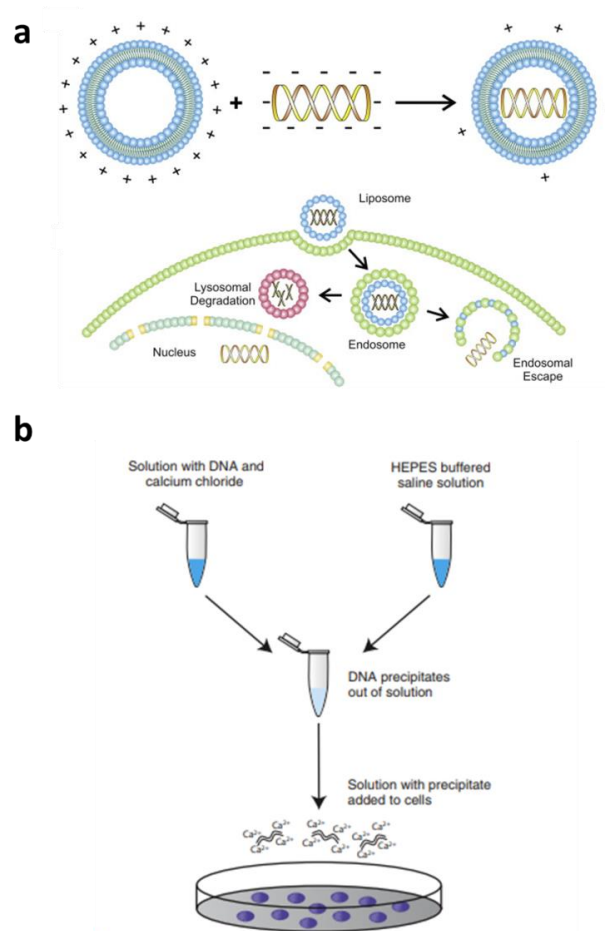


Fig. 1.9 Gene delivery achieved by **a)** Lipofection (from Koirala *et al.* 2013) and **b)** Calcium phosphate precipitation (from Carter *et al.* 2015).

Calcium phosphate precipitation shares many of the advantages as that of lipofection, being a rapid, relatively inexpensive method for achieving transfection. The vectors are biodegradable and as such there are few issues with cytotoxicity or advocating an adverse host immune response. As with liposomes, transfection efficiency is strongly dependent on the operating parameters and heavily influenced by ion and DNA concentration, pH, temperature, aeration, mixing and time between precipitation and transfection (due to precipitate aggregation).

Whilst these factors can be modulated to optimise transfection efficiency, they are also the cause of a high degree of variability and low reproducibility in the technique. Whilst some transfection efficiencies can be as high as 90%, others can be as low as 1% (Carter *et al.*, 2015); this is strongly dependent on cell type and requires a high level of front-end methodology optimisation to improve DNA incorporation in each individual case.

As with lipofection, calcium phosphate precipitation is also amenable to modification to improve transfection and vector stability. Examples include a multi-shell approach of repeating coats of DNA and calcium phosphate to improve colloid stability and act as a protective barrier against lysosomal degradation (Sokolova *et al.*, 2006). Via a similar thought process, the introduction of a lipid (Li *et al.* 2010), protein (Chowdhury *et al.*, 2005; Liu *et al.*, 2005) , ionic additives (Khan *et al.*, 2016) or block co-polymer (PEG-PAA) (Kakizawa and Kataoka, 2002) coat to the precipitate showed improvements in therapeutic effect through better release kinetics, stability and mitigated vector aggregation. Host cell targeting can also be modulated by studding the surface of the precipitates with cellular membrane entry peptides to improve delivery and transfection (Liu *et al.*, 2011).

1.4.2.2 Physical

1.4.2.2.1 Electroporation

Gene transfer into a host cell can also be achieved by exposing the cell membrane to an electric field, thus polarising the phospholipid bilayer and lowering the energy barrier for water penetration. This leads to the reversible formation of nanopores in the membrane and thus an entrance route for DNA in to the cell; this process is termed “electroporation”(Nayerossadat, Maedeh and Ali, 2012; Carter *et al.*, 2015).

Electroporation has a number of advantages in that it is applicable to a wide range of tissue tropisms and can be applied at all stages of the cell life cycle whilst also having applicability for *in vivo* treatments. Unlike viral vector-based therapies, electroporation does not have cytotoxic risks, whilst also being particularly amenable to vaccine therapies; this is due to an enhanced adjuvant-based activation of the host immune response mediated by higher levels of antigen expression and cytokine release at the site of treatment, as a result of moderate tissue damage at the treatment site. In addition, parameters such as electrode placement and timing of the pulses can be controlled to influence specific spatial and temporal responses and expression levels *in vivo*.

There are, however, concerns with the feasibility of electrode placement within certain tissue groups as well as the risk of significant localised tissue damage or DNA modification as a

consequence of excessive voltage conditions. In addition, mass transport across the membrane is non-specific and as such, intra-cellular ionic environments could be adversely affected. These issues require rigorous optimisation of the treatment parameters to modulate appropriate transfection and gene expression whilst also limiting any host tissue damage (Lambricht *et al.*, 2016).

1.4.2.2.2 Gene Gun

The concept of the “gene gun” falls within the remit of biolistics (biological ballistics) and functions by electrostatically coating the transfer DNA onto the surface of heavy metal particles, usually either tungsten or gold.

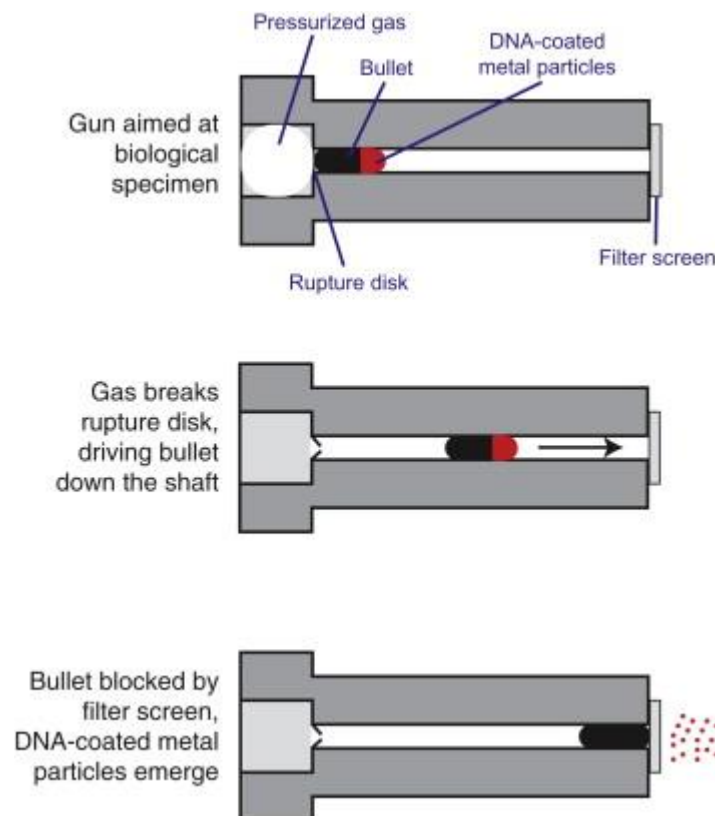


Fig. 1.10 Mechanism of the “gene gun” as a technique to deliver therapeutic DNA to host tissue (from Carter *et al.* 2015).

Transfection occurs through a build of helium gas pressure which eventually breaks a rupture disk, causing a plastic bullet (tipped with the DNA-coated metallic microparticles) to travel at high velocity down the shaft of the gun. The bullet is halted at the end of the shaft by a filter screen; however the excessive force built up by the gas pressure causes the microparticles to fire past the screen and through the cell membrane of the target cells (Carter *et al.*, 2015).

Advantages of using the “gene gun” include its *in vivo* applicability (currently in both skin and liver cells) and broad tissue application (including neurons) as it is cell-receptor independent (Thomas, Ehrhardt and Kay, 2003). As with all the non-viral methods, there are little immunogenic or

toxicity considerations, when compared to viral-mediated treatments. It is a relatively simplistic technique and does not require modification by ligands, liposomes or polymers to achieve cellular entry and can deliver large volumes of therapeutic DNA, depending on the surface area of the microparticles used (Lin *et al.*, 2000). Furthermore, the gene gun can achieve transfection deep into a tissue and the transfection pattern can be well dispersed, targeting specific cells within a tissue amongst a background of un-touched cells.

The main disadvantages of the technique are the risk of high shear damage to cells due to high projectile velocity and as such the pressure and geometric parameters need to be optimised prior to treatment. Expression is also transient and therefore repeat treatments are required for sustained gene therapy to be achieved (Lin *et al.*, 2000; Nayerossadat, Maedeh and Ali, 2012; Carter *et al.*, 2015).

1.4.2.2.3 Naked / Plasmid DNA

“Vector-less” or naked DNA can be injected via micro-injection directly into a cell by puncturing the cell membrane with a needle. Often packaged into a plasmid, therapeutic DNA can theoretically be transfected into any cell type at relatively high delivery capacity (2 – 19 kb), with some cases of long term expression of over a year (Nayerossadat, Maedeh and Ali, 2012). It is a particularly efficient technique, as the amount of therapeutic DNA in each dose is entirely injected into the cell and little is lost via a transduction process, as is the case with other vector systems. As with other physical methods, the tissue tropism is not entry-mediated and there are little safety/immunological concerns given the lack of viral components.

The fundamental disadvantage of this technique is the degree of manual labour involved, as each cell needs to be treated individually using micromanipulation techniques and a skilled operator. This can be both time consuming and have low reproducibility, given human factors such as fatigue and microscope image interpretation. There are also issues in treating certain cell types, particularly neurons given their morphology and cellular sensitivity (Carter *et al.*, 2015).

Whilst having applicability in germ line gene therapy in creating transgenic animals, a somatic gene therapy using microinjection is still too slow and not scalable, though there have been efforts to improve microinjection techniques, using automated platforms for microinjection to speed up throughput (Chow *et al.*, 2016).

Plasmid DNA can also be utilised in DNA vaccines, whereby an intravenous injection of naked DNA, encoding for a specific antigen, can transfect host cells and elicit a cellular and humoral immune response. This is advantageous as it is possible to generate a broad immune response and develop host immunity without the need for a replicating viral vector, whilst also being relatively simple and non-toxic. However, there have been issues with low immunogenicity with first generation DNA vaccines with little to no activation of T-cells, likely due to DNA degradation by host endonucleases and issues with cellular integration due to the physical size and strong negative charge of plasmid DNA (Ferraro *et al.*, 2011).

Significant work has gone into developing the immunogenicity of DNA vaccines by increasing antigen expression and activation of CD8⁺ T-cell responses. DNA vaccines have also seen improvements in promoters, enhancers and introns, whilst also utilising adjuvants to stimulate host responses and engineering better formulation and delivery methods, including those listed here (e.g. the gene gun). The use of a number of additions, including transferrin, solvents, surfactant, polymers and endonuclease-inhibitors have demonstrated improvements in the transfection efficiency of naked and plasmid DNA (Karnchanasri, 2012).

This has opened the door for a number of DNA vaccines, including those against malaria (Doolan and Hoffman, 2001), AIDS (Chen, Wang and Lu, 2014), Ebola (Sridhar, 2015), Influenza (Stachyra, Góra-Sochacka and Sirko, 2014) and certain cancer indications, such as cervical carcinoma (Bharadwaj *et al.*, 2009; Khan, 2013).

1.4.2.2.4 Ultrasound

Ultrasound can also be an effective tool for achieving gene transfer through a technique known as “sonoporation.” Here, pores are created in the cellular membrane through sonication, which creates microbubbles in solution that oscillate in size in response to the frequency of the ultrasonic source applied through the solution. Acoustic cavitation of the membrane occurs as the ultrasound mediated acoustic pressure increases and the microbubble burst, creating nanopores (~ 100 nm) which allow therapeutic DNA to enter the cells (Newman and Bettinger, 2007).

Whilst having the benefits of other non-viral, physical gene transfer techniques, there are some drawbacks to the method; expression is often transient and the efficiency of transfection is usually low as the cavitation mechanism is short lived. Localised increased temperature and pressure can lead to cell death and as such operating parameters such as duration, intensity and frequency of ultrasound pulses need to be optimised to balance transfection efficiency and host cell damage (Kim *et al.*, 1996; Liang *et al.*, 2004; Newman and Bettinger, 2007).

1.4.2.2.5 Magnetofection

Gene delivery can also be mediated through the use of cationic superparamagnetic iron oxide nanoparticles as part of a DNA complex to deliver therapeutic genetic material to host cells under a magnetic field. The concept relies on a magnetic field facilitating a high localised concentration of the nanoparticle-DNA complex around the host cells, improving the rate of endocytosis and thus transfection of DNA (Prosen *et al.*, 2013).

Importantly, the nanoparticles are biodegradable and will dissociate with DNA in the host cytoplasm and have demonstrated the potential to increase transfection efficiency several hundred-fold, whilst also dramatically increasing the rate of transfection to increase treatment throughput time (Scherer *et al.*, 2002).

The main advantage of magnetofection is the rapid rate (as fast as 15 minutes) at which the DNA-nanoparticle complexes sediment onto the surface of target cells, under a magnetic field. This coupled with transfection efficiencies as high as 73% make the technique an attractive option. As

with other techniques detailed here, operating parameters need to be optimised and tailored to specific cell types, including the strength of the magnetic field, morphology of the nanoparticles and DNA conjugation chemistry (e.g. mediated by PEI) to optimise the transfection efficiency (Plank *et al.*, 2003).

To summarise, both viral and non-viral methods of gene therapy offer viable means for achieving efficient therapeutic nucleic acid delivery for gene therapy. Viral vectors have a number of advantages in that they can target specific cell types, can achieve long term, stable transgene expression as well as having high transfection efficiencies. Of the viruses, adenovirus and herpes virus offer promise due to their high insert capacities, though retrovirus vectors have gained popularity due to their stable transgene expression, with lentiviral vectors also able to infect non-dividing cells. The four viral vector groups represent ~ 50% of all vectors used in gene therapy up to 2017 (Hanna *et al.*, 2017).

Non-viral vectors have also showed a great deal of promise; they avoid the complexity of viral vector manufacture with respect to lengthy and expensive cloning and propagation methods as well as the safety implications of using viral vectors. Vectors can be produced rapidly and at scale, with little cell type dependency, high throughput and in some cases high gene transfer efficiency.

The main issue is the lack of stable and pro-longed gene expression, though this could be overcome through hybrid nonviral-viral plasmid vector engineering; including replication signals sourced from HPV and Epstein-Barr Virus in the plasmid which encode both *cis*- and *trans*- elements could aid in mediating episomal replication and allow for stable long term gene expression using non-viral vectors (Robbins and Ghivizzani, 1998). Further research is needed to overcome some associated issues such as localised tissue damage, expensive specialised equipment and lengthy manual handling techniques to improve *in vivo* applications.

1.5 Nanoplex Purification

An important facet of using plasmid DNA and viral vectors in clinical gene therapy is their purification strategy. The regulatory authorities, whether it be the Food and Drug Administration (FDA), European Medicines Agency (EMA) or Medicines and Healthcare products Regulatory Agency (MHRA) will require adherence to strict ICH (International Council for Harmonisation of Technical Requirements for Registration of Pharmaceuticals for Human Use) guidelines on vector quality characteristics, including their identity, potency, purity, infectivity and stability as well as stringent upper limits on process and product impurities that require removal prior to formulation (White *et al.*, 2017).

Exemplary cases for impurity removal for a therapeutic plasmid DNA and AAV vector product are provided in Table 1.3. It should be noted that there are a multitude of critical quality attributes (CQA) requirements that need to be fulfilled, depending on the product type and regulatory body. These CQAs relate not only to purity, but also to product quality and safety and will involve the reporting of a number of other parameters (e.g. final pH, osmolality, visual appearance, protein concentration, viral titre, potency and seal integrity).

Purification strategies are designed based on the characteristics of the feedstock and the target product of interest. Each vector has its own set of unique characteristics which need to be considered when optimising its purification train, including its hydrodynamic radius, net charge, isoelectric point, hydrophobicity, ligand affinity, density, intra-/extra- cellular release fraction, stability, lability etc.

Each unit operation and the sequence they are run in are designed with the aim of meeting product quality and safety requirements as stipulated by the regulatory agency, whilst also being robust, cost efficient, productive and scalable (Morenweiser, 2005; Carvalho, Sepodes and Martins, 2017).

Table 1.2 *Clinical testing parameters and specifications for the manufacture of an example plasmid vector and adeno-associated vector* (Diogo *et al.*, 2000; Stadler, Lemmens and Nyhammar, 2004; Allay *et al.*, 2011; Lloyd-Evans, 2017; Penaud-Budloo *et al.*, 2018) .

Product Type	Parameter	Assay	Acceptability Range
Plasmid Vector	Genomic DNA	TaqMan-PCR	< 10 ng gDNA / μ g pDNA
	Host Cell Proteins	Bicinchoninic Acid Assay or Silver Staining Gel	Undetectable
	RNA	0.8% Agarose Gel or Analytical HPLC	Not visible or < 0.2 μ g / mg pDNA
	Endotoxins	Limulus Amebocyte Lysate	< 0.1 EU / μ g pDNA
	Circular Closed Covalent over Open Circular form of pDNA	Capillary Gel Electrophoresis	> 97 %
	DNA Purity	Optical Density A260/A280	1.7 – 2.0
	Sterility - Bacteria / Fungi Static Activity	Inoculation of Fluid Thioglycollate Medium (European Pharmacopoeia	Undetectable

Product Type	Parameter	Assay	Acceptability Range
Specification – 2.6.14)			
Adeno-Associated Viral Vector	Replication-competent AAV	Serial Infection / <i>rep</i> or <i>cap</i> qPCR	< 1 rcAAV per 1 x 10 ⁸ vector genomes (vg)
	Residual BSA	ELISA	< 50 ng / ml
	Residual Host DNA	qPCR	≤ 10 ng / dose
	Protein Purity	SDS-PAGE	≥ 80 %
	Endotoxins	Limulus Amebocyte Lysate	< 2 EU / dose
	Residual Process-related Contaminants (e.g. Benzonase, PEG, Detergent etc.)	HPLC, MS, ELISA etc.	Quantitative results should be reported
	Sterility - Bacteria / Fungi Static Activity	Inoculation of Fluid Thioglycollate Medium (European Pharmacopoeia Specification – 2.6.14)	Undetectable
	Empty Capsids / Intermediate Viral Particles	vg (qPCR) / vp (ELISA), EM or AUC	Quantitative results should be reported
	Aggregation	Dynamic Light Scattering	Quantitative results should be reported

Table 1.3 Characteristics pertinent to the purification of common gene therapy viral vectors (adapted from Kieff *et al.* 1971; Francis & Bradford 1976; Lankinen *et al.* 1991; Baxby 1996; Müller *et al.* 2000; Gray *et al.* 2010; Michen & Graule 2010; Segura *et al.* 2011a; Venkatakrishnan *et al.* 2013). Important to note here is that the characteristics may vary depending on virus serotype and buffer conditions.

	Adenovirus (Ad5)	Adeno- Associated Virus (AAV 2)	Retrovirus / Lentivirus	Herpes Simplex Virus (HSV-1)	Poxvirus
Genome	dsDNA	ssDNA	ssRNA	dsDNA	dsDNA
Envelope	✗	✗	✓	✓	✓
Fraction	Lysate	Lysate	Supernatant	Supernatant	Lysate or Supernatant
Stability	↑	↑	↓	↓	Moderate
Density (g/cm³)	1.34	1.39	1.16	1.73	1.27
Hydrodynamic Size (nm)	80 – 100	20 – 30	100	100	140 – 450
Net charge (at pH 7)	Negative	Neutral – Positive	Positive	Positive	Negative
Isoelectric Point	4.5	6.3-6.8	6.8-7.9	5.3 – 7.28	6.56

Plasmid DNA, for example, is characterised by its large hydrodynamic size (100 – 250 nm), with a strong net negative charge resulting from the negatively charged phosphate groups on the nucleic acid backbone of the plasmid molecule, thus the overall charge increases with increasing number of bases (Ferreira *et al.*, 2000). Viral vectors vary in their morphology and characteristics; Table 1.4 summarises some of the key features of some of the salient viruses used in gene therapy which become useful when considering their purification strategy.

Given low transfection efficiencies (approximately 1 in 1000 pDNA molecules in a dose successfully transfects a target cell and is expressed) (Varley *et al.*, 1999) and high dosage requirements (sometimes as high as mg levels of pDNA), as well as the growing popularity of gene therapy and DNA vaccine therapies, large volumes of plasmid DNA and viral vectors need to be produced. Large scale manufacture of plasmid DNA and viral vectors usually involves

fermentation-based cell culture, usually followed by a cell lysis step (depending on if the vector is located intracellularly or is released into the culture supernatant) to release product into the bulk feedstock (Ferreira *et al.*, 2000; Levy *et al.*, 2000; Segura, Kamen and Garnier, 2011b).

When required, cell lysis can be achieved by thermal, mechanical or chemical means; thermal lysis is less favoured due to the complexity and lengthy of the heat-shock method (repeated cycles of freeze thaw -80 °C/ 37 °C), as well the lack of feasible scale up options due to the requirement for efficient and controlled heat transfer equipment to treat large feedstock volumes (Florencio *et al.*, 2015). Mechanical disruption, including ultrasonication, microfluidisation and bead milling, offers a scalable alternative with recoveries of up to 74% for plasmid DNA (Ferreira *et al.* 2000) and successful application also demonstrated with viral vectors too (Burova and Ioffe, 2005; Wright, 2008a; Allay *et al.*, 2011; Segura, Kamen and Garnier, 2011b; Potter *et al.*, 2014). Viral vectors can also be liberated from the host cell through hypotonic shock or small pressure changes e.g. via a cross-flow filtration system (Segura, Kamen and Garnier, 2011b).

However, optimisation is required to achieve an appropriate trade-off between cell disruption and vector recovery, as well as to limit the micronisation of cell debris through prolonged mechanical cell disruption which can complicate higher resolution purification steps further downstream (Balasundaram, Harrison and Bracewell, 2009); plasmid DNA (and its polynucleotide components) is particularly shear sensitive and mechanical stress can cause a break/relaxation of the supercoiled structure of pDNA to form open circular DNA, which ultimately leads to a reduction in the transfection efficiency of the genetic material (Levy *et al.*, 2000; Schmidt, Friehs and Flaschel, 2007), whilst high shear forces can cause a shedding effect on the envelope of viruses, leading to a loss of infectivity (Morenweiser, 2005).

Alkaline lysis appears to be the most favourable approach for large scale cell disruption for plasmid DNA (Ferreira *et al.*, 2000; Urthaler, Buchinger and Necina, 2004) and is based on the method first described by Birnboim and Doly (Birnboim and Doly, 1979). Cells are separated from the broth by an initial centrifugation or microfiltration step and then re-suspended in a lysis buffer (0.2 M NaOH, 1% SDS), designed to disrupt the lipid-protein hydrogen and ionic bonds within the bacterial outer and plasma membranes.

The buffer will often also contain ethylene diamine tetra-acetic acid (EDTA) as a chelating agent for Ca²⁺ -and Mg²⁺ cations, which facilitates a reduction in membrane integrity whilst also reducing the efficacy of Mg²⁺ dependent endonucleases, preserving the quality of the released plasmid DNA (Prazeres *et al.*, 1999).

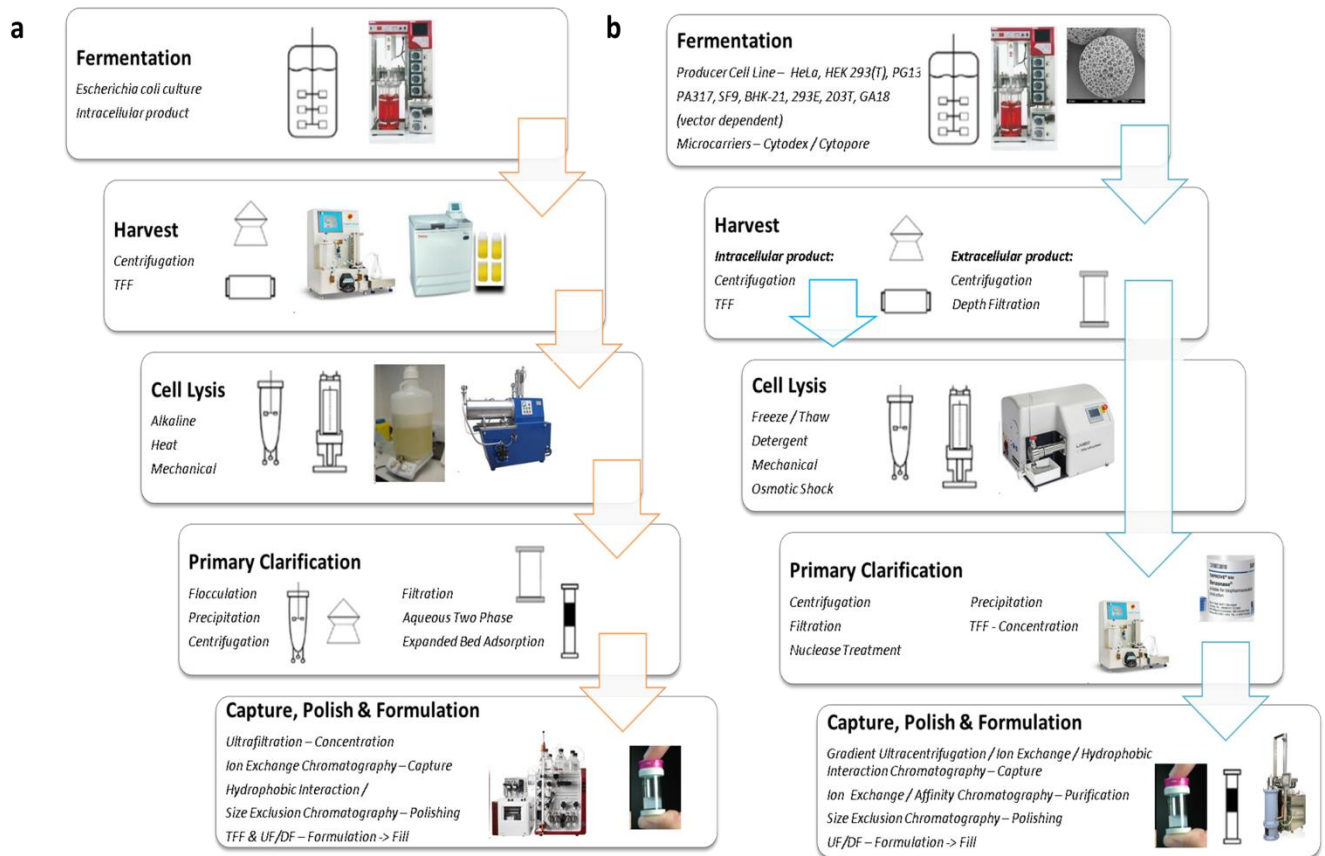


Fig. 1.11 Purification strategies for generic **a)** plasmid DNA and **b)** viral vector products (adapted from Prazeres *et al.* 1999; Ferreira *et al.* 2000; Fuerstenau-Sharp *et al.* 2003; Shi *et al.* 2009; Allay *et al.* 2011; Merten *et al.* 2014; Florencio *et al.* 2015; van der Loo & Wright 2016; Lloyd-Evans 2017; Terova *et al.* 2018).

Mixing is a key parameter here which needs to be carefully monitored as the released genomic DNA greatly increases the viscosity of the lysate and consequently the P/V (power input per unit volume) increases (Marquet *et al.*, 1997). Mixing is complicated as the lysate displays non-Newtonian rheological characteristics and thus the geometrical design of the mixing vessel, impellers and flow properties of the material need to be carefully considered to preserve the quality of the plasmid DNA (Stephenson, Norman and Cumming, 1992; Ciccolini *et al.*, 1999; Levy *et al.*, 2000).

Whilst rapid mixing is required to achieve homogenous distribution of the buffer, consistent cell disruption and the avoidance of localised high pH regions in the lysis tank (which can lead to significant plasmid denaturation (Rush and Warner, 1970; Prazeres, Schluep and Cooney, 1998a)), a balance must be struck to avoid agitation-related shear damage of the released plasmid DNA and fragmentation of host chromosomal DNA which pose difficulties further downstream in separating from target plasmid DNA (Ciccolini *et al.*, 1999; Urthaler, Buchinger and Necina, 2004). Often additives such as glucose and sucrose are included in the lysis buffer as a shear-protectant to mitigate this issue (Prazeres *et al.*, 1999).

In the case of viral vectors, cell disruption can be achieved by addition of non-ionic detergents, such as Triton X-100 or Tween-80, which can disrupt both the viral envelope and the cell membrane whilst leaving the viral nucleocapsid intact. The cell disruption step does, however, often lead to nucleic acid-protein and viral particle aggregation in the cell lysate. This can be offset by addition of either 150 mM NaCl or a non-ionic surfactant which prevents electrostatic interaction between cell debris and host cell proteins, whilst use of a divalent salt buffer such as citrate or 200 mM MgSO₄ can also mediate better viral particle dispersion in future processing steps and storage (Merten *et al.*, 2014; Penaud-Budloo *et al.*, 2018).

Cell disruption is not 100% selective and consequently a high percentage of the cell lysate or cell supernatant consists of product-related impurities. In the case of bacterial production of plasmid DNA the percentage of plasmid DNA can be as low as 3%, with impurities including RNA, host genomic DNA, endotoxins (lipopolysaccharides), cell debris and host cell proteins (Stadler, Lemmens and Nyhammar, 2004). In the case of viral vectors, impurities can also include empty or intermediate capsids, cell membrane vesicles, as well as helper viruses used to facilitate vector production; these will also need to be purified away from the fully formed viral vector (Merten and Al-Rubeai, 2011).

As many of these impurities exhibit a negative charge (nucleic acids, endotoxins) and have similar physiochemical properties such as hydrophobicity (endotoxins) and size (empty capsids, membrane vesicles) to the target plasmid or viral vector, multiple sequential purification steps are required to recover the target species at sufficiently high levels of purity (Stadler, Lemmens and Nyhammar, 2004; Segura, Kamen and Garnier, 2011b). Endotoxin removal is particularly critical; they are lipopolysaccharides derived from bacterial cell walls and can cause toxic shock syndrome *in vivo* and thus should be stringently monitored (de Azavedo *et al.*, 1985).

Prior to these impurities being removed, a chilled high-salt neutralisation buffer is added the alkaline lysate which facilitates the formation of genomic DNA aggregates and proteins complexed by SDS, creating a precipitate/floc (Ciccolini *et al.*, 1999; Prazeres *et al.*, 1999). Whilst the potassium acetate buffer causes irreversible denaturation of chromosomal DNA which form part of the floc, plasmid DNA is able to renature into its supercoiled conformation and are re-solubilised, given the pH conditions are not excessive (Levy *et al.*, 2000). The floc is separated either by a centrifugation or filtration step prior to plasmid precipitation using sequential isopropanol and ethanol wash steps (Prazeres *et al.*, 1999).

Primary clarification of the cell lysate or supernatant is then required to remove cellular debris and any low molecular weight impurities, whilst also concentrating the feedstock volume for subsequent lower capacity, high resolution purification steps. This initial clarification step tends to be low resolution, though must have a high volumetric capacity to handle the large volumes of a cell lysate / supernatant direct from fermentation harvest (Ferreira *et al.*, 2000).

Further intermediate purification and concentration steps are also required to exclude product-related impurities, including enzymatic endonuclease degradation of host RNA and DNA, though issues arise due to the animal source of the enzyme, which makes process validation and regulatory

approval trickier and thus tends to be avoided during commercial, large-scale manufacture (Ferreira *et al.*, 2000; Gustavsson *et al.*, 2004a; Stadler, Lemmens and Nyhammar, 2004). This can be remedied through endogenous endonucleases; incubation of the cell lysate at 37 °C can reduce RNA levels by 40%, including problematic high molecular weight RNA (Monteiro *et al.*, 1999).

Removal of other host impurities (at large scale) can be achieved by a series of precipitation reactions; a wide range of host cell proteins and high molecular weight RNA can be salted out using chaotropic salts such as lithium chloride and ammonium or potassium acetate or co-precipitated with high molecular weight polymers such as PEG, which aids in removing smaller nucleic acid impurities (Ferreira *et al.*, 2000).

Aqueous-two phase extraction (ATPS) is another scalable technique which can be utilised on cleared lysates and have showed high removal of impurities such as RNA (98%) and endotoxins (68%), whilst achieving high levels of plasmid recovery (91%) in systems such as PEG 600 and sodium citrate / ammonium sulphate.

The technique is particularly useful preceding a hydrophobic interaction chromatography step as no buffer exchange is required saving both cost and time, thus improving process efficiency (Gomes *et al.*, 2009). In a similar vein, AAV vectors have shown to be successfully purified using a PEG 8000 / ammonium sulphate ATPS system as faster alternative to density gradient ultracentrifugation (Guo *et al.*, 2013).

Higher resolution purification of plasmid DNA and viral vectors tend to be carried out by either density gradient ultracentrifugation or by column chromatography. Whilst both have the ability to achieve the high levels of recovery and purity demanded by regulatory agencies (Garger, Griffith and Grill, 1983; Sambrook and Russell, 2006; Merten and Al-Rubeai, 2011; Segura, Kamen and Garnier, 2011b; Blom *et al.*, 2014; Florencio *et al.*, 2015), gradient ultracentrifugation is plagued by a lack of scalability, expensive capital costs, long processing times which can induce product aggregation as well as the use of difficult to remove, toxic reagents such as ethidium bromide, caesium chloride and iodixanol (Ferreira *et al.*, 2000; Burova and Ioffe, 2005; Merten *et al.*, 2014; Kramberger, Urbas and Štrancar, 2015a; Terova *et al.*, 2018).

Given the nature of this research project, we will now look at the variety of chromatography options available in downstream processing to understand the versatility and wide scope of the technique as well as its applicability in addressing various nanoplex purification challenges.

1.6 Chromatographic Purification

Chromatography has been the work-horse of the bioprocessing field since the early 1940s (Martin and Synge, 1941), providing a robust and flexible platform for the isolation and purification of high value compounds with a variety of applications. Chromatography appears to be the most favourable downstream processing technique having the highest resolution, whilst also being scalable, robust and well characterised (Urthaler, Buchinger and Necina, 2004; Przybylowski *et al.*, 2007). Indeed, chromatography is an over-arching term and there are a multitude of variations to the technique that achieve separation through various physical and chemical principles.

1.6.1 Ion Exchange Chromatography

Ion-exchange chromatography has been widely employed in the intermediate, conditioning stages as well as the capture and polishing steps of nanoplexes. The purification strategy relies on the high negative surface charge of the target species; for plasmid DNA and most viral vectors, the ζ -potential in typical aqueous buffers and neutral pH is between -30 to -50 mV (Ledley 1996; Michen & Graule 2010) and as such, anion-exchange chromatography is favoured for both vector types (Prazeres, Schluep and Cooney, 1998b; Steppert *et al.*, 2016).

Plasmid DNA binding and elution behaviour on ion-exchangers are also mediated by their hydrodynamic size and shape, which will determine their overall net charge and charge density. For plasmid DNA, these physiochemical characteristics are a function of their nucleic acid composition; nucleic acids in general exhibit a negative charge stemming from their sugar-phosphate backbone, whilst for supercoiled plasmid DNA (> 1000 bp) regions of charge compression can occur in “bend” regions, as a consequence of poly-adenine sequences leading to localised dipole and electrostatic interactions with chromatographic supports (Huber, 1998).

Anion-exchange chromatography offers a number of benefits over other competitive techniques, including scalability across preparative and analytical scales and robust media with facile sanitation options (as with most chromatographic unit operations), high throughput purification of plasmids from low charge density impurities (and in some cases other plasmid DNA isoforms) and a wide range of tailored media options, including strong and weak ion-exchangers (Eon-Duval and Burke, 2004).

Some of the fundamental drawbacks of anion-exchange chromatography are its low-resolution and selectivity, particularly in instances of high concentrations of polyanionic molecules such as endotoxins, genomic DNA and RNA³ in the feed stream which can lead to co-elution and diminished purity levels of the eluent (Prazeres, Schluep and Cooney, 1998b; Eon-Duval and Burke, 2004).

³ A RNA-depleting conditioning step often precedes anion-exchange runs and involves treatment of the feedstock with ribonuclease A to degrade the RNA impurities. This does, however, have both cost and regulatory implications due to the enzyme being sourced from the bovine pancreas (Hines *et al.*, 1992; Prazeres, Schluep and Cooney, 1998b; Eon-Duval and Burke, 2004).

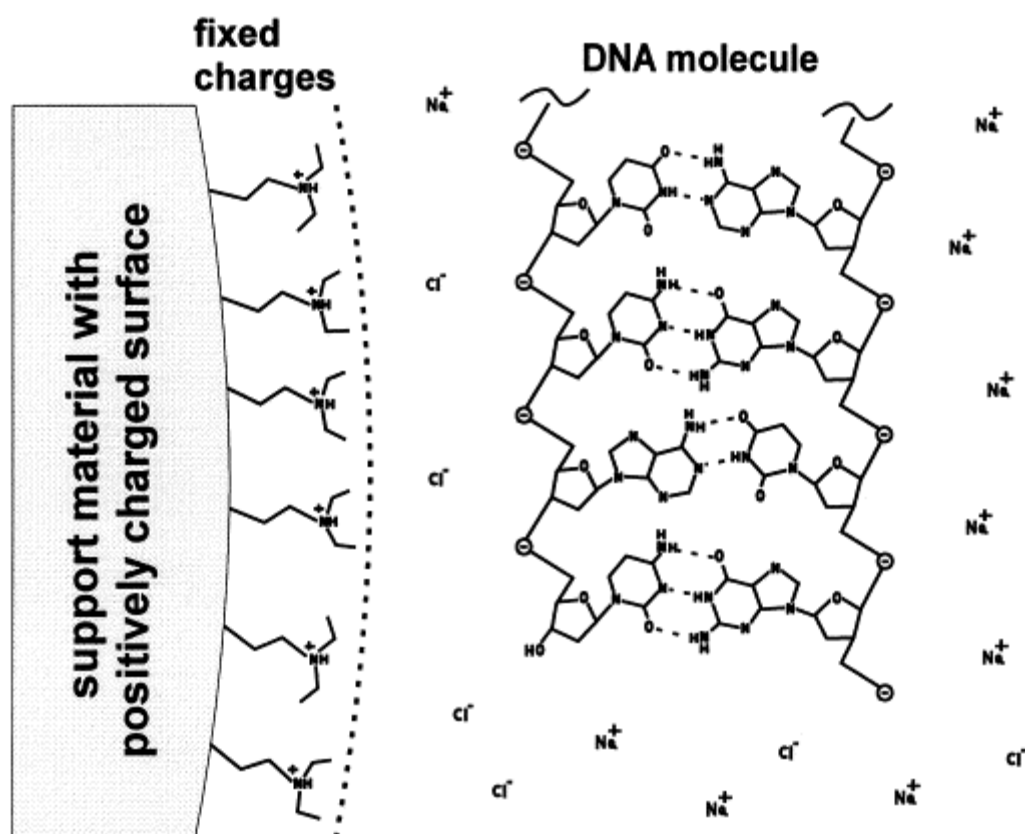


Fig. 1.12 Theoretical schematic of the electrostatic interaction between a positively charged anion-exchange stationary phase (in this case a weak AEX matrix, DEAE) and the negatively charged phosphodiester functional groups of double stranded DNA (sourced from Huber 1998).

In the case of viral vectors, their net surface charge (and thus interaction behaviour with ion-exchange supports) is derived from their surface composition; this includes the proteins which make up their capsid or the overall composition of their envelope (Segura, Kamen and Garnier, 2011b). Compared to smaller protein therapeutics, viral vectors exhibit stronger binding interactions and elute at higher ionic strengths (Trilisky and Lenhoff, 2007). This is likely due to an energetics scaling effect, as stronger colloidal interactions will occur with increasing particle size (Oberholzer and Lenhoff, 1999) as well as multiple sites for electrostatic interaction on virion surfaces due to their complexity and multi-protein composition.

This enhanced binding capacity allows a wide-range of viral vectors to be purified using anion-exchange chromatography⁴ and allows for high ionic loading conditions and salt elution gradients to facilitate isolation and fractionation of the target species away from impurities such as host cell proteins. However, as with plasmid DNA, viral vectors also suffer from low resolution anion-exchange runs due to co-elution of similarly densely charged nucleic acids and endotoxins, which compete for binding sites on the stationary support (Segura, Kamen and Garnier, 2011b).

⁴ Table 1 from Segura et al. 2011 provides an apt summary of the applications of AEX chromatography for a variety of viral vectors.

Interestingly, the ability of AAVs to tolerate substantial pH changes without impacting vector functionality (Gruntman *et al.*, 2015) can aid in its purification by ion-exchange chromatography. It has been demonstrated that “charge-switching” of the vector surface by pH modulation of the viral feedstock (below the vector’s isoelectric point) of AAV serotypes 2, 5 and 8 can result in better selectivity and elevated vector yields (Gao *et al.*, 2000; Brument *et al.*, 2002; Davidoff *et al.*, 2004; Qu *et al.*, 2007). It should be noted that this does not apply to the majority of viral vectors, given their high sensitivity to pH changes (Kramberger, Urbas and Štrancar, 2015a).

One of the major stumbling blocks of ion-exchange purification of both plasmid DNA and viral vectors is the low capacity of the resins due to a lack of pore-penetration; indeed this is one of the issues this research project aims to address. As a result, anion-exchange chromatography is often coupled with sequential chromatographic in a downstream processing train, using alternative separation principles including those discussed throughout Section 1.6.

1.6.2 Affinity Chromatography

Affinity chromatography offers a more selective and higher resolution approach to the purification of nanoplexes. The technique relies on the reversible, specific interaction between a target biomolecule and a ligand coupled to a stationary phase. Affinity chromatography utilises the nanoplex’s unique biological function or chemical structure and purification is based on highly specific molecular recognition between a natural or synthetic ligand and the target species. Elution can subsequently be achieved by modification of the ligand-target interaction, through modulation of the pH, polarity or ionic strength, or by competitive inhibition by introduction of a second ligand (Cuatrecasas, 1970; Platonova and Tennikova, 2005; Janson, 2011).

1.6.2.1 Triple Helix Affinity Chromatography

There are a number of variations to affinity chromatography, with applicability across protein, plasmid DNA and viral vector purification. In the case of plasmid DNA, Triple-Helix affinity chromatography (THAC) has been one of the more prevalent purification techniques; it relies on a specific recognition between a triple helix-forming stationary phase-immobilised oligonucleotide sequence and a sequence on the double stranded target plasmid. The ligand is usually a single stranded homo-pyrimidine oligonucleotide sequence which binds to an inserted, complimentary homo-purine sequence on the major groove of the duplex DNA. Molecular recognition between thymine on the third strand thymine (T) and adenine-thymine (A.T) base pairs on the plasmid facilitate the formation of (T.A.T) triplexes, whilst the complex is stabilised by protonated cytosine (C⁺) interacting with guanine-cytosine (G.C) base pairs to form C⁺.G.C triplexes. The interaction relies on Hoogsteen hydrogen bonding and requires cytosine protonation, thus loading should be at mildly acidic pH, followed by dissociation in alkaline buffer (Wils *et al.*, 1997).

Whilst offering a promising, economical, single-step chromatography step for significantly reducing the levels of contaminants such as genomic DNA, RNA and endotoxins two fold, THAC is hampered by a number of issues. Triple helix formation kinetics are slow and consequently binding steps require ≥ 60 minutes, which limits process throughput. In addition, support binding capacity is low (28 μg / ml support) and as such plasmid recovery is low (32% - 62%), whilst some

reports also suggest plasmid denaturation and loss of plasmid during wash stages, perhaps due to long processing times. To combat this, new resin designs have been employed for THAC, including wide-pored resins (Schluep and Cooney, 1998) and thermo-responsive affinity macro-ligands, which have seen yields jump to 70 – 90% (Costioli *et al.*, 2003).

1.6.2.2 Protein / Amino Acid – DNA Affinity Chromatography

An alternative to THAC is the use of protein-DNA affinity chromatography, which facilitates the isolation of plasmids from a crude alkaline lysate. The principle is based on a zinc finger (ZF) DNA binding protein coupled with a glutathione S-transferase (GST), creating an affinity ligand with bi-functionality; here the GST links to a glutathione Sepharose media, whilst the ZF domain recognises a 5'-GGGGCGGCT-3' sequence motif on the target plasmid (Woodgate *et al.*, 2002). Elution is achieved by competitive inhibition with the addition of reduced glutathione, resulting in high resolution plasmids but with modest yields (23-27%) (Ghose, Forde and Slater, 2004).

Via a less specific, yet more robust approach, amino acid-DNA affinity chromatography has been applied to plasmid DNA purification, facilitated by the use of histidine (Sousa *et al.*, 2006) ligands coupled to a stationary support. Histidine affinity chromatography has been demonstrated to resolve supercoiled plasmid DNA from host impurities as well as open circular DNA. The histidine-base recognition is based on a number of potential interactions, including hydrogen bonding, hydrophobic interaction and ring stacking (Luscombe, Laskowski and Thornton, 2001).

The interaction is particularly specific to supercoiled DNA, likely due to the higher exposure and availability of bases (particularly high percentage adenine or guanidine sequences) for interaction, relative to the open circular form of DNA (Sousa, Prazeres and Queiroz, 2007). Despite strong endotoxin column retention, it is possible to isolate plasmid DNA via an ammonium sulphate elution gradient (Sousa *et al.*, 2005, 2006).

Despite high purities (up to 100%, with removal of gDNA, endotoxins, RNA and host cell proteins to acceptable limits) and dynamic binding capacities in the range of 500 µg/ ml support, one of the fundamental issues of the technique is the relatively low yield and high salt conditions required for elution (Sousa *et al.* 2008). Studies have suggested that the use of arginine may overcome this issue, with better specificity for supercoiled plasmid DNA (stemming from more stable, multiple contact point-interactions between arginine and the nucleic acid chains, particularly guanine rich sequences) and an option to elute by competitive inhibition with arginine-spiked buffer (Sousa *et al.* 2008).

1.6.2.3 Thiophilic Aromatic Chromatography

Thiophilic Aromatic Chromatography (TAC) utilises chromatographic resins functionalised with aromatic thioether ligands which are capable of separating plasmid DNA from other DNA isoforms. The recognition is suggested to be two-fold; an intercalating π - π hydrophobic interaction between the aromatic ring of the thioether ligand and the double helix plasmid DNA. The second is possibly the ligand's sulphur residue behaving as an electron donor to specific nucleotides on

the plasmid, allowing a hydrophilic interaction with the highly available phosphate backbone of the supercoiled DNA isoform (Sandberg *et al.*, 2004).

The main drawbacks of the technique are the requirement for high concentrations of ammonium sulphate (or other lyotropic salt) to facilitate conformational compression of the nucleic acid moieties to enhance separation. Furthermore, elution kinetics can be slow and maximum yields of ~ 70% are reported; in all, this technique may have application as a polishing step after a series of group separation unit operations (Lemmens *et al.*, 2003; Sandberg *et al.*, 2004).

1.6.2.4 Immobilised Metal Affinity Chromatography

Immobilised metal affinity chromatography (IMAC) matrices are supports coupled with chelating agents, usually nitrilotriacetic acid (NTA) or iminodiacetic acid (IDA) which coordinate transition metal ions, such as Co, Zn, Ca, Mg, Ni or Cu in a 2⁺ oxidation state. Their separation principle relies on the relative affinity of target species to the immobilised transition ions; the interaction is reversible and can be eluted under gentle conditions using a competitive inhibitor such as imidazole or glycine, or by modifying the pH (Chaga, 2001; Murphy *et al.*, 2003; Nastasijevic *et al.*, 2008).

IMAC can be utilised in the purification of both plasmid DNA and viral vectors, though by different principles. For viral vectors, IMAC has been demonstrated to be a successful bind-and-elute purification strategy for a number of vectors, including HSV-1 (Jiang *et al.*, 2004), Adenovirus (Huyghe *et al.*, 1995), AAV (Koerber *et al.*, 2007), baculovirus (His-tagged) (Hu *et al.*, 2003) and γ -retrovirus (McNally *et al.*, 2014), with yields of ~ 50 – 90 % and purities comparable to gradient ultracentrifugation. A significant advantage of IMAC is its tolerance to high salt conditions and as such, an eluate from a preceding ion-exchange run can be loaded directly onto the column, without the need for buffer exchange (Burova and Ioffe, 2005).

With respect to plasmids, the step aims to remove single stranded nucleic acids and endotoxins from the feedstream and thus increase the purity of plasmid DNA in the flow through. The technique relies on both endotoxins and RNA having a higher avidity for the chelated metal ion (relative to the plasmid DNA) because of a higher availability of aromatic nitrogen (purine – adenine and guanine) bases available for interaction (Murphy *et al.*, 2003; Tan *et al.*, 2007). The main drawback of the technique is co-elution of genomic DNA, unless a conditioning step precedes IMAC to disrupt the gDNA, exposing the aromatic bases for metal affinity interactions (Cano *et al.*, 2005).

1.6.2.5 Viral Affinity Chromatography

There are a variety of options for affinity chromatography of viral vectors which rely on recognition between antigens on the viral capsid or envelope and an immobilised receptor. One such example of this is the use of immune-affinity including monoclonal antibodies, such as A20, which has a high affinity for AAV-2 capsids (Grimm *et al.*, 1998) or antibody fragments, such as the Camelid or Llama single domain heavy chain ligands which make up the commercially available

CaptureSelect™ (Thermo Fischer) and AVB Sepharose HP (GE Healthcare) resins, respectively and provide high affinity for the capsid proteins of a range of AAV serotypes (Terova *et al.* 2018).

An alternative to immune-affinity is the use of either cellulose or heparin sulphate affinity columns, exploiting the biological function of the heparin sulphate proteoglycan on viral vector surfaces which mediates cellular entry. Recoveries of ~ 70% have been reported on the POROS HE/M (PerSeptive Biosystems) heparin affinity column for the AAV-2 vector (Clark *et al.*, 1999), whilst applicability has also been demonstrated for retrovirus, HSV and vaccinia viruses (Segura, Kamen and Garnier, 2011b). Mucin has also been utilised as an immobilised ligand in the purification of AAV type 5 vectors, based on its high 2-3, linked sialic acid content and the fact that, similar to heparin, its requirement for cellular entry of AAV-5 (Walters *et al.*, 2001); studies have demonstrated higher viral vector yield with mucin conjugated-Sepharose media, than that of conventional gradient ultracentrifugation (Auricchio *et al.*, 2001).

1.6.2.6 Immobilised Metal Affinity Viral Chromatography

Viruses can also be engineered to display markers which aid in affinity-based capture. Examples of this approach include the use of hexahistidine tags displayed on AAV-2 and AAV-8 (yields > 90%), which have high affinity for Ni-IMAC columns (Koerber *et al.*, 2007), as well as HSV-1 engineered to present the histidine affinity tag (HAT) peptide which has high avidity in Co-IMAC purification columns (Jiang *et al.*, 2004), whilst adenoviruses naturally bind to Zn-IMAC columns without genetic modification. In a similar vein, the commonly used biotin-avidin interaction can be exploited for viral purification, with vectors biotinylated via metabolic engineering or chemical conjugation reactions, the latter achieved through fusion of a viral structural protein to a biotin acceptor peptide, though this comes at the risk of compromising viral transduction efficiency (Segura, Kamen and Garnier, 2011b).

In general, affinity chromatography techniques offer highly selective and often significantly high resolution separation compared to alternative chromatographic unit operations. They are particularly attractive as they present a one-step solution to target purification, which can increase product yield, process throughput and is economically favourable.

The main setbacks of the approach tend to be the fragility of the ligands, their biological source, high cost of manufacture and functionalisation, low binding capacities and their occasional propensity to leak into the product stream (Gribnau and Tesser, 1974; Lowe, Lowe and Gupta, 2001; Jozala *et al.*, 2016). Research continues into the development of synthetic ligands to offset these limitations and though the manufacture of artificial, biomimetic ligands can be resource-intensive, this work is justified given the potential long-term economic benefits of robust, one-step affinity chromatography (Sousa, Prazeres and Queiroz, 2008).

1.6.3 Hydrophobic Interaction Chromatography

Hydrophobic interaction chromatography (HIC) exploits differences in the hydrophobicity of solutes to achieve efficient separation. Non-polar groups on the biological species interact with hydrophobic alkyl or aryl ligands on the stationary phase; loading occurs at high ionic

concentrations to displace ordered water molecules which shield both the solute species in the mobile phase and the ligands functionalised on the stationary phase, whilst elution is achieved by either decreasing the salt concentration or by introduction of an organic solvent to modify the polarity of the mobile phase (Queiroz, Tomaz and Cabral, 2001).

The technique is particularly amenable to the purification of plasmid DNA given the differences in hydrophobicity of the plasmid DNA and its other isoforms, as well as other process impurities such as endotoxins, with some reporting yields as high as 98% (Bo *et al.*, 2013). Denatured nucleic acids from the alkaline lysis step, as well as single stranded nucleic acids, exhibit higher non-polar character, whilst lipid A on endotoxins provides a moiety for hydrophobic interaction (Diogo *et al.*, 2000; Diogo, Queiroz and Prazeres, 2001).

The technique has been applied with less success for viral vectors, with low recoveries (5 – 30%) reported, likely due to either viral degradation or aggregation resulting from high salt concentrations (Burova and Ioffe, 2005; Segura, Kamen and Garnier, 2011b). The high salt requirement means the operation is associated with high economical cost as well as adding an additional step to re-buffer the product for further purification / formulation, which can further reduce yield (Sousa, Prazeres and Queiroz, 2008).

1.6.4 Reverse Phase Chromatography

Similar to HIC, reverse phase chromatography (RPC) is dependent on hydrophobic interactions between solute species and the stationary phase. The key difference is the higher concentration of non-polar ligands on the stationary phase (commonly silica, polystyrene or linear hydrocarbons, e.g. C8-C18 are used) and consequently the need for highly non-polar solvents for elution. In order to improve separation, ion pairing molecules such as triethylamine or trifluoroacetic acid are used to suppress charges for ionic interaction and thus enhance hydrophobic interaction with the stationary phase (Neville, 1996).

Due to its particularly high resolution, RPC is mainly used as an analytical tool for assessing the quality of purified plasmid or viral vector, though can be run in flow-through mode for preparative purification of adenoviral vectors (Green *et al.*, 2002) as well for plasmid DNA, with nearly 100% recovery for the latter (Colote, Ferraz and Liautard, 1986).

One of the main disadvantages of RPC is the requirement for organic solvents, which can be costly, volatile and mutagenic, which have process, environmental and regulatory safety implications (Yabré *et al.*, 2018). Furthermore, the solvents can denature the biological product and lead to diminished product yield (McNay, O'Connell and Fernandez, 2001).

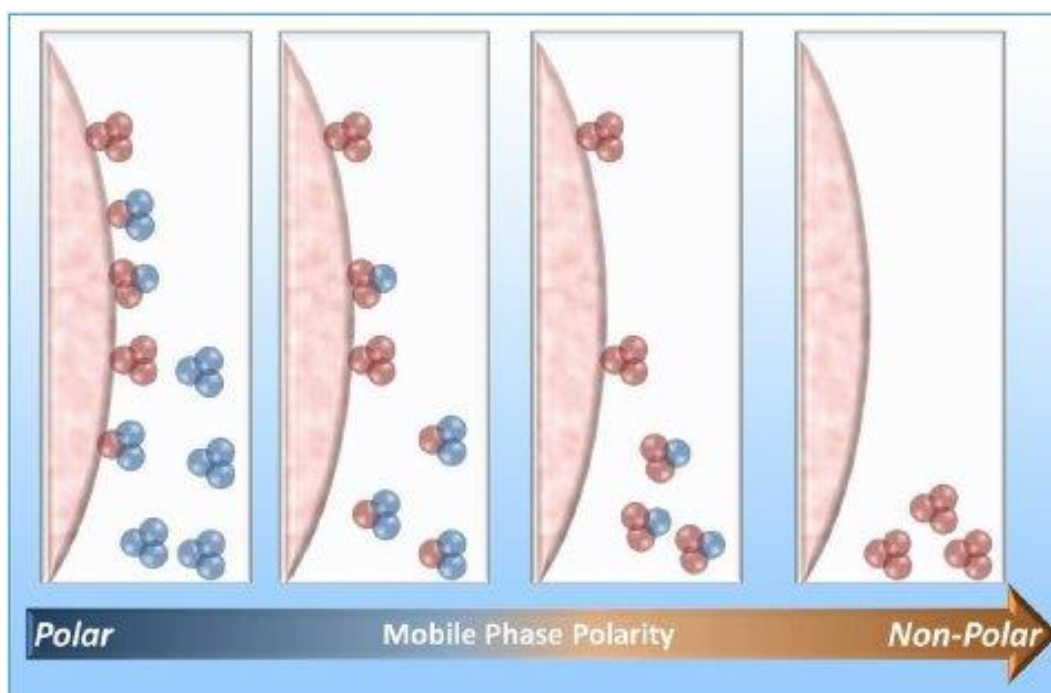


Fig. 1.13 A schematic detailing the principles of reverse-phase chromatography, whereby it is possible to elute species based by modulating the polarity of the mobile phase (from Salvato *et al.* 2012) .

1.6.5 Size Exclusion Chromatography

Size Exclusion Chromatography (SEC), also known as gel filtration, relies on the principle of differences in species' size to achieve separation and given the comparatively large sizes of both plasmid DNA and viral vectors compared to other feedstock impurities, the technique serves as a useful tool for purification.

Species will elute from the column in order of size, with smaller and lower molecular weight feedstock components such as RNA and endotoxins retained for longer in the column, whilst larger targets will elute earlier or even in the earliest void volume of the column, being completely excluded from entering the pores of the matrix (Varley *et al.*, 1999). An appropriate media should be selected based on the exclusion limit, fractionation range and porosity of the beads, as well as the composition of the feedstream and product characteristics, in order to achieve optimum separation; for instance, large pored resins such as Sephacryl S-1000 SF (GE Healthcare), which has exclusion limits of 1×10^8 Da and 20 kb for globular proteins and linear DNA, respectively, can achieve better resolution of target plasmid against similar high molecular weight impurities such as genomic DNA (Ferreira *et al.*, 2000), plasmid DNA isoforms (Latulippe and Zydney, 2009), proteoglycans and empty viral capsids (Qu *et al.*, 2015).

However, to achieve high resolution, there are limitations to loading capacity (usually $< 10\%$ of the column volume) and linear flow rates (< 15 cm/hr); as such concentration of the feedstock is required prior to SEC, which may lead to loss of yield through particle aggregation (Kamen and Henry, 2004). Low flow rates lead to long processing times and potential product degradation as well as hampering process productivity (Segura, Kamen and Garnier, 2011b).

In all, the technique offers a gentle method of purification; there is no media-target chemical interaction and as SEC is usually run isocratically, no harsh elution conditions are required. High recoveries are regularly achieved and the step also has the additional benefit of being able to buffer exchange / de-salt (ideal for post-IEX elution or HIC chromatography) the target species for either pre-conditioning for the next unit operation or for formulation. As such, SEC is often used as a polishing step towards the end of the downstream processing train, when feed volumes and process impurity concentrations are low and re-constitution of the product to its final fill buffer is required (Varley *et al.*, 1999; Urthaler, Buchinger and Necina, 2004; Segura, Kamen and Garnier, 2011b).

1.7 Developments in Chromatographic Separation

In order to meet the challenge of purifying higher titre, diverse and more problematic feedstocks composed of larger, sensitive and more complex bio-products, purification platforms such as chromatography have had to adapt and evolve. As product titre increases, upstream capacity can facilitate this without impacting cost, whilst process bottlenecks and costs shift to downstream processing, as its “capacity scales at least linearly with costs due to its physical principles of separation” (Gronemeyer, Ditz and Strube, 2014).

Chromatographic separation accounts for approximately 50% of the total bioprocess cost and product yield falls with each additional unit operation added to the bioprocess train (Ladisch, 2001). Conventional chromatography matrices were custom built for the purification of small protein complexes at low concentrations and consequently have to be retro-fitted to purify large vectors such as viruses or plasmid DNA (Lyddiatt and O’Sullivan, 1998). This is somewhat of an inefficient approach as the diffusivity of a nanoplex such as plasmid DNA is 10-fold lower than a typical therapeutic protein (Subramanian, 2012) and given the small pore sizes of conventional chromatography beads, large target molecules can only interact with the bead’s surface, representing a dramatic loss in binding capacity (Stadler, Lemmens and Nyhammar, 2004).

This has driven research into new types of chromatography media for the purification of large nanoplexes, innovating conventional methodologies and techniques to handle more complex, concentrated feed streams, whilst maintaining an economically feasible bioprocess.

1.7.1 Mixed Mode Chromatography

One such example of innovative chromatography is the relatively novel mixed-mode (MMC) approach. As the name suggests, the stationary phase is composed of ligands which can interact with at least two or more interaction types, which often leads to higher selectivity, better retention and more favourable yields. The technique grants better flexibility whereby the mobile phase can be modulated to promote and tailor specific solute interactions with the stationary phase (Zhang and Liu, 2016).

GE Healthcare’s Capto Adhere MMC resin utilises an N-Benzyl-N-Methyl ethanol amine ligand to interact with target species by ionic, hydrogen bonding and hydrophobic interaction. Whilst developed for the purification of mAbs, it has also been successfully applied to the purification of

plasmid DNA, with dynamic binding capacities of 60 µg/ml of resin reported (Matos, Queiroz and Bülow, 2014).

The technique is particularly amenable to viral purification, as certain viral populations can bind to both anion and cation exchange resins at neutral pH; this mixed binding character is due to the complex and non-uniform charge distribution of the viral surface, with multiple capsid proteins exhibiting both positive and negative charge surface charges. This subsequently aids the removal of impurities as a cation-exchanger and anion exchanger will successfully deplete chromosomal DNA and host cell proteins, respectively (Gagnon, 1996; Carta and Jungbauer, 2010).

Hydroxyapatite chromatography (HAC) is another good example of MMC whereby viruses are able to bind to both the positively charged calcium ions as well as the negatively charged phosphate groups, even at high salt concentrations, with subsequent elution using a phosphate gradient (Segura, Kamen and Garnier, 2011b). HAC has been demonstrated for the successful purification of HPV-like particles, with yields of 59% reported (Baek *et al.*, 2011).

One of the main disadvantages of MMC is its time consuming method development and front end optimisation requirements. Particularly in the case of pH-sensitive viral vectors, loading and elution conditions need to be carefully optimised to avoid compromising product integrity in an effort to strive for higher recoveries (Segura, Kamen and Garnier, 2011b; Kramberger, Urbas and Štrancar, 2015).

1.7.2 Membrane & Monolithic Chromatography

Next generation chromatography materials such as membrane and monolithic systems aim to move away from the traditional, beaded chromatography supports, towards macroporous (700 – 1000 nm) stationary phases with elevated porosities which facilitate better mass transfer characteristics through convection and so separation is not limited by diffusion. This also creates lower pressure drops across the column, which allows for rapid flow rates and all of this ultimately leads to higher binding capacities (Urthaler *et al.*, 2005; McNally *et al.*, 2014).

The membrane adsorber Mustang Q (Pall Life Sciences), which utilises the same quaternary amine as many beaded media, has demonstrated significantly higher binding capacities for both plasmid DNA (10 mg/ml resin) (Teeters *et al.*, 2003) and lentiviral vectors (140 fold concentration factor) (Kutner *et al.*, 2009). In a similar fashion, monolithic columns, such as BIA's DEAE Convective Interaction Media (CIM), have been used successfully for the purification of nanoplexes, with improvements in binding capacity up to 13 mg/ml media for plasmid DNA (Tarmann and Jungbauer, 2008) and recoveries of up to 80% for a range of viral particles, including lentivirus (Bandeira *et al.*, 2012) and bacteriophages (Kramberger, Urbas and Štrancar, 2015).

1.7.3 Tentacular Supports

In an effort to improve the overall surface area for interaction between stationary phases and the target solutes, long poly-electrolyte “tentacles”, with elongated spacer arms, have been functionalised into supports, aiming to combat the issue of low pore penetration of nanoplexes

(Müller, 1990; Merten and Al-Rubeai, 2011). For canine adenoviral vectors, yields of up to 88% have been achieved using Merck's Fractogel propyl-tentacle resins (Segura *et al.*, 2012). Fractogel EMD and Sepharose Q XL also have tentacle structures extending from their exterior which could facilitate plasmid DNA clustering onto the surface of the beads (Theodossiou, Søndergaard and Thomas, 2001).

1.7.4 Wide-Pore Matrices

To maximise the interior surface area of beaded media, wide-pored media have also been employed to improve the separation and recovery of large nanoplexes. These include Celbeads DEAE and PL SAX 4000 Å resins, with pores larger than 500 nm to support better convective mass transfer of target species. Celbeads and PL SAX were demonstrated to have static binding capacities of 1.76 and 5.03 mg/ml resin of plasmid DNA, respectively and correlate well with the available surface area for anion-exchange interactions on each media (Tarmann and Jungbauer, 2008). One of the main drawbacks of wide-pored matrices is the risk of comprising the bead's physical integrity and compressibility under packed-bed conditions (Lyddiatt, 2002).

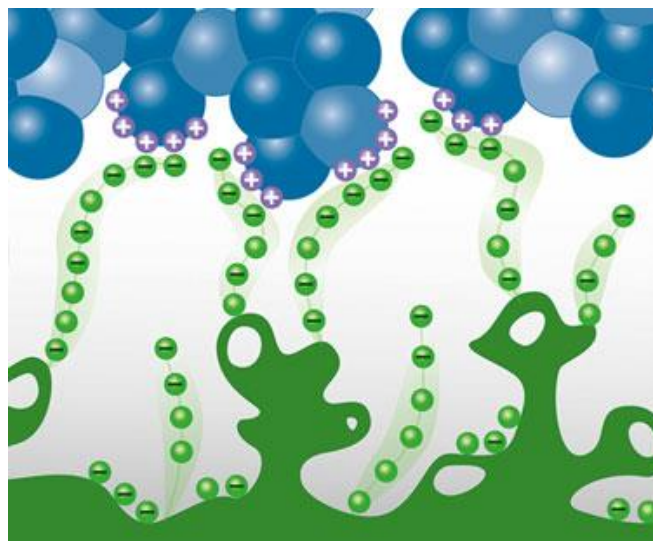


Fig. 1.14 A cartoon depiction of Fractogel's tentacular arms interaction with target solute species in the mobile phase (courtesy of Aldridge 2009).

1.7.5 Multi-Layer Chromatography Beads

At the focal point of this research is the employment of multi-layer chromatography matrices which aims to isolate nanoplexes using a purification-by-flow-through strategy. Here, a bi-layered media is created, whereby large particulates, such as plasmid DNA and viral vectors, are excluded from the porous support, whilst smaller impurities are “hoovered” into the core. The first example of this methodology was reported by Gustavsson and co-workers, who utilised a multi-column approach to achieve 89% recovery of plasmid DNA and 99.5% and 96% removal of RNA and proteins, respectively (Gustavsson *et al.*, 2004).

Two commercial resins from GE Healthcare, Capto™ Core 700 and 400, were released in 2012 and 2018, respectively, with the former shown to be effective at purifying H3N2 A influenza from egg allantoic fluid, achieving recoveries of 69% and an ovalbumin binding capacity of 14.1 mg /ml resin, using a multimodal octylamine ligand functionalised within the core (Blom *et al.*, 2014). An alternative approach is that of laminating or coating ion-exchange resins with non-reactive polymer such as agarose to create a bi-layered media with an inert shell; whilst this has proven to be somewhat effective, there are challenges in achieving a sufficiently thin pellicle around the bead to avoid compromising mass transfer of smaller impurities into the core of the bead (Zhang *et al.*, 2001; Jahanshahi, Zhang and Lyddiatt, 2005; Jahanshahi, Partida-Martinez and Hajizadeh, 2008).

This approach is particularly effective as it combines the capture and resolution potential of both ion-exchange and size-exclusion chromatography, whilst overcoming capacity and volume limitations of the unit operations if run in isolation. This allows the bi-layered-based separation to be run higher up the downstream processing train and simultaneously cuts down on the number of subsequent steps which will help in dramatically improving process efficiency through lowering overall cost and increasing process throughput.

1.8 Virus Mimics

As research continues into new types of chromatography media to meet the ever increasing demands of gene therapy and DNA vaccines, as well as the continual battle to drive down bioprocess costs, a key issue is the availability and cost of nanoplex material to optimise with. Plasmid DNA and live viral vectors can take days to produce in conventional cell culture systems and the cost of manufacture and subsequent purification of sufficient material to test novel chromatography systems often becomes an inhibitory factor (Lyddiatt and O'Sullivan, 1998). As such there is a niche to create a cheap and readily available nanoplex mimic which can provide valuable process data on new chromatographic supports, at a fraction of the price whilst also circumventing some of the associated safety concerns of using live viral vectors.

1.8.1 Inclusion Bodies

One of the first accounts of surrogate virus mimics was the use of nanoparticulate inclusion bodies (IBs) for the optimisation of aqueous two phase systems. The inclusion bodies were harvested from *E. coli* culture producing yeast α -glucosidase, expressed as IBs in the cytoplasm. The IBs were found to have similar physiochemical properties to that of adeno- and retro- viruses, in terms of hydrodynamic size and buoyant density, with concentration in the order of $\sim 5 \times 10^{14}$ particles/ml produced (Braas *et al.*, 2000; Braas, Walker and Lyddiatt, 2000).

The main disadvantage of using IBs as viral mimics is the lengthy production time and cost of equipment and materials associated with *E. coli* culture and subsequent cell disruption steps, as well as a lack of process control in terms of quantity or physiochemical characteristics of the nanoparticulate IBs produced.

1.8.2 Silica Nanoparticles

Silica nanoparticles have been utilised as mimics of viruses for a range of applications, including as surrogates for rotavirus in characterising filtration media (Pang *et al.*, 2014) and mimicking the surface topography of enveloped viruses such as HSV, influenza and HIV to monitor nanoparticulate uptake into cells (Niu *et al.*, 2013). Some examples are particularly sophisticated, mimicking the protruding capsid proteins of non-enveloped viruses using grafted silica nanotubes onto the surface of silica nanoparticles (Wang *et al.*, 2017).

Silica nanoparticles are advantageous as they can be functionalised with protein and/or DNA (Farkas, Varsani and Pang, 2015), in part due to the high density of silanol groups available on their surface (Wu, Hung and Mou, 2011). They are also mesoporous and can be “loaded” with therapeutic agents such as doxorubicin for drug delivery, particularly in cancer applications (Watermann and Brieger, 2017). One of the major drawbacks is the complexity involved in the synthesis of silica nanoparticles; the precursor tetraethyl orthosilicate requires the use of organic solvent due to its poor aqueous solubility and the formation of nanoparticles requires toxic reagents such as tetramethylammonium hydroxide and concentrated sodium hydroxide solutions (Bharti *et al.*, 2015).

1.8.3 Gold Nanoparticles

Metallic nanoparticles such as gold have also been extensively characterised for their use as drug delivery vehicles (Ghosh *et al.*, 2008; Schäffler *et al.*, 2014), in part due to their high amenability for surface functionalisation with protein and DNA (Giljohann *et al.*, 2010; Patel *et al.*, 2010; Tiwari *et al.*, 2011; Singh *et al.*, 2012). Gold nanoparticles have also been demonstrated as useful surrogate mimics in the characterisation of ion-exchange filtration membranes and are particularly useful due to their ease of assaying given their signature surface plasmon resonance band at 520 nm (Matsushita *et al.*, 2006).

Whilst gold nanoparticles are useful mimics of most viral species owing to their strong negative surface charge (Giljohann *et al.*, 2010), the nanoparticles are tricky to synthesise and require boiling steps, reflux condensers, as well as reducing agents and expensive hydrogen tetrachloroaurate precursor material (Frens, 1973; Zhou *et al.*, 2009; Yeh, Czeran and Rotello, 2012). Gold nanoparticles are also particularly dense ($\sim 19 \text{ g/cm}^3$) (Akbulut *et al.*, 2012) and experimental observations have found nanoparticles of similar hydrodynamic radius to some viral vectors ($\sim 100 \text{ nm}$) readily collapse out of suspension.

1.8.4 Polymeric Nanoparticles

Nanoparticles formed using polymeric sub-units have also been successfully applied as mimics of a variety of viruses, including bacteriophage (Patel, 2017) and enveloped viruses such as HIV and influenza (Lou *et al.*, 2019) using cationic polymers such as azide or cross-linked ϵ -poly-lysine conjugated to 1,2-epoxytetradecane polymers. As with silica nanoparticles, there have been demonstrations of conjugated viral “spikes” to the surface of the nanoparticles using a zinc coordinate ligand to aid in cell surface recognition and entry for drug delivery (Liu *et al.*, 2018).

Much of the focus on polymeric nanoparticles has been their utility as drug delivery vehicles, using biocompatible polymers such as polyhydroxyalkanoates (PHA) and poly-(lactic-co-glycolic) acid (PGLA) as starting materials for nanoparticle formation (Masood, 2016). As with many synthetic nanoparticles, polymer-based nanoparticles are often manufactured using complex emulsion or emulsification techniques, including difficult to control polymerisation reactions. Furthermore, toxic impurities can accumulate within or in proximity to the nanoparticles, including organic solvents, cross-linkers, initiators and monomeric components, which need to be extensively dialysed to ensure high levels of nanoparticle purity (Crucho and Barros, 2017).

1.8.5 Virus-Like Particles

The gold standard of viral mimics is that of virus-like particles (VLPs), i.e. viral structure proteins which form into nanoparticulate structures during expression and can often very closely resemble the parent virus, making ideal surrogates. As with most viral vectors, VLPs can also be utilised for drug delivery; one example of this is the use of HPV-VLPs utilised as vectors for the delivery of pDNA in a murine model, with successful antigen presentation recorded (Malboeuf *et al.*, 2007).

VLPs can also be modified to aid in targeted drug delivery; a good example of this is where a model green fluorescent protein was fused to an SV40 VP2/3 minor protein of a VLP, with successful cellular delivery observed (Inoue *et al.*, 2008). Despite their significant advantages and close resemblance to *bona fide* virus species, VLPs do not circumvent some of the key issues of using live viral material which justify the need for viral mimics. VLPs, like live viral material, still require proper containment and have similar safety concerns to live or attenuated viral material, whilst their use is hampered by the same cost and resource requirements given their production in cell culture and purification requirements (Lai *et al.*, 2010; Somiya, Liu and Kuroda, 2017).

1.8.6 Protein Nanoparticles

One promising approach for the development of appropriate viral vector mimics is the use of cross-linked protein nanoparticles. These particles offer a cheap, readily available and easy to manufacture mimic and logically fit well given that non-enveloped viruses are encased by a composite of proteins and it is this capsid which is responsible for its interaction with purification media.

Much of the work into the formation of protein nanoparticles concerns their use as drug delivery vehicles (Mehravar, Jahanshahi and Saghatoleslami, 2009; Lohcharoenkal *et al.*, 2014) and relies upon the coacervation/cross-linking method first detailed by Marty *et al.* in 1978. The focus has generally been on albumin-based nanoparticles, due to the high availability of lysine residues available for cross-linking (Habeeb and Hiramoto, 1968), though there have also been accounts of the use of self-associating viral protein nanoparticles which have been utilised in vaccine applications (López-Sagasetta *et al.*, 2016).

Work by Langer and co-workers has looked at optimising the desolvation procedure to tailor specific sizes of albumin nanoparticles, including organic solvent, protein and cross-linker ratios,

as well as experimental conditions such as pH, temperature and ionic strength (Weber *et al.*, 2000; Langer *et al.*, 2003, 2008; von Storp *et al.*, 2012).

Some initial research was carried out by Lyddiatt *et al.* on characterising chromatography media and aqueous two phase systems using both inclusion bodies and BSA nanoparticles as surrogate mimics of viruses. The intent was to utilise these mimics in lieu of difficult to attain gene therapy vectors to test the chromatography of polymer-coated resins. Here a weak anion-exchange matrix (Streamline DEAE, GE Healthcare) was coated with polymer to form a “subtractive adsorbent” and subsequently incubated with BSA nanoparticles of 95 nm average size to observe binding kinetics (Lyddiatt and O’Sullivan, 1998; Braas, Walker and Lyddiatt, 2000; Zhang *et al.*, 2001; Jahanshahi *et al.*, 2004; Jahanshahi, Zhang and Lyddiatt, 2005).

The research detailed here looks to refine this approach; particularly in the production of viral mimics, with more stringent characterisation and systematic variance of processing conditions, to tailor nanoparticles to specific virus species and utilise the manufactured surrogates in informing the chromatographic performance of a range of novel bi-layered matrices manufactured in house.

1.9 Nanoplex Market Analysis

A market appraisal demonstrating the dosage requirement and patient population of an exemplary disease state treatable by gene therapy was carried out in order to estimate the requirement of scale of manufacture of viral vectors (and thus viral mimics required to characterise chromatography media).

The example disease used in this analysis is Epidermolysis Bullosa (EB), referring to the Phase I clinical trial carried out by Siprashvili *et al.* in 2016. In this study, autologous recessive dystrophic epidermolysis bullosa (RDEB) keratinocytes were subjected to retroviral-mediated transduction of a COL17A1 gene, contained within an epidermal sheet graft. A 70% transduction efficiency was reported with graft longevity of more than 5 years (Siprashvili *et al.*, 2016). Similar work transfecting HEK 293T cells with COL17A1 via retroviral vectors demonstrated high titres of 2.1×10^6 infectious particles per ml with transduction efficiencies of $\sim 60\%$ (Titeux *et al.*, 2010).

To provide context, a similar study for the treatment of EB employed lentiviral vectors transducing human keratinocytes, demonstrating the successful transduction of 10^7 infectious particles per graft and used a green fluorescent protein (GFP) marker to illustrate $\sim 50\%$ transduction efficiency (Kuhn *et al.*, 2002).

The estimated prevalence of EB in the United States and Europe is 1 per 100,000 people though this continues to grow as it is estimated inherited EB incidence is 8 per 1 million new births (Fine, 2016; Maldonado-Colin *et al.*, 2017). Estimating the population of the US and Europe at ~ 1 billion, as per the latest ONS figures, the EB patient population can be approximated to be 1×10^7 .

If we optimistically assume each patient requires one successful graft once per lifetime, i.e. one dose (assuming a 50% transduction efficiency) would be $\sim 2 \times 10^7$ infectious particles, then effectively the total patient population demand for potent, infectious viral particles would be $\sim 2 \times 10^{14}$, not considering the difficulties and costs of acquiring sufficient skin graft material as well as the complications of dose administration, including host-graft rejection. Nonetheless, a requirement in the order of 10^{14} particles for just one disease state is a huge demand in the context of bio-processing; particularly when manufacturing a product at such a large scale.

The associated costs of producing infectious viral particles can be huge; cell culture, clarification, viral particle isolation, concentration and purification as well as final formulation and filling and also product quality testing and validation (all this even before the transfection stage) are all extremely costly; an example from GE Healthcare for producing adenovirus particles for therapeutic use estimates a cost per batch of $\sim \$500,000$ to produce a batch in the order of $\sim 10^{13}$ viral particles per litre (GE Healthcare, 2019).

When considering such high costs of manufacture, decisions at each stage of the process design are vital and small scale optimisation studies to determine optimum purification trains are crucial. Consequently, using protein nanoparticles as a proxy for *bona fide* viral particles can provide, both cheaply and rapidly, informative bioprocess data (e.g. by screening various chromatography media and other processing steps for purification performance prior to scale up) to inform important decisions with respect to maintaining product integrity, purity and yield and can aid in saving time and driving down product costs, as well as improving process throughput to deliver gene and cell therapy products to meet the ever increasing patient population demand.

1.10 References

- Akbulut, O. *et al.* (2012) 'Separation of Nanoparticles in Aqueous Multiphase Systems through Centrifugation', *Nano Letters*. American Chemical Society, 12(8), pp. 4060–4064. doi: 10.1021/nl301452x.
- Aldridge, S. (2009) 'Bringing Greater Efficiency to Antibody Manufacturing', *Genetic Engineering and Biotechnology News*, 29(14). Available at: <https://www.genengnews.com/magazine/117/bringing-greater-efficiency-to-antibody-manufacturing/2/> (Accessed: 31 December 2018).
- Allay, J. A. *et al.* (2011) 'Good manufacturing practice production of self-complementary serotype 8 adeno-associated viral vector for a hemophilia B clinical trial.', *Human gene therapy*. Mary Ann Liebert, Inc., 22(5), pp. 595–604. doi: 10.1089/hum.2010.202.
- Anderson, W. F. (2000) 'The Best of Times, the Worst of Times', *Science (New York, N.Y.)*. American Association for the Advancement of Science, 288(5466), pp. 627–629. doi: 10.1126/science.256.5058.808.
- Anson, D. S. (2004) 'The use of retroviral vectors for gene therapy-what are the risks? A review of retroviral pathogenesis and its relevance to retroviral vector-mediated gene delivery.', *Genetic vaccines and therapy*. BioMed Central, 2(1), p. 9. doi: 10.1186/1479-0556-2-9.
- Artusi, S. *et al.* (2018) 'Herpes Simplex Virus Vectors for Gene Transfer to the Central Nervous System', *Diseases*. Multidisciplinary Digital Publishing Institute, 6(3), p. 74. doi: 10.3390/diseases6030074.
- Auricchio, A. *et al.* (2001) 'A Single-Step Affinity Column for Purification of Serotype-5 Based Adeno-associated Viral Vectors', *Molecular Therapy*, 4(4), pp. 372–374. doi: 10.1006/mthe.2001.0462.
- de Azavedo, J. C. *et al.* (1985) 'Gram-negative endotoxins and staphylococcal toxic shock syndrome.', *Progress in clinical and biological research*, 189, pp. 419–32. Available at: <http://www.ncbi.nlm.nih.gov/pubmed/4048216> (Accessed: 3 December 2018).
- Baek, J.-O. *et al.* (2011) 'Production and purification of human papillomavirus type 33 L1 virus-like particles from *Spodoptera frugiperda* 9 cells using two-step column chromatography', *Protein Expression and Purification*, 75(2), pp. 211–217. doi: 10.1016/j.pep.2010.08.005.
- Balasundaram, B., Harrison, S. and Bracewell, D. G. (2009) 'Advances in product release strategies and impact on bioprocess design', *Trends in Biotechnology*. Elsevier Current Trends, 27(8), pp. 477–485. doi: 10.1016/J.TIBTECH.2009.04.004.
- Bandeira, V. *et al.* (2012) 'Downstream Processing of Lentiviral Vectors: Releasing Bottlenecks', *Human Gene Therapy Methods*. Mary Ann Liebert, Inc. 140 Huguenot Street, 3rd Floor New Rochelle, NY 10801 USA , 23(4), pp. 255–263. doi: 10.1089/hgtb.2012.059.
- Baum, C. *et al.* (2011) 'Concise Review: Managing Genotoxicity in the Therapeutic Modification of Stem Cells', *STEM CELLS*, 29(10), pp. 1479–1484. doi: 10.1002/stem.716.

Baxby, D. (1996) *Poxviruses, Medical Microbiology*. University of Texas Medical Branch at Galveston. Available at: <http://www.ncbi.nlm.nih.gov/pubmed/21413326> (Accessed: 27 November 2018).

Benjaminsen, R. V *et al.* (2013) ‘The Possible “Proton Sponge ” Effect of Polyethylenimine (PEI) Does Not Include Change in Lysosomal pH’, *Molecular Therapy*. Cell Press, 21(1), pp. 149–157. doi: 10.1038/MT.2012.185.

Bharadwaj, M. *et al.* (2009) ‘HPV & HPV vaccination: issues in developing countries.’, *The Indian journal of medical research*, 130(3), pp. 327–33. Available at: <http://www.ncbi.nlm.nih.gov/pubmed/19901442> (Accessed: 26 November 2018).

Bharti, C. *et al.* (2015) ‘Mesoporous silica nanoparticles in target drug delivery system: A review.’, *International journal of pharmaceutical investigation*. Wolters Kluwer -- Medknow Publications, 5(3), pp. 124–33. doi: 10.4103/2230-973X.160844.

Birnboim, H. C. and Doly, J. (1979) ‘A rapid alkaline extraction procedure for screening recombinant plasmid DNA.’, *Nucleic acids research*, 7(6), pp. 1513–23. Available at: <http://www.ncbi.nlm.nih.gov/pubmed/388356> (Accessed: 30 November 2018).

Blaese, R. M. *et al.* (1995) ‘T Lymphocyte-Directed Gene Therapy for ADA- SCID: Initial Trial Results After 4 Years’, *Science*, 270(5235), pp. 475–480. doi: 10.1126/science.270.5235.475.

Blom, H. *et al.* (2014) *Efficient chromatographic reduction of ovalbumin for egg-based influenza virus purification*, *Vaccine*. doi: 10.1016/j.vaccine.2014.04.033.

Bo, H. *et al.* (2013) ‘Using a single hydrophobic-interaction chromatography to purify pharmaceutical-grade supercoiled plasmid DNA from other isoforms’, *Pharmaceutical Biology*. Taylor & Francis, 51(1), pp. 42–48. doi: 10.3109/13880209.2012.703678.

Bordignon, C. *et al.* (1995) ‘Gene therapy in peripheral blood lymphocytes and bone marrow for ADA- immunodeficient patients.’, *Science (New York, N.Y.)*, 270(5235), pp. 470–5. Available at: <http://www.ncbi.nlm.nih.gov/pubmed/7570000> (Accessed: 13 November 2018).

Braas, G. M. F. *et al.* (2000) ‘Recovery and Manipulation of Nanoparticulate Bioproducts : Relevance To the Up-Scaled Manufacture of Gene Therapy Vectors’, *Trans IChemE*, 78(March), pp. 11–18.

Braas, G. M. F., Walker, S. G. and Lyddiatt, A. (2000) ‘Recovery in aqueous two-phase systems of nanoparticulates applied as surrogate mimics for viral gene therapy vectors’, *Journal of Chromatography B: Biomedical Sciences and Applications*, 743(1–2), pp. 409–419. doi: 10.1016/S0378-4347(00)00056-6.

Brument, N. *et al.* (2002) ‘A versatile and scalable two-step ion-exchange chromatography process for the purification of recombinant adeno-associated virus serotypes-2 and -5.’, *Molecular therapy: the journal of the American Society of Gene Therapy*, 6(5), pp. 678–86. Available at: <http://www.ncbi.nlm.nih.gov/pubmed/12436964> (Accessed: 27 December 2018).

Buchschacher, G. L. (2003) *Lentiviral vector systems for gene transfer*. Springer US. Available at: <https://www.springer.com/gb/book/9780306477027> (Accessed: 21 November 2018).

Burova, E. and Ioffe, E. (2005) 'Chromatographic purification of recombinant adenoviral and adeno-associated viral vectors: methods and implications', *Gene Therapy*, 12, pp. S5–S17. doi: 10.1038/sj.gt.3302611.

Cano, T. *et al.* (2005) 'Separation of Genomic DNA from Plasmid DNA by Selective Renaturation with Immobilized Metal Affinity Capture', *Biotechnology Progress*, 21(5), pp. 1472–1477. doi: 10.1021/bp050155g.

Carta, G. and Jungbauer, A. (2010) *Protein chromatography : process development and scale-up*. Wiley-VCH.

Carter, M. *et al.* (2015) 'Gene Delivery Strategies', *Guide to Research Techniques in Neuroscience*. Academic Press, pp. 239–252. doi: 10.1016/B978-0-12-800511-8.00011-3.

Carvalho, M., Sepodes, B. and Martins, A. P. (2017) 'Regulatory and Scientific Advancements in Gene Therapy: State-of-the-Art of Clinical Applications and of the Supporting European Regulatory Framework.', *Frontiers in medicine*. Frontiers Media SA, 4, p. 182. doi: 10.3389/fmed.2017.00182.

Chaga, G. S. (2001) 'Twenty-five years of immobilized metal ion affinity chromatography: past, present and future.', *Journal of biochemical and biophysical methods*, 49(1–3), pp. 313–34. Available at: <http://www.ncbi.nlm.nih.gov/pubmed/11694287> (Accessed: 28 December 2018).

Chen, Y., Wang, S. and Lu, S. (2014) 'DNA Immunization for HIV Vaccine Development.', *Vaccines*. Multidisciplinary Digital Publishing Institute (MDPI), 2(1), pp. 138–59. doi: 10.3390/vaccines2010138.

Cho, I. K. *et al.* (2019) 'Combination of stem cell and gene therapy ameliorates symptoms in Huntington's disease mice', *Regenerative Medicine*. Nature Publishing Group, 4(1), p. 7. doi: 10.1038/s41536-019-0066-7.

Chow, Y. T. *et al.* (2016) 'Single Cell Transfection through Precise Microinjection with Quantitatively Controlled Injection Volumes', *Scientific Reports*. Nature Publishing Group, 6(1), p. 24127. doi: 10.1038/srep24127.

Chowdhury, E. H. *et al.* (2005) 'Integrin-Supported Fast Rate Intracellular Delivery of Plasmid DNA by Extracellular Matrix Protein Embedded Calcium Phosphate Complexes', *Biochemistry*, 44(37), pp. 12273–12278. doi: 10.1021/bi050595g.

Christian, M. *et al.* (2010) 'Targeting DNA double-strand breaks with TAL effector nucleases.', *Genetics*. Genetics, 186(2), pp. 757–61. doi: 10.1534/genetics.110.120717.

Ciccolini, L. A. S. *et al.* (1999) 'Rheological properties of chromosomal and plasmid DNA during alkaline lysis reaction', *Bioprocess Engineering*. Springer-Verlag, 21(3), p. 231. doi: 10.1007/s004490050669.

Clark, K. R. *et al.* (1999) 'Highly Purified Recombinant Adeno-Associated Virus Vectors Are Biologically Active and Free of Detectable Helper and Wild-Type Viruses', *Human Gene Therapy*, 10(6), pp. 1031–1039. doi: 10.1089/10430349950018427.

Collins, M. and Thrasher, A. (2014) 'Gene therapy: progress and predictions', *Proc. R. Soc. B*, 282. doi: 10.1098/rspb.2014.3003.

Collins, M. and Thrasher, A. (2015) 'Gene therapy: progress and predictions.', *Proceedings. Biological sciences*. The Royal Society, 282(1821), p. 20143003. doi: 10.1098/rspb.2014.3003.

Colote, S., Ferraz, C. and Liautard, J. P. (1986) 'Analysis and purification of plasmid DNA by reversed-phase high-performance liquid chromatography.', *Analytical biochemistry*, 154(1), pp. 15–20. Available at: <http://www.ncbi.nlm.nih.gov/pubmed/3706719> (Accessed: 30 December 2018).

Costioli, M. D. *et al.* (2003) 'DNA purification by triple-helix affinity precipitation', *Biotechnology and Bioengineering*. John Wiley & Sons, Ltd, 81(5), pp. 535–545. doi: 10.1002/bit.10497.

Cotrim, A. P. and Baum, B. J. (2008) 'Gene Therapy: Some History, Applications, Problems, and Prospects', *Toxicologic Pathology*, 36(1), pp. 97–103. doi: 10.1177/0192623307309925.

Crucho, C. I. C. and Barros, M. T. (2017) 'Polymeric nanoparticles: A study on the preparation variables and characterization methods', *Materials Science and Engineering: C*. Elsevier, 80, pp. 771–784. doi: 10.1016/J.MSEC.2017.06.004.

Cuatrecasas, P. (1970) 'Protein Purification by Affinity Chromatography', *Journal of Biological Chemistry*. American Society for Biochemistry and Molecular Biology, 245(12), pp. 3059–3065. Available at: <http://www.jbc.org/content/245/12/3059.short> (Accessed: 27 December 2018).

Culver, K. W. (1994) *Gene therapy: a handbook for physicians*. Liebert. Available at: https://books.google.co.uk/books/about/Gene_Therapy.html?id=Q4FrAAAAMAAJ&redir_esc=y (Accessed: 8 November 2018).

Cyranoski, D. and Ledford, H. (2018) 'Genome-edited baby claim provokes international outcry', *Nature*, 563(7733), pp. 607–608. doi: 10.1038/d41586-018-07545-0.

Danos, O. and Mulligan, R. C. (1988) 'Safe and efficient generation of recombinant retroviruses with amphotropic and ecotropic host ranges.', *Proceedings of the National Academy of Sciences of the United States of America*. National Academy of Sciences, 85(17), pp. 6460–4. doi: 10.1073/PNAS.85.17.6460.

Davidoff, A. M. *et al.* (2004) 'Purification of recombinant adeno-associated virus type 8 vectors by ion exchange chromatography generates clinical grade vector stock', *Journal of Virological Methods*, 121(2), pp. 209–215. doi: 10.1016/j.jviromet.2004.07.001.

Daya, S. and Berns, K. I. (2008) 'Gene therapy using adeno-associated virus vectors.', *Clinical microbiology reviews*. American Society for Microbiology (ASM), 21(4), pp. 583–93. doi: 10.1128/CMR.00008-08.

Diogo, M. M. *et al.* (2000) 'Purification of a cystic fibrosis plasmid vector for gene therapy using hydrophobic interaction chromatography', *Biotechnology and Bioengineering*. Wiley-Blackwell, 68(5), pp. 576–583. doi: 10.1002/(SICI)1097-0290(20000605)68:5<576::AID-BIT13>3.0.CO;2-5.

Diogo, M. M., Queiroz, J. A. and Prazeres, D. M. (2001) 'Studies on the retention of plasmid DNA

and Escherichia coli nucleic acids by hydrophobic interaction chromatography.’, *Bioseparation*, 10(4–5), pp. 211–20. Available at: <http://www.ncbi.nlm.nih.gov/pubmed/12233744> (Accessed: 6 November 2017).

Doolan, D. L. and Hoffman, S. L. (2001) ‘DNA-based vaccines against malaria: status and promise of the Multi-Stage Malaria DNA Vaccine Operation.’, *International journal for parasitology*, 31(8), pp. 753–62. Available at: <http://www.ncbi.nlm.nih.gov/pubmed/11403765> (Accessed: 26 November 2018).

Dunbar, C. E. *et al.* (2018) ‘Gene therapy comes of age.’, *Science (New York, N.Y.)*. American Association for the Advancement of Science, 359(6372), p. eaan4672. doi: 10.1126/science.aan4672.

Eon-Duval, A. and Burke, G. (2004) ‘Purification of pharmaceutical-grade plasmid DNA by anion-exchange chromatography in an RNase-free process’, *Journal of Chromatography B*. Elsevier, 804(2), pp. 327–335. doi: 10.1016/J.JCHROMB.2004.01.033.

Eyquem, J. *et al.* (2017) ‘Targeting a CAR to the TRAC locus with CRISPR/Cas9 enhances tumour rejection’, *Nature*, 543(7643), pp. 113–117. doi: 10.1038/nature21405.

Farkas, K., Varsani, A. and Pang, L. (2015) ‘Adsorption of Rotavirus, MS2 Bacteriophage and Surface-Modified Silica Nanoparticles to Hydrophobic Matter’, *Food and Environmental Virology*, 7(3), pp. 261–268. doi: 10.1007/s12560-014-9171-3.

Ferraro, B. *et al.* (2011) ‘Clinical applications of DNA vaccines: current progress.’, *Clinical infectious diseases : an official publication of the Infectious Diseases Society of America*. Oxford University Press, 53(3), pp. 296–302. doi: 10.1093/cid/cir334.

Ferreira, G. N. *et al.* (2000) ‘Downstream processing of plasmid DNA for gene therapy and DNA vaccine applications.’, *Trends in biotechnology*, 18(9), pp. 380–8. Available at: <http://www.ncbi.nlm.nih.gov/pubmed/10942962> (Accessed: 27 November 2018).

Ferrua, F. *et al.* (2019) ‘Lentiviral haemopoietic stem/progenitor cell gene therapy for treatment of Wiskott-Aldrich syndrome: interim results of a non-randomised, open-label, phase 1/2 clinical study’, *The Lancet Haematology*. Elsevier, 6(5), pp. e239–e253. doi: 10.1016/S2352-3026(19)30021-3.

Fine, J.-D. (2016) ‘Epidemiology of Inherited Epidermolysis Bullosa Based on Incidence and Prevalence Estimates From the National Epidermolysis Bullosa Registry’, *JAMA Dermatology*. American Medical Association, 152(11), p. 1231. doi: 10.1001/jamadermatol.2016.2473.

Fink, D. J. *et al.* (1996) ‘Gene Transfer to Neurons Using Herpes Simplex Virus-Based Vectors’, *Annual Review of Neuroscience*, 19(1), pp. 265–287. doi: 10.1146/annurev.ne.19.030196.001405.

Fischer, A., Hacein-Bey-Abina, S. and Cavazzana-Calvo, M. (2010) ‘20 years of gene therapy for SCID’, *Nature Immunology*, 11(6), pp. 457–460. doi: 10.1038/ni0610-457.

Florencio, G. D. *et al.* (2015) ‘Simple downstream process based on detergent treatment improves yield and in vivo transduction efficacy of adeno-associated virus vectors’, *Molecular Therapy. Methods*

✂ *Clinical Development*. American Society of Gene & Cell Therapy, 2, p. 15024. doi: 10.1038/MTM.2015.24.

Francis, R. D. and Bradford, H. B. (1976) *Some Biological and Physical Properties of Molluscum Contagiosum Virus Propagated in Cell Culture*, *JOURNAL OF VIROLOGY*. Available at: <http://jvi.asm.org/> (Accessed: 27 November 2018).

Frens, G. (1973) 'Controlled Nucleation for the Regulation of the Particle Size in Monodisperse Gold Suspensions', *Nature Physical Science*, 241(105), pp. 20–22. doi: 10.1038/physci241020a0.

Fuerstenau-Sharp *et al.* (2003) 'Scalable purification of viral vectors for gene therapy: An appraisal of downstream processing approaches', *BioProcess International*. BioProcess International, 15(2), pp. 1–5. Available at: <https://ora.ox.ac.uk/objects/uuid:5a606126-0cd9-4538-a2f9-1894c133c24f> (Accessed: 3 December 2018).

Gagnon, P. (1996) *Purification tools for monoclonal antibodies*. Validated Biosystems, Inc.

Gao, G. *et al.* (2000) 'Purification of Recombinant Adeno-Associated Virus Vectors by Column Chromatography and Its Performance in Vivo', *Human Gene Therapy*, 11(15), pp. 2079–2091. doi: 10.1089/104303400750001390.

Garger, S. J., Griffith, O. M. and Grill, L. K. (1983) 'Rapid purification of plasmid DNA by a single centrifugation in a two-step cesium chloride-ethidium bromide gradient.', *Biochemical and biophysical research communications*, 117(3), pp. 835–42. Available at: <http://www.ncbi.nlm.nih.gov/pubmed/6199024> (Accessed: 3 December 2018).

GE Healthcare (2019) *Manufacturing of viral vectors*. Available at: <https://www.gelifesciences.com/en/us/solutions/bioprocessing/knowledge-center/viral-vectors>.

Ghose, S., Forde, G. M. and Slater, N. K. H. (2004) 'Affinity Adsorption of Plasmid DNA', *Biotechnology Progress*. American Chemical Society (ACS), 20(3), pp. 841–850. doi: 10.1021/bp034257n.

Ghosh, P. *et al.* (2008) 'Gold nanoparticles in delivery applications☆', *Advanced Drug Delivery Reviews*, 60(11), pp. 1307–1315. doi: 10.1016/j.addr.2008.03.016.

Giljohann, D. A. *et al.* (2010) 'Gold Nanoparticles for Biology and Medicine', *Angewandte Chemie International Edition*. John Wiley & Sons, Ltd, 49(19), pp. 3280–3294. doi: 10.1002/anie.200904359.

Ginn, S. L. *et al.* (2018) 'Gene therapy clinical trials worldwide to 2017: An update', *The Journal of Gene Medicine*, 20(5), p. e3015. doi: 10.1002/jgm.3015.

Gomes, G. A. *et al.* (2009) 'Purification of plasmid DNA with aqueous two phase systems of PEG 600 and sodium citrate/ammonium sulfate', *Separation and Purification Technology*. Elsevier, 65(1), pp. 22–30. doi: 10.1016/J.SEPPUR.2008.01.026.

Gray, S. J., Woodard, K. T. and Samulski, R. J. (2010) 'Viral vectors and delivery strategies for

CNS gene therapy.’, *Therapeutic delivery*. NIH Public Access, 1(4), pp. 517–34. Available at: <http://www.ncbi.nlm.nih.gov/pubmed/22833965> (Accessed: 27 November 2018).

Green, A. P. *et al.* (2002) ‘A New Scalable Method for the Purification of Recombinant Adenovirus Vectors’, *Human Gene Therapy*, 13(16), pp. 1921–1934. doi: 10.1089/10430340260355338.

Gribnau, T. C. and Tesser, G. I. (1974) ‘Ligand-leakage in affinity chromatography, a mathematical approach.’, *Experientia*, 30(10), pp. 1228–30. Available at: <http://www.ncbi.nlm.nih.gov/pubmed/4435146> (Accessed: 13 February 2018).

Grimm, D. *et al.* (1998) ‘Novel Tools for Production and Purification of Recombinant Adenoassociated Virus Vectors’, *Human Gene Therapy*, 9(18), pp. 2745–2760. doi: 10.1089/hum.1998.9.18-2745.

Gronemeyer, P., Ditz, R. and Strube, J. (2014) ‘Trends in Upstream and Downstream Process Development for Antibody Manufacturing’, *Bioengineering*. Multidisciplinary Digital Publishing Institute, 1(4), pp. 188–212. doi: 10.3390/bioengineering1040188.

Gruntman, A. M. *et al.* (2015) ‘Stability and Compatibility of Recombinant Adeno-Associated Virus Under Conditions Commonly Encountered in Human Gene Therapy Trials’, *Human Gene Therapy Methods*. Mary Ann Liebert, Inc., 26(2), p. 71. doi: 10.1089/HGTB.2015.040.

Guo, P. *et al.* (2013) ‘A simplified purification method for AAV variant by polyethylene glycol aqueous two-phase partitioning.’, *Bioengineered*. Taylor & Francis, 4(2), pp. 103–6. doi: 10.4161/bioe.22293.

Gustavsson, P.-E. *et al.* (2004) ‘Purification of plasmid DNA with a new type of anion-exchange beads having a non-charged surface’, *Journal of Chromatography A*. Elsevier, 1038(1–2), pp. 131–140. doi: 10.1016/J.CHROMA.2004.03.050.

Habeeb, A. F. S. A. and Hiramoto, R. (1968) ‘Reaction of proteins with glutaraldehyde’, *Archives of Biochemistry and Biophysics*, 126(1), pp. 16–26. doi: 10.1016/0003-9861(68)90554-7.

Hanna, E. *et al.* (2017) ‘Gene therapies development: slow progress and promising prospect.’, *Journal of market access & health policy*. Taylor & Francis, 5(1), p. 1265293. doi: 10.1080/20016689.2017.1265293.

Hawkes, N. (2018) ‘Childhood leukaemia: Novartis immunotherapy drug approved after deal with NHS.’, *BMJ (Clinical research ed.)*. British Medical Journal Publishing Group, 362, p. k3799. doi: 10.1136/bmj.k3799.

Hill, L., Lulla, P. and Heslop, H. E. (2019) ‘CAR-T cell therapy for non-Hodgkin lymphomas: A new treatment paradigm’, *ADVANCES IN CELL AND GENE THERAPY*. John Wiley & Sons, Ltd, p. e54. doi: 10.1002/acg2.54.

Hines, R. N. *et al.* (1992) ‘Large-scale purification of plasmid DNA by anion-exchange high-performance liquid chromatography.’, *BioTechniques*, 12(3), pp. 430–4. Available at: <http://www.ncbi.nlm.nih.gov/pubmed/1571155> (Accessed: 27 December 2018).

Hu, Y.-C. *et al.* (2003) 'Generation of chimeric baculovirus with histidine-tags displayed on the envelope and its purification using immobilized metal affinity chromatography', *Enzyme and Microbial Technology*. Elsevier, 33(4), pp. 445–452. doi: 10.1016/S0141-0229(03)00143-1.

Huber, C. G. (1998) 'Micropellicular stationary phases for high-performance liquid chromatography of double-stranded DNA', *Journal of Chromatography A*. Elsevier, 806(1), pp. 3–30. doi: 10.1016/S0021-9673(97)01124-2.

Huyghe, B. G. *et al.* (1995) 'Purification of a Type 5 Recombinant Adenovirus Encoding Human p53 by Column Chromatography', *Human Gene Therapy*, 6(11), pp. 1403–1416. doi: 10.1089/hum.1995.6.11-1403.

Inoue, T. *et al.* (2008) 'Engineering of SV40-based nano-capsules for delivery of heterologous proteins as fusions with the minor capsid proteins VP2/3', *Journal of Biotechnology*, 134(1–2), pp. 181–192. doi: 10.1016/j.jbiotec.2007.12.006.

Jahanshahi, M. *et al.* (2004) 'Preparation and purification of synthetic protein nanoparticulates', *IEE Proceedings - Nanobiotechnology*, 151(5), p. 176. doi: 10.1049/ip-nbt:20041085.

Jahanshahi, M., Partida-Martinez, L. and Hajizadeh, S. (2008) 'Preparation and evaluation of polymer-coated adsorbents for the expanded bed recovery of protein products from particulate feedstocks', *Journal of Chromatography A*. Elsevier, 1203(1), pp. 13–20. doi: 10.1016/J.CHROMA.2008.07.028.

Jahanshahi, M., Zhang, Z. and Lyddiatt, A. (2005) 'Subtractive chromatography for purification and recovery of nano-bioproducts', *IEE Proceedings - Nanobiotechnology*, 152(3), p. 121. doi: 10.1049/ip-nbt:20045004.

Janson, J.-C. (2011) *Protein Purification: Principles, High Resolution Methods and Applications*. 3rd edn. Wiley. Available at: https://books.google.co.uk/books?id=2RCbtWQJ2SsC&dq=principles+of+affinity+chromatography&lr=&source=gbs_navlinks_s (Accessed: 27 December 2018).

Jenks, S. (2000) 'Gene Therapy Death —“Everyone Has to Share in the Guilt”', *Journal of the National Cancer Institute*. Oxford University Press, 92(2), pp. 98–100. doi: 10.1093/jnci/92.2.98.

Jiang, C. *et al.* (2004) 'Immobilized cobalt affinity chromatography provides a novel, efficient method for herpes simplex virus type 1 gene vector purification.', *Journal of virology*. American Society for Microbiology (ASM), 78(17), pp. 8994–9006. doi: 10.1128/JVI.78.17.8994-9006.2004.

Jinek, M. *et al.* (2012) 'A programmable dual-RNA-guided DNA endonuclease in adaptive bacterial immunity.', *Science (New York, N.Y.)*. American Association for the Advancement of Science, 337(6096), pp. 816–21. doi: 10.1126/science.1225829.

Joseph M. Fedeyko, Dionisios G. Vlachos, * and Lobo*, R. F. (2005) 'Formation and Structure of Self-Assembled Silica Nanoparticles in Basic Solutions of Organic and Inorganic Cations'. American Chemical Society . doi: 10.1021/LA0468390.

Jozala, A. F. *et al.* (2016) 'Biopharmaceuticals from microorganisms: from production to purification', *Brazilian Journal of Microbiology*. Elsevier, 47, pp. 51–63. doi: 10.1016/J.BJM.2016.10.007.

Kakizawa, Y. and Kataoka, K. (2002) 'Block Copolymer Self-Assembly into Monodisperse Nanoparticles with Hybrid Core of Antisense DNA and Calcium Phosphate', *Langmuir*. American Chemical Society, 18(12), pp. 4539–4543. doi: 10.1021/LA011736S.

Kamen, A. and Henry, O. (2004) 'Development and optimization of an adenovirus production process', *The Journal of Gene Medicine*. John Wiley & Sons, Ltd., 6(S1), pp. S184–S192. doi: 10.1002/jgm.503.

Kanda, H. *et al.* (2017) 'Gene therapy with HSV encoding p55TNFR gene for HIV neuropathic pain: an evidence-based mini-review.', *Translational perioperative and pain medicine*, 2(4), pp. 24–32. Available at: <http://www.ncbi.nlm.nih.gov/pubmed/29130055> (Accessed: 21 November 2018).

Karnchanasri, K. (2012) *Bi-Layered Chromatography Matrices for the Purification of Biological Nanoplexes*. University of Birmingham.

Kay, M. A. *et al.* (2000) 'Evidence for gene transfer and expression of factor IX in haemophilia B patients treated with an AAV vector', *Nature Genetics*, 24(3), pp. 257–261. doi: 10.1038/73464.

Kay, M. A., Glorioso, J. C. and Naldini, L. (2001) 'Viral vectors for gene therapy: the art of turning infectious agents into vehicles of therapeutics', *Nature Medicine*. Nature Publishing Group, 7(1), pp. 33–40. doi: 10.1038/83324.

Kessler, P. D. *et al.* (1996) 'Gene delivery to skeletal muscle results in sustained expression and systemic delivery of a therapeutic protein.', *Proceedings of the National Academy of Sciences of the United States of America*. National Academy of Sciences, 93(24), pp. 14082–7. doi: 10.1073/PNAS.93.24.14082.

Khan, K. H. (2013) 'DNA vaccines: roles against diseases.', *Germes*. European Academy of HIV/AIDS and Infectious Diseases, 3(1), pp. 26–35. doi: 10.11599/germes.2013.1034.

Khan, M. A. *et al.* (2016) 'Gene delivery using calcium phosphate nanoparticles: Optimization of the transfection process and the effects of citrate and poly(l-lysine) as additives.', *Journal of colloid and interface science*. NIH Public Access, 471, pp. 48–58. doi: 10.1016/j.jcis.2016.03.007.

Kieff, E. D., Bachenheimer, S. L. and Roizman, B. (1971) *Size, Composition, and Structure of the Deoxyribonucleic Acid of Herpes Simplex Virus Subtypes 1 and 2* Downloaded from, *JOURNAL OF VIROLOGY*. Available at: <http://jvi.asm.org/> (Accessed: 27 November 2018).

Kim, H. J. *et al.* (1996) 'Ultrasound-Mediated Transfection of Mammalian Cells', *Human Gene Therapy*, 7(11), pp. 1339–1346. doi: 10.1089/hum.1996.7.11-1339.

Koerber, J. T. *et al.* (2007) 'Engineering Adeno-Associated Virus for One-Step Purification via Immobilized Metal Affinity Chromatography', *Human Gene Therapy*. Mary Ann Liebert, Inc. 2 Madison Avenue Larchmont, NY 10538 USA , 18(4), pp. 367–378. doi: 10.1089/hum.2006.139.

Koirala, A., Conley, S. M. and Naash, M. I. (2013) 'A review of therapeutic prospects of non-viral gene therapy in the retinal pigment epithelium', *Biomaterials*. Elsevier, 34(29), pp. 7158–7167. doi: 10.1016/J.BIOMATERIALS.2013.06.002.

Kramberger, P., Urbas, L. and Štrancar, A. (2015) 'Downstream processing and chromatography based analytical methods for production of vaccines, gene therapy vectors, and bacteriophages.', *Human vaccines & immunotherapeutics*. Taylor & Francis, 11(4), pp. 1010–21. doi: 10.1080/21645515.2015.1009817.

Kuhn, U. *et al.* (2002) 'In Vivo Assessment of Gene Delivery to Keratinocytes by Lentiviral Vectors', *Journal of Virology*. American Society for Microbiology (ASM), 76(3), p. 1496. doi: 10.1128/JVI.76.3.1496-1504.2002.

Kumar, S. R. *et al.* (2016) 'Clinical development of gene therapy: results and lessons from recent successes.', *Molecular therapy. Methods & clinical development*. Elsevier, 3, p. 16034. doi: 10.1038/mtm.2016.34.

Kutner, R. H. *et al.* (2009) 'Simplified production and concentration of HIV-1-based lentiviral vectors using HYPERFlask vessels and anion exchange membrane chromatography', *BMC Biotechnology*. BioMed Central, 9(1), p. 10. doi: 10.1186/1472-6750-9-10.

Ladisch, M. R. (2001) *Bioseparations engineering: principles, practice, and economics*. Wiley. Available at: <https://www.wiley.com/en-gb/Bioseparations+Engineering%3A+Principles%2C+Practice%2C+and+Economics-p-9780471244769> (Accessed: 31 December 2018).

Lai, J. C. C. *et al.* (2010) 'Formation of virus-like particles from human cell lines exclusively expressing influenza neuraminidase', *Journal of General Virology*, 91(9), pp. 2322–2330. doi: 10.1099/vir.0.019935-0.

Laine, R. F. *et al.* (2015) 'Structural analysis of herpes simplex virus by optical super-resolution imaging', *Nature Communications*. Nature Publishing Group, 6(1), p. 5980. doi: 10.1038/ncomms6980.

Lambricht, L. *et al.* (2016) 'Clinical potential of electroporation for gene therapy and DNA vaccine delivery', *Expert Opinion on Drug Delivery*, 13(2), pp. 295–310. doi: 10.1517/17425247.2016.1121990.

Langer, K. *et al.* (2003) 'Optimization of the preparation process for human serum albumin (HSA) nanoparticles', *International Journal of Pharmaceutics*, 257(1–2), pp. 169–180. doi: 10.1016/S0378-5173(03)00134-0.

Langer, K. *et al.* (2008) 'Human serum albumin (HSA) nanoparticles: reproducibility of preparation process and kinetics of enzymatic degradation.', *International journal of pharmaceutics*, 347(1–2), pp. 109–17. doi: 10.1016/j.ijpharm.2007.06.028.

Lankinen, H. *et al.* (1991) 'Purification and characterization of the herpes simplex virus type 1 ribonucleotide reductase small subunit following expression in *Escherichia coli*', *Journal of General Virology*. Microbiology Society, 72(6), pp. 1383–1392. doi: 10.1099/0022-1317-72-6-1383.

de Larrea, C. F. *et al.* (2019) 'Future Prospects of CAR T Cell Therapy for Multiple Myeloma', *Advances in Cell and Gene Therapy*. John Wiley & Sons, Ltd, 2(3), p. acg2.72. doi: 10.1002/acg2.72.

Latulippe, D. R. and Zydney, A. L. (2009) 'Size exclusion chromatography of plasmid DNA isoforms', *Journal of Chromatography A*, 1216(35), pp. 6295–6302. doi: 10.1016/j.chroma.2009.07.009.

Ledley, F. D. (1996) 'Pharmaceutical Approach to Somatic Gene Therapy', *Pharmaceutical Research*. Kluwer Academic Publishers-Plenum Publishers, 13(11), pp. 1595–1614. doi: 10.1023/A:1016420102549.

Lee, C. S. *et al.* (2017) 'Adenovirus-mediated gene delivery: Potential applications for gene and cell-based therapies in the new era of personalized medicine', *Genes & Diseases*, 4(2), pp. 43–63. doi: 10.1016/j.gendis.2017.04.001.

Lemmens, R. *et al.* (2003) 'Supercoiled plasmid DNA: selective purification by thiophilic/aromatic adsorption.', *Journal of chromatography. B, Analytical technologies in the biomedical and life sciences*, 784(2), pp. 291–300. Available at: <http://www.ncbi.nlm.nih.gov/pubmed/12505777> (Accessed: 31 December 2018).

Levy, M. S. *et al.* (2000) 'Biochemical engineering approaches to the challenges of producing pure plasmid DNA', *Trends in Biotechnology*. Elsevier Current Trends, 18(7), pp. 296–305. doi: 10.1016/S0167-7799(00)01446-3.

Li, J. *et al.* (2010) 'Biodegradable calcium phosphate nanoparticle with lipid coating for systemic siRNA delivery', *Journal of Controlled Release*, 142(3), pp. 416–421. doi: 10.1016/j.jconrel.2009.11.008.

Li, L. *et al.* (2013) 'Genomic Editing of the HIV-1 Coreceptor CCR5 in Adult Hematopoietic Stem and Progenitor Cells Using Zinc Finger Nucleases', *Molecular Therapy*, 21(6), pp. 1259–1269. doi: 10.1038/mt.2013.65.

Li, T. *et al.* (2011) 'TAL nucleases (TALNs): hybrid proteins composed of TAL effectors and FokI DNA-cleavage domain', *Nucleic Acids Research*, 39(1), pp. 359–372. doi: 10.1093/nar/gkq704.

Liang, H.-D. *et al.* (2004) 'Optimisation of ultrasound-mediated gene transfer (sonoporation) in skeletal muscle cells', *Ultrasound in Medicine & Biology*. Elsevier, 30(11), pp. 1523–1529. doi: 10.1016/J.ULTRASMEDBIO.2004.08.021.

Lin, M. T. S. *et al.* (2000) 'The gene gun: current applications in cutaneous gene therapy', *International Journal of Dermatology*. Wiley/Blackwell (10.1111), 39(3), pp. 161–170. doi: 10.1046/j.1365-4362.2000.00925.x.

Liu, S. *et al.* (2018) 'Virus Spike and Membrane-Lytic Mimicking Nanoparticles for High Cell Binding and Superior Endosomal Escape', *ACS Applied Materials & Interfaces*. American Chemical Society, 10(28), pp. 23630–23637. doi: 10.1021/acsami.8b06934.

Liu, T. *et al.* (2005) 'Calcium Phosphate Nanoparticles as a Novel Nonviral Vector for Efficient Transfection of DNA in Cancer Gene Therapy', *Cancer Biotherapy and Radiopharmaceuticals*, 20(2),

pp. 141–149. doi: 10.1089/cbr.2005.20.141.

Liu, X.-Y., Pestka, S. and Shi, Y. (2012) *Recent advances in cancer research and therapy*. Elsevier Science.

Liu, Y. *et al.* (2011) ‘An efficient calcium phosphate nanoparticle-based nonviral vector for gene delivery.’, *International journal of nanomedicine*. Dove Press, 6, pp. 721–7. doi: 10.2147/IJN.S17096.

Lloyd-Evans, P. (2017) *Manufacturing of Plasmids for Gene Therapies*. Available at: <https://atmpmanufacture.org/wp-content/uploads/2018/01/amc-oct-2017-paul-lloyd-evans-nhsbt.pdf> (Accessed: 27 November 2018).

Lohcharoenkal, W. *et al.* (2014) ‘Protein nanoparticles as drug delivery carriers for cancer therapy.’, *BioMed research international*. Hindawi, 2014, p. 180549. doi: 10.1155/2014/180549.

van der Loo, J. C. M. and Wright, J. F. (2016) ‘Progress and challenges in viral vector manufacturing.’, *Human molecular genetics*. Oxford University Press, 25(R1), pp. R42–52. doi: 10.1093/hmg/ddv451.

López-Sagaseta, J. *et al.* (2016) ‘Self-assembling protein nanoparticles in the design of vaccines’. doi: 10.1016/j.csbj.2015.11.001.

Lou, B. *et al.* (2019) ‘Modular core-shell polymeric nanoparticles mimicking viral structures for vaccination’, *Journal of Controlled Release*. Elsevier, 293, pp. 48–62. doi: 10.1016/J.JCONREL.2018.11.006.

Lowe, C. R., Lowe, A. R. and Gupta, G. (2001) ‘New developments in affinity chromatography with potential application in the production of biopharmaceuticals.’, *Journal of biochemical and biophysical methods*, 49(1–3), pp. 561–74. Available at: <http://www.ncbi.nlm.nih.gov/pubmed/11694302> (Accessed: 28 December 2018).

Luscombe, N. M., Laskowski, R. A. and Thornton, J. M. (2001) ‘Amino acid-base interactions: a three-dimensional analysis of protein-DNA interactions at an atomic level.’, *Nucleic acids research*, 29(13), pp. 2860–74. Available at: <http://www.ncbi.nlm.nih.gov/pubmed/11433033> (Accessed: 28 December 2018).

Lyddiatt, A. (2002) ‘Process chromatography: current constraints and future options for the adsorptive recovery of bioproducts’, *Current Opinion in Biotechnology*. Elsevier Current Trends, 13(2), pp. 95–103. doi: 10.1016/S0958-1669(02)00293-8.

Lyddiatt, A. and O’Sullivan, D. A. (1998) ‘Biochemical recovery and purification of gene therapy vectors’, *Current Opinion in Biotechnology*, 9(2), pp. 177–185. doi: 10.1016/S0958-1669(98)80112-2.

Malboeuf, C. M. *et al.* (2007) ‘Human papillomavirus-like particles mediate functional delivery of plasmid DNA to antigen presenting cells in vivo’, *Vaccine*, 25(17), pp. 3270–3276. doi: 10.1016/j.vaccine.2007.01.067.

Maldonado-Colin, G. *et al.* (2017) ‘Inherited epidermolysis bullosa: A multisystem disease of skin and mucosae fragility’, *Indian Journal of Paediatric Dermatology*. Medknow Publications and Media Pvt. Ltd., 18(4), p. 267. doi: 10.4103/ijpd.IJPD_16_17.

Mali, P. *et al.* (2013) 'RNA-Guided Human Genome Engineering via Cas9', *Science*, 339(6121), pp. 823–826. doi: 10.1126/science.1232033.

Mann, R., Mulligan, R. C. and Baltimore, D. (1983) 'Construction of a retrovirus packaging mutant and its use to produce helper-free defective retrovirus.', *Cell*, 33(1), pp. 153–9. Available at: <http://www.ncbi.nlm.nih.gov/pubmed/6678608> (Accessed: 15 November 2018).

Manno, C. S. *et al.* (2006) 'Successful transduction of liver in hemophilia by AAV-Factor IX and limitations imposed by the host immune response', *Nature Medicine*, 12(3), pp. 342–347. doi: 10.1038/nm1358.

Marquet, M. *et al.* (1997) 'Characterization of plasmid DNA vectors for use in human gene therapy, Part 1', *BioPharm*, 10(5), pp. 42–50. Available at: <https://www.scopus.com/record/display.uri?eid=2-s2.0-0030909317&origin=inward&txGid=4fc0aedb2ec4a43e4223e2750c3cdecf> (Accessed: 30 November 2018).

Martin, A. J. and Synge, R. L. (1941) 'A new form of chromatogram employing two liquid phases: A theory of chromatography. 2. Application to the micro-determination of the higher monoamino-acids in proteins.', *The Biochemical journal*. Portland Press Ltd, 35(12), pp. 1358–68. Available at: <http://www.ncbi.nlm.nih.gov/pubmed/16747422> (Accessed: 3 December 2018).

Marty, J. J., Oppenheim, R. C. and Speiser, P. (1978) 'Nanoparticles--a new colloidal drug delivery system.', *Pharmaceutica acta Helvetiae*, 53(1), pp. 17–23. Available at: <http://www.ncbi.nlm.nih.gov/pubmed/643885> (Accessed: 16 April 2016).

Masood, F. (2016) 'Polymeric nanoparticles for targeted drug delivery system for cancer therapy', *Materials Science and Engineering: C*. Elsevier, 60, pp. 569–578. doi: 10.1016/J.MSEC.2015.11.067.

Matos, T., Queiroz, J. A. and Bülow, L. (2014) 'Plasmid DNA purification using a multimodal chromatography resin', *Journal of Molecular Recognition*. John Wiley & Sons, Ltd, 27(4), pp. 184–189. doi: 10.1002/jmr.2349.

Matsushita, T. *et al.* (2006) 'Behavior of gold colloid as model viruses during filtration through adsorptive ion exchange membranes', *Desalination*, 199(1–3), pp. 105–107. doi: 10.1016/j.desal.2006.03.152.

McFadden, G. (2005) 'Poxvirus tropism', *Nature Reviews Microbiology*. Nature Publishing Group, 3(3), pp. 201–213. doi: 10.1038/nrmicro1099.

McNally, D. J. *et al.* (2014) 'Optimised concentration and purification of retroviruses using membrane chromatography', *Journal of Chromatography A*. Elsevier, 1340, pp. 24–32. doi: 10.1016/J.CHROMA.2014.03.023.

McNay, J. L., O'Connell, J. P. and Fernandez, E. J. (2001) 'Protein unfolding during reversed-phase chromatography: II. Role of salt type and ionic strength.', *Biotechnology and bioengineering*, 76(3), pp. 233–40. Available at: <http://www.ncbi.nlm.nih.gov/pubmed/11668459> (Accessed: 30 December 2018).

Mehravar, R., Jahanshahi, M. and Saghatoleslami, @bullet Naser (2009) '(HSA) Nanoparticles as Drug Delivery System: Preparation, Optimization and Characterization Study', *Dynamic Biochemistry, Process Biotechnology and Molecular Biology*, 51. Available at: <https://pdfs.semanticscholar.org/1841/a789b5dbfdbc2b3523cd3ddb4d1e2949821d.pdf> (Accessed: 30 April 2018).

Merten, O.-W. *et al.* (2014) 'Manufacturing of viral vectors: part II. Downstream processing and safety aspects', *Pharmaceutical Bioprocessing*, 2(3), pp. 237–251. doi: 10.4155/PBP.14.15.

Merten, O.-W. and Al-Rubeai, M. (2011) *Viral Vectors for Gene Therapy*. Humana Press. doi: 10.1007/978-1-61779-095-9.

Michen, B. and Graule, T. (2010) 'Isoelectric points of viruses', *Journal of Applied Microbiology*. Blackwell Publishing Ltd, 109(2), pp. 388–397. doi: 10.1111/j.1365-2672.2010.04663.x.

Miller, A. D. *et al.* (1991) 'Construction and properties of retrovirus packaging cells based on gibbon ape leukemia virus.', *Journal of virology*. American Society for Microbiology Journals, 65(5), pp. 2220–4. Available at: <http://www.ncbi.nlm.nih.gov/pubmed/1850008> (Accessed: 15 November 2018).

Miller, A. D. (1992) 'Human gene therapy comes of age', *Nature*. Nature Publishing Group, 357(6378), pp. 455–460. doi: 10.1038/357455a0.

Mingozzi, F. and High, K. A. (2011) 'Immune responses to AAV in clinical trials.', *Current gene therapy*, 11(4), pp. 321–30. Available at: <http://www.ncbi.nlm.nih.gov/pubmed/21557723> (Accessed: 13 November 2018).

Monteiro, G. A. *et al.* (1999) 'Analysis and use of endogenous nuclease activities in Escherichia coli lysates during the primary isolation of plasmids for gene therapy.', *Biotechnology and bioengineering*, 66(3), pp. 189–94. Available at: <http://www.ncbi.nlm.nih.gov/pubmed/10577473> (Accessed: 3 December 2018).

Montini, E. *et al.* (2009) 'The genotoxic potential of retroviral vectors is strongly modulated by vector design and integration site selection in a mouse model of HSC gene therapy', *Journal of Clinical Investigation*, 119(4), pp. 964–975. doi: 10.1172/JCI37630.

Morenweiser, R. (2005) 'Downstream processing of viral vectors and vaccines', *Gene Therapy*, 12, pp. S103–S110. doi: 10.1038/sj.gt.3302624.

Mullen, C. A. *et al.* (1996) 'Molecular Analysis of T Lymphocyte-Directed Gene Therapy for Adenosine Deaminase Deficiency: Long-Term Expression *In Vivo* of Genes Introduced with a Retroviral Vector', *Human Gene Therapy*, 7(9), pp. 1123–1129. doi: 10.1089/hum.1996.7.9-1123.

Müller, B. *et al.* (2000) 'Human immunodeficiency virus type 1 Vpr protein is incorporated into the virion in significantly smaller amounts than gag and is phosphorylated in infected cells.', *Journal of virology*, 74(20), pp. 9727–31. Available at: <http://www.ncbi.nlm.nih.gov/pubmed/11000245> (Accessed: 27 November 2018).

Müller, W. (1990) 'New ion exchangers for the chromatography of biopolymers', *Journal of*

Chromatography A. Elsevier, 510, pp. 133–140. doi: 10.1016/S0021-9673(01)93746-X.

Mulligan, R. (1993) ‘The basic science of gene therapy’, *Science*. American Association for the Advancement of Science, 260(5110), pp. 926–932. doi: 10.1126/science.2734614.

Murphy, J. C. *et al.* (2003) ‘Nucleic Acid Separations Utilizing Immobilized Metal Affinity Chromatography’, *Biotechnology Progress*, 19(3), pp. 982–986. doi: 10.1021/bp025563o.

Naldini, L. *et al.* (1996) ‘In vivo gene delivery and stable transduction of nondividing cells by a lentiviral vector.’, *Science (New York, N.Y.)*, 272(5259), pp. 263–7. Available at: <http://www.ncbi.nlm.nih.gov/pubmed/8602510> (Accessed: 15 November 2018).

Nastasijevic, B. *et al.* (2008) ‘Sequence-specific binding of DNA and RNA to immobilized Nickel ions’, *Biochemical and Biophysical Research Communications*, 366(2), pp. 420–425. doi: 10.1016/j.bbrc.2007.11.169.

Nayerossadat, N., Maedeh, T. and Ali, P. A. (2012) ‘Viral and nonviral delivery systems for gene delivery.’, *Advanced biomedical research*. Wolters Kluwer -- Medknow Publications, 1, p. 27. doi: 10.4103/2277-9175.98152.

Neville, B. (1996) ‘Reversed-Phase Chromatography of Proteins’, in *Protein Purification Protocols*. New Jersey: Humana Press, pp. 277–292. doi: 10.1385/0-89603-336-8:277.

Newman, C. M. H. and Bettinger, T. (2007) ‘Gene therapy progress and prospects: Ultrasound for gene transfer’, *Gene Therapy*, 14(6), pp. 465–475. doi: 10.1038/sj.gt.3302925.

Nienhuis, A. W. (2008) ‘Development of gene therapy for blood disorders’, *Blood*, 111(9), pp. 4431–4444. doi: 10.1182/blood-2007-11-078121.

Nienhuis, A. W., Dunbar, C. E. and Sorrentino, B. P. (2006) ‘Genotoxicity of Retroviral Integration In Hematopoietic Cells’, *Molecular Therapy*, 13(6), pp. 1031–1049. doi: 10.1016/j.ymthe.2006.03.001.

Niu, Y. *et al.* (2013) ‘Nanoparticles Mimicking Viral Surface Topography for Enhanced Cellular Delivery’, *Advanced Materials*. Wiley-Blackwell, 25(43), pp. 6233–6237. doi: 10.1002/adma.201302737.

Oberholzer, M. R. and Lenhoff, A. M. (1999) ‘Protein Adsorption Isotherms through Colloidal Energetics’. doi: 10.1021/la981199k.

Orkin, S. H., Motulsky, A. G. and Varmus, H. (1995) *REPORT AND RECOMMENDATIONS OF THE PANEL TO ASSESS THE NIH INVESTMENT IN RESEARCH ON GENE THERAPY Executive Summary of Findings and Recommendations*. Available at: https://osp.od.nih.gov/wp-content/uploads/2014/11/Orkin_Motulsky_Report.pdf (Accessed: 13 November 2018).

Pang, L. *et al.* (2014) ‘Mimicking filtration and transport of rotavirus and adenovirus in sand media using DNA-labeled, protein-coated silica nanoparticles’, *Water Research*. Pergamon, 62, pp. 167–179. doi: 10.1016/J.WATRES.2014.05.055.

Patel, P. (2017) 'Polymer nanoparticles mimic bacteriophages', *C&EN Global Enterprise*. American Chemical Society Washington, DC, 95(35), pp. 9–9. doi: 10.1021/cen-09535-notw6.

Patel, P. C. *et al.* (2010) 'Scavenger Receptors Mediate Cellular Uptake of Polyvalent Oligonucleotide-Functionalized Gold Nanoparticles', *Bioconjugate Chemistry*. American Chemical Society, 21(12), pp. 2250–2256. doi: 10.1021/bc1002423.

Penaud-Budloo, M. *et al.* (2018) 'Pharmacology of Recombinant Adeno-associated Virus Production.', *Molecular therapy. Methods & clinical development*. American Society of Gene & Cell Therapy, 8, pp. 166–180. doi: 10.1016/j.omtm.2018.01.002.

Peng, Z. (2005) 'Current Status of Gendicine in China: Recombinant Human Ad-p53 Agent for Treatment of Cancers', *Human Gene Therapy*. Mary Ann Liebert, Inc. 2 Madison Avenue Larchmont, NY 10538 USA , 16(9), pp. 1016–1027. doi: 10.1089/hum.2005.16.1016.

Perez, E. E. *et al.* (2008) 'Establishment of HIV-1 resistance in CD4+ T cells by genome editing using zinc-finger nucleases', *Nature Biotechnology*, 26(7), pp. 808–816. doi: 10.1038/nbt1410.

Plank, C. *et al.* (2003) 'The Magnetofection Method: Using Magnetic Force to Enhance Gene Delivery', *Biological Chemistry*. Walter de Gruyter, 384(5), pp. 737–747. doi: 10.1515/BC.2003.082.

Platonova, G. A. and Tennikova, T. B. (2005) 'Chromatographic investigation of macromolecular affinity interactions.', *Journal of chromatography. A*, 1065(1), pp. 75–81. Available at: <http://www.ncbi.nlm.nih.gov/pubmed/15782953> (Accessed: 27 December 2018).

Potter, M. *et al.* (2014) 'A simplified purification protocol for recombinant adeno-associated virus vectors.', *Molecular therapy. Methods & clinical development*. American Society of Gene & Cell Therapy, 1, p. 14034. doi: 10.1038/mtm.2014.34.

Power, C. (2001) 'Retroviral diseases of the nervous system: pathogenic host response or viral gene-mediated neurovirulence?', *Trends in neurosciences*. Elsevier, 24(3), pp. 162–9. doi: 10.1016/S0166-2236(00)01737-9.

Prazeres, D. M. F. *et al.* (1999) 'Large-scale production of pharmaceutical-grade plasmid DNA for gene therapy: problems and bottlenecks', *Trends in Biotechnology*. Elsevier Current Trends, 17(4), pp. 169–174. doi: 10.1016/S0167-7799(98)01291-8.

Prazeres, D. M., Schluep, T. and Cooney, C. (1998a) 'Preparative purification of supercoiled plasmid DNA using anion-exchange chromatography.', *Journal of chromatography. A*, 806(1), pp. 31–45. Available at: <http://www.ncbi.nlm.nih.gov/pubmed/9639879> (Accessed: 8 February 2018).

Prazeres, D. M., Schluep, T. and Cooney, C. (1998b) 'Preparative purification of supercoiled plasmid DNA using anion-exchange chromatography.', *Journal of chromatography. A*, 806(1), pp. 31–45. Available at: <http://www.ncbi.nlm.nih.gov/pubmed/9639879> (Accessed: 2 November 2017).

Prosen, L. *et al.* (2013) 'Magnetofection: a reproducible method for gene delivery to melanoma cells.', *BioMed research international*. Hindawi, 2013, p. 209452. doi: 10.1155/2013/209452.

Przybylowski, M. *et al.* (2007) 'Production of clinical-grade plasmid DNA for human Phase I

clinical trials and large animal clinical studies', *Vaccine*, 25(27), pp. 5013–5024. doi: 10.1016/j.vaccine.2007.04.077.

Puumalainen, A.-M. *et al.* (1998) 'β-Galactosidase Gene Transfer to Human Malignant Glioma *In Vivo* Using Replication-Deficient Retroviruses and Adenoviruses', *Human Gene Therapy*, 9(12), pp. 1769–1774. doi: 10.1089/hum.1998.9.12-1769.

Qasim, W. *et al.* (2017) 'Molecular remission of infant B-ALL after infusion of universal TALEN gene-edited CAR T cells.', *Science translational medicine*. American Association for the Advancement of Science, 9(374), p. eaaj2013. doi: 10.1126/scitranslmed.aaj2013.

Qu, G. *et al.* (2007) 'Separation of adeno-associated virus type 2 empty particles from genome containing vectors by anion-exchange column chromatography', *Journal of Virological Methods*, 140(1–2), pp. 183–192. doi: 10.1016/j.jviromet.2006.11.019.

Qu, W. *et al.* (2015) 'Scalable downstream strategies for purification of recombinant adeno-associated virus vectors in light of the properties.', *Current pharmaceutical biotechnology*. Bentham Science Publishers, 16(8), pp. 684–95. doi: 10.2174/1389201016666150505122228.

Queiroz, J. A., Tomaz, C. T. and Cabral, J. M. S. (2001) 'Hydrophobic interaction chromatography of proteins', *Journal of Biotechnology*. Elsevier, 87(2), pp. 143–159. doi: 10.1016/S0168-1656(01)00237-1.

Razi Soofiyan, S. *et al.* (2013) 'Gene therapy, early promises, subsequent problems, and recent breakthroughs.', *Advanced pharmaceutical bulletin*. Tabriz University of Medical Sciences, 3(2), pp. 249–55. doi: 10.5681/apb.2013.041.

Reyon, D. *et al.* (2012) 'FLASH assembly of TALENs for high-throughput genome editing', *Nature Biotechnology*, 30(5), pp. 460–465. doi: 10.1038/nbt.2170.

Robbins, P. D. and Ghivizzani, S. C. (1998) 'Viral Vectors for Gene Therapy', *Pharmacology & Therapeutics*. Pergamon, 80(1), pp. 35–47. doi: 10.1016/S0163-7258(98)00020-5.

Rogers, S. and Pfuderer, P. (1968) 'Use of Viruses as Carriers of Added Genetic Information', *Nature*. Nature Publishing Group, 219(5155), pp. 749–751. doi: 10.1038/219749a0.

Rosenberg, S. A. *et al.* (1990) 'Gene Transfer into Humans — Immunotherapy of Patients with Advanced Melanoma, Using Tumor-Infiltrating Lymphocytes Modified by Retroviral Gene Transduction', *New England Journal of Medicine*, 323(9), pp. 570–578. doi: 10.1056/NEJM199008303230904.

Rush, M. G. and Warner, R. C. (1970) 'Alkali denaturation of covalently closed circular duplex deoxyribonucleic acid.', *The Journal of biological chemistry*, 245(10), pp. 2704–8. Available at: <http://www.ncbi.nlm.nih.gov/pubmed/5445805> (Accessed: 30 November 2018).

Russell, D. W. and Miller, A. D. (1996) 'Foamy virus vectors.', *Journal of virology*. American Society for Microbiology Journals, 70(1), pp. 217–22. Available at: <http://www.ncbi.nlm.nih.gov/pubmed/8523528> (Accessed: 15 November 2018).

Salmikangas, P., Kinsella, N. and Chamberlain, P. (2018) 'Chimeric Antigen Receptor T-Cells (CAR T-Cells) for Cancer Immunotherapy - Moving Target for Industry?', *Pharmaceutical research*. Springer, 35(8), p. 152. doi: 10.1007/s11095-018-2436-z.

Salvato, F., Gallo de Carvalho, M. C. da C. and Lima Leite, A. de (2012) 'Strategies for Protein Separation', in *Integrative Proteomics*. InTech. doi: 10.5772/29363.

Sambrook, J. and Russell, D. W. (2006) 'Purification of Closed Circular DNA by Equilibrium Centrifugation in CsCl-Ethidium Bromide Gradients: Discontinuous Gradients', *Cold Spring Harbor Protocols*. Cold Spring Harbor Laboratory Press, 2006(1), p. pdb.prot3913. doi: 10.1101/PDB.PROT3913.

Sandberg, L. M. *et al.* (2004) 'Thiophilic interaction chromatography for supercoiled plasmid DNA purification', *Journal of Biotechnology*. Elsevier, 109(1–2), pp. 193–199. doi: 10.1016/J.JBIOTEC.2003.10.036.

Schäffler, M. *et al.* (2014) 'Blood protein coating of gold nanoparticles as potential tool for organ targeting', *Biomaterials*, 35(10), pp. 3455–3466. doi: 10.1016/j.biomaterials.2013.12.100.

Scherer, F. *et al.* (2002) 'Magnetofection: enhancing and targeting gene delivery by magnetic force in vitro and in vivo', *Gene Therapy*. Nature Publishing Group, 9(2), pp. 102–109. doi: 10.1038/sj.gt.3301624.

Schluep, T. and Cooney, C. L. (1998) 'Purification of plasmids by triplex affinity interaction.', *Nucleic acids research*. Oxford University Press, 26(19), pp. 4524–8. Available at: <http://www.ncbi.nlm.nih.gov/pubmed/9742258> (Accessed: 28 December 2018).

Schmidt, T., Friehs, K. and Flaschel, E. (2007) 'Structures of Plasmid DNA', in *Plasmids for Therapy and Vaccination*. Weinheim, Germany: Wiley-VCH Verlag GmbH, pp. 29–43. doi: 10.1002/9783527612833.ch02.

Segura, M. M. *et al.* (2012) 'Chromatography Purification of Canine Adenoviral Vectors', *Human Gene Therapy Methods*, 23(3), pp. 182–197. doi: 10.1089/hgtb.2012.058.

Segura, M. M., Kamen, A. A. and Garnier, A. (2011a) 'Overview of Current Scalable Methods for Purification of Viral Vectors', in. Humana Press, pp. 89–116. doi: 10.1007/978-1-61779-095-9_4.

Segura, M. M., Kamen, A. A. and Garnier, A. (2011b) 'Overview of Current Scalable Methods for Purification of Viral Vectors', in. Humana Press, pp. 89–116. doi: 10.1007/978-1-61779-095-9_4.

Shi, X. *et al.* (2009) 'Biodegradable Polymeric Microcarriers with Controllable Porous Structure for Tissue Engineering', *Macromolecular Bioscience*. Wiley-Blackwell, 9(12), pp. 1211–1218. doi: 10.1002/mabi.200900224.

Singh, J. *et al.* (2012) 'Bovine Serum Albumin Bioconjugated Gold Nanoparticles: Synthesis, Hemolysis, and Cytotoxicity toward Cancer Cell Lines', *J. Phys. Chem. C*, 116(15), pp. 8834–8843. doi: 10.1021/jp300585d.

Siprashvili, Z. *et al.* (2016) 'Safety and Wound Outcomes Following Genetically Corrected

Autologous Epidermal Grafts in Patients With Recessive Dystrophic Epidermolysis Bullosa', *JAMA*, 316(17), p. 1808. doi: 10.1001/jama.2016.15588.

Sokolova, V. V. *et al.* (2006) 'Effective transfection of cells with multi-shell calcium phosphate-DNA nanoparticles', *Biomaterials*, 27(16), pp. 3147–3153. doi: 10.1016/j.biomaterials.2005.12.030.

Somiya, M., Liu, Q. and Kuroda, S. (2017) 'Current Progress of Virus-mimicking Nanocarriers for Drug Delivery.', *Nanotheranostics*. Ivyspring International Publisher, 1(4), pp. 415–429. doi: 10.7150/ntno.21723.

Son, K. K., Tkach, D. and Hall, K. J. (2000) 'Efficient in vivo gene delivery by the negatively charged complexes of cationic liposomes and plasmid DNA', *Biochimica et Biophysica Acta (BBA) - Biomembranes*. Elsevier, 1468(1–2), pp. 6–10. doi: 10.1016/S0005-2736(00)00311-4.

Sousa, F. *et al.* (2005) 'Separation of supercoiled and open circular plasmid DNA isoforms by chromatography with a histidine–agarose support', *Analytical Biochemistry*, 343(1), pp. 183–185. doi: 10.1016/j.ab.2005.03.011.

Sousa, F. *et al.* (2006) 'Selective purification of supercoiled plasmid DNA from clarified cell lysates with a single histidine–agarose chromatography step', *Biotechnology and Applied Biochemistry*, 45(3), p. 131. doi: 10.1042/BA20060082.

Sousa, F. *et al.* (2008) 'Specific recognition of supercoiled plasmid DNA in arginine affinity chromatography', *Analytical Biochemistry*, 374(2), pp. 432–434. doi: 10.1016/j.ab.2007.11.005.

Sousa, F., Prazeres, D. M. F. and Queiroz, J. A. (2007) 'Circular dichroism investigation of the effect of plasmid DNA structure on retention in histidine chromatography', *Archives of Biochemistry and Biophysics*, 467(2), pp. 154–162. doi: 10.1016/j.abb.2007.08.027.

Sousa, F., Prazeres, D. M. F. and Queiroz, J. A. (2008) 'Affinity chromatography approaches to overcome the challenges of purifying plasmid DNA', *Trends in Biotechnology*, 26(9), pp. 518–525. doi: 10.1016/j.tibtech.2008.05.005.

Sridhar, S. (2015) 'Clinical development of Ebola vaccines.', *Therapeutic advances in vaccines*. SAGE Publications, 3(5–6), pp. 125–38. doi: 10.1177/2051013615611017.

Stachyra, A., Góra-Sochacka, A. and Sirko, A. (2014) 'DNA vaccines against influenza.', *Acta biochimica Polonica*, 61(3), pp. 515–22. Available at: <http://www.ncbi.nlm.nih.gov/pubmed/25210719> (Accessed: 26 November 2018).

Stadler, J., Lemmens, R. and Nyhammar, T. (2004) 'Plasmid DNA purification', *The Journal of Gene Medicine*. Wiley-Blackwell, 6(S1), pp. S54–S66. doi: 10.1002/jgm.512.

Stephenson, D., Norman, F. and Cumming, R. H. (1992) 'Shear thickening of DNA in SDS lysates.', *Bioseparation*, 3(5), pp. 285–9. Available at: <http://www.ncbi.nlm.nih.gov/pubmed/1369427> (Accessed: 30 November 2018).

Steppert, P. *et al.* (2016) 'Purification of HIV-1 gag virus-like particles and separation of other extracellular particles', *Journal of Chromatography A*. Elsevier, 1455, pp. 93–101. doi:

10.1016/J.CHROMA.2016.05.053.

Stolberg, S. G. (1999) 'The biotech death of Jesse Gelsinger.', *The New York times magazine*, pp. 136–140, 149–150. Available at: <http://www.ncbi.nlm.nih.gov/pubmed/11647737> (Accessed: 13 November 2018).

von Storp, B. *et al.* (2012) 'Albumin nanoparticles with predictable size by desolvation procedure.', *Journal of microencapsulation*, 29(2), pp. 138–46. doi: 10.3109/02652048.2011.635218.

Subramanian, G. (2012) *Biopharmaceutical production technology*. 2nd edn. Wiley-VCH..

Szybalska, E. H. and Szybalski, W. (1962) 'Genetics of human cell lines, IV. DNA-mediated heritable transformation of a biochemical trait.', *Proceedings of the National Academy of Sciences of the United States of America*. National Academy of Sciences, 48(12), pp. 2026–34. doi: 10.1073/PNAS.48.12.2026.

Tan, L. *et al.* (2007) 'Differential interactions of plasmid DNA, RNA and endotoxin with immobilised and free metal ions.', *Journal of chromatography. A*, 1141(2), pp. 226–34. doi: 10.1016/j.chroma.2006.12.023.

Tarmann, C. and Jungbauer, A. (2008) 'Adsorption of plasmid DNA on anion exchange chromatography media', *Journal of Separation Science*. John Wiley & Sons, Ltd, 31(14), pp. 2605–2618. doi: 10.1002/jssc.200700654.

Tebas, P. *et al.* (2014) 'Gene Editing of CCR5 in Autologous CD4 T Cells of Persons Infected with HIV', *New England Journal of Medicine*, 370(10), pp. 901–910. doi: 10.1056/NEJMoa1300662.

Teeters, M. A. *et al.* (2003) 'Adsorptive membrane chromatography for purification of plasmid DNA', *Journal of Chromatography A*. Elsevier, 989(1), pp. 165–173. doi: 10.1016/S0021-9673(03)00027-X.

Terova, O. *et al.* (2018) 'Overcoming downstream purification challenges for viral vector manufacturing: enabling advancement of gene therapies in the clinic'. doi: 10.18609/CGTI.2018.017.

Theodossiou, I., Søndergaard, M. and Thomas, O. R. T. (2001) 'Design of expanded bed supports for the recovery of plasmid DNA by anion exchange adsorption', *Bioseparation*. Kluwer Academic Publishers, 10(1/3), pp. 31–44. doi: 10.1023/A:1012078605874.

Thomas, C. E., Ehrhardt, A. and Kay, M. A. (2003) 'Progress and problems with the use of viral vectors for gene therapy.', *Nature reviews. Genetics*, 4(5), pp. 346–58. doi: 10.1038/nrg1066.

Thomas, S. K. *et al.* (2002) 'A protein encoded by the herpes simplex virus (HSV) type 1 2-kilobase latency-associated transcript is phosphorylated, localized to the nucleus, and overcomes the repression of expression from exogenous promoters when inserted into the quiescent HSV genome.', *Journal of virology*, 76(8), pp. 4056–67. Available at: <http://www.ncbi.nlm.nih.gov/pubmed/11907244> (Accessed: 21 November 2018).

Titeux, M. *et al.* (2010) 'SIN retroviral vectors expressing COL7A1 under human promoters for ex

vivo gene therapy of recessive dystrophic epidermolysis bullosa.’, *Molecular therapy : the journal of the American Society of Gene Therapy*. American Society of Gene & Cell Therapy, 18(8), pp. 1509–18. doi: 10.1038/mt.2010.91.

Tiwari, P. M. *et al.* (2011) ‘Functionalized Gold Nanoparticles and Their Biomedical Applications’, *Nanomaterials*, 1(1), pp. 31–63. doi: 10.3390/nano1010031.

Trilisky, E. I. and Lenhoff, A. M. (2007) ‘Sorption processes in ion-exchange chromatography of viruses’, *Journal of Chromatography A*, 1142(1), pp. 2–12. doi: 10.1016/j.chroma.2006.12.094.

Urnov, F. D. *et al.* (2010) ‘Genome editing with engineered zinc finger nucleases’, *Nature Reviews Genetics*, 11(9), pp. 636–646. doi: 10.1038/nrg2842.

Urthaler, J. *et al.* (2005) ‘Application of monoliths for plasmid DNA purification: Development and transfer to production’, *Journal of Chromatography A*. Elsevier, 1065(1), pp. 93–106. doi: 10.1016/J.CHROMA.2004.12.007.

Urthaler, J., Buchinger, W. and Necina, R. (2004) *Improved downstream process for the production of plasmid DNA for gene therapy* □, *International Review Conference on Biotechnology*. Available at: www.actabp.pl (Accessed: 30 November 2018).

Vannucci, L. *et al.* (2013) ‘Viral vectors: a look back and ahead on gene transfer technology.’, *The new microbiologica*, 36(1), pp. 1–22. Available at: <http://www.ncbi.nlm.nih.gov/pubmed/23435812> (Accessed: 21 November 2018).

Varley, D. L. *et al.* (1999) ‘Production of plasmid DNA for human gene therapy using modified alkaline cell lysis and expanded bed anion exchange chromatography.’, *Bioseparation*, 8(1–5), pp. 209–17. Available at: <http://www.ncbi.nlm.nih.gov/pubmed/10734573> (Accessed: 27 November 2018).

Venkatakrishnan, B. *et al.* (2013) ‘Structure and dynamics of adeno-associated virus serotype 1 VP1-unique N-terminal domain and its role in capsid trafficking.’, *Journal of virology*. American Society for Microbiology Journals, 87(9), pp. 4974–84. doi: 10.1128/JVI.02524-12.

Walters, R. W. *et al.* (2001) ‘Binding of Adeno-associated Virus Type 5 to 2,3-Linked Sialic Acid Is Required for Gene Transfer’, *Journal of Biological Chemistry*, 276(23), pp. 20610–20616. doi: 10.1074/jbc.M101559200.

Wang, W. *et al.* (2017) ‘Facile Synthesis of Uniform Virus-like Mesoporous Silica Nanoparticles for Enhanced Cellular Internalization’, *ACS Central Science*. American Chemical Society, 3(8), pp. 839–846. doi: 10.1021/acscentsci.7b00257.

Watanabe, S. and Temin, H. M. (1983) ‘Construction of a helper cell line for avian reticuloendotheliosis virus cloning vectors.’, *Molecular and cellular biology*. American Society for Microbiology Journals, 3(12), pp. 2241–9. doi: 10.1128/MCB.3.12.2241.

Watermann, A. and Brieger, J. (2017) ‘Mesoporous Silica Nanoparticles as Drug Delivery Vehicles in Cancer.’, *Nanomaterials (Basel, Switzerland)*. Multidisciplinary Digital Publishing Institute (MDPI), 7(7). doi: 10.3390/nano7070189.

Weber, C. *et al.* (2000) 'Desolvation process and surface characterisation of protein nanoparticles.', *International journal of pharmaceutics*, 194(1), pp. 91–102. doi: 10.1016/S0378-5173(99)00370-1.

White, M. *et al.* (2017) 'A Guide to Approaching Regulatory Considerations for Lentiviral-Mediated Gene Therapies.', *Human gene therapy methods*. Mary Ann Liebert, Inc., 28(4), pp. 163–176. doi: 10.1089/hgtb.2017.096.

Wils, P. *et al.* (1997) 'Efficient purification of plasmid DNA for gene transfer using triple-helix affinity chromatography', *Gene Therapy*, 4(4), pp. 323–330. doi: 10.1038/sj.gt.3300388.

Wirth, T., Parker, N. and Ylä-Herttuala, S. (2013) 'History of gene therapy', *Gene*. Elsevier, 525(2), pp. 162–169. doi: 10.1016/J.GENE.2013.03.137.

Woodgate, J. *et al.* (2002) 'Protein-mediated isolation of plasmid DNA by a zinc finger-glutathione S-transferase affinity linker', *Biotechnology and Bioengineering*, 79(4), pp. 450–456. doi: 10.1002/bit.10296.

Wright, J. (2008) 'Manufacturing and characterizing AAV-based vectors for use in clinical studies Overview of Good Manufacturing Practice', *Gene Therapy*, 1565, pp. 840–848. doi: 10.1038/gt.2008.65.

Wu, S.-H., Hung, Y. and Mou, C.-Y. (2011) 'Mesoporous silica nanoparticles as nanocarriers', *Chemical Communications*. The Royal Society of Chemistry, 47(36), p. 9972. doi: 10.1039/c1cc11760b.

Xiao, X., Li, J. and Samulski, R. J. (1996) 'Efficient long-term gene transfer into muscle tissue of immunocompetent mice by adeno-associated virus vector.', *Journal of virology*. American Society for Microbiology Journals, 70(11), pp. 8098–108. Available at: <http://www.ncbi.nlm.nih.gov/pubmed/8892935> (Accessed: 15 November 2018).

Yabré, M. *et al.* (2018) 'Greening Reversed-Phase Liquid Chromatography Methods Using Alternative Solvents for Pharmaceutical Analysis', *Molecules*. Multidisciplinary Digital Publishing Institute, 23(5), p. 1065. doi: 10.3390/molecules23051065.

Yeh, Y.-C., Creran, B. and Rotello, V. M. (2012) 'Gold nanoparticles: preparation, properties, and applications in bionanotechnology.', *Nanoscale*. NIH Public Access, 4(6), pp. 1871–80. doi: 10.1039/c1nr11188d.

Young, A. T. L. *et al.* (2002) *Gene Therapy: A Lipofection Approach for Gene Transfer Into Primary Endothelial Cells, Cell Transplantation*. Available at: www.cognizantcommunication.com (Accessed: 22 November 2018).

Yu, S. F. *et al.* (1986) 'Self-inactivating retroviral vectors designed for transfer of whole genes into mammalian cells.', *Proceedings of the National Academy of Sciences of the United States of America*. National Academy of Sciences, 83(10), pp. 3194–8. doi: 10.1073/PNAS.83.10.3194.

Zhang, K. and Liu, X. (2016) 'Mixed-mode chromatography in pharmaceutical and biopharmaceutical applications', *Journal of Pharmaceutical and Biomedical Analysis*. Elsevier, 128, pp. 73–88. doi: 10.1016/J.JPBA.2016.05.007.

Zhang, W.-W. *et al.* (2018) 'The First Approved Gene Therapy Product for Cancer Ad- β 53 (Gendicine): 12 Years in the Clinic', *Human Gene Therapy*, 29(2), pp. 160–179. doi: 10.1089/hum.2017.218.

Zhang, Z. *et al.* (2001) 'Design and assembly of solid-phases for the effective recovery of nanoparticulate bioproducts in fluidised bed contactors.', *Bioseparation*, 10(1–3), pp. 113–32. Available at: <http://www.ncbi.nlm.nih.gov/pubmed/11787793> (Accessed: 27 April 2015).

Zhou, J. *et al.* (2009) 'Functionalized gold nanoparticles: Synthesis, structure and colloid stability', *Journal of Colloid and Interface Science*. Academic Press, 331(2), pp. 251–262. doi: 10.1016/J.JCIS.2008.12.002.

Zufferey, R. *et al.* (1998) *Self-Inactivating Lentivirus Vector for Safe and Efficient In Vivo Gene Delivery*, *JOURNAL OF VIROLOGY*. Available at: <https://www.ncbi.nlm.nih.gov/pmc/articles/PMC110499/pdf/jv009873.pdf> (Accessed: 21 November 2018).

CHAPTER II

MANUFACTURE & CHARACTERISATION OF MULTIFUNCTIONAL BI-LAYERED CHROMATOGRAPHY MATERIALS

Abstract

The manufacture of bi-layered chromatography materials intended for the purification of nanoplex products for gene therapy and vaccine applications is described. Three size exclusion chromatography matrices (Sephacrose 6 Fast Flow, Superose 6 Prep Grade, and Superose 12 Prep Grade) differing with respect to agarose content, cross-linker chemistry, particle and pore size distributions, were transformed into bi-layered supports featuring anion exchange functionalised cores and exterior size excluding shells in five sequential steps (i.e. allyl glycidyl ether activation, partial bromination, hydrolysis, full bromination, ligand coupling).

In the second ‘key’ step two different approaches were employed to balance bromine’s reaction with immobilised allyl functions against its depth of diffusion into the porous allylated matrices, namely the inclusion of the viscosity enhancing agents (sucrose or Carbopol® 934) in the reaction cocktail, and single mode microwave heating immediately prior to adding the reactant.

The resulting media were evaluated with respect to loss of surface and core binding, *cf.* control Q-coupled anion exchangers constructed from the same base matrices in finite bath studies allied with confocal scanning laser microscopic imaging. Plasmid DNA and bovine serum albumin in native and fluorescently tagged forms were respectively as surface and core binding probes, and the binding selectivities of different bi-layered support materials were compared by means of a simple selectivity ratio (μg of pDNA bound per mg of BSA bound); the lower the number the more selective the support.

Whilst all media received 10% bromination to achieve a thin, inert shell, the best performing bi-layered matrix was Superose 6 Prep Grade manufactured using the viscosity enhanced 64% sucrose route, which displayed a similar core binding capacity to the control, with nearly 100% reduction in surface plasmid DNA binding, recording an overall SI of 0.04. Sepharose 6 Fast Flow bi-layered resins manufactured using the microwave 60% ethylene glycol route displayed strong plasmid binding and only a 50% reduction compared to the control, with confocal images suggesting patches of functionality on the bead’s surface.

Abbreviations

AGE: Allyl Glycidyl Ether

AU: Absorbance Units

bp: Base Pairs

BSA: Bovine Serum
Albumin

CLSM: Confocal Laser
Scanning Microscopy

DMSO: Dimethyl
Sulfoxide

DNA: Deoxyribonucleic
Acid

EBA: Expanded Bed
Adsorption

dH₂O: Deionised Water

EU: Endotoxin Units

E-SEM: Environmental
Scanning Electron
Microscopy

IEC: Ion Exchange
Chromatography

kDa: kilo Daltons

pDNA: Plasmid DNA

LB: Lysogeny Broth

LM: Light Microscopy

NaBH₄: Sodium
Borohydride

NaCl: Sodium Chloride

OD: Optical Density

PSD: Particle Size
Distribution

SEC: Size Exclusion
Chromatography

SBC: Static Binding
Capacity

SI: Selectivity Index

Tris-HCl:
Trisaminomethane
hydrochloride

Q: Trimethylamine
Chloride

Table of Contents

2.1	Introduction.....	95
2.1.1	Gene Therapy & Vaccines.....	95
2.1.2	Downstream Processing.....	95
2.1.3	Chromatographic Separation.....	96
2.1.4	Novel Chromatography Designs.....	96
2.1.5	Multi-Layer Chromatography Designs.....	97
2.2	Materials & Methods.....	102
2.2.1	Materials & Reagents.....	102
2.2.2	Allyl Glycidyl Ether Activation.....	102
2.2.3	Partial Bromination.....	102
2.2.4	Hydrolysis.....	104
2.2.5	Full Bromination & Q Coupling.....	104
2.2.6	Particle Size Distribution.....	105
2.2.7	Viscosity Measurements.....	105
2.2.8	Temperature Stability.....	105
2.2.9	Bromine Stability.....	105
2.2.10	Plasmid Production.....	106
2.2.11	Analysis.....	106
2.3	Results & Discussion.....	112
2.3.1	Particle Size Distribution.....	112
2.3.2	Viscosity Measurements.....	114
2.3.3	Viscosity Enhanced & Microwave Assisted Partial Bromination.....	115
2.3.4	Bromine Stability.....	118
2.3.5	Temperature Stability & Ramping Rates.....	121
2.3.6	Plasmid Map & Quality Assessment.....	124
2.3.7	Static Chromatography.....	126
2.3.8	Confocal Laser Scanning Microscopy.....	136
2.3.9	Environmental Scanning Electron Microscopy.....	142
2.4	Conclusions.....	145
2.5	References.....	146

List of Figures

Fig. 2.1 Purification of a virus feed-stream using beads with a bi-layered architecture (Courtesy of Dr. E. Theodosiou).

Fig. 2.2 Schematics illustrating: a) plasma surface etching of a chromatography adsorbent bead to form a bi-layered bi-functional support; b) sectioning of through the resulting support to highlight the 'ligand free' exterior and ligand functionalised core; and c) the underwater fluidized bed plasma treatment reactor operating with He-O₂ at an input power of 3.7 W. Also shown d) is a photograph of the plasma reactor in operation (Reproduced from Olszewski *et al.*, 2013).

Fig. 2.3 Schematic illustrating the manufacture of functionalised, bi-layered beads using an AGE Activation/Partial Bromination technique (Courtesy of Prof. O.R.T. Thomas).

Fig. 2.4 Mode of operation of the CEM Microwave reactor with chromatography resin mixed with microwave assisting buffer to form a slurry. This is placed in the round bottom flask prior to heating (Karnchanasri, 2013).

Fig. 2.5 A general schematic of the methodology involved in a finite bath study; starting from resin in a 20% Ethanol storage buffer through to isolation of the pelleted beads for microscopy and analysis of supernatant concentrations for mass balancing and calculations of static binding capacities.

Fig. 2.6 Schematic illustrating how a three-dimensional image can be generated using a confocal microscope. The confocal pinhole facilitates focus on individual layers, as thin as 1 μm , and these slices can be scanned and subsequently re-stacked to construct a three dimensional image of a bead with a fluorescent probe bound (Hubbuck and Kula, 2008).

Fig. 2.7 Particle size distribution data for **a)** the commercial multi-functional resin, Capto™ Core 700 and the three base size exclusion matrices used, i.e. **b)** Superose 12 Prep Grade, **c)** Sepharose 6 Fast Flow, and **d)** Superose 6 Prep Grade.

Fig. 2.8 Molecular structure of cross-linked agarose which forms the basic make up of all three starting matrices used in this study (Sigma Aldrich, 2018b).

Fig. 2.9 a) Relationship between viscosity & temperature for deionised water. **b)** k/D – temperature profile for the bromination of a double bond (Gilbert and Martin, 2011).

Fig. 2.10 Bromine stability studies with respect to time on **a)** viscosity-enhanced and **b)** microwave-assisted reaction buffers. Symbols: -□- 80% (w/v) sucrose; -■- 64% (w/v) sucrose; -○- 0.4% (w/v) Carbopol® 934; -●- 85% (v/v) ethylene glycol; -△- 60% (v/v) ethylene glycol; -▲- 50% (v/v) ethylene glycol; -▽- 60% (v/v) DMSO; and -▼- deionised water.

Fig. 2.11 The monomer molecular structure of Carbopol® 934 (GenScript, 2018; Thermo Fisher Scientific, 2018b).

Fig. 2.12 Temperature ramps and stability assessment for microwave assisting buffers composed of varying percentages of **a)** ethylene glycol and **b)** DMSO. Symbols: -□- 50% (v/v) ethylene glycol; -■- 60% (v/v) ethylene glycol; -○- 85% (v/v) ethylene glycol; -●- 100% (v/v) ethylene glycol; -△- 50% (v/v) DMSO; -▲- 60% (v/v) DMSO; -▽- 100% (v/v) DMSO; and -▼- deionised water.

Fig. 2.13 Temperature ramps of the chromatography matrices in **a)** deionised water and **b)** 60% (v/v) ethylene glycol. Symbols: -□- Sepharose 6 Fast Flow; -■- Superose 6 Prep Grade; and -○- Superose 12 Prep Grade.

Fig. 2.14 Plasmid map of pBR322-P170 used as probe for assessing the chromatography media manufactured in-house.

Fig. 2.15 Equilibrium adsorption Isotherm for plasmid DNA on fully functionalised ('control') supports: **a)** Superose 6 Prep Grade; **b)** Superose 12 Prep Grade; and **c)** Sepharose 6 Fast Flow. The lines through the data represent fitted Langmuir curves (*Equation 11*) with the parameters given in Table 2.3.

Fig. 2.16 a) Plasmid DNA and BSA static binding capacity (SBC) values for each base resin and manufacturing condition. Selectivity indices (SI) are calculated via *Equations 7 and 8*. **b)** Percentage binding reduction for plasmid DNA and BSA probes for each sample type relative to the fully functionalised control samples. EG refers to ethylene glycol.

Fig. 2.17 Illustration of auto-fluorescence of the base (a) and functionalised (b & c) matrices, and the use of thresholding (d) to eliminate the effect. Panels: **a)** Sepharose 6 Fast Flow; **b)** Sepharose 6 Fast Flow fully functionalised with the anion exchange ligand Q; **c)** sample B incubated with fluorescent plasmid DNA (pDNA-Syto™ 9); and **d)** sample C post-thresholding to remove auto-fluorescence from the chromatography bead. Note that the value in the bottom left corner of each image corresponds to the gain value.

Fig. 2.18 Light Microscopy (LM) & Confocal Laser Scanning Fluorescent Microscopy (FM) images of the fully functionalised samples and bi-layered resins.

Fig 2.19 Light Microscopy (LM) & Confocal Laser Scanning Fluorescent Microscopy (FM) images comparing the **a)** commercial Capto™ Core 700 resin against the **b)** worst & **c)** best performing resins.

Fig 2.20 Scanning electron micrographs of a number of commercial chromatography resins, taken at low and high magnifications to gauge bead size and surface morphology/porosity, respectively. Panels: **a)** Capto™ Core 700; **b)** Q Sepharose Fast Flow; **c)** Sepharose 6 Fast Flow; **d)** Superose 6 Prep Grade; **e)** Superose 12 Prep Grade; and **f)** Capto™ Q.

Fig. 2.21 Scanning electron micrographs of the functionalised control chromatography resins and bi-layered matrices, organised by method and type of starting matrix. Images were taken at high

magnification only as, at lower magnifications, the resins were qualitatively similar to the original starting matrices.

List of Tables

Table 2.1 Allyl contents introduced into commercial agarose base matrices following reaction with AGE.

Table 2.2 Comparison table of the loss tangents of a variety of potential microwave-assisted reaction buffers (2.45 GHz, 20°C) (Kappe, Stadler and Dallinger, 2012)

Table 2.3 A comparison of the three chromatography resins used as base matrices in this study, compared with **a)**, a commercial, bi-functional matrices currently on the market. Mean particle sizes of the experimental Mastersizer data are compared against the manufacturers stated values. Comparison of the relative pore sizes are also given, with molecular weight exclusion limits (kDa) and base pairs (bp) quoted for globular proteins and DNA, respectively.

Table 2.4 The experimental design matrix. Summary table highlighting the sample types and treatment conditions carried forward for static binding assessment.

Table 2.5 Quality assessment of a sample of the master stock of purified plasmid DNA used during the static binding studies.

Table 2.6 Langmuir fitting parameters for each of the control samples for the plasmid DNA probe.

Table 2.7 Quantitation of allyl group generation and partial bromination achieved accompanied by the % reduction in probe binding and overall selectivity index (SI) for each sample type.

2.1 Introduction

2.1.1 Gene Therapy & Vaccines

In recent times, the landscape of bioprocessing has seen a gradual transition to manufacturing more complex bio-products. Traditionally, a bioprocess train would be challenged with a simple, small protein to purify from a typical bacterial cell culture (Jozala, Geraldles, Tundisi, Feitosa, Breyer, Cardoso, Mazzola, Oliveira-Nascimento, Rangel-Yagui, Magalhães, Oliveira, Pessoa, *et al.*, 2016). The modern bioprocess is now challenged with being more flexible, as well as having to handle more convoluted feed streams from a variety of cell lines, with the task of removing problematic contaminants and impurities, as well as isolating larger, more sensitive and ultimately more complex products (Morenweiser, 2005; Tran, 2011; Kramberger, Urbas and Štrancar, 2015b).

The industry has also found itself having to adapt to meet new demands, responding to global epidemics and new diseases, having to be flexible whilst generating product at large scale and at high throughput. An example of this was the 2009 influenza A (H1N1) pandemic, which prompted the World Health Organisation to lead a revolution in vaccine-based therapeutic production platforms (Li and Qiu, 2013).

The advent of gene therapy and novel, more effective vaccine treatments has seen a rise in the development of large, complex and fragile therapeutic products (Collins and Thrasher, 2014). This grouping will often include macromolecular drug delivery vehicles such as viral vectors, virus-like particles, as well as non-viral vectors such as supercoiled plasmid DNA. Whilst boasting huge potential, especially in the field of cancer treatment, these nanoplex products pose a number of similar challenges in the context of a bioprocess purification chain (Wold and Toth, 2013).

The burden of separating a complex and large bio-product runs throughout the bioprocess, from fermentation harvest to primary clarification, intermediate purification, capture and finally polishing. The large size of the macromolecules, their shear sensitive nature, the existence of similarly sized and charged non-functional vectors as well as the need to maintain potency (or virulence in the case of viral vectors) all require thought when designing an efficient separation train for gene therapy vectors. Isolation and capture methods for these molecules require continuous development to maintain standards of purity, efficacy and safety (Segura, Kamen and Garnier, 2011b).

2.1.2 Downstream Processing

Whilst the entire bioprocess requires adaptation to gene therapy considerations, this work will focus primarily downstream of a cell harvest, as this tends to be the main cost driver for most conventional bioprocesses, as well as the bottleneck in terms of process throughput (Chon and Zarbis-Papastoitsis, 2011; Gronemeyer, Ditz and Strube, 2014; Kelley, 2016).

Downstream processing unit operations have traditionally been optimised for the purification and isolation of small protein targets. They therefore require re-engineering and re-thinking to cope with the challenges presented by novel gene therapy products. As Levy *et al.* 2000 put it; “By

acknowledging these challenges and using bio-process design information based on fundamental studies of the system's properties, it will be possible to create efficient and consistent processes for these materials.”

Whilst there are a number of downstream operations that could be considered, including initial disruption by centrifugation, homogenisation or cell lysis, and primary clarification steps such as filtration, the focus of this thesis chapter is on re-thinking the chromatographic-based steps. This particular unit is considered the most expensive (in terms of capital and consumables) and in many scenarios suffers from low productivity and high amounts of waste generation and thus directing optimisation will likely have a large impact on the overall process efficiency (Przybycien *et al.*, 2004).

2.1.3 Chromatographic Separation

In order to achieve high resolution separation of gene therapy vectors, at least one or usually multiple chromatography steps are an essential requirement especially for clinical application (Horn *et al.*, 1995).

In the case of viral vectors and plasmid DNA, mis-folded and non-functional structures (usually of a similar size to the target product) require removal from the feed-stream. Therapeutic formulations for plasmid DNA should also be free of host genomic DNA ($<0.05 \mu\text{g}/\mu\text{g}$ plasmid DNA), host proteins, endotoxins ($<0.1 \text{ EU}/\mu\text{g}$ plasmid DNA) as well as being over 90% super-coiled to be considered an effective gene therapy product (Prazeres *et al.*, 2001; Diogo, Queiroz and Prazeres, 2005).

In the case of viral vectors, removal of host cell proteins and host DNA ($<10 \text{ ng}/\text{dose}$), cell debris (product dependent) and product-related impurities, such as empty capsids (non-detectable) and viral DNA ($100 \text{ pg} / 10^9$ vectors) require removal from a cell lysate feedstock (Wright, 2008b). In addition, due consideration to infectivity and potency is needed when assessing the bulk drug substance prior to clinical application.

In the context of industrial downstream processing, chromatographic methods employing orthogonal separation principles of size, charge, hydrophobicity and specific interaction are utilised in complementary manner to separate and purify target species free of impurities. For instance, size exclusion chromatography (SEC) utilises differences in molecular size or hydrodynamic radius, whereas adsorptive techniques such as ion exchange adsorption chromatography (IEC), hydrophobic interaction chromatography (HIC) and affinity chromatography (AC) respectively exploit differences in electrostatic charge, hydrophobicity and molecular recognition to achieve separation of targets and impurities.

2.1.4 Novel Chromatography Designs

In an effort to meet ever-changing demands in downstream processing, recent years have seen a plethora of advancements in chromatography systems directed towards new media designs,

column and ligand designs and operational modes, all aimed at improving product yields, purity and process economics (Lowe, Lowe and Gupta, 2001; Orr *et al.*, 2013).

Expanded Bed Adsorption (EBA) was a novel development in the '90s which was an innovative method of operating a column, effectively as a fluidised bed where the beads are suspended in a stable manner under up-flow. EBA, due to its larger void volumes, allow for applications much earlier in the purification chain and handling of solid-containing feedstocks (Arpanaei *et al.*, 2010; Tran, 2011).

Monolith columns and membrane adsorbers aim to move away from the traditional beaded column towards a macro-porous support design which facilitate larger surface areas and better mass transfer mechanistics, improving binding capacity and flow rates (Segura, Kamen and Garnier, 2011b). There has also been work done on expanding the surface area of beads through designs with surface pellicular/tentacular ligands; aiming to improve resolution, throughput and recovery (Janzen *et al.*, 1990), as well as the development of environmentally responsive polymer brushes to aid elution, cleaning and column lifetimes (Cao *et al.*, 2015; Müller *et al.*, 2013; Willett, 2009).

2.1.5 Multi-Layer Chromatography Designs

A major challenge of a crude virus feedstock is that many of the impurities bear similar physical and chemical characteristics to the target vector and therefore multiple columns of different functionality are required in succession to achieve target purity and acceptable yields. Generally, SEC and IEC chromatography are the most prevalent and arguably most successful techniques at accommodating the issues associated with nanoplex purification. Their popularity stems from their ability to their scalability options, as well as being able to resolve target vectors away from similarly sized, mis-folded vectors and smaller feed impurities based on both molecular weight and charge variations (Gustavsson *et al.*, 2004b; Burova and Ioffe, 2005; Kramberger, Urbas and Štrancar, 2015b).

IEC, on its own, affords poor binding capacities for large viral vectors, mainly due to intra-particle mass transfer issues, lack of pore penetration and weak binding. SEC, though good for separating molecules of disparate molecular size is unable to separate similarly sized yet misfolded and non-functioning vectors from one another, nor resolve different charge isoforms of DNA from target plasmid species (Latulippe and Zydney, 2009).

One major innovation built on by the work described in this chapter is the development of chromatography media that combine two different separation principles, namely SEC and IEC, spatially separated from one another within the same chromatographic bead (Arpanaei *et al.*, 2010; Daniak *et al.*, 2002; Gustavsson *et al.*, 2004a,b; Jahanshahi *et al.*, 2008; Karnchanasri, 2013; Olszewski *et al.*, 2013; Vilorio-Cols *et al.*, 2004) In this fashion, it should be possible to synergistically exploit the benefits of both technologies, namely high capacities (for small, charged molecules), throughput and scalability options achievable through ion-exchange, whilst also achieving separation of large vectors from smaller impurities by size exclusion (the former species eluting in the void volume), whilst eliminating the inherent disadvantages of employing IEC

followed by SEC, i.e. low target binding capacities of ion exchangers, and, limited sample volume and throughput of SEC (Gustavsson *et al.*, 2004a; Karnchanasri, 2013).

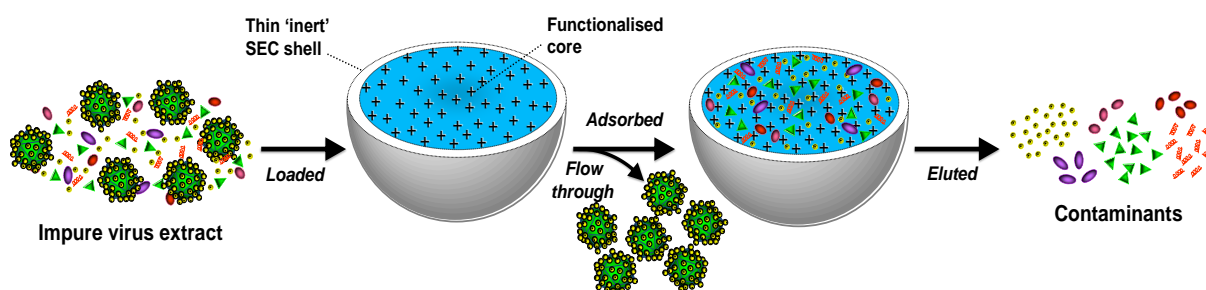


Fig. 2.1 Purification of a virus feed-stream using beads with a bi-layered architecture (Courtesy of Dr. E. Theodosiou).

If successful, such bi-layered SEC-IEC matrices would enable efficient and gentle separation of nanoplex products from smaller chemically similar contaminants in a ‘one column-one bead’ based process (Fig. 2.1), that promises overall improvements in process performance, costs (capital and consumables) and sustainability without compromising on purity or yield.

In 2012, GE Healthcare released its first multi-modal chromatography core/shell media, Capto™ Core 700, designed specifically for intermediate purification and polishing of viruses and other large biomolecules, and recently introduced its second, Capto™ Core 400. Both of these media⁵ feature bi-layered architectures with a thin ‘inert’ shells with 700 kDa or 400 kDa size-exclusion cut off, too small for large therapeutic viruses to penetrate and bind (i.e. 700 kDa for Capto™ Core 700 and 400 kDa for Capto™ Core 400). The cores of both media are functionalised with octylamine, a hydrophobic and positively charged mixed-mode ligand that binds protein impurities small enough to pass through the shell strongly over a broad pH and ionic strength range. In this way, the target virus is isolated in the flow through fraction, whilst the smaller impurities are “hoovered” into the core, as illustrated in Fig. 2.1.

This “negative mode” chromatography (Jahanshahi, Partida-Martinez and Hajizadeh, 2008b) is particularly useful for large nanoplex vectors due to limited interaction with the functionalised matrix, allowing for a “gentler” form of purification and limited impact on the structure and activity of the final vector product (Burova and Ioffe, 2005). There are a number of routes to achieve a “negative mode” beaded bi-layered architecture featuring a “non-stick” surface and functionalised core.

The earliest reports employed coating strategies. For example, Daniak and co-workers (2002) grafted a small pored Amberlite anion exchange adsorbent with an oppositely charged ‘cell

⁵ GE Healthcare claims for these multimodal chromatography media include: significant improvements in productivity of SEC through the use of 100 fold higher sample loads and significantly higher flow rates; and straightforward optimization arising from robust flow-through operation and a wide operating window (GE Data file 28998307AC).

repelling' layer of poly(acrylic acid) physically adsorbed and subsequently cross-linked *in situ*, whereas others (Viloria-Cols, Hatti-Kaul and Mattiasson, 2004; Jahanshahi, Partida-Martinez and Hajizadeh, 2008b) simply laminated adsorbent particles with thick underivatized layers of agarose. Lamination is the more promising approach for eradicating surface binding of large species to meso-macroporous chromatography media appropriate for unhindered binding of protein. However, a major stumbling block is the difficulty in casting sufficiently thin, uniform and mechanically sound shells; failure to do so will result in reduced protein mass transfer and binding capacity, compromised inertness and performance life span (Arpanaei *et al.*, 2010).

An alternative approach is to modify the surface of the chromatography matrix using plasma⁶ irradiation. Arpanaei and co-workers (2010) modified the exterior surfaces of the rigid 'gel-in-a-shell' expanded bed adsorbent Q HyperZ with low temperature low pressure plasmas in a purpose built reactor. The authors detailed two different approaches namely 'plasma etching and oxidation' and 'plasma polymerization coating'. The former approach involved shaving anion exchange ligands away from the exterior surface and replacing with polar oxygen containing functions using an air plasma, whilst the latter involved using various monomers in an argon carrier gas to coat exterior surface bound ligands beneath an anti-fouling polymer layer.

Whilst showing much promise, the broad application of low temperature low pressure plasma for the modification of chromatography media seems unlikely, as it requires base matrices that can tolerate gross removal of water without suffering major changes to their physical dimensions⁷.

Though eminently suitable for rigid 'gel-in-a shell' or 'controlled pore glass' media it is not appropriate for softer porous hydrogels (90+% water), which represent the bulk of chromatography materials used for macromolecule separation today. In recognition of this, Olszewski *et al.* (2013) turned to cold atmospheric plasma and devised a means to modify chromatography adsorbents in their wet state (Fig. 2.2). In their work reactive oxygen species (ROS) transported to aqueous slurries of anion exchange media (Q Sepharose Fast Flow, DEAE Sepharose Fast Flow and EMD Fractogel DEAE) by ignited He-O₂ plasma gas bubbles in an underwater fluidised bed reactor (Fig. 2c and 2d), reduced the 'surface' binding of large plasmid DNA molecules threefold at the expense of a ~10% drop in core protein binding.

⁶ Fisher (2002) defines plasma as a partially or wholly ionized medium consisting of electrons, ions and possibly neutrals and photons.

⁷ Low pressure plasma treatment requires application of a vacuum which draws out all of the water. In the case of soft hydrogel based matrices this will lead to (i) support collapse; and (ii) on rehydration post treatment to deep modification of the support.

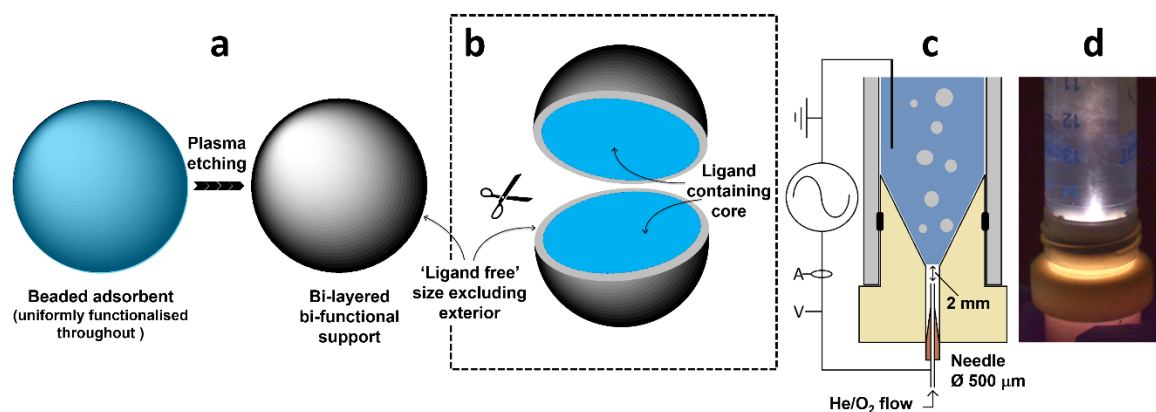


Fig. 2.2 Schematics illustrating: a) plasma surface etching of a chromatography adsorbent bead to form a bi-layered bi-functional support; b) sectioning of through the resulting support to highlight the 'ligand free' exterior and ligand functionalised core; and c) the underwater fluidized bed plasma treatment reactor operating with He-O₂ at an input power of 3.7 W. Also shown d) is a photograph of the plasma reactor in operation (Taken from Olszewski *et al.*, 2013).

Various chemical methods to manufacture bilayered chromatography media, exploiting fast reactions of anchored groups with limiting amounts of soluble reactant, have been described (Bergstrom *et al.*, 1998; Gustavsson *et al.*, 2004; Berg *et al.*, 2005; Karnchanasri, 2013). Gustavsson and coworkers (2004) and Karnchanasri (2013) created a bi-layered SEC-AEC matrices from Sephacryl S500 HR and Sepharose CL6B base matrices respectively using broadly similar five step processes. Briefly, these involved activation of un-functionalised base matrix with allyl glycidyl ether (AGE) to introduce allyl groups throughout the matrix (step 1). In the next crucial step (step 2) a calculated amount of bromine sufficient to react with a small percentage (typically <30%) of the AGE activated support's allyl groups is added.

The electrophilic addition reaction of bromine with the carbon-carbon double bonds of the anchored allyl functions as it diffuses into the porous support gives rise to a bilayered support intermediate featuring an allylated core and brominated shell. As the reaction of allyl groups with bromine is carried out in aqueous solution the brominated reaction product is a likely a mixture of bromoalcohol (bromohydrin) and dibromo adducts, the precise balance of these is dependent both on the rate of addition and the additives present (Zabicky, 1986). In the subsequent steps bromo-alkyl groups in the outer layer are hydrolysed to render it inert (step 3), the allylated core is then reacted with excess bromine (step 4), before finally coupling the strong anion exchange quaternary amine ligand, tri-methylamine chloride, Q (step 5).

In her work, Karnchansri (2013) employed two different reaction-diffusion balancing approaches to reduce the thickness of the outer inert layer, namely increasing the viscosity of the reaction solvent so as to slow the reactant's diffusion into the activated support, and microwave heating immediately prior to adding the reactant to preferentially increase bromine's reaction with anchored allyl functions over its diffusion into the allylated support. These two techniques are discussed further in 2.2.6.2 and 2.2.6.3.

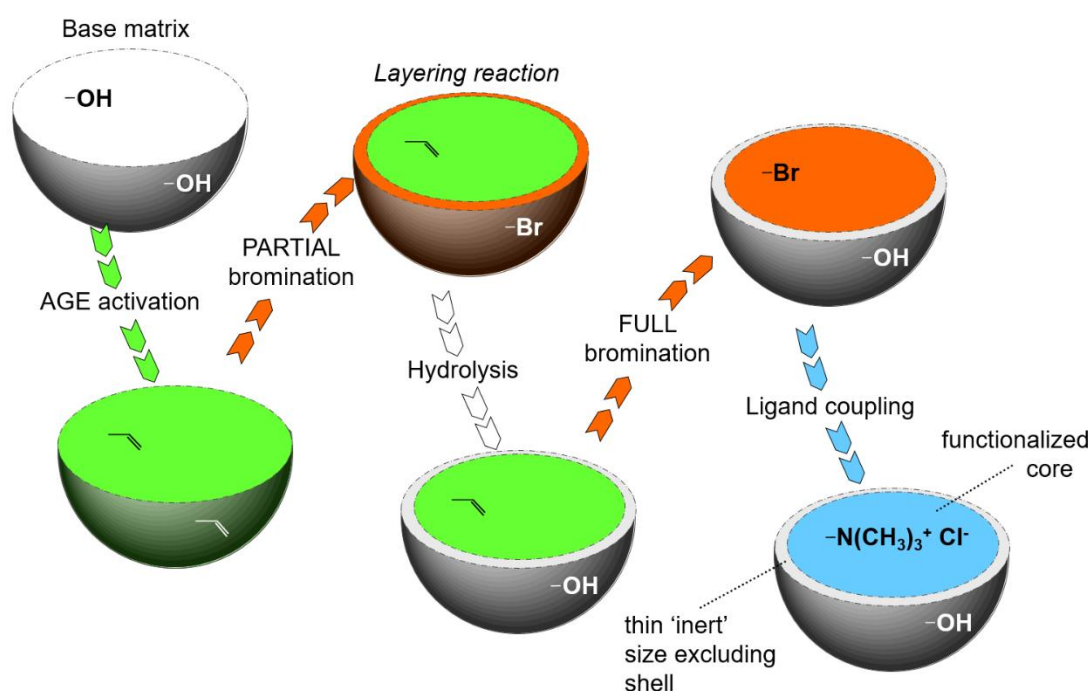


Fig. 2.3 Schematic illustrating the manufacture of functionalised, bi-layered beads using an AGE Activation/Partial Bromination technique (Reproduced courtesy of Prof. O.R.T. Thomas).

There is an incentive to improve the fabrication process to create bilayered media with outer shells as thin, uniform and inert as possible, so that maximal functionalised core volume and therefore binding capacity for the smaller contaminants is achieved.

Accordingly, the work described in this chapter builds on Karnchanasri's (2013) studies on the manufacture of bi-layered SEC-IEC supports by viscosity-enhanced (VE) and microwave-assisted (MW) reaction-diffusion (R-D) balancing approaches, with the aim of generating agarose-based SEC-IEC media with improved binding selectivity. Specifically, this involved replacing Karnchanasri's chosen starting material, Sepharose CL6B, with three different matrices (Sepharose 6 Fast Flow, Superose 6 Prep Grade, Superose 12 Prep Grade) differing with respect to particle size distribution, agarose content and pore size distribution, and cross-linker chemistry (Cao *et al.*, 2015), and screening four different reaction solvents (ethylene glycol, water, 64% w/v sucrose in water, 0.4% w/v Carbopol® 934 in water). The resulting supports were initially evaluated in static binding studies conducted with plasmid DNA and BSA as probes for surface and core binding respectively, and subsequently by fluorescent microscopy using the same probes tagged with fluorophores to localise binding to the chromatographic beads.

2.2 Materials & Methods

2.2.1 Materials & Reagents

Sephacrose 6 Fast Flow, Superose 6 Prep Grade and Superose 12 Prep Grade and PD-10 desalting columns were purchased from GE Healthcare (Uppsala, Sweden).

Bromine (99.9%), sodium hydroxide pellets (NaOH), trimethylamine chloride (Q), sodium borohydride (99%) (NaBH_4), dimethyl sulphoxide (DMSO), ethylene glycol, allyl glycidyl ether (AGE), sodium chloride (NaCl), triaminomethane hydrochloride (100 X Concentrate), potassium bromate (0.1 M), methanol (99%), ethanol (99%), sucrose and bovine serum albumin (BSA) were obtained from Sigma-Aldrich (Poole, UK).

Carbopol® 934 was procured from Lubrizol (Wickliffe, USA), whilst sulphuric acid (99%), Syto™ 9 Green Fluorescent Nucleic Acid Stain, Texas Red-X succinimidyl ester and Bicinchoninic Acid assay Protein Kit (BCA) were obtained from Fisher Scientific (Loughborough, UK). Buffers and all aqueous solutions were prepared using electro-deionised water (resistivity 5–15 $\text{M}\Omega\text{-cm}$ at 22°C) purified by a Sartorius Arium® Advanced EDI Pure Water System (Sartorius AG, Göttingen, Germany).

2.2.2 Allyl Glycidyl Ether Activation

Ten millilitre (wet settled bed volume) portions of size exclusion matrix were washed copiously (300 ml) with deionised water under vacuum on a sintered glass filter funnel to remove traces of 20% (v/v) ethanol storage buffer. The matrix was then transferred to a 100 ml conical flask containing 12.5 mg of NaBH_4 . Four millilitres of 50% (w/v) NaOH was then added before incubating at 50 °C in a reciprocating (170 rpm) water bath for 1 h. The supports were then suction dried under vacuum before being transferred back to the flask and adding 8.5 ml of AGE, sealing and placing in a reciprocating (170 rpm) water bath held at 40 °C for 16 h. Thereafter the AGE-activated matrices were recovered from the reaction liquor on a sintered glass filter funnel, before washing sequentially with deionised water, 70% (v/v) ethanol and finally deionised water, and storing in 20% (v/v) ethanol at 4 °C in tightly sealed tubes.

2.2.3 Partial Bromination

Three millilitre aliquots of allylated chromatography matrices were recovered from storage solution by vacuum filtration and then equilibrated in either 64% (w/v) sucrose or 0.4% (w/v) Carbopol® for viscosity enhanced reaction-diffusion balancing, or 60% (v/v) ethylene glycol or water for microwave enhanced reaction-diffusion balancing reactions. After equilibration the matrices were subsequently suction dried before slurring with 2.4 ml of fresh solution (to yield 55% v/v slurries) and transferring to 100 ml conical flasks.

2.2.3.1 Viscosity Enhanced Partial Bromination

Calculated amounts (based on a bromine assay) of pure liquid bromine were supplied to each conical flask to brominate 10% of the allyl groups present in each AGE-activated support (Table 2.1). After addition of the bromine solution, the flasks were immediately sealed and shaken manually until the orange colour disappeared.

Table 2.1 Allyl contents introduced into commercial agarose base matrices following reaction with AGE.

Matrix	Allyl content ($\mu\text{mol/ml}$)
AGE-activated Sepharose 6 Fast Flow	326.6 ± 26.5 (n=9)
AGE-activated Superose 6 Prep Grade	348.4 ± 14.4 (n=9)
AGE-activated Superose 12 Prep Grade	477.6 ± 20.5 (n=9)
AGE-activated Sepharose CL6B	315.7 ± 25.5 (n=24)

2.2.3.2 Microwave Assisted Partial Bromination

A conical flask was placed into the cavity of a CEM Discover S Class mono-modal microwave reactor⁸ (CEM Corporation, NC, USA). A magnetic stirrer flea was placed inside the flask to allow for uniform mixing before the heating the vessel to a stable 83 °C. This was carried out at 60 W and under “dynamic” heating mode, where the target temperature can be maintained via a feedback loop. Importantly, the round bottom glass flask behaves as an insulator and is transparent to the microwaves. The buffers and chromatography beads both act as absorbers of microwave radiation (Jones *et al.*, 2002).

As with the viscosity enhanced protocol in Section 2.2.3.1, a calculated amount of bromine was added to achieve 10% bromination. The flask was immediately sealed and the temperature and

⁸ This microwave reactor has numerous benefits including accurate temperature and pressure control as well as magnetic stirring to facilitate a well-mixed suspension and avoidance of hot and cold spots in the vessel (Wiesbrock *et al.*, 2004; Karnchanasri, 2013).

mixing held for a further 60 s and until the orange colour had disappeared, as per the set up described in Fig. 2.3.

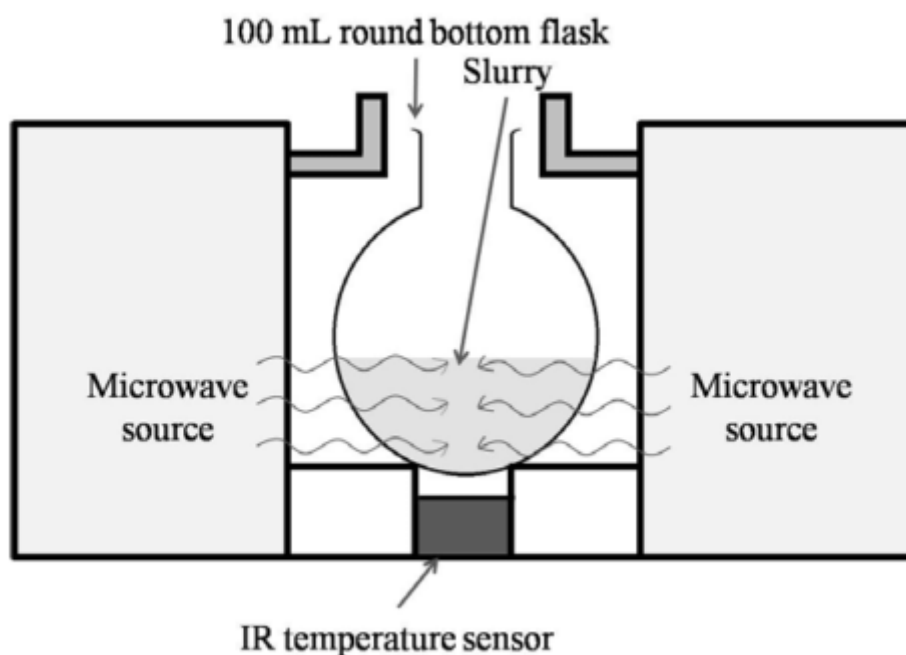


Fig. 2.3 Mode of operation of the CEM Microwave reactor with chromatography resin mixed with microwave assisting buffer to form a slurry. This is placed in the round bottom flask prior to heating (Reproduced from Karnchanasri, 2013).

The supports were subsequently washed with copious amounts of deionised water under vacuum on a sintered glass filter funnel. A small aliquot ($\sim 20 \mu\text{L}$) of each partially brominated sample was taken for a bromine assay to measure the actual level of bromination achieved.

2.2.4 Hydrolysis

Portions (2.9 ml) of partially brominated supports were then transferred to a conical flask containing 11.2 mg of NaBH_4 and subsequently $314 \mu\text{L}$ of 50% (w/v) NaOH and 1 ml of deionised water were added before sealing and placing the flask in a 40°C water bath agitating at 170 rpm for 18 h.

After 18 h, matrices were washed with deionised water under vacuum on a sintered glass filter funnel in order to remove excess hydrolysing agents.

2.2.5 Full Bromination & Q Coupling

The entire portion of vacuum dried, hydrolysed support was aliquoted into a fresh conical flask containing 4 ml before steady drop-wise addition of bromine until a permanent orange colour was

observed. The matrix was then washed with deionised water under vacuum on a sintered glass filter funnel.

The fully brominated supports were transferred to a fresh screw cap tube containing 11.2 mg of NaBH_4 , before adding 730 μL of 50% (w/v) NaOH and 1.22 ml of deionised water and gently mixing the suspension on a vortex mixer operated at low speed. Once mixed, 1.87 ml of 65% (w/v) trimethylamine chloride (a quaternary amine, strong anion exchange ligand) was added before immediately sealing and left to agitate end-over-end on an SB1 blood tube rotator (Stuart Scientific, Stone, UK) for 18 h.

The modified supports were then thoroughly washed through two cycles of water and 1 M NaCl before being stored at 4°C in 20% (v/v) ethanol. Control supports were created by skipping the partial bromination and hydrolysis steps and performing full bromination and Q coupling directly after AGE activation.

2.2.6 Particle Size Distribution

The particle size distributions of the three base SEC matrices used to create the modified supports were measured using a Malvern Mastersizer 2000 (Malvern Instruments, Malvern, UK). Briefly, 10% (v/v) matrix slurries were made up in deionised water before mixing and gradual addition into the unit's dispersion tank. Addition of the support was terminated once laser obscuration had reached a pre-determined optimum of 12% (a background measurement is taken prior to addition of the sample). The Malvern Mastersizer 2000 software then generates a particle size distribution based on the scattering pattern of the sample.

2.2.7 Viscosity Measurements

The rheology of the viscosity enhancing solutions was measured using a Bohlin C-VOR Rheometer (Malvern Instruments, Malvern, UK), equipped with a 60 mm, 1° angle stainless steel cone geometry. Changes in viscosity were measured at a shear rate of 10 s^{-1} .

2.2.8 Temperature Stability

The temperature stability of a variety of solvents and base size exclusion chromatography media, whilst in the microwave cavity, were assessed with respect to time. 3 ml of each solvent or 5.4 ml of chromatography resin slurry (55% v/v) were aliquoted into a round bottom flask with a magnetic stirrer before being placed into the microwave reactor, with a target temperature set at 83°C and held for a further minute once reached.

2.2.9 Bromine Stability

In order to assess the stability of the highly reactive bromine species in either the viscosity enhancing or microwave reaction solutions, a starting concentration of 200 mM bromine in each solution was made up to a volume of 3 ml. Loss of bromine in solution was assessed by measuring, in triplicate, the absorbance at 410 nm, at 3 min intervals over a time course of 21 min. For this,

an Evolution 300 UV-Vis Spectrophotometer (Thermo Scientific, Stafford, UK) and a High Precision Quartz Cell (Hellma Analytics, Müllheim, Switzerland), with each solution blanked against an identical solution without the added bromine.

2.2.10 Plasmid Production

Plasmid DNA material (used to characterise the chromatography resins) were generated in a 5 L batch *Escherichia coli* fermentation. Briefly, 10 ml aliquots of Luria Bertani (LB) broth supplemented with 50 µg/ml ampicillin were inoculated with a single fresh colony of *Escherichia coli* DH5α cells, contained within them the 26.7 kbp plasmid pIT14 (from pBR322-P170), kindly donated by Dr. Eirini Theodosiou, Aston University, Birmingham, UK. This inoculum culture was shaken overnight at 37 °C and 220 rpm before a 1 ml aliquot was added to a 250 ml shake flask containing 80 ml of LB broth (containing 50 µg/ml ampicillin) and left to agitate on an orbital shaker at 37°C and 220 rpm.

Once an optical density (OD_{600nm}) of 0.6 was reached (measured on an Evolution 300 UV-Vis Spectrophotometer (Thermo Scientific, Stafford, UK)), the inoculum was transferred to a 5 L Fermac 310/60 fermenter (Electrolab, Tewkesbury, UK) with an impeller equipped with two six-blade Rushton turbines for agitation. Growth media for the fermentation was an LB broth with a final volume of 4 L, with 30 g/L glucose, 100 µg/ml ampicillin and antifoam (polypropylene glycol) added as required.

The batch fermentation employed starting conditions of 37°C, controlled by a cooling jacket, an agitator speed of 400 rpm and air-flow rate set at 1.0 VVM. The pH was maintained at 7.0 throughout the fermentation by the automatic addition of 5 M NaOH. The dissolved oxygen tension (DOT) was controlled above 50% by adjusting either the aeration or agitation. After the cells reached late exponential phase, the fermentation was terminated and cells harvested.

Plasmid DNA (pDNA) was isolated using a QIAGEN Plasmid Giga Kit (QIAGEN, Manchester, UK) with pDNA quality and concentrations measured using a UV Spectrophotometric assay (see Section 2.3.6 for more details).

Cell harvest was achieved via centrifugation in a J2-21 centrifuge (Beckman, High Wycombe, UK) operated at 6,000 rpm (4°C) for 15 min. The cell paste weighed 24.5 g (wet cell weight), 1.17 g/L dry cell weight, generating a plasmid yield of 615 µg/g of wet cell weight; the paste and purified pDNA was stored at -20°C.

2.2.11 Analysis

2.2.11.1 Environmental Electron Scanning Electron Microscopy

Chromatography resins were visualised via environmental electron scanning microscopy with the assistance of Paul Stanley and Theresa Morris, both from the School of Metallurgy & Materials, University of Birmingham. Chromatography resins were subjected to a methanol drying gradient; re-suspended firstly in a 50% methanol solution, before gently spinning down and re-buffering

(over 3 cycles) into consecutively increasing methanol concentrations until suspended in 100% dry methanol (100% methanol & molecular sieve).

The beads were subsequently mounted onto aluminium stubs prior to critical point drying and sputter coating with a thin layer of platinum to minimise the effect of charging and improve image contrast. Imaging of the samples was on a Philips XL-30 FEG Environmental Scanning Electron Microscope (FEI Company, OR, USA).

2.2.11.2 Bromine Assay

Supports were quantified for the allyl groups generated during AGE activation and post-partial bromination by exposing 0.05 ml of vacuum dried resin to 1 ml of an acidified bromine solution (sulphuric acid 0.5 M, potassium bromate 0.1 M ratio, 2: 1). The acidified bromine solution was prepared by mixing the two reagents, then left for 10 min to develop a strong yellow colour, before mixing again by inversion then adding to the chromatographic supports.

Once added, the suspension was mixed by vortex for 10 s and subsequently separated by a brief centrifugation spin (1000 rpm, 10 s) using a benchtop micro-centrifuge (VWR MiniStar Silverline, VWR International, Radnor, USA). Each supernatant was removed and measured for absorbance at 410 nm using an Evolution 300 UV-Vis Spectrophotometer (Thermo Scientific, Stafford, UK) and a High Precision Quartz Cell (Hellma Analytics, Müllheim, Switzerland).

0.5 M sulphuric acid was utilised as a diluent and a blank and the original, underivatised size exclusion matrices used as controls. A bromine standard curve was constructed by measuring the absorbance at 410 nm of a range of bromine stock solutions ranging from 0 – 10 mM, made up in sulphuric acid. The moles of bromine disappearing from solution corresponds, in a 1 : 1 ratio, with the moles of allyl groups present on the chromatography supports, relative to the underivatised control supports. This assay is repeated after the partial bromination step on a small aliquot of sample to assess the level of partial bromination achieved.

2.2.11.3 Static Binding Studies

Chromatography matrices were washed with deionised water before buffer exchanging and equilibrated 3 times in 1 ml of 0.05 M Tris-HCl (pH 8.0), such that the settled bed volume of the resin was 0.05 ml. Each chromatography matrix was then exposed to either a 5 mg/ml BSA or a 15 µg/ml pIT14 plasmid solution and allowed to incubate for 2 h with end-over-end mixing on an SB1 blood tube rotator (Bibby Scientific Ltd., Stone, UK). Binding isotherms for plasmid DNA were generated for the control matrices by applying an identical methodology but by varying the load concentration, as determined by UV spectrophotometry (see 2.2.11.5).

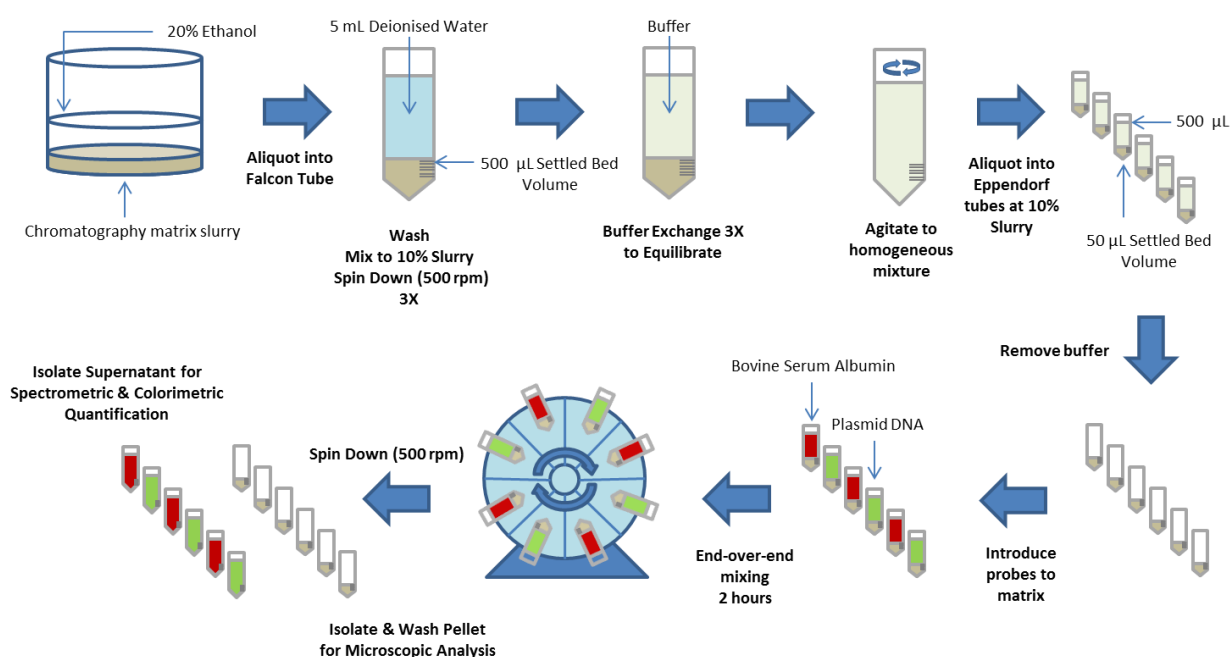


Fig. 2.4 A general schematic of the methodology involved in a finite bath study starting from resin in a 20% Ethanol storage buffer through to isolation of the pelleted beads for microscopy and analysis of supernatant concentrations for mass balancing and calculations of static binding capacities.

Each loading condition would be measured in triplicate to determine averages and standard deviations. Post-incubation, the chromatography matrices were pelleted via a brief 10 s pulse of 500 rpm on a benchtop micro-centrifuge (VWR MiniStar Silverline, VWR International, Radnor, USA). The supernatants were carefully removed for quantification for either protein or pDNA concentration using a bicinchoninic acid (BCA) or ultraviolet (UV) spectrophotometric assay, respectively.

2.2.11.4 Bicinchoninic Acid Assay for Protein

For protein quantitation during the static binding studies, a Pierce® Bicinchoninic acid (BCA) assay kit was purchased from Thermo Fischer (Thermo Scientific, Stafford, UK). Working reagent

was prepared by mixing 50 parts reagent A (sodium carbonate, sodium bicarbonate, bicinchoninic acid, sodium tartrate in 0.1 M sodium hydroxide) with 1 part reagent B (4% cupric sulphate). The microplate protocol was applied, whereby 0.2 ml of the working reagent was aliquoted into each well of a 96-well microplate (Thermo Scientific, Stafford, UK) before addition of a 0.025 ml protein sample to each individual well. Samples were aspirated three times to ensure uniform mixing in each well before the plate was sealed and placed in a microplate shaker-incubator for 30 mins at 350 rpm at 37°C (Infors AG, Bottmingen, Switzerland).

For each plate analysed, a BSA standard curve was generated by including standards in the (absorbance linear) range of 0.02 - 2 mg/ml and thus the concentration of the unknown protein sample on the plate can be ascertained based on the well's absorbance reading. Absorbance values were read at 562 nm using a Synergy Neo2 HTS Multi-Mode Microplate Reader (BioTek, Vermont, USA).

2.2.11.5 Ultraviolet Spectrophotometric Assay for pDNA

Plasmid DNA (pDNA) was assessed for both quality and concentration using an Ultraviolet Spectrophotometric assay with the aid of a quartz cuvette; an Evolution 300 UV-Vis Spectrophotometer (Thermo Scientific, Stafford, UK) and a High Precision Quartz Cell (Hellma Analytics, Müllheim, Switzerland) were both used in this methodology.

Plasmid DNA stocks and aliquots were assessed for concentration, purity and salt carryover by measuring absorbance values at four different wavelengths; 230, 260, 280 and 320 nm, each in triplicate. Samples were diluted to within the linear range of the instrument (absorbance values between 0.1-0.9) to allow for accurate determination of concentration.

2.2.11.6 Confocal Laser Scanning Microscopy

In order to compliment the static binding data for the two probes, BSA and pDNA, confocal laser scanning microscopy has been employed to provide images of the spatial location of the probes with respect to the optically transparent chromatography beads.

To achieve this, the two probes need to be conjugated with fluorescent dyes prior to contact with the chromatography matrices. BSA was conjugated with Texas-Red X; briefly, 1 mg of Texas Red-X dye was dissolved in 1 ml DMSO and incubated for one hour at room temperature on an SB1 blood tube rotator.

Using a molar dye/protein ratio of 1: 100 (Hubbuch and Kula, 2008), aliquots of BSA were tagged by incubating with the dye in a light-free environment (an Eppendorf wrapped in aluminium foil) for one hour with end-over-end mixing on an SB1 blood rotator. The dye/protein ratio was chosen to reduce the contribution of emitted fluorescence re-adsorption to light attenuation as well as to allow for efficient purification of conjugated protein-dye complexes.

Free, un-conjugated dye was separated from the bio-conjugated proteins using single-use PD-10 desalting columns packed with Sephadex G-25 media (GE Healthcare, Uppsala, Sweden) operated in gravity flow mode.

With respect to the pDNA, Syto™ 9 was utilised as a minor groove-binding fluorescent dye. Here the probe was added to a pDNA stock solution with a dye/DNA ratio of 1 dye molecule to 100 DNA base pairs, as per the manufacturer recommendations. No purification was required in the case of pDNA-Syto™ 9 conjugates due to the fact that the intensity of fluorescence is much higher when the Syto™ 9 probe is conjugated to pDNA, than free, unconjugated Syto™ 9 in solution.

Therefore, by adjusting fluorescent detection settings on the microscope, it is possible to threshold such that any fluorescence from the unconjugated dye is eliminated. Effects of dye labelling on protein surface characteristics (and therefore binding behaviour) were assessed using cation exchange chromatography and isoelectric focussing, as discussed in Chapter III. Dye labelling effects on pDNA were adjudged to be minimal as trials were conducted to assess differences between labelling of the pDNA pre- and post- binding to chromatography resin, for which little difference in fluorescent intensity was found.

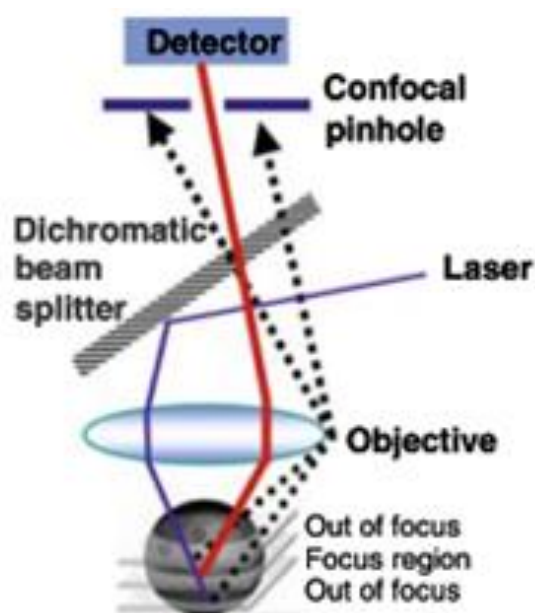


Fig. 2.5 Schematic illustrating how a three-dimensional image can be generated using a confocal microscope. The confocal pinhole facilitates focus on individual layers, as thin as 1 μm , and these slices can be scanned and subsequently re-stacked to construct a three dimensional image of a bead with a fluorescent probe bound (Hubbuck and Kula, 2008).

Protein-dye and pDNA-dye conjugates were then diluted to the correct loading concentrations before being used in static binding studies as described in 2.2.11.3, running in parallel to the non-fluorescent, quantitative static binding studies. As opposed to isolating the supernatant after centrifugation, the chromatography matrix pellet was washed three times in fresh TRIS-HCl buffer in order to remove non-specific bound and free BSA or pDNA in solution. For sample

preparation, resin, in 5 μ L aliquots, were pipetted onto microscope slides, with a cover slip carefully placed on top to hold the samples in place. Precautions were taken to minimise fluorophore bleaching; the use of low laser powers, minimised exposure times and use of aluminium foil to cover all samples during conjugation, transition and storage.

Image acquisition was conducted using a confocal laser scanning microscope (Leica TCS SPE 102A, Leica Microsystems, GmbH, Mannheim, Germany) equipped with krypton/argon ($\lambda = 488$ nm and $\lambda = 568$ nm) and helium/neon ($\lambda = 633$ nm) lasers. A 40x oil emersion objective was used to image the samples on a microscope slide with a cover slip. For the BSA experiments, samples were excited with the 568 laser to visualise the protein species labelled with Texas Red-X (excitation and emission maxima at $\lambda = 596$ and 615 nm, respectively). For the pDNA experiments, the 488 nm was used for excitation as Syto™ 9 has excitation and emission maxima at $\lambda = 485$ and 498 nm, respectively.

Images were captured and processed using the Leica Application Suite (LAS X) software (Version 1.9) (Leica Microsystems, GmbH). Settings were optimised to ensure minimisation of auto-fluorescence (see Fig. 2.17), including laser intensity, signal gain, offset and emission detection range. Control tests ensured that the detected emitted light intensity was within detection range and blank tests ensured no auto-fluorescence of untagged protein or the chromatography resin (Close *et al.*, 2013). Emission detection ranges for the photomultiplier tube, gain, offset and thresholds were all optimised on the confocal microscopy software in order to enhance fluorescence detection and remained constant within a set method across all samples to allow for effective comparative across samples. For each sample type, five beads were imaged to confirm similar binding characteristics were taking place across the entire sample set.

2.3 Results & Discussion

2.3.1 Particle Size Distribution

In order to assess the distribution of bead sizes within each commercial resin suspension, a light scattering technique was employed using a Mastersizer 2000. This provided insight into both a distribution of size as well as an average particle diameter. This allowed a comparison to be made between the stated sizes from the manufacturer and the actual size characteristics of the batch used for the manufacturing of the bi-layered materials as well as a direct comparison between the bead types used in this study.

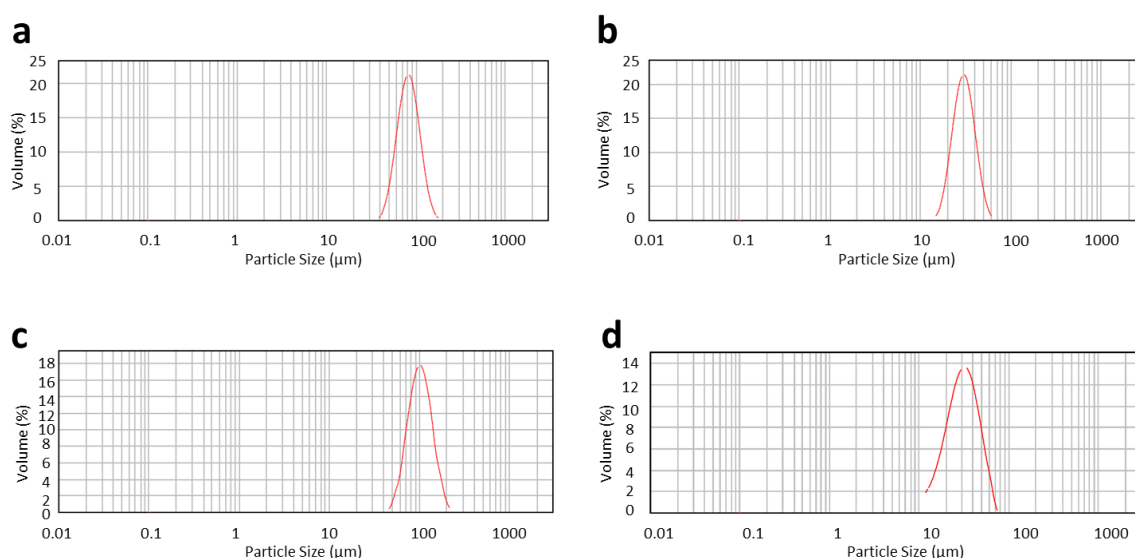


Fig. 2.6 Particle size distribution data for **a)** the commercial multi-functional resin, Capto™ Core 700 and the three base size exclusion matrices used; **b)** Superose 12 Prep Grade **c)** Sepharose 6 Fast Flow & **d)** Superose 6 Prep Grade.

Table 2.2 A comparison of the three chromatography resins used as base matrices in this study, compared with a), a commercial, bi-functional matrices currently on the market. Mean particle sizes of the experimental Mastersizer data are compared against the manufacturers stated values. Comparison of the relative pore sizes are also given, with molecular weight exclusion limits (kDa) and base pairs (bp) quoted for globular proteins and DNA, respectively (Dublin 1988, Tayyab et al. 2001, DePhillips and Lenhoff, 2000, Saber et al. 2011 and GE Healthcare 2015).

	Mastersizer d _{50V} (µm)	GE Healthcare d _{50V} (µm)	Pore Size		
			(kDa)	(nm)	(bp)
a) Capto™ Core 700	85	90	700	35	-
b) Superose 12 Prep Grade	30	30 – 40	300	25	150
c) Sepharose 6 Fast Flow	100	90	4, 000	50	165
d) Superose 6 Prep Grade	35	30 - 40	5,000	40	450

The mean particle size of the cumulative volume distribution corroborate with manufacturer's specifications.

The three size exclusion base matrices vary in terms of their average sizes and pore structure, with the Superose media tending to have much smaller average wet bead diameters than the Sepharose or Capto™ media. While information on the Capto™ media is currently proprietary, the Superose and Sepharose media are both beaded media formed by cooling aqueous agarose in a non-polar organic solvent and subsequently covalently cross-linking the repeating 1-3-linked β-D galactose and 1,4-linked 3,6-anhydro-α-L-galactose polymers to preserve the 3-D network fibre structure, as indicated in Fig. 2.7 (Nweke, McCartney and Bracewell, 2017).

The percentage of agarose in the matrix gives rise to the nomenclature of the bead (e.g. Sepharose 6 Fast Flow and Superose 6 PG are composed of 6% agarose, whereas Superose 12 has an agarose content of 12%) and this has an impact on the porosity of the media, allowing for varied selectivity and exclusion limits, as well as flow, hydrophilicity and rigidity properties. Thus the media have different applications, (Pääkkönen, Pursiainen and Lajunen, 2010). These characteristics will be exploited to create a varied set of bi-layered and functionalised materials with a diverse set of properties.

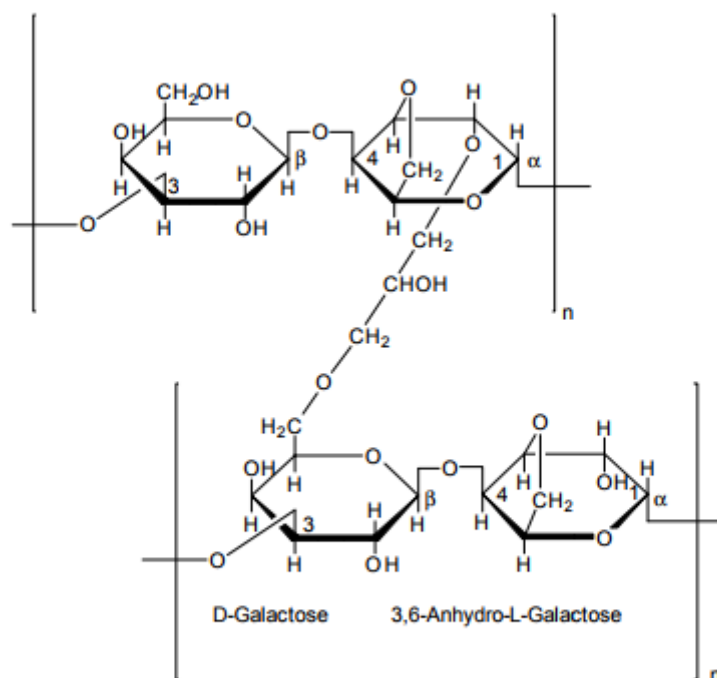


Fig. 2.7 Molecular structure of cross-linked agarose which form the basic make up of all three starting matrices used in this study (Sigma Aldrich, 2018b).

2.3.2 Viscosity Measurements

As this methodology of viscosity enhanced reaction diffusion balancing had been the subject of a PhD thesis within the O.R.T Thomas Research Group prior to commencement of this work. The thesis titled “Bi-layered chromatography matrices for the purification of biological nanoplexes” (Karnchanasri, 2013) looked to optimise the conditions of viscosity enhanced- and microwave assisted- manufacture of bi-layered beads using the chromatography media Sepharose CL-6B. It is important to note at this stage that as Sepharose CL-6B was not available at the point of manufacture, Sepharose 6 Fast Flow was employed as a comparative point of reference; the two are similar though Sepharose 6 is mechanically stronger. They both have a similar average particle size and are both 6% cross-linked agarose particles, spherical in shape and employ the same cross-linker, but only differ in the extent of cross-linking.

Karnchanasri (2013) optimised the viscosity enhanced protocol, concluding that the optimal bi-layered Sepharose CL-6B based matrix was achieved using a viscosity of 0.007 Pa.s at 25°C during the partial bromination step (corresponding to the use of 64% (w/v) sucrose in water). This work looks to build upon this, replicating these viscosity conditions with both sucrose and a new viscosity enhancer, Carbopol® 934, employed at a concentration of 0.4% (w/v) in water to give a viscosity (0.006 Pa.s, 25 °C) close to Karnchanasri’s (2013) identified optimum. . Carbopol® 934 is a poly-acrylic acid polymer cross-linked with allyl ethers of sucrose and was chosen as an alternative to sucrose to circumvent some of Karnachanasri’s observations of sucrose

consumption of bromine; it was hypothesised that Carbopol would be less reactive with bromine and therefore aid in the partial bromination of the resins.

2.3.3 Viscosity Enhanced & Microwave Assisted Partial Bromination

In order to achieve a thin outer shell and maximise the functionalised core within each bead, the partial bromination step can be improved by either viscosity enhancement or microwave assistance (Karncahnasri, 2013). The principles behind these techniques are based on the Arrhenius, Arrhenius-Guzman and Stokes-Einstein equations.

Equation 1: Arrhenius Equation

$$k = Ae^{\left(\frac{-E_a}{RT}\right)}$$

Equation 2: Arrhenius-Guzman Equation

$$\eta = 0.5 \times 10^{-3} \times e^{\left(\frac{B}{RT}\right)}$$

Equation 3: Stokes-Einstein Equation

$$D = \frac{k_B T}{6\pi\eta r}$$

Where:

- k is the rate constant (mol/L.s)
- A is the frequency factor (the frequency of collisions between reactant molecules) (s⁻¹)
- E_a is the activation energy (~238.7 kJ/mol for the bromination of a double bond (Islam and Poirier, 2007))
- R is the universal gas constant (8.314 J /K.mol)
- T is the absolute temperature (K)
- η is viscosity (kg/m.s)
- B is an empirical constant dependent on the properties of the liquid (Morris, 1992)
- D is the diffusion coefficient (m² /s)
- k_B is the Boltzmann constant (1.381 x 10⁻²³ J/K)(k_B = R ÷ N_A, where N_A is the Avogadro constant, 6.022 x 10²³) (Reeks, 2011)
- r is the radius of a spherical particle in a fluid of dynamic viscosity

Evidently, adjusting the viscosity of the reaction buffer will lower the diffusion coefficient, the magnitude of which is dependent on the empirical constant, B, of the experimental buffer chosen. Theoretically, the more viscous the solution, the slower the diffusion coefficient and thus diffusion into the chromatography resin is limited, allowing bromination of the carbon-carbon double bond to occur only at or near the surface of the matrix, given a finite amount of bromine is added.

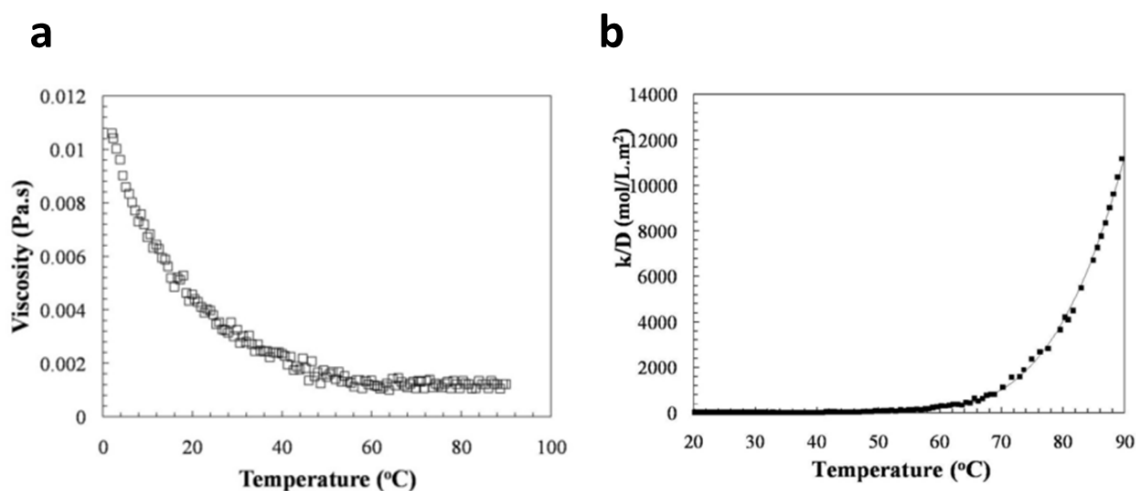


Fig. 2.8 a) Relationship between viscosity & temperature for deionised water. **b)** k/D – temperature profile for the bromination of a double bond (Gilbert and Martin, 2011).

With regards to microwave assisted reaction-diffusion balancing, Equation 1 highlights an increase in the rate constant with increasing experimental temperature. This allows the bromination reaction to occur quicker and thus the loaded bromine is used up at a faster rate. Increasing temperature was conducted by microwave heating due to its multiple advantages over conventional heating. These include better energy transfer, faster heating and cooling rates, higher energy efficiency due to minimal heat loss and uniform sample heating, as well as minimal heat conduction within the vessel (Agrawal, 1998) and finally relatively lower capital costs (Pääkkönen, Pursiainen and Lajunen, 2010).

The fundamentals of microwave heating are dependent on the interaction of the sample with an electromagnetic field, either by dipole rotation or ionic conduction. The former represents an interaction where heat is generated through polar molecules attempting to align in the alternating electrical field. Heat generation is strongly dependent on the dipole involved and the radiation frequency, in a range (usually 2.45 GHz) whereby the dipole can respond to the oscillating field but is not able to accurately align with it, causing a phase difference between the field orientation and the dipole orientation, resulting in a loss of energy from the dipole through molecular friction, collisions and dielectric heating (Kappe, Stadler and Dallinger, 2012).

Heat generation can also occur through ionic conduction, whereby the electrical field generates ionic movement as dissolved charged particles oscillate and attempt to align to the oscillating field, causing increased molecular collisions with neighbouring atoms, resulting in agitation and

ultimately conversion of the electrical energy to heat. Of the two mechanisms, ionic conduction is the more prominent though both work in tandem to effect sample heating (Thostenson and Chou, 1999; Lidström *et al.*, 2001; Hayes, 2002; Kappe, Stadler and Dallinger, 2012; Karnchanasri, 2013).

The efficiency of heating a material in an electromagnetic field is dependent on its dielectric loss tangent ($\tan \delta$), which is a measure of reactance (resistance in a capacitor), i.e. how well the material is able to absorb microwave radiation. The dielectric loss tangent is described with respect to two parameters, as per Equation 4.

Equation 4:

$$\tan \delta = \frac{\epsilon''}{\epsilon'}$$

Where:

- ϵ'' is the dielectric loss factor (imaginary permittivity) which indicates the efficiency of dissipation of electrical energy as heat within the bulk substance
- ϵ' is the dielectric constant (real permittivity) which illustrates how polarisable the molecules in the sample are and thus describes the proportion of microwave radiation reflected vs. the proportion absorbed

To achieve an efficient conversion of microwave energy into thermal energy, a significant dielectric loss factor and low dielectric constant are required to achieve a high $\tan \delta$ value, which would result in efficient absorption and rapid heating. Classification of materials, with respect to $\tan \delta$, are listed as follows: high ($\tan \delta > 0.5$), medium ($0.5 > \tan \delta > 0.1$) and low ($0.1 > \tan \delta$) (Kappe, Stadler and Dallinger, 2012).

Table 2.2 illustrates some of the buffers available for microwave-assisted bi-layering and their respective $\tan \delta$ values. Previous work by Karnchanasri (2013) looked to optimise the partial bromination step with microwave assistance using water as a buffer system. The work presented here expands on this by using different microwave-assisting buffers alongside water, as elaborated upon in section 2.3.3 and 2.3.5.

However, a balance is required as, although increasing temperature increases the reaction rate, it also increases both the diffusion rate directly and also reduces the buffer's viscosity (Fig. 2.8 a)) which will also increase the diffusion rate. Karnchanasri (2013) demonstrated that the relationship between reaction/diffusion rates (k/D) for the bromination reaction has a greater impact on the rate of reaction when the temperature is ramped to 60 °C or higher, whilst diffusion remains relatively constant above this temperature. Therefore operating above 60 °C for the microwave reactions should theoretically have a minimal impact on diffusion whilst greatly improving the rate of formation of bromo-alkyl groups on the surface of the beads, forming a thin and well defined shell on the surface.

Table 2.3 Comparison table of the loss tangents of a variety of potential microwave-assisted reaction buffers (2.45 GHz, 20 °C) (Kappe, Stadler and Dallinger, 2012).

Solvent	$\tan \delta$	Solvent	$\tan \delta$
Ethylene Glycol	1.350	N,N-Dimethylformamide	0.161
DMSO	0.825	Water	0.123
2-Propanol	0.799	Chlorobenzene	0.101
Formic Acid	0.722	Chloroform	0.091
Methanol	0.659	Acetonitrile	0.062
Nitrobenzene	0.589	Ethyl Acetate	0.059
1-Butanol	0.571	Acetone	0.054
2-Butanol	0.447	Tetrahydrofuran	0.047
1,2-Dichlorobenzene	0.280	Dichloromethane	0.042
1-Methyl-2-pyrrolidone	0.275	Toluene	0.040
Acetic Acid	0.174	Hexane	0.020

It is important to note that the $\tan \delta$ values for polysaccharides (i.e. chromatography matrices) are much higher than any of the solvent and under heating conditions the polar, hydroxyl-rich polysaccharides will interact directly with the microwaves, heating up much faster than the solvent. This will result in a tight banding effect as the bromine should, in theory, react instantly upon contact with the outer surface of the bead.

2.3.4 Bromine Stability

A point of concern during the partial and full bromination studies was the stability of the highly reactive bromine in its buffer prior to contact with the chromatography resins. For this reason, a

number of different solvents were assessed for their efficacy as a buffer system for the bromination reactions. The aim was to find a buffer that is minimally oxidised by bromine allowing more of the originally loaded bromine to interact with the chromatography media and not the buffer.

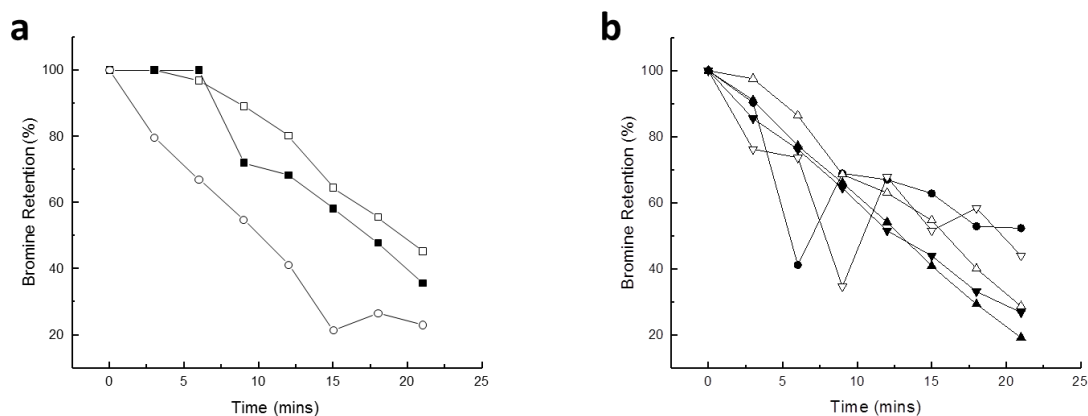
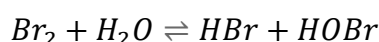


Fig. 2.9 Bromine stability studies with respect to time on **a)** viscosity-enhanced; \square - 80% Sucrose, \blacksquare - 64% Sucrose, \circ - 0.4% Carbopol 934 and **b)** microwave-assisted reaction buffers; \bullet - 85% Ethylene Glycol, Δ - 60% Ethylene Glycol, \blacktriangle - 50% Ethylene Glycol, ∇ - 60% DMSO & \blacktriangledown - Deionised Water.

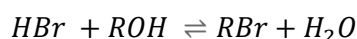
To this end, a range of concentrations of a variety of buffers were assessed for bromine loss with respect to time, as illustrated in Fig. 2.9, aiming to optimise buffer conditions for a) viscosity enhancement and b) microwave assisted partial bromination.

Although bromine stability studies were conducted at room temperature (conditions for the viscosity enhanced reactions only), and assumption is made that the trends observed would be a useful indicator (and in fact be accelerated at the experimental 83 °C temperature) for the microwave reactions too.

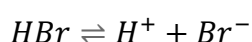
Equation 5:



Equation 6:



Equation 7:



With respect to the viscosity-enhanced buffers, it is evident that sucrose-based buffers are a better choice with respect to bromine loss, with 80% (w/v) sucrose performing the better of the two

over the time course. This can be attributed to the % water in the buffer causing increased loss of bromine, as shown in Equation 5 (Willett, 2009). The higher the percentage of water, the further the equilibrium will be pushed towards the formation of hydrogen bromide, ultimately limiting the reactivity of bromine with the allyl groups on the chromatographic supports. Carbopol® 934 in Fig. 2.9 a) and 50% ethylene glycol in b) performed comparatively poorly as the buffers are also aqueous and the water content is the main contributor responsible for the loss of bromine.

Equation 5 goes some way to illustrating the performance of high percentage of sucrose and also ethylene glycol buffers, with respect to time (Gilbert and Martin, 2011). Not only is lack of water a factor here, but also the interaction with the additional hydroxyl residues of the sucrose and ethylene glycol molecules, whereby in aqueous solution, sucrose, Carbopol, ethylene glycol and DMSO are being oxidised by bromine.

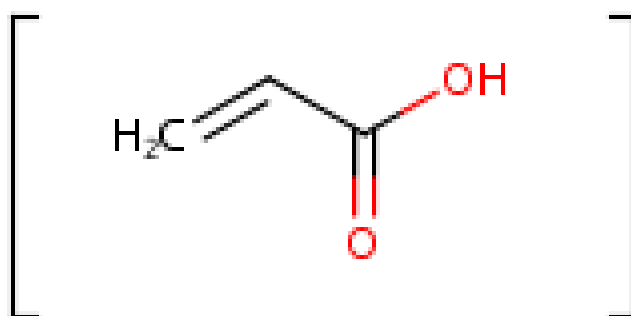


Fig. 2.10 The monomer molecular structure of Carbopol® 934 (GenScript, 2018; Thermo Fisher Scientific, 2018b).

Equation 6 highlights the equilibrium between the dissociation of HBr in solution allowing Br⁻ ions to carry out nucleophilic attacks of carbon-carbon double bonds, such as the carbonyl group in Carbopol® 934 and the sulfinyl group in DMSO, explaining why the two also performed poorly (Aida *et al.*, 1976; Willett, 2009). To further confirm this, 85% (v/v) DMSO was also assessed for bromine stability, however within seconds the absorbance value dropped below the linear range of the instrument indicating a rapid and high loss of bromine in solution. Whilst ethylene glycol has two terminal hydroxyl groups which can also undergo nucleophilic attack from the bromine, Fig. 2.9 indicates that bromine's reactivity is higher with DMSO's sulfinyl double bond.

What is also interesting to note is the peak and trough behaviour of some buffers with respect to time and it is hypothesised that this is as result of pre-equilibrium fluctuations as bromine dissolves in solution and fluctuates between HBr, HOBr and Br⁻ and back to Br₂ until equilibrium is reached.

According to Karnchanasri (2013), bromine concentration would stabilise to ~ 50% of the original loaded concentration after between 5 – 50 min after point of addition, depending on the buffer system used. Identifying suitable buffer conditions which limit this bromine interaction and maintains bromine concentration in a stable fashion for an extended period of time is vital. This will facilitate the use of smaller volumes of pure bromine whilst improving the efficiency of the

partial bromination step by having more bromine in solution readily available to interact with the allyl groups on the surface of the resin rather than being used up by the buffer.

Karnchanasri (2013) also determined 64% (w/v) sucrose as optimal for partial bromination, in essence demonstrating that a balance must be struck between viscosity enhancement of the layering action and bromine loss within the buffer. In addition, the time from adding bromine to the slurry of beads and buffer is < 5 min until complete mixing occurs, whereby there is little oxidation of the buffer and bromine concentration is relatively constant for the two sucrose-based buffers. For these reasons, 64% (w/v) sucrose was carried forward for the bi-layering reactions. Similarly, for the microwave assisted reactions, 60% (v/v) ethylene glycol was found to hold bromine in the most stable fashion up to 5 min and therefore was also carried forward. This is further justified after testing various microwave assisting buffers for temperature ramp times and stability, as described in 2.3.5.

Carbopol® 934 (at a concentration of 0.4% w/v in water), despite having a similar viscosity to 64% (w/v) aqueous solution of sucrose, whilst envisaged to perform better with respect to bromine stability, was still carried forward as an alternative viscosity enhancing reaction buffer. Its high water content, carbonyl and hydroxyl groups are possible explanations for its high bromine reactivity. The rationale for including it in subsequent experiments derives from the idea that due to its highly aqueous composition, it would be easy to remove the viscosity enhancer from the chromatography beads after the viscosity enhancing step. This has been an issue in screening tests for other viscosity enhancers in the past, whereby washing of the beads would take hours and remnants of viscosity enhancing buffers would remain and thus influence subsequent probe binding experiments.

2.3.5 Temperature Stability & Ramping Rates

Karnchanasri demonstrated that the optimum condition for bi-layering via microwave assistance was 83°C, which would allow the bromination reaction to proceed at a quicker rate before the reagent diffuses into the core of the bead, thus creating a thin, outer shell.

With this in mind, a variety of buffers were assessed in temperature ramping experiments. Figs 2.11 and 2.12 highlight the performance of the various buffers and chromatography media, respectively. Varying concentrations of ethylene glycol and DMSO were assessed for ramp rates based on their high $\tan \delta$ values, as detailed in Table 2.2. Deionised water has the lowest tangential loss factor and also the lowest dipole moment, compared to both ethylene glycol and DMSO (1.85, 2.36 and 3.96, respectively; measured as Debye units (D)) (Lide, 2004).

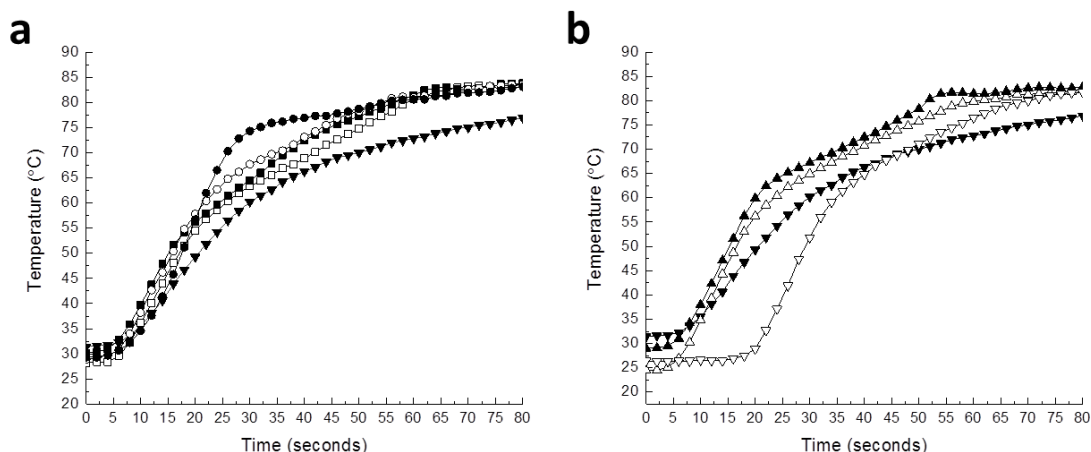


Fig. 2.11 Temperature ramps and stability assessment for microwave assisting buffers composed of varying percentages of **a)** Ethylene Glycol and **b)** DMSO. Symbols: -□- 50% Ethylene Glycol, -■- 60% Ethylene Glycol, -○- 85% Ethylene Glycol, -●- 100% Ethylene Glycol, -△- 50% DMSO, -▲- 60% DMSO, -▽- 100% DMSO & -▼- Deionised Water.

It is important to note that, as per Equation 4, $\tan \delta$ will decrease upon heating and has varying impacts dependent on the solvent; for instance at 25 °C, DMSO has the highest dielectric loss, however between 55 – 90 °C, ethylene glycol has a higher overall dielectric loss tangent. This is because the reduction in the dielectric loss factor (ϵ''), which occurs upon heating, is less for ethylene glycol compared to DMSO (Horikoshi and Serpone, 2013). This is likely due to the molecular composition of the two solvents, with the two hydroxyl groups present on an ethylene glycol molecule contributing heavily to its high heat capacity. This explains the deceleration in ramping rate for all samples at ~ 55 °C and also the slow ramp rate for 100% DMSO, compared to its ethylene glycol equivalent.

Hydrophobic interactions from the non-polar groups, the formation of cage structures by water molecules around these groups, as well as extensive hydrogen bonding and low entropy can increase the apparent heat capacity of the solution, facilitating rapid heat adsorption and rapid temperature ramps (Sturtevant, 1977). These interactions are all readily available in both ethylene glycol and DMSO, corroborating their accelerated heat adsorption characteristics.

In the case of both Fig. 2.11 a) and b), however, a 60% concentration of the aqueous buffer reached the target temperature the quickest, indicating a balance is required between high tangential loss values and the aqueous nature of the buffer. It is likely that 60% provides an optimum compromise condition whereby the water content of the buffer allows sufficient formation of structural cages around the non-polar groups in the solvent whilst also providing a high enough dipole moment and dielectric loss tangent contribution from the organic solvent to achieve rapid heating.

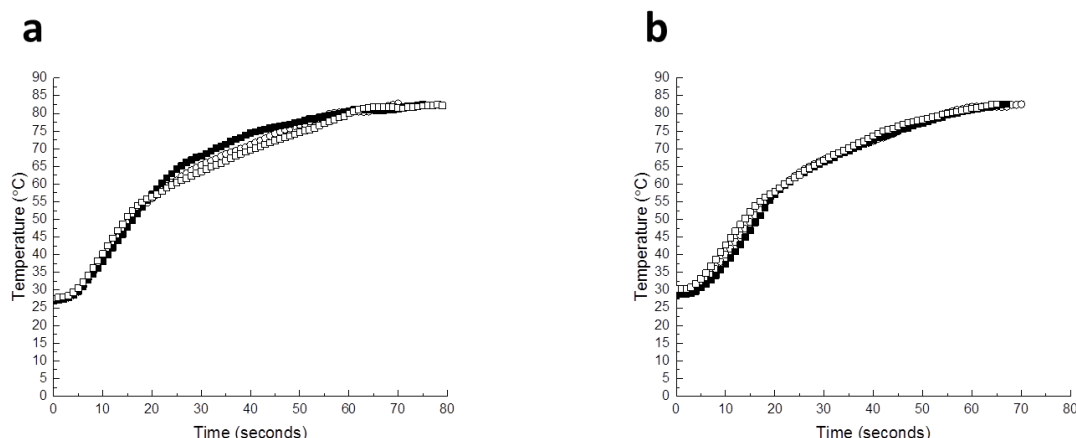


Fig. 2.12 Temperature ramps of the chromatography matrices in **a)** Deionised water and **b)** 60% ethylene glycol. Symbols: \square - Sepharose 6 Fast Flow, \blacksquare - Superose 6 Prep Grade, \circ - Superose 12 Prep Grade.

Another important experimental factor to take into consideration is the temperature ramp rates of the chromatography bead slurries in both deionised water and 60% ethylene glycol. Fig. 2.7 indicates the general dipole-rich molecular structure of all of the cross-linked agarose chromatography beads and all of them had relatively similar temperature ramp profiles.

The three supports heated in 60% ethylene glycol experienced the quickest temperature ramp, reaching target temperature between 66 – 71 s, compared to deionised water, which had resins reaching target temperature between 71 – 80 s. This trend was also observed previously when considering the heating profiles of the buffers on their own. The existence of the two terminal hydroxyl groups and high $\tan \delta$ value of ethylene glycol relative to deionised water aids in explaining these observations.

Despite their different size distributions, surface area: volume ratios and degrees of cross-linking, the temperature profiles for the three resins in each buffer were comparatively similar. Superose 12 Prep Grade performing the best in deionised water and Sepharose 6 Fast Flow in 60% ethylene glycol, but with < 10 s to reach target temperature between each resin type for each buffer set.

An ideal microwave assisting buffer would meet the criteria of balancing a rapid ramp rate whilst having low bromine interaction. For the microwave reaction buffers, ethylene glycol was carried forward for the partial bromination reactions alongside deionised water, whilst DMSO was discarded due to its strong interaction with bromine, as detailed in section 2.3.3. 60% ethylene glycol was selected due its ability to retain bromine in a stable fashion up to five minutes as well as its temperature stability and rapid ramp rate to 83 °C. This information becomes relevant when considering the process at a larger bioprocess scale, as a rapid temperature ramp can result in higher process throughput and ultimately a more economical bioprocess. In addition, limiting bromine interaction can save litres of buffer and limit the use of expensive and dangerous pure liquid bromine.

Table 2.4 The experimental design matrix. Summary table highlighting the sample types and treatment conditions carried forward for static binding assessment.

Base Resins	Bi-layering Technique	Buffer
Sephacrose 6 Fast Flow	Viscosity Enhanced	64 % Sucrose
		0.4% Carbopol® 934
Superose 6 Prep Grade	Microwave Assisted	60% Ethylene Glycol
Superose 12 Prep Grade		Deionised Water

With all the above taken into consideration with regard to screening for bromine stability, temperature ramping and buffer characteristics, Table 2.3 details the partial bromination conditions selected to create the bi-layered matrices. All three resins undergo the same partial bromination step, aiming for 10% bromination based on allyl quantification from the bromine assay with only the technique (viscosity enhanced or microwave assisted) and buffer being varied as points of comparison.

2.3.6 Plasmid Map & Quality Assessment

In order to critically assess the binding performance of the bi-layered matrices, the manufactured chromatography beads were challenged with two biological probes. The first of these was bovine serum albumin, a negatively charged (at pH 7.2) protein capable of infiltrating the entirety of the porous structure of all three media and binding to the ligands present.

The second is plasmid DNA, a much larger probe (see Fig. 2.14) which exceeds the exclusion limit of all three pores structures of the bi-layered resins (see Table 2.2). However, plasmid DNA is also negatively charged and will therefore bind to conventional anion exchange matrices as well as any surface ligands that still exist due to an inefficient bi-layering step. Both probes are well characterised and commonly used as analytical tools in the field of purification (Janzen *et al.*, 1990; Ljunglöf and Thömmes, 1998; Gustavsson *et al.*, 2004a; Latulippe and Zydney, 2009; Arpanaei *et al.*, 2010); bovine serum albumin is often used as a “model” protein while adsorption data concerning plasmid DNA is especially useful due to its use as a vector for gene therapy and DNA vaccines (Lara, Ramírez and Wunderlich, 2012; Scholz and Wagner, 2012).

Whilst the protein probe can be purchased as a lyophilised powder, the plasmid DNA is generated through a recombinant *Escherichia coli* fermentation and purified after cell lysis using filtration and capture anion exchange chromatography (see Section 2.2.10).

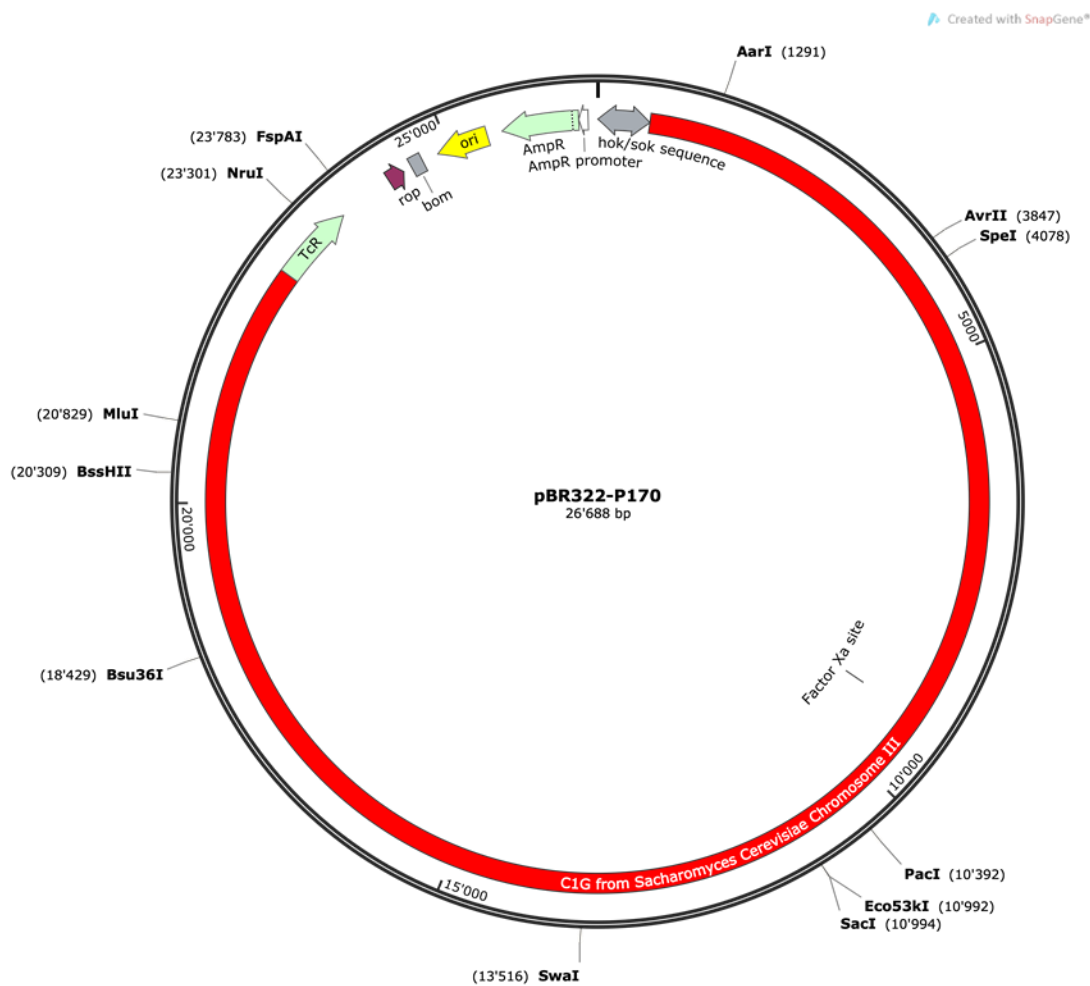


Fig. 2.13 Plasmid map of pBR322-P170 used as probe for assessing the chromatography media manufactured in-house.

Post-purification, it is important to determine the purity of the plasmid DNA sample and to ensure little co-purification of impurities such as cell debris, host cell proteins, RNA, organic compounds and chaotropic salts. This can be done using a spectrophotometric assay, across wavelengths 230, 260, 280 and 320 nm and using Equations 8, 9 & 10 to determine concentration, purity and salt carryover, respectively.

Equation 8:

$$pDNA \text{ Concentration } (\mu g/ml) = (A_{260} - A_{320}) \times 50 (\mu g/ml)$$

Equation 9:

$$pDNA \text{ Purity } (\mu g) = \frac{(A_{260} - A_{320})}{(A_{280} - A_{320})}$$

Equation 10:

$$\text{Salt Carryover} = \frac{A_{260}}{A_{230}}$$

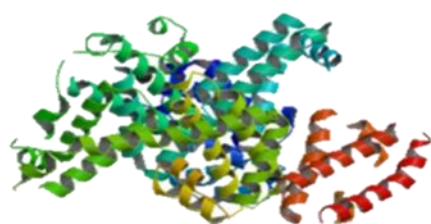
The results of this assay are summarised in Table 2.5 and are a result of scanning a small aliquot of the plasmid DNA stock (1 ml of the 270 ml stock created). According to Promega (Madison, NI, USA), an acceptable value for purity will lie in the range of 1.7 – 2. A value of 1.84 indicates low to no levels of impurities in the purified stock; the low absorbance value at 320 nm also emphasises low turbidity and further reaffirms the lack of presence of impurities in solution. Furthermore, Promega also state that ratios of 1.5 and greater indicate low to no carryover of organic compounds or chaotropic salts from the purification process, thus a ratio of 2.27 is another confirmation of a pure sample with little contamination present.

Table 2.5 Quality assessment of a sample of the master stock of purified plasmid DNA used during the static binding studies.

Concentration	Purity	Salt Carryover	Turbidity
(µg/ml)	(-)	(-)	(A _{320 nm})
56	1.84	2.27	0.02

2.3.7 Static Chromatography

Characterising and comparing the newly manufactured chromatography resins are carried out using static or “finite-bath” chromatography. In this methodology, chromatography beads are incubated with a solution containing a probe which interacts and binds to the matrix ligands under end-over-end mixing. A mass balance of the finite bath provides data on binding capacity and adsorption kinetics for each of the chromatography resins. These metrics are useful as points of comparison to assess the performance of each of the resins manufactured.



Bovine Serum Albumin

66.4 kDa

7 nm



Plasmid DNA

16.5 MDa

75 nm

Fig. 2.14 Comparison of the molecular weights and hydrodynamic radii of the two probes used in the chromatographic studies (GenScript, 2018; Thermo Fisher Scientific, 2018b). Probes with and without fluorescent dyes conjugated to the surface are contacted with the manufactured resins to assess their binding performance.

The two probes used in this study are indicated in Fig. 2.14 and, whilst both being negatively charged at the operating pH of 7.2, their size difference is exploited to characterise how well the bi-layering of the beads has been carried out. Plasmid DNA is a much larger molecule, with a molecular weight of 16.5×10^6 Da compared to 6.64×10^4 Da for Bovine Serum Albumin (Erickson, 2009). It is therefore expected that pDNA should only be able to bind to ligands (if present) on the surface of the supports, as the exclusion limits of all the supports are too small for the probe to diffuse further than the shell (see Table 2.2 for more detail). Conversely, Bovine Serum Albumin is a much smaller, negatively charged (at pH 5 and above) probe, capable of passing the shell of the matrix and infiltrating the bead to its core, saturating the trimethylamine (Q) ligands throughout the porous structure of the bead.

The relative degree of penetration explains why the plasmid DNA static binding capacity values are much lower than those obtained for Bovine Serum Albumin, as only the protein can diffuse throughout the bead and is thus exposed to and can interact with a higher concentration of ligands. This is illustrated in the relative binding capacities in Fig. 2.16 and is further demonstrated in subsequent confocal images in Section 2.3.8, where binding localisation is clearly illustrated and thus justifies their use as useful tools in assessing the degree to which bi-layering has been achieved.

The size and physiochemical properties of the probes are dependent on the environment that the probe is in, as the supercoiled plasmid DNA and quaternary structure of BSA will adopt varying conformations dependent on pH, temperature, ionic strength and polarity of the buffer that surrounds it (Damodaran and Kinsella, 1980; Takeda *et al.*, 1989; Kongraksawech *et al.*, 2006; Arkhangelsky *et al.*, 2008; Li *et al.*, 2008; Jiang *et al.*, 2013; Pabbathi, Patra and Samanta, 2013).

These changes are due to the species adjusting size and shape to achieve the most thermodynamically stable conformation in response to its surroundings, with respect to both its hydrophobic and hydrophilic/polar residues/chains that make up its structure. Provided the experimental conditions remain constant throughout the static binding studies, accurate comparisons can be drawn from each of the finite bath studies.

Finally, it is important to state that the two probes were challenged onto the beads in separate finite bath experiments. A “mixed-feed” study was avoided, to maintain clean binding to the resin for each individual probe and to prevent competitive binding and charge repulsion between the two species as well as complexes forming between the probes in solution due to hydrogen bonding (Seeman, Rosenberg and Rich, 1976); separating the probes into individual feeds would provide a more accurate indication of the performance of each of the manufactured chromatography media.

2.3.7.1 Control Isotherm Analysis

As a precursor to designing the static binding experiments, it is important to determine the maximum probe binding capacity for each fully functionalised resin type. This determines the highest amount a probe should bind to the resins with total functionalisation and provides a useful indication as to an appropriate loading concentration of the probe for static binding studies on the manufactured bi-layered matrices.

Adsorption isotherms were constructed for each of the fully functionalised (i.e. not core-shell) control matrices for both BSA and plasmid DNA, as highlighted in Fig. 2.15. Here, an increase in challenge concentration of the probe is applied, measuring free probe concentration (C^*) against mass of A bound to the supports (Q^*). A Langmuir model was applied to the experimental data as per Equation 11, resulting in quantification of Q_{\max} (the static binding capacity) and K_d (the adsorption coefficient - a measure of the rate of adsorption onto the chromatography beads). Comparative data for the three resins are detailed in Table 2.5.

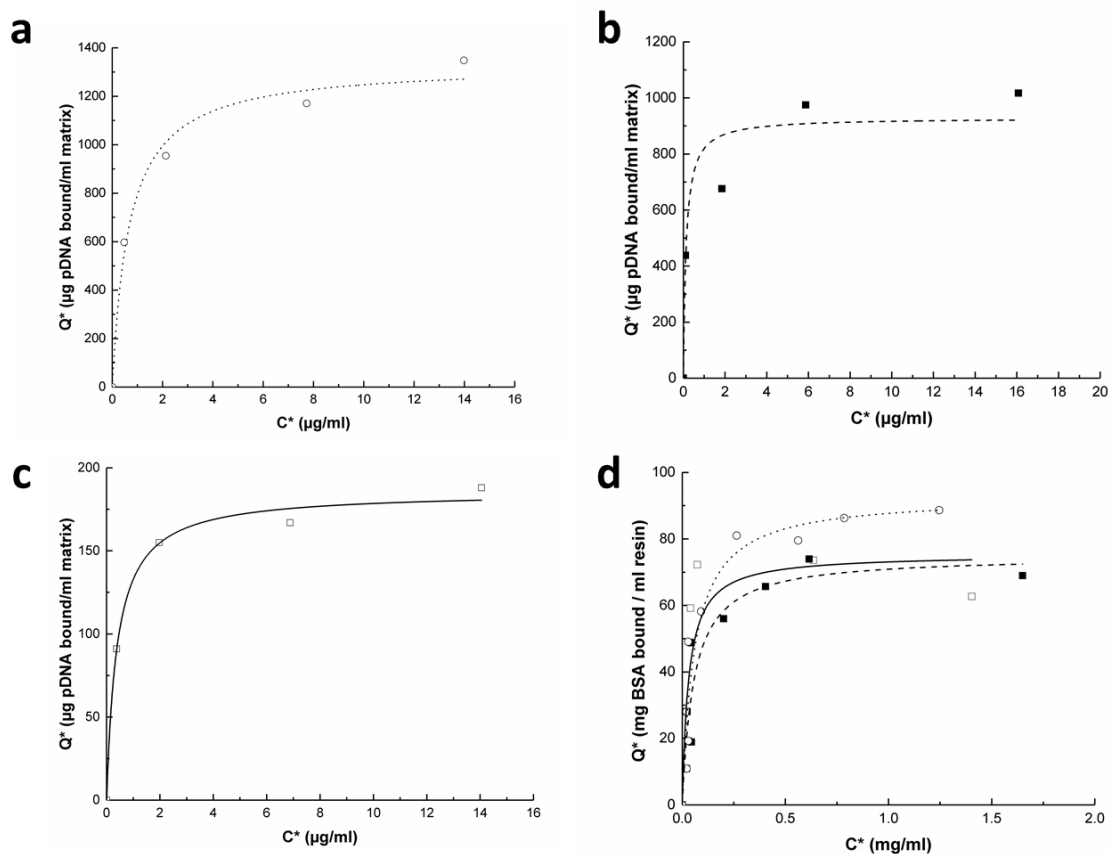


Fig. 2.15 Adsorption Isotherm data for BSA and plasmid DNA adsorption onto the fully functionalised supports which act as controls in this study. Plasmid DNA binding onto **a)** Superose 12 Prep Grade, **b)** Superose 6 Prep Grade and **c)** Sepharose 6 Fast Flow. **d)** BSA binding characteristics for all three resins as described above. Symbols: \square - Sepharose 6 Fast Flow, \blacksquare - Superose 6 Prep Grade, \circ - Superose 12 Prep Grade. A Langmuir model was fitted to each data set using Equation 11. Table 2.6 describes in detail the parameters derived from this set of curves.

Equation 11:

$$Q^* = \frac{Q_{max} \cdot C^*}{K_d + C^*}$$

Where:

- Q^* is the amount of pDNA or BSA bound to the support matrix
- C^* is the amount of free protein in solution
- Q_{max} (µg pDNA or mg BSA / ml resin) is the static or equilibrium binding capacity

- K_d (μg or mg/ml) is the adsorption coefficient (given the method of addition of plasmid DNA to the same batch of media for each data point, K_d is less valid and therefore not reported here).

Table 2.6 Langmuir fitting parameters for each of the control samples for the plasmid DNA probe (mean \pm SD, $n = 3$) as well as two commercial resins, *Q-Sepharose Fast Flow* (Anion Exchanger) and *Capto™ Core 700* (Bi-layered media)

		Sepharose 6	Superose 6	Superose 12	Q	Capto™
		Fast Flow	Prep Grade	Prep Grade	Sepharose Fast Flow	Core 700
Q_{\max}	pDNA					
	($\mu\text{g} / \text{ml}$ resin)	161 ± 5	929 ± 84	1332 ± 61	175	18
	BSA					
	(mg / ml resin)	75.35 ± 11.48	74.92 ± 6.69	92.82 ± 6.51	59	52
K_d	pDNA					
	($\mu\text{g} / \text{ml}$ resin)	0.40 ± 0.06	3.54 ± 0.65	0.68 ± 0.15	-	-
	BSA					
	(mg / ml resin)	0.03 ± 0.02	0.06 ± 0.02	0.06 ± 0.02	-	-

The adsorption isotherm data reveal interesting characteristics about each of the respective resins. Both Superose 6 & 12 resins exhibited a significantly higher (~ 8 fold) binding capacity for plasmid DNA than the Sepharose 6 resin. This can be attributed to the smaller average bead size of the Superose media and thus higher surface area: volume ratio available for interaction with plasmid DNA. With respect to BSA, the maximum binding capacities are relatively similar, though as with plasmid DNA, Superose 12 has the highest binding capacity. As we will see later in later analysis of the bromine assay, Superose 12 samples generated the highest number of allyl groups of all three samples and thus a higher concentration of ligand can be conjugated onto the beads, resulting in larger binding capacities for both plasmid DNA and BSA.

Adsorption isotherm analysis was also carried out for two commercial resins as a point of comparison. The first was Q Sepharose Fast Flow; a strong anion-exchanger with a similar size distribution, pore size and cross-linking chemistry as Sepharose 6 Fast Flow, also functionalised with an identical trimethylamine chloride (Q) ligand used in this study. The second was Capto™ Core 700, a bi-layered media similar to those being manufactured in this study; both commercial resins are manufactured by GE Healthcare.

For Q Sepharose Fast Flow, static binding capacities of 59 mg and 175 µg / ml resin were established experimentally for Bovine Serum Albumin and plasmid DNA, respectively. This data corroborates well with the Bovine Serum albumin binding data observed in other studies (in similar buffer conditions) (Liu *et al.*, 2007) as well as the control binding data in Fig. 2.16. The functionalised Sepharose 6 Fast Flow control in Table 2.5 for plasmid DNA also corroborates well with this figure for plasmid DNA binding in Q Sepharose Fast Flow. For Capto™ Core 700, static binding capacities of 52 mg and 18 µg / ml resin were established for Bovine Serum Albumin and plasmid DNA, respectively.

The data for the two probes on both types of resin were then utilised as decisional tools for informing an appropriate loading concentration in the subsequent static binding studies. The data provides an indication of suitable ranges for the loading concentration such that an appropriate challenge can be selected which will provide sufficient material to detect binding differences between samples whilst also avoiding over saturation of the chromatography media (and thus exaggerated aggregative pseudo-binding characteristics on the surface of the beads, especially for plasmid DNA). In addition, the load concentration also considers economical experimental design, preserving finite probe and chromatography resin material.

Against this, a load of 5 mg of Bovine Serum Albumin and 15 µg of plasmid DNA were challenged onto 0.05 ml of the manufactured bi-layered resin to determine the matrices' performance, as detailed in Section 2.2.11.3. In this way, a sufficient amount of probe material would remain in the bulk liquid phase to draw accurate comparisons between the matrices tested.

2.3.7.2 Bi-layered Beads Performance Characterisation

A facile method of comparing the various bi-layered matrices for their adsorption performance is via a selectivity index, as detailed in Equations 12 and 13. In essence, the selectivity index (SI) quantifies how well the bi-layered sample retains core-binding (Bovine Serum Albumin binding capacity) and how well it excludes shell-binding (plasmid DNA binding capacity) compared to the fully functionalised control made from the same base matrix. The lower the value of the selectivity index, the better performing the resin, as an ideal bi-layered matrix will maximise core BSA binding with minimal surface plasmid DNA binding.

Equation 12:

$$\% \text{ Reduction in probe SBC} = \frac{\text{Probe SBC}_{\text{Control}} - \text{Probe SBC}_{\text{Sample}}}{\text{Probe SBC}_{\text{Control}}}$$

Equation 13:

$$\text{Selectivity Index } (\mu\text{g pDNA} / \text{mg BSA}) = \frac{\text{SBC pDNA}}{\text{SBC BSA}}$$

Where:

- The probe refers to either plasmid DNA or BSA
- SBC is the static binding capacity for a matrix (mg or μg / ml resin)
- The control sample is one which has been fully functionalised without any bi-layering
- Sample refers to any material which has been partially brominated to create a bi-layered matrix

Table 2.7 *Allyl contents introduced into commercial agarose base matrices following reaction with AGE.*

Matrix	Allyl content ($\mu\text{mol/ml}$)
AGE-activated Sepharose 6 Fast Flow	326.6 ± 26.5 (n=9)
AGE-activated Superose 6 Prep Grade	348.4 ± 14.4 (n=9)
AGE-activated Superose 12 Prep Grade	477.6 ± 20.5 (n=9)
AGE-activated Sepharose CL6B	315.7 ± 25.5 (n=24)

Table 2.7 shows the allyl contents of the various agarose based supports following full activation with AGE. Included for sake of comparison are values obtained by Karchanasi (2013) for the AGE activation of Sepharose CL6B. Allyl groups are generated by reacting allyl glycidyl ether with the hydroxyl residues present on the agarose matrix, as illustrated in Fig. 2.3. Not surprisingly, the allyl densities of AGE activated reflected their agarose contents. Allyl densities of the three 6% agarose base matrices were roughly similar while that of Superose 12 PG was ca. 50% higher. As noted earlier (2.2.3.1) the values in Table 2.7 were employed to calculate the amount of bromine required to react with 10% of the reactive allyl groups in each support type.

The relative success of viscosity enhanced compared to microwave assisted appears dependent on the type of resin and buffer system, with no evident superior partial bromination technique based on the bromine assay. Fig. 2.16 summarises the reduction in static binding capacity and raw static binding data across all the samples, with controls included for reference. One would expect a high

level of partial bromination would result in a complete reduction in plasmid DNA binding and a significant proportion of core BSA reduction.

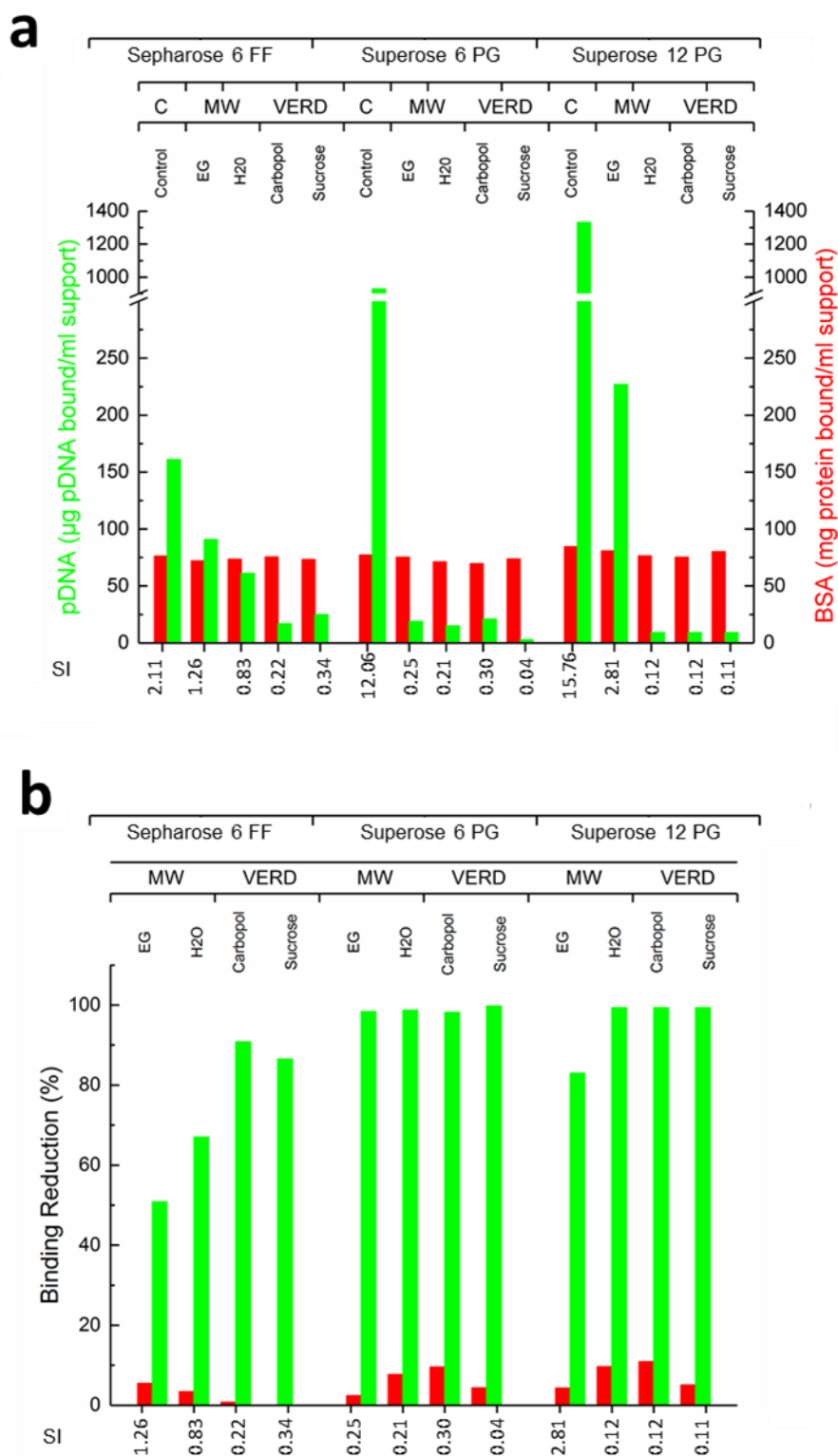


Fig. 2.16 a) Percentage binding reduction for probes *plasmid DNA* & *BSA* for each base resin and manufacturing condition, relative to the fully functionalised control samples; selectivity indices (SI) are calculated via Equations 12 & 13. **b)** Original static binding capacity data for each sample type. H₂O & EG refer to deionised water and Ethylene Glycol, respectively.

Comparing across the three resins, the Superose Prep Grade media displayed significantly higher selectivity indices, with all but one eliminating $\geq 98\%$ of plasmid DNA binding. Some of these were at the cost of a reduction in BSA binding, for instance Superose 12 Prep Grade partially brominated with a 0.4% (w/v) Carbopol® viscosity enhancing buffer, which reduced the core binding by nearly 11%.

Sepharose 6 Fast Flow was the poorest performing resin; although reduction in core binding capacity was generally low, the partial bromination failed to sufficiently eliminate surface plasmid DNA binding. Despite the high partial bromination percentages across the samples, the low selectivity indices can be attributed to the physical size of the beads, being much larger than the other two media can lead to mixing issues and lack of exposure of the entire surface of the beads to the brominating buffer. This can be observed in Section 2.3.8.3, with “patchy” plasmid DNA binding, which explains the limited 50 – 90% reduction in surface binding and thus the low selectivity indices.

In evaluating the partial bromination techniques across the Superose media, for the microwave assisting buffers, deionised water performed consistently better than 60% ethylene glycol, predominantly due to the incomplete elimination of surface binding. In the case of Superose 6 Prep Grade, both conditions achieved similar selectivity indices but for opposing reasons. With deionised water, a more significant proportion of core binding is lost but a higher degree of shell binding is eliminated. The reverse is true for 60% (v/v) ethylene glycol, where core binding is preserved at the expense of a small proportion of shell binding.

This trend is strongly apparent in the Superose 12 Prep Grade media; where a high proportion of allyl groups are generated and the bromine that has been added is either insufficient in quantity and/or is reacting too quickly (with the supports and the buffer) to cover the entire surface of the resin. The rapid reaction time can be attributed to the high $\tan \delta$ value of 60% (v/v) ethylene glycol relative to deionised water. This can result, again, in “patchy” surface binding, as is evident in the fluorescent images in Fig. 2.1.8.

This hypothesis is further supported in that very little core binding of the protein is compromised in the 60% Ethylene Glycol samples compared to the deionised water sample (which should theoretically react slower due to a lower tangential loss factor). This gives the bromine molecules sufficient time to diffuse around the surface of the beads as well as into the porous support before the bromine reaction can take place, resulting in more complete elimination of surface binding, but at the cost of some loss of core binding, as is reflected in Fig. 2.16.

The 64% Sucrose technique produced the highest selectivity indices for a viscosity enhancer and as a technique overall, eliminating 99% of plasmid DNA at the expense of only 4% and 5% compromise in core Bovine Serum Albumin binding for Superose 12 and 6 Prep Grade samples, respectively. Compared to the 64% Sucrose samples, surface binding of the plasmid DNA was lower for Carbopol® samples, which correlates with the slightly reduced partial bromination achieved.

Interestingly, the Carbopol® samples had inferior selectivity indices mainly as a result of significant core binding loss (compared to the 64% Sucrose samples) indicating that the buffer facilitates better mass transport of bromine molecules into the core of the porous support rather than reacting with the surface of the beads, even at lower partial bromination percentages. As these are highly porous resins, with an intra-particle porosity in the range of 85% (Carta and Jungbauer, 2010), the buffer the beads are suspended in (and “filled” with) will have an impact on both the experimental pore size and mass transfer characteristics within the resin.

Although both buffers have similar viscosities, the high percentage of sucrose can both “close-off” pores and hinder diffusion into the resin through molecular interactions, including hydrogen bonding, between the sucrose polymer and the agarose beads. This can lead to steric hindrance of the bromine molecules as they diffuse via the buffer into the porous supports. Conversely, the highly aqueous nature of the Carbopol® buffer can aid mass transfer of the bromine into the porous support. This benefits the sucrose buffers in that bromination is limited mainly to the surface and thus preserves core binding, consequentially leading to better selectivity indices.

2.3.8 Confocal Laser Scanning Microscopy

Whilst the static binding data provides a solid foundation for a comparative assessment of the chromatography samples, a useful corroborative study was run in parallel using fluorescent probes. Bovine Serum Albumin was labelled with Texas-Red X, attaching covalently to the abundant lysine residues on the protein via a succinimidyl ester on the dye whilst plasmid DNA was labelled with Syto™ 9, a minor-groove binding dye. Both labelling reactions were carried out in a controlled fashion to ensure an appropriate probe: dye ratio was attained (see Section 2.2.11.6 for more details) as well as any un-conjugated dye either removed or accounted for.

The fluorescent studies were run as identical experiments to the original static binding capacity studies utilising the same load concentrations for the probes and settled bed volumes for the chromatographic media.

2.3.8.1 Correcting for Auto-Fluorescence

It is important to optimise microscope and image acquisition settings prior to excitation of the sample, imaging and interpretation of the images. Fig. 2.17 highlights the importance of correcting for auto-fluorescence which can occur when the sample is excited by a photon source. In this case, no auto-fluorescence was observed when the beads were excited with a 568 nm laser, which was used to visualise the Bovine Serum Albumin-Texas Red X samples.

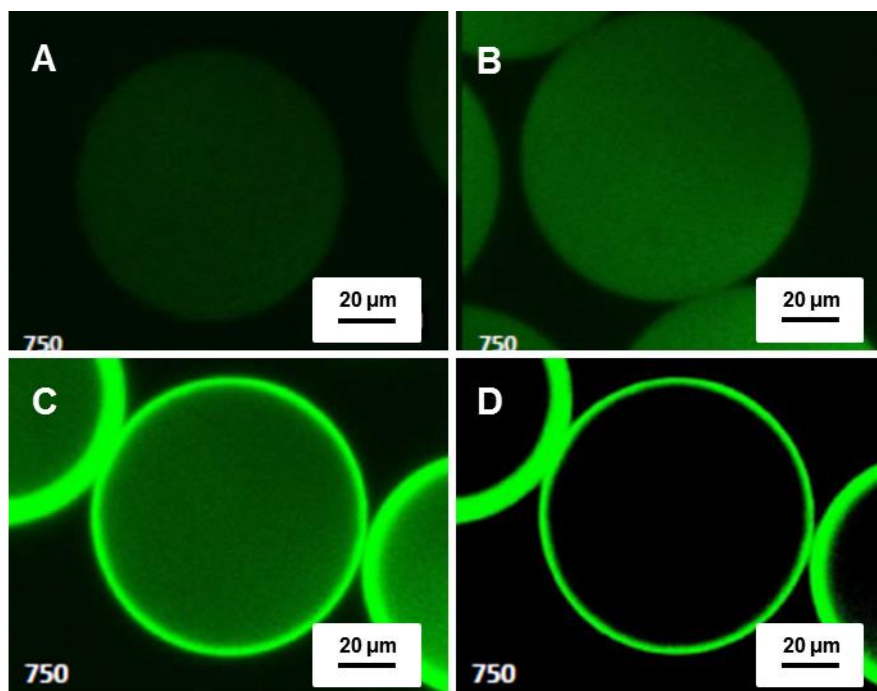


Fig. 2.17 Illustration of auto-fluorescence of the base and functionalised matrices and thresholding to eliminate the effect; **a)** Sepharose 6 Fast Flow, **b)** Sepharose 6 Fast Flow fully functionalised with the anion exchange ligand Q, **c)** sample B incubated with fluorescent plasmid DNA (pDNA-Syto™ 9) & **d)** sample C post-thresholding to remove auto-fluorescence from the chromatography bead. Note that the value in the bottom left corner corresponds to the gain value for each image.

However, for the plasmid DNA, which is excited by a 488 nm laser, a small degree of auto-fluorescence can be observed from the agarose base matrix and a slightly higher degree with the anion-exchange ligand functionalised to the matrix (Fig. 2.17 a) and b), respectively).

Interestingly, this indicates that some emission is being detected from both the agarose backbone and from the trimethylamine (Q) ligand.

Control samples were run loading the beads with solely un-labelled plasmid DNA to assess auto-fluorescence of the probe itself. Similar studies were run for Syto™ 9 label without DNA (at equivalent concentrations to the original samples), to trial levels of fluorescence of the Syto™ 9 dye binding to the anion-exchange ligands on the beads. The images attained for both control tests were qualitatively similar to Image B in Fig. 2.17, indicating little additional fluorescence for both.

Without correction, as seen in Image C, one could interpret this result as ingress of plasmid DNA into the core of the media, which, by reasonable size-exclusion principles, is not possible. In reality, this interior fluorescence is as a result of either un-conjugated dye binding to the core anion-exchange ligands (due to the relatively small size of the Syto-9 label) or auto-fluorescence of the beads themselves (likely a combination of both). This can be corrected when you consider that the Syto-9 stain “exhibits enhanced fluorescence upon binding (to plasmid DNA)” (Thermo Fisher Scientific, 2018c).

By evaluating the level of auto-fluorescence in Image B, it is possible to correct Image C by either adjusting the gain value, lowering the laser intensity, or in this case, a method known as thresholding. The former two require adjustments needed to be carried out prior to image acquisition, whereas image thresholding can be carried out post-acquisition. For the sake of comparison, the laser intensity and gain were kept constant across all samples unless otherwise stated. On occasion, the gain will be adjusted in order to pick up sufficient signal to generate a comprehensible image; corresponding values for each sample are stipulated in each individual image shown.

The gain value corresponds to the sensitivity of the photomultiplier tube, which collects the electronic signal from the sample after it has been excited with the laser. This data is processed and digitised by the computer and each pixel has an associated intensity value assigned (grey levels) for 8-bit storage, ranging from 0 – 255 (Nikon, 2018). This range of grey levels can be thresholded to remove any noise or, in this case, background auto-fluorescence. The result of this thresholding can be seen in Image D, where only plasmid DNA-Syto™ 9 probe binding can be observed.

2.3.8.2 Control Samples

A natural starting point for the confocal laser scanning microscopy studies was to assess the functionalised control samples; these are the samples that have undergone complete saturation with bromine and subsequently hydrolysed and coupled with trimethylamine chloride (Q). These samples exhibit no bi-layering and are used as yardsticks to compare the bi-layered matrices against. Fig. 2.18 illustrates the light microscopy and corresponding florescent microscopy for each sample.

The disparity in fluorescence visualised in the samples is a useful insight into the importance of time in fluorescence work and how the age of samples and fluorophore conjugates has an impact on the quality of the image attained.

The brighter images (Sephacrose 6 Fast Flow – Plasmid DNA, Superose 6 – Bovine Serum Albumin & Superose 6 – Plasmid DNA) were all imaged within min of completing the incubation time; however the other samples in the set were inhibited by a time delay of up to one day. Fluorescence can be lost with respect to time, usually by a photo-bleaching mechanism where the fluorophore is destroyed via exposure to excitation light, or by a quenching mechanism due to short-range interactions between the fluorophore and the local molecular environment (Thermo Fisher Scientific, 2018a).

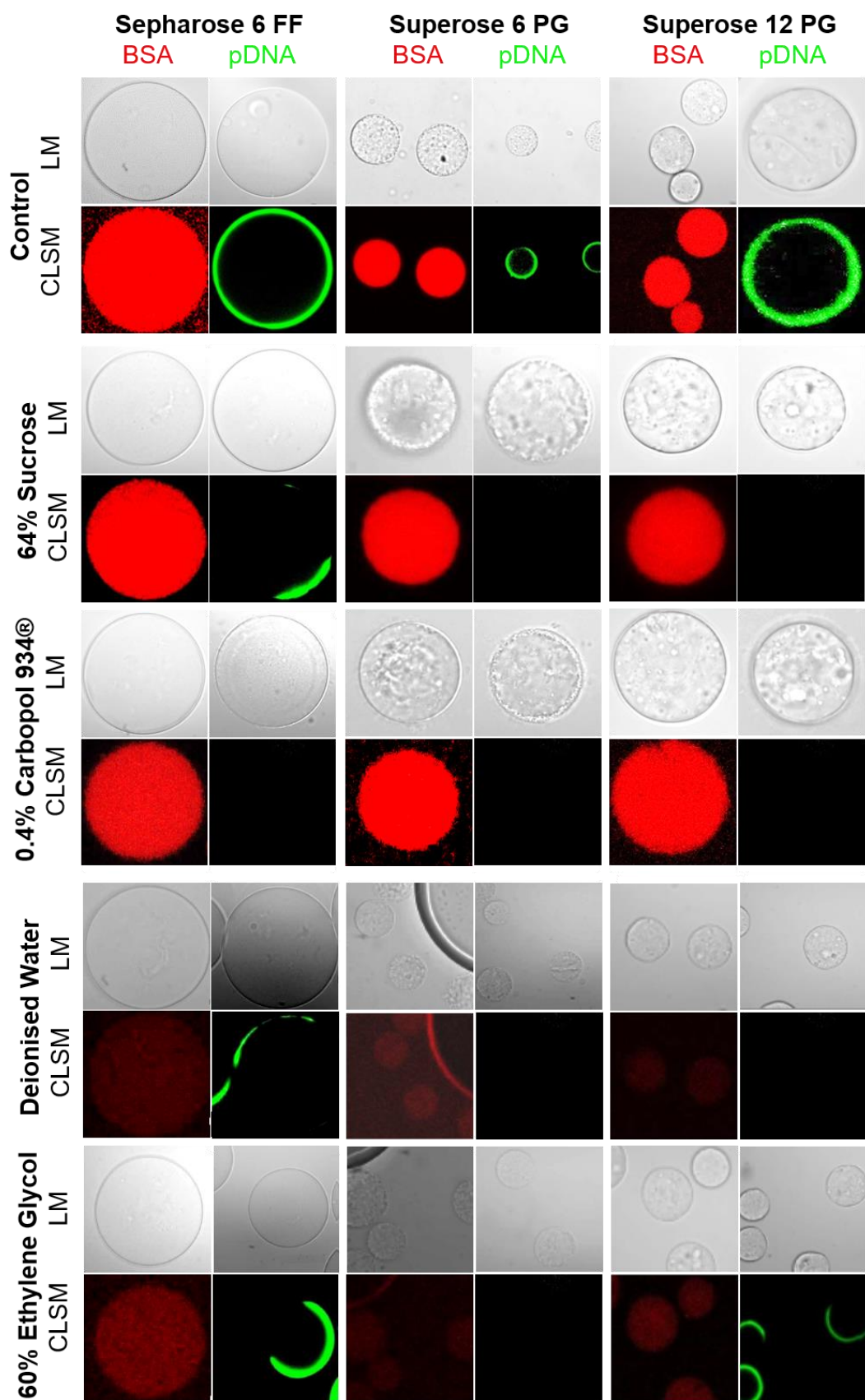


Fig. 2.18 Light Microscopy (LM) & Confocal Laser Scanning Fluorescent Microscopy (CLSM) images for the fully functionalised samples and bi-layered materials challenged with BSA and plasmid DNA.

In addition to fluorescent degradation by either bleaching or quenching, a second reason of matrix age may aid in rationalising the contrasting fluorescent intensities. An example of this is Superose 6 Prep Grade – BSA; as a result of a damaged original batch, the sample was manufactured and incubated with its respective probe within one day, thus giving it a different “age” to the other samples. The particularly striking fluorescence (even at a lowered gain value) may point to some degree of probe loss, or “ligand leakage” with respect to time; a phenomenon common in both ion-exchange and especially affinity chromatography (Gribnau and Tesser, 1974; Johansson, Hellberg and Wennberg, 1987; Levison and Pathirana, 1996). Importantly, for the quantitative static binding studies, all three resins were from their original batches and thus challenged with probes at the same matrix age.

All three resin types had similar BSA static binding capacities (~ 68 mg / ml resin) and quite varied plasmid DNA static binding capacities, ranging from 161 – 1332 μ g / ml resin). The fluorescence in the images does not equate perfectly with the static binding data and emphasises the need to have static binding data as a quantitative measure of comparison between the manufactured resins. However, the confocal microscopic data can be a useful tool if used qualitatively to corroborate trends illustrated in the finite bath studies and identify potential inconsistencies in binding, such as “patchy” binding, as observed in Section 2.3.8.3.

2.3.8.3 Bi-Layered Samples

Fig. 2.18 also summarises the bi-layered samples by light microscopy and confocal laser scanning microscopy images, grouping them by base matrix and type of bi-layering technique. The light microscopy images are useful as they provide supporting evidence that the bead(s) being imaged are in the correct focal plane, even if a fluorescent image is not visible (in the case of some of the high SI matrices incubated with plasmid DNA).

On the whole, the image panels marry well across to the static binding studies results. For instance, the poor selectivity indices for the Sepharose 6 Prep Grade bi-layered materials is clearly due to incomplete elimination of plasmid DNA binding on the surface of the beads.

This is likely a direct result of both bromine reactivity with the buffer and inefficient mixing during the partial bromination step, especially for the microwave samples, where the increased in temperature has accelerated reaction rates with both the buffer and supports. This has resulted in the remaining limited bromine molecules to react rapidly and only on a limited surface area of the beads, leaving allyl groups exposed on the surface to allow for Q-coupling. This ultimately leads to “patchy” binding of plasmid DNA, clearly evident in multiple bi-layered samples manufactured from Sepharose 6 Fast Flow.

Additionally, the degree to which the plasmid DNA binding capacity has been reduced is also evident in the Sepharose 6 Fast Flow fluorescent images, with the two microwave samples (60% v/v ethylene glycol - 50% reduction in plasmid DNA binding and Deionised water - 60% reduction in plasmid DNA binding) showing high amounts of fluorescent plasmid DNA around the surface of the beads whilst 0.4% Carbopol® (90% reduction in plasmid DNA binding) exhibits no visible plasmid DNA fluorescence around the beads and 64% Sucrose (86% reduction in

plasmid DNA binding) exhibiting some patches of plasmid DNA binding but significantly less than the microwave assisted samples.

With respect to the two Superose Prep Grade media, the percentages of plasmid DNA binding reduction are $\geq 98\%$, barring the Superose 12 Prep Grade microwave assisted sample with 60% Ethylene Glycol (82% reduction), which again exhibits some patchy binding of plasmid DNA to the surface of the beads.

2.3.8.4 Commercial Resin Comparison

Naturally it makes sense to draw comparisons between the commercially available Capto™ Core 700 bi-layered material and the resins manufactured in house. Importantly, Capto™ Core 700 is functionalised with a different ligand, octylamine, as opposed to trimethylamine chloride (Q); due to its different structure, octylamine has both anion-exchange and hydrophobic interaction capabilities.

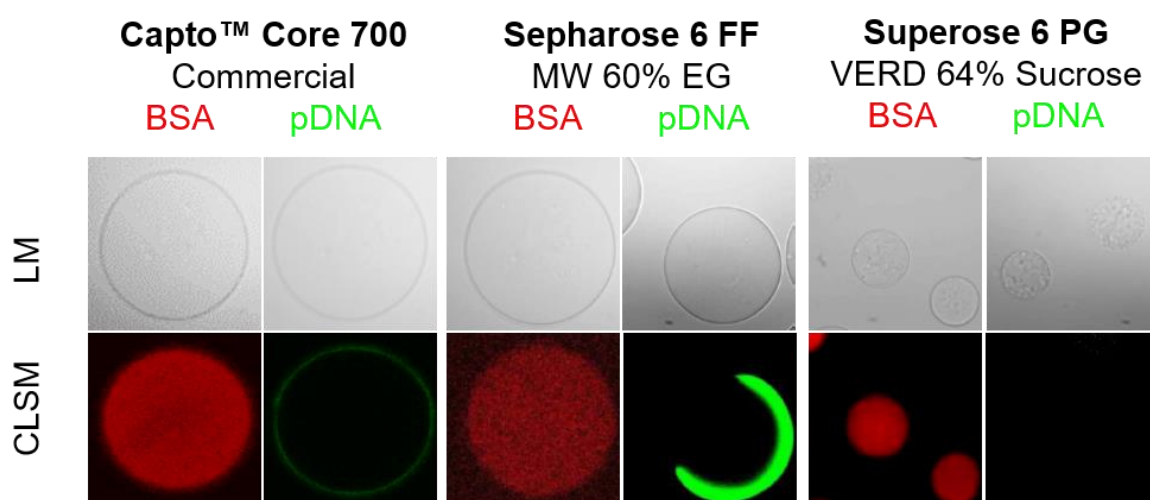


Fig 2.19 Light Microscopy (LM) & Confocal Laser Scanning Fluorescent Microscopy (FM) images comparing the commercial Capto™ Core 700 resin against the worst & best performing resins.

Here we compare the commercial resin against the best and worst performing manufactured chromatography resins. As no commercial resin fully functionalised with octylamine exists as a control for Capto™ Core 700, static binding capacities are used as a point of comparison in lieu of selectivity indices.

The bi-layering process has had little impact on the static binding capacities of the proteins for the two manufactured resins, with a comparable amount also bound to the commercial bead, despite the difference in ligand. Notably, some plasmid DNA binding is picked up for the Capto™ Core 700 resin, supported by the spectrophotometric data indicating that the shell is not completely inert. This is likely due to ligands still present on the surface of the beads, with a more accentuated

effect seen with the Capto™ Core 700 due to its highly potent, bi-functional octylamine ligand. In the context of maximising plasmid DNA yield in a bioprocess, it is clear that the Superose 6 Prep Grade media performs the best of the three.

2.3.9 Environmental Scanning Electron Microscopy

Electron Microscopy facilitates high resolution visualisation of the surface of the chromatography beads and Fig. 2.21 highlights differences in the surface morphology of the base matrices and bi-layered beads manufactured in this study. The rationale was to observe differences in bead morphology and surface porosity between the three starting matrices and any significant differences in surface configuration once the beads have been functionalised fully or in bi-layering.

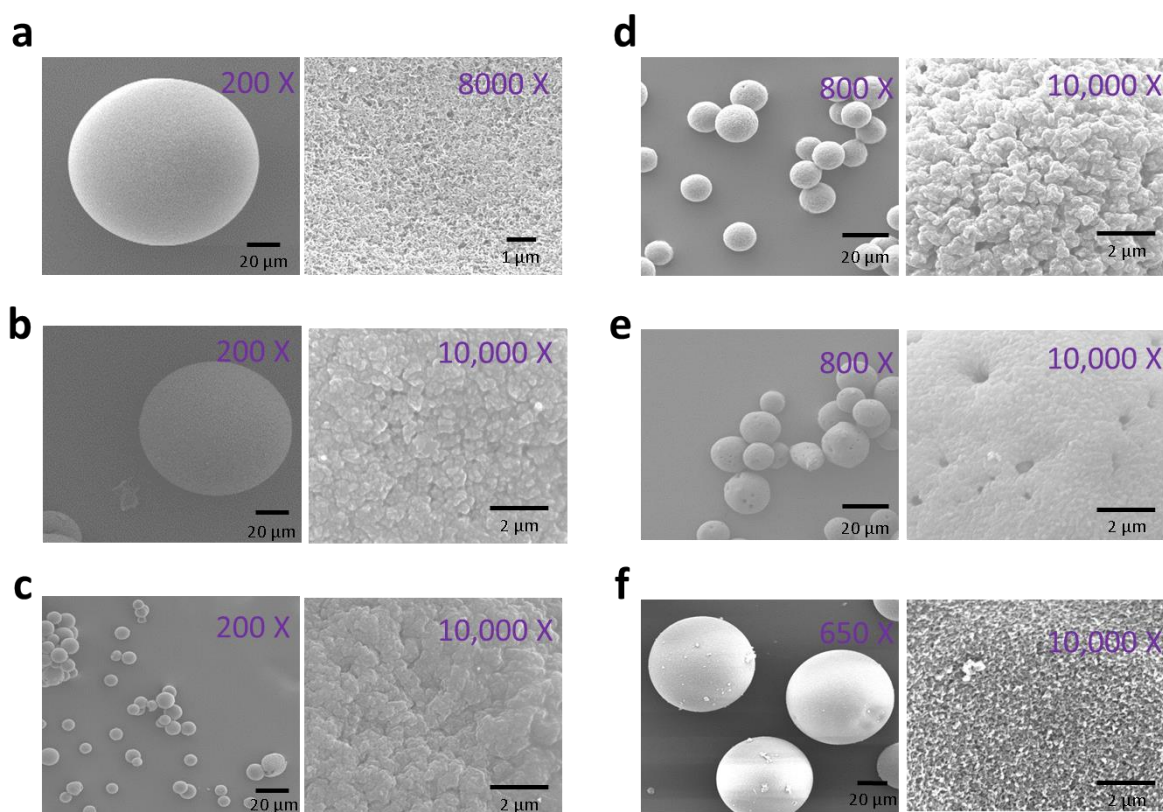


Fig. 2.20 Scanning electron micrographs of a number of commercial chromatography resins, taken at low and high magnifications (in purple text) to gauge bead size and surface morphology/porosity, respectively. **a)** Capto™ Core 700, **b)** Q Sepharose Fast Flow, **c)** Sepharose 6 Fast Flow, **d)** Superose 6 Prep Grade, **e)** Superose 12 Prep Grade & **f)** Capto™ Q. Wherever possible, images were taken which were representative of the entire sample, i.e. significantly damaged/difficult to image beads were avoided.

The micrographs reveal interesting differences between the various commercial resins; purely in terms of size the sizes corroborate well with sizing data illustrated in Fig. 2.6, with the Capto™ and Sepharose media much larger compared with the two Superose media. The composition and starting polymer gives the Capto™ resin better bead uniformity, in terms of size and also fewer defects.

Fig. 2.20 also highlights how the degree of cross-linking affects the porosity of the media that can be seen on the surface of the media. At 10,000 X magnification, the Sepharose 6 and Superose 6 media appear to be much more porous than the Superose 12 surface, appearing to have clusters with nanometre scale spaces in between them. The Superose 12 surface, at the same magnification, has no such apparent gaps, with a smoother, sheet-like surface.

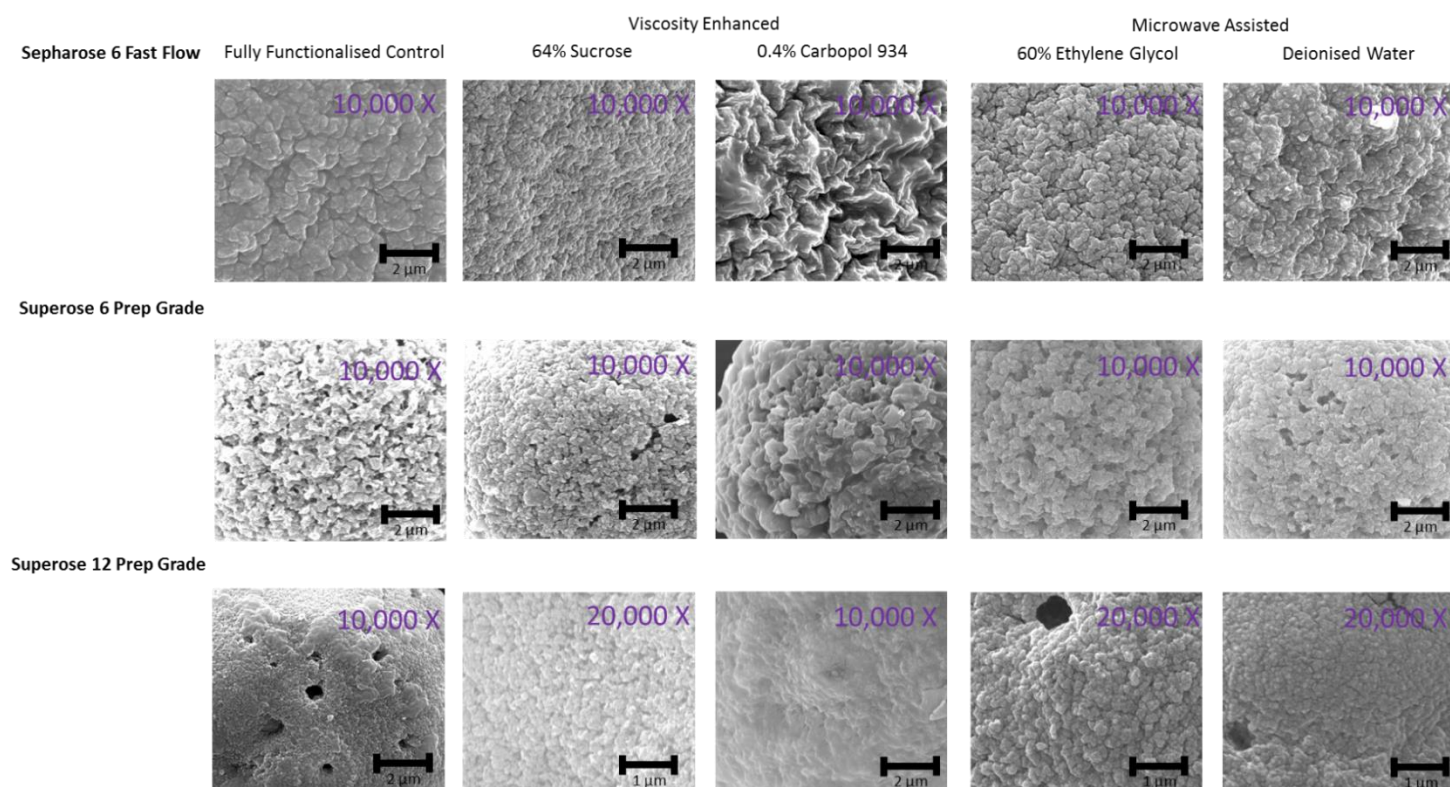


Fig. 2.21 Scanning electron micrographs of the functionalised control chromatography resins and bi-layered matrices, organised by method and type of starting matrix. Images were taken at high magnification only as, at lower magnifications, the resins were qualitatively similar to the original starting matrices.

The micrographs for the treated samples reveal intriguing differences between the bead types and partial bromination routes. The fully functionalised control beads bear a great deal of resemblance to their base matrices illustrated in Fig. 2.21. For Sepharose 6 Fast Flow, the most striking difference is the sample partially brominated with 0.4% Carbopol® 934, which appears much rougher with much taller peaks and deeper crevices than the other samples of its type, which exhibit a pockmark effect on the surface. This deep crevice effect can also be seen to some degree with the Superose 6 media, though not at all with the Superose 12 media, perhaps due to its close knit cross-linking structure.

This surface effect may be due to an interaction between the polymer and the matrix, effectively leading to a thin coating/film of Carbopol® 934 forming over the surface of the bead, even after multiple washes of the bead. The effect seems to be more prominent in the 6% cross-linked

matrices, perhaps due to the larger porosity providing more surface area for the polymer to interact with.

This corroborates well with the static binding data, as this thin film can improve selectivity indices in two ways, either by restricting bromine diffusion into the bead and thus forcing bromination solely on the surface, or by “sealing off” both the pores and the ligands on the surface to limit plasmid DNA binding. This is further emphasised in that, compared with 64% Sucrose, and for all three media, the partial bromination route with 0.4% Carbopol® 934 has a higher percentage reduction in binding in BSA, indicating that a 0.4% Carbopol® 934 film is restricting access to both probes. From an experimental front, it was noticed during washing steps that the Carbopol® 934 samples took abnormally long to vacuum dry, which is a further inference that the Carbopol® 934 is hindering mass transfer within the beads.

Another interesting feature highlighted by the electron micrograph images is the presence of round holes in the media, most predominantly in the Superose 12 matrices. The worst of the samples was that of the microwave assisted 60% Ethylene Glycol, which marries up well with the static binding data, with this sample binding the highest proportion of plasmid DNA for the bead type. Depending on when and how these holes formed, these structural defects could have an impact on the partial bromination step as well as the probe binding experiments. The holes could aid diffusion of bromine into the core of the bead, which supports the relatively high loss of BSA binding and low reduction in plasmid DNA binding for the Superose 12 samples.

With respect to the probe binding experiments, the holes could either be providing additional surface area on the exterior of the bead for the plasmid DNA to bind, or, given the size of some of holes, providing channels into the core of the bead, providing access to the abundance of functionalised ligands present in the interior of the bead. It seems more likely that the holes, much like the roughed surfaces of the beads, provide additional surface area for the plasmid DNA to interact with thus diminishing the selectivity indices of these particular beads.

It is important to consider at this point that these features, including the pockmarking, deep crevices and holes, could potentially stem from the bead’s manufacturing process. Multiple cycles of washing, scraping the beads off vacuum filters, centrifugation and re-suspension during their manufacture may have caused shear damage to the bead’s surface, resulting in a much rougher exterior.

Alternatively, the method of dehydration required for electron microscopy may be the underlying cause for the diverse surface appearances. It could be envisaged that, as the beads are highly porous and principally composed of (and thus structurally supported by) an aqueous buffer, removing this water could have a detrimental impact on the structure and morphology of the beads. Curiously, the beads that have the highest percentage of cross-linking (and theoretically the most rigid structure) have the highest degree of damage. This may be due to adverse effects of dehydration on the cross-linker itself, causing disruption in the agarose backbone chains, leading to holes forming in the surface of the beads.

Environmental Scanning Electron Microscopy – Energy Dispersive X-Ray (E-SEM/EDX) analysis was attempted on the samples shown in this section in an attempt to pick up changes in elemental composition on the surface of the resins. Unfortunately, the resolution of this technique is not high enough to observe incremental changes in the surface composition of the beads, i.e. changes in concentration of nitrogen from the Q ligand. It is suggested that either Cryo-SEM is utilised, whereby the samples are sliced using a microtome, revealing interior sections of the bead which can be scanned for elemental composition.

Conversely, the signal from EDX can be enhanced by using a heavier element probe, which would need to be designed to bind to the anion-exchange ligand prior to imaging (e.g. Au nanoparticles covalently linked to a protein which could bind to the ligands and highlight, albeit indirectly, the spatial distribution of the ligand within the bead using E-SEM/EDX).

2.4 Conclusions

This study demonstrates the manufacture of chromatography resins with a bi-layered architecture, formulated under varying conditions and subsequently tested to determine binding performance using both quantitative colorimetric assays and qualitative microscopic imaging.

The results from this study highlight that bi-layering is achievable with all three matrices tested, with varying degrees of success. Both viscosity enhanced and microwave assisted partial bromination proved to be viable techniques, though with variable performances, depending on the type of buffer and starting resin used. The most effective of the three resins was Superose 6 Prep Grade, partially brominated with 64% Sucrose, with a selectivity index of 370, mainly due to its smaller bead volume and comparatively larger pore sizes, which aid mass transfer mechanisms during the partial bromination step. Superose 12 also achieved notably high selectivity indices for both 64% Sucrose as a viscosity enhancer and deionised water as a microwave assisting buffer.

The confocal laser scanning images corroborated well with the quantification data and illustrates its use as a powerful tool for assessing and troubleshooting chromatography resins in both analytical and process purification contexts. It is hoped that the data attained from the screening studies, static binding quantification and microscopy can be used as tools for informing the development of an even better generation of chromatography materials which can ultimately be used at process chromatography scale in the purification of gene therapy vectors and vaccines.

2.5 References

- Agrawal, D.K., 1998. Microwave processing of ceramics. *Curr. Opin. Solid State Mater. Sci.* 3, 480–485. doi:10.1016/S1359-0286(98)80011-9
- Aida, T., Akasaka, T., Furukawa, N., Oae, S., 1976. Catalytic Reduction of Sulfoxide by Bromine-Hydrogen Bromide System. *Bull. Chem. Soc. Jpn.* 49, 1117–1121. doi:10.1246/bcsj.49.1117
- Arkhangelsky, E., Steubing, B., Ben-Dov, E., Kushmaro, A., Gitis, V., 2008. Influence of pH and ionic strength on transmission of plasmid DNA through ultrafiltration membranes. *Desalination* 227, 111–119. doi:10.1016/J.DESAL.2007.07.017
- Arpanaei, A., Winther-Jensen, B., Theodosiou, E., Kingshott, P., Hobley, T.J., Thomas, O.R.T., 2010. Surface modification of chromatography adsorbents by low temperature low pressure plasma. *J. Chromatogr. A* 1217, 6905–6916. doi:10.1016/j.chroma.2010.08.069
- Bergstrom, J., Berglund, R., Soderberg, L., 1998. Process for introducing a functionality.
- Burova, E., Ioffe, E., 2005. Chromatographic purification of recombinant adenoviral and adeno-associated viral vectors: methods and implications. *Gene Ther.* 12, S5–S17. doi:10.1038/sj.gt.3302611
- Carta, G., Jungbauer, A., 2010. Protein chromatography: process development and scale-up. Wiley-VCH.
- Chon, J.H., Zarbis-Papastoitis, G., 2011. Advances in the production and downstream processing of antibodies. *N. Biotechnol.* 28, 458–463. doi:10.1016/j.nbt.2011.03.015
- Close, E.J., Salm, J.R., Iskra, T., Sørensen, E., Bracewell, D.G., 2013. Fouling of an anion exchange chromatography operation in a monoclonal antibody process: Visualization and kinetic studies. *Biotechnol. Bioeng.* 110, 2425–2435. doi:10.1002/bit.24898
- Collins, M., Thrasher, A., 2014. Gene therapy: progress and predictions. *Proc. R. Soc. B* 282. doi:10.1098/rspb.2014.3003
- Damodaran, S., Kinsella, J.E., 1980. Stabilization of Proteins by Solvents Effect of pH and anions on the positive cooperativity of 2-nonanone binding to bovine serum albumin. *J. Biol. Chemistry* 255, 8503–8508.
- Diogo, M.M., Queiroz, J.A., Prazeres, D.M.F., 2005. Chromatography of plasmid DNA. *J. Chromatogr. A* 1069, 3–22.
- GenScript, 2018. Nucleic Acids and Protein Calculations [WWW Document]. URL <https://www.genscript.com/conversion.html> (accessed 1.23.18).
- Gilbert, J.C., Martin, S.F., 2011. Experimental organic chemistry: a miniscale and microscale approach. Brooks/Cole Cengage Learning.
- Greenwood, N., Earnshaw, A., 1997. Chemistry of the Elements, 2nd ed. Butterworth-Heinemann.
- Gribnau, T.C., Tesser, G.I., 1974. Ligand-leakage in affinity chromatography, a mathematical approach. *Experientia* 30, 1228–30.
- Gronemeyer, P., Ditz, R., Strube, J., 2014. Trends in Upstream and Downstream Process Development for Antibody Manufacturing. *Bioengineering* 1, 188–212.

doi:10.3390/bioengineering1040188

- Gustavsson, P.-E., Lemmens, R., Nyhammar, T., Busson, P., Larsson, P.-O., 2004a. Purification of plasmid DNA with a new type of anion-exchange beads having a non-charged surface. *J. Chromatogr. A* 1038, 131–140. doi:10.1016/J.CHROMA.2004.03.050
- Gustavsson, P.-E., Lemmens, R., Nyhammar, T., Busson, P., Larsson, P.-O., 2004b. Purification of plasmid DNA with a new type of anion-exchange beads having a non-charged surface. *J. Chromatogr. A* 1038, 131–140. doi:10.1016/J.CHROMA.2004.03.050
- Hayes, B.L., 2002. Microwave synthesis : chemistry at the speed of light. CEM Pub.
- Horikoshi, S., Serpone, N., 2013. Microwaves in nanoparticle synthesis : fundamentals and applications. Wiley-VCH.
- Horn, N.A., Meek, J.A., Budahazi, G., Marquet, M., 1995. Cancer Gene Therapy Using Plasmid DNA: Purification of DNA for Human Clinical Trials. *Hum. Gene Ther.* 6, 565–573. doi:10.1089/hum.1995.6.5-565
- Hubbich, J., Kula, M.R., 2008. Confocal laser scanning microscopy as an analytical tool in chromatographic research. *Bioprocess Biosyst. Eng.* 31, 241–259. doi:10.1007/s00449-008-0197-5
- Islam, S.M., Poirier, R.A., 2007. New Insights into the Bromination Reaction for a Series of Alkeness A Computational Study. *J. Phys. Chem. A* 111, 13218–13232. doi:10.1021/jp075674b
- Jahanshahi, M., Partida-Martinez, L., Hajizadeh, S., 2008. Preparation and evaluation of polymer-coated adsorbents for the expanded bed recovery of protein products from particulate feedstocks. *J. Chromatogr. A* 1203, 13–20. doi:10.1016/J.CHROMA.2008.07.028
- Janzen, R., Unger, K.K., Müller, W., Hearn, M.T.W., 1990. Adsorption of proteins on porous and non-porous poly(ethyleneimine) and tentacle-type anion exchangers. *J. Chromatogr. A* 522, 77–93. doi:10.1016/0021-9673(90)85179-Y
- Jiang, X., Qu, W., Pan, D., Ren, Y., Williford, J.-M., Cui, H., Luijten, E., Mao, H.-Q., 2013. Plasmid-Templated Shape Control of Condensed DNA-Block Copolymer Nanoparticles. *Adv. Mater.* 25, 227–232. doi:10.1002/adma.201202932
- Johansson, B.L., Hellberg, U., Wennberg, O., 1987. Determination of the leakage from Phenyl-Sepharose Cl-4B, Phenyl-Sepharose FF and Phenyl-Superose in bulk and column experiments. *J. Chromatogr.* 403, 85–98.
- Jones, D.A., Lelyveld, T.P., Mavrofidis, S.D., Kingman, S.W., Miles, N.J., 2002. Microwave heating applications in environmental engineering—a review. *Resour. Conserv. Recycl.* 34, 75–90. doi:10.1016/S0921-3449(01)00088-X
- Jozala, A.F., Geraldés, D.C., Tundisi, L.L., Feitosa, V. de A., Breyer, C.A., Cardoso, S.L., Mazzola, P.G., Oliveira-Nascimento, L. de, Rangel-Yagui, C. de O., Magalhães, P. de O., Oliveira, M.A. de, Pessoa, A., Jr, 2016. Biopharmaceuticals from microorganisms: from production to purification. *Braz. J. Microbiol.* 47 Suppl 1, 51–63. doi:10.1016/j.bjm.2016.10.007
- Kappe, C.O., Stadler, A., Dallinger, D., 2012. Microwaves in organic and medicinal chemistry. Wiley-VCH.

- Karnchanasri, K., 2013. Bi-layered chromatography matrices for the purification of biological nanoplexes, PhD thesis, University of Birmingham, UK.
- Kelley, B., 2016. Industrialization of mAb production technology: the bioprocessing industry at a crossroads. *MAbs* 1, 443–52.
- Kongraksawech, T., Vázquez-Landaverde, J., Huerta-Ruelas, J., Torres, J.A., 2006. IONIC STRENGTH AND pH EFFECTS ON OPTICAL THERMOGRAPHS FOR BOVINE SERUM ALBUMIN (BSA) EFECTOS DE LA FUERZA IÓNICA Y EL pH SOBRE LOS TERMOGRAMAS ÓPTICOS DE LA SEROALBÚMINA BOVINA (BSA).
- Kramberger, P., Urbas, L., Štrancar, A., 2015. Downstream processing and chromatography based analytical methods for production of vaccines, gene therapy vectors, and bacteriophages. *Hum. Vaccin. Immunother.* 11, 1010–21. doi:10.1080/21645515.2015.1009817
- Lara, A.R., Ramírez, O.T., Wunderlich, M., 2012. Plasmid DNA Production for Therapeutic Applications, in: *Methods in Molecular Biology* (Clifton, N.J.). pp. 271–303. doi:10.1007/978-1-61779-433-9_14
- Latulippe, D.R., Zydney, A.L., 2009. Size exclusion chromatography of plasmid DNA isoforms. *J. Chromatogr. A* 1216, 6295–6302. doi:10.1016/j.chroma.2009.07.009
- Levison, P.R., Pathirana, N.D., 1996. Rapid ion chromatographic method for the quantitative determination of ligand leakage from ion-exchange media. *J. Chromatogr. A* 742, 79–86. doi:10.1016/0021-9673(96)00194-X
- Levy, M.S., O’Kennedy, D. R., Ayazi-Shamlou, P., Dunnill, P., 2000. Biochemical engineering approaches to the challenges of producing pure plasmid DNA. *Trends Biotechnol.* 18, 296–305. doi:10.1016/S0167-7799(00)01446-3
- Li, M., Qiu, Y.X., 2013. A review on current downstream bio-processing technology of vaccine products. *Vaccine* 31, 1264–1267. doi:10.1016/j.vaccine.2012.12.056
- Li, Y., Lee, J., Lal, J., An, L., Huang, Q., 2008. Effects of pH on the Interactions and Conformation of Bovine Serum Albumin: Comparison between Chemical Force Microscopy and Small-Angle Neutron Scattering. *J. Phys. Chem. B* 112, 3797–3806. doi:10.1021/jp077392h
- Liddy, A.M., 2009. Multifunctional Chromatography Supports. PhD Thesis.
- Lide, D.R., 2004. *Handbook of Chemistry and Physics*, 8th ed. CRC Press.
- Lidström, P., Tierney, J., Wathey, B., Westman, J., 2001. Microwave assisted organic synthesis - a review. *Tetrahedron* 57, 9225–9283.
- Liu, X., Atwater, M., Wang, J., Huo, Q., 2007. Extinction coefficient of gold nanoparticles with different sizes and different capping ligands. *Colloids Surf. B. Biointerfaces* 58, 3–7. doi:10.1016/j.colsurfb.2006.08.005
- Ljunglöf, A., Thömmes, J., 1998. Visualising intraparticle protein transport in porous adsorbents by confocal microscopy. *J. Chromatogr. A* 813, 387–395. doi:10.1016/S0021-9673(98)00378-1
- Lowe, C.R., Lowe, A.R., Gupta, G., 2001. New developments in affinity chromatography with potential application in the production of biopharmaceuticals. *J. Biochem. Biophys. Methods* 49, 561–74.

- Morenweiser, R., 2005. Downstream processing of viral vectors and vaccines. *Gene Ther.* 12, S103–S110. doi:10.1038/sj.gt.3302624
- Morris, C.G., 1992. Dictionary of Science and Technology. Academic Press.
- Müller, T.K.H., Cao, P., Ewert, S., Wohlgemuth, J., Liu, H., Willett, T.C., Theodosiou, E., Thomas, O.R.T., Franzreb, M., 2013. Integrated system for temperature-controlled fast protein liquid chromatography comprising improved copolymer modified beaded agarose adsorbents and a travelling cooling zone reactor arrangement. *J. Chromatogr. A* 1285, 97–109. doi:10.1016/j.chroma.2013.02.025
- Nikon, 2018. Critical Aspects of Confocal Microscopy | MicroscopyU [WWW Document]. URL <https://www.microscopyu.com/techniques/confocal/critical-aspects-of-confocal-microscopy> (accessed 2.8.18).
- Nweke, M.C., McCartney, R.G., Bracewell, D.G., 2017. Mechanical characterisation of agarose-based chromatography resins for biopharmaceutical manufacture. *J. Chromatogr. A* 1530, 129–137. doi:10.1016/J.CHROMA.2017.11.038
- Orr, V., Zhong, L., Moo-Young, M., Chou, C.P., 2013. Recent advances in bioprocessing application of membrane chromatography. *Biotechnol. Adv.* 31, 450–465. doi:10.1016/J.BIOTECHADV.2013.01.007
- Pääkkönen, S., Pursiainen, J., Lajunen, M., 2010. Fast Oxidation of Secondary Alcohols by the Bromate-Bromide System Using Cyclic Microwave Heating in Acidic Water. *ChemInform* 51, 6695–6699. doi:10.1016/j.tetlet.2010.10.009
- Pabbathi, A., Patra, S., Samanta, A., 2013. Structural Transformation of Bovine Serum Albumin Induced by Dimethyl Sulfoxide and Probed by Fluorescence Correlation Spectroscopy and Additional Methods. *ChemPhysChem* 14, 2441–2449. doi:10.1002/cphc.201300313
- Prazeres, D.M., Monteiro, G.A., Ferreira, G.N., Diogo, M.M., Ribeiro, S.C., Cabral, J.M., 2001. Purification of plasmids for gene therapy and DNA vaccination. *Biotechnol. Annu. Rev.* 7, 1–30.
- Prazeres, D.M., Schluep, T., Cooney, C., 1998. Preparative purification of supercoiled plasmid DNA using anion-exchange chromatography. *J. Chromatogr. A* 806, 31–45.
- Promega, 2018. How do I determine the concentration, yield and purity of a DNA sample? [WWW Document]. PubHub. URL <https://www.promega.co.uk/resources/pubhub/enotes/how-do-i-determine-the-concentration-yield-and-purity-of-a-dna-sample/> (accessed 2.5.18).
- Przybycien, T.M., Pujar, N.S., Steele, L.M., 2004. Alternative bioseparation operations: life beyond packed-bed chromatography. *Curr. Opin. Biotechnol.* 15, 469–478. doi:10.1016/j.copbio.2004.08.008
- Reeks, M.W., 2011. STOKES-EINSTEIN EQUATION, in: A-to-Z Guide to Thermodynamics, Heat and Mass Transfer, and Fluids Engineering. Begellhouse. doi:10.1615/AtoZ.s.stokes-einstein_equation
- Schleef, M., 1999. Issues for large-scale plasmid DNA manufacturing. *Biotechnol. a Multi-Volume Compr. Treatise. Recomb. Proteins, Monoclon. Antibodies, Ther. Genes* 5a, 443–470.
- Scholz, C., Wagner, E., 2012. Therapeutic plasmid DNA versus siRNA delivery: Common and different tasks for synthetic carriers. *J. Control. Release* 161, 554–565.

doi:10.1016/j.jconrel.2011.11.014

- Seeman, N.C., Rosenberg, J.M., Rich, A., 1976. Sequence-specific recognition of double helical nucleic acids by proteins. *Proc. Natl. Acad. Sci. U. S. A.* 73, 804–8.
- Segura, M.M., Kamen, A.A., Garnier, A., 2011. Overview of Current Scalable Methods for Purification of Viral Vectors. Humana Press, pp. 89–116. doi:10.1007/978-1-61779-095-9_4
- Sigma Aldrich, 2018. SEPHAROSE AND SEPHAROSE CL GEL FILTRATION MEDIA PRODUCT INFORMATION SHEET.
- Sturtevant, J.M., 1977. Heat capacity and entropy changes in processes involving proteins. *Proc. Natl. Acad. Sci. U. S. A.* 74, 2236–40.
- Takeda, K., Wada, A., Yamamoto, K., Moriyama, Y., Aoki, K., 1989. Conformational change of bovine serum albumin by heat treatment. *J. Protein Chem.* 8, 653–9.
- Thermo Fisher Scientific, 2018a. Plasmid DNA Miniprep Kits.
- Thermo Fisher Scientific, 2018b. SYTO 9 Stain [WWW Document]. URL <https://www.thermofisher.com/uk/en/home/life-science/cell-analysis/fluorophores/syto-9.html> (accessed 2.13.18).
- Thermo Fisher Scientific, 2018c. Fluorescence Fundamentals [WWW Document]. URL <https://www.thermofisher.com/uk/en/home/references/molecular-probes-the-handbook/introduction-to-fluorescence-techniques.html> (accessed 2.13.18).
- Thostenson, E.T., Chou, T.-W., 1999. Microwave processing: fundamentals and applications. *Compos. Part A Appl. Sci. Manuf.* 30, 1055–1071. doi:10.1016/S1359-835X(99)00020-2
- Tran, R., 2011. Evaluation of challenges to the ubiquitous nature of chromatography.
- Viloria-Cols, M.E., Hatti-Kaul, R., Mattiasson, B., 2004. Agarose-coated anion exchanger prevents cell-adsorbent interactions. *J. Chromatogr. A* 1043, 195–200.
- Wiesbrock, F., Hoogenboom, R., Abeln, C.H., Schubert, U.S., 2004. Single-Mode Microwave Ovens as New Reaction Devices: Accelerating the Living Polymerization of 2-Ethyl-2-Oxazoline. *Macromol. Rapid Commun.* 25, 1895–1899. doi:10.1002/marc.200400369
- Willett, T.C., 2009. Magnetic adsorbents displaying switchable ion-exchange behaviour. *Sch. Chem. Eng.* 250.
- Wils, P., Escriou, V., Warnery, A., Lacroix, F., Lagneaux, D., Ollivier, M., Crouzet, J., Mayaux, J.-F., Scherman, D., 1997. Efficient purification of plasmid DNA for gene transfer using triple-helix affinity chromatography. *Gene Ther.* 4, 323–330. doi:10.1038/sj.gt.3300388
- Wold, W.S.M., Toth, K., 2013. Adenovirus vectors for gene therapy, vaccination and cancer gene therapy. *Curr. Gene Ther.* 13, 421–33.
- Wright, J., 2008. Manufacturing and characterizing AAV-based vectors for use in clinical studies Overview of Good Manufacturing Practice. *Gene Ther.* 1565, 840–848. doi:10.1038/gt.2008.65

CHAPTER III

MANUFACTURE & CHARACTERISATION OF PROTEIN NANOPARTICLES AS SURROGATE VIRUS MIMICS

Abstract

Biological nanoplexes are a fast growing and diverse product group in the current biopharmaceutical environment, particularly for gene therapy and vaccine treatments. They generally consist of plasmid DNA, viral vectors, virus-like particles (VLPs), mega-molecular vaccines, mega protein complexes and IgMs. They are characterised by their large physical size, fragility, complex surfaces and chemical similarity to smaller contaminating macromolecular components.

The acquisition of representative virus feedstock, sufficient in quantity and particle concentration, as well as the methods for monitoring these species during purification, poses several practical issues in the realm of virus particle purification. We have developed a platform for the manufacture of protein nanoparticles as surrogate virus mimics. The nanoparticles can be manufactured cost effectively, in high volume and rapidly in the context of characterising viral chromatographic media.

The reproducible manufacture of protein nanoparticles within a defined size range using varying ratios of organic solvent as desolvation agents is detailed herein. Tailoring bovine serum albumin to mimic adenovirus virus particles facilitates the creation of crude virus analogues with similar size and surface characteristics. These characteristics are assayed using a number of techniques to determine efficiency of manufacture and demonstrate how well the nanoparticulate solutions represent their *bone fide* viral counterparts.

This chapter will focus on the groundwork of manufacturing the protein nanoparticles and the concept of tailoring this process to target a specific virus, human adenovirus type 5. In order to produce adenoviral mimics, a 70:30 Methanol: Ethanol mix was employed to desolvate a 10% BSA solution under continuous stirring. In the long term, these sophisticated nanoparticles serve to broaden the scope of virus chromatography and enable the collection of effective and novel data to improve recovery and purification of viruses. It is envisioned that the manufacture of reproducible, well characterised and multi-functional nanoparticles will provide a platform for assessment of established and novel viral purification media in the near future. The concept of characterising chromatography media with these viral mimics is taken forward in future chapters of this thesis

Abbreviations

AdV: Adenovirus Type V

As: Asymmetry Factor

BCA: Bicinchoninic Acid

BSA: Bovine Serum Albumin

CCD: Charge-Coupled Device

CD: Circular Dichroism

CV: Column Volumes

DLS: Dynamic Light Scattering

h: Theoretical Plate Height

HCl: Hydrochloric Acid

HSA: Human Serum Albumin

NTA: Nano-tracking Analysis

PDI: Polydispersity Indices

PES: Polyethersulfone

PSD: Particle Size Distribution

PTFE: Polytetrafluoroethylene

Tris: Tris(hydroxymethyl) aminomethane

USD: Ultra Scale Down

Table of Contents

CHAPTER III.....	146
Abstract.....	151
Abbreviations.....	152
List of Figures.....	155
3.1 Introduction	158
3.1.1 Viral Vectors.....	158
3.1.2 Virus Mimics.....	159
3.1.3 Protein Nanoparticles.....	160
3.2 Materials & Methods	161
3.2.1 Materials & Reagents.....	161
3.2.2 Preparation of Bovine Serum Albumin Nanoparticles	161
3.2.3 Analysis.....	163
3.3 Results & Discussion	168
3.3.1 Desolvation.....	168
3.3.2 Cross-Linking	169
3.3.3 Nanoparticle Purification.....	169
3.3.4 Particle Yield Analysis	172
3.3.5 Molecular Weight Analysis	174
3.3.6 Dynamic Light Scattering vs. Nano-Tracking Analysis.....	175
3.3.7 DLS Validation.....	182
3.3.8 Impact of the Organic Solvent Composition on Nanoparticulation	183
3.3.9 Relationship between Size & PDI	188
3.3.10 Relationship between Size & Ionic Strength	189
3.3.11 Zeta Potential & Isoelectric Focussing.....	190
3.3.11 Scale Down of Nanoparticle Fabrication	194
3.3.12 Influence of Process Parameters	198
3.3.13 Nanoparticle Reproducibility	205
3.3.14 Protein 2 ^o Structure Analysis	206
3.3.15 Nanoparticle Morphology	208
3.3.16 Adenovirus Type V Mimic	209

3.4	Conclusions.....	210
3.5	References	212

List of Figures

Fig. 3.1 Experimental set up for the formation of protein nanoparticles using a syringe pump (1) to control the rate of addition of organic solvent contained within the syringe (2) before it enters the glass beaker (3). Stirring is controlled using a magnetic stirrer plate (4) and prior to addition the solvent is filtered using a 0.22 μm syringe filtration unit (5). The solvent flows through a PTFE tube before making physical contact with the glass rod (6), allowing the solvent to flow down the rod and allow uniform droplets to fall into the centre of the protein solution (7) to initiate protein unfolding.

Fig. 3.2 The process of desolvation (adapted from Paik et al. 2013); a thermodynamically driven, self-assembling process to produce protein nanoparticles from their respective monomeric form (Holban, Grumezescu and Giri, 2016).

Fig. 3.3 a) The result of harsh centrifugation conditions on a nanoparticle preparation, whereby the nanoparticles would aggregate heavily onto the interior surface of the Eppendorf™ tube and could not be effectively re-dispersed using an L&R T-9 ultrasonic bath (L&R Ultrasonics, NJ, USA). **b)** An improved purification method (as stipulated in Section 3.2.2) whereby a centrifuge concentrator is used to dialyse the crude nanoparticle preparation against a 300 kDa membrane, allowing for removal of unreacted reagents, diafiltration and re-constitution of the nanoparticles into fresh buffer (3 times)..

Fig. 3.4 Crude protein nanoparticles sampled direct from manufacture (bars & —) and purified nanoparticles after three cycles of dialysis against a 300,000 MWCO centrifugal concentrator membrane (bars & —). **a)** Changes in average particle size pre- and post- purification for BSA nanoparticles with respect to increasing Ethanol concentration in the desolvating “cocktail”. **b)** Size exclusion chromatograms illustrating the efficacy of purification in removing residual protein species from final nanoparticle preparations;

Fig. 3.5 NativePAGE™ Gel of Bovine Serum Albumin & Bovine Serum Albumin Nanoparticles of various sizes: **(i)** Invitrogen model protein ladder superimposed alongside the gel; **(ii)** NativeMark™ protein ladder utilised as a molecular weight standard; Nanoparticles of a variety of sizes: **(iii)** 49 nm; **(iv)** 75 nm; **(v)** 113 nm; **(vi)** 73 nm; **(vii)** 63 nm & **(viii)** Bovine Serum Albumin.

Fig. 3.6 Bovine Serum Albumin nanoparticles manufactured using varying ratios of Ethanol & Methanol (mean \pm SD, $n = 3$); the line & scatter plot represents protein yield whilst the bars represent the average particle size for each preparation.

Fig. 3.7 Theoretical determination of particle size distributions using DLS. **a)** Particles causing a scattering of light creating **b)** a resultant speckle pattern on a detector screen. **c)** The relationship between particle size and correlation function decay rate and **d)** the three types of distribution achievable using the Zetasizer Nano ZS (Malvern Instruments, 2004).

Fig. 3.8 Particle size distribution of a BSA nanoparticle preparation using DLS (---) and NTA (—) analytical techniques.

Fig. 3.9 Particle size -□- & polydispersity indices -■- for **a)** un-purified & **b)** purified nanoparticles as a function of nanoparticle concentration (mean \pm SD, $n = 3$). The data illustrates the importance of a correct dilution factor prior to analysis via DLS, to avoid issues of noise and contaminants skewing the average particle size and PDI data.

Fig. 3.10 The impact of variations in organic solvent on **a)** average BSA nanoparticle size and polydispersity index & **b)** the relationship between the dielectric constant of the organic solvent mixture and the eventual average particle size produced (mean \pm SD, $n = 3$). Note that these protein solutions were initially dissolved in 10 mM NaCl, rather than in Deionised Water as with Fig. 3.4 & 3.6, though the trend holds true in both instances. See 3.3.10 for further discussion into the importance of ionic concentration on nanoparticle formation.

Fig. 3.11 The relationship between increasing Ethanol concentration (in an Ethanol-Methanol desolvating mixture) on the average particle size (grey columns) with respect to polydispersity indices -□- and ζ -potential (at pH 8) -■- of the BSA nanoparticles (mean \pm SD, $n = 3$).

Fig. 3.12 The impact of 10 mM NaCl (circles -○-/-●-) vs. deionised water (squares -■-/-□-) on the average particle size (filled symbols) and polydispersity indices (open symbols) of the BSA nanoparticles, with respect to increasing Ethanol concentration (in an Ethanol / Methanol mixture (mean \pm SD, $n = 3$)).

Figure 3.13 a) An illustration of the electrical double layer that surrounds each protein nanoparticle in a suspension. A two-part liquid layer surrounds each particle, the inner layer is known as the Stern layer, where counter-ions are strongly attached and an outer, more diffuse layer where there is a significantly weaker interaction between the ions and the particle. A boundary exists within the diffuse layer where the ions and particle are stable, whereby when the particle moves the ions within the boundary move with the particle; this boundary is termed the slipping plane, or the surface of hydrodynamic shear. It is the potential at this boundary that is the zeta potential. **b)** The folded capillary cell used to carry out micro-electrophoresis to determine the electrophoretic mobility of the particles. **c)** Laser Doppler Velocimetry measuring fluctuations in intensity signals from scattered light to determine the velocity of the migrating particles. Images and theory courtesy of Malvern Instruments 2004.

Figure 3.14 a) Isoelectric focussing curves of BSA & BSA Nanoparticles of various sizes and **b)** changes in ζ -potential -■- and average particle size -□- of an 85 nm BSA nanoparticle as a function of varying pH.

Fig. 3.15 Scale down approach for the manufacture of protein nanoparticles; **a)** large scale Simax 50 ml beaker utilising a 25 \times 6 Spinbar® polygon stirrer, **b)** 2 ml Safe-Lock Eppendorf tube with a 5 \times 2 Spinbar® microflea for stirring. Note that all dimensions are in mm and drawings are not to scale. **c)** key dimensions and metrics for both scales. The Reynolds number (Re) was calculated based on a 10% BSA solution desolvated by a 70: 30 MeOH: EtOH solvent mixture at a volumetric ratio of 1: 4, resulting in $\rho = 836.32 \text{ kg/m}^3$ & $\mu = 0.000872 \text{ N.s/m}^2$ (Chick and Lubrzynska, 1913; Doran, 1995). This dimensionless value would increase proportionally with additional Methanol in the mixture. **d)** The impact on scale down on average particle size over a range of

dielectric constants for 50 ml scale -■- and 0.5 ml scale -○-. The native protein was dissolved in 10 mM NaCl prior to desolvation, in order to stabilise the high concentrations of protein at lower working volumes. **e)** The effect of increasing stirring rate on a 10% BSA solution desolvated by a 70: 30 MeOH: EtOH solvent mixture at 0.5 ml scale and the equivalent size for the same conditions at 50 ml scale (mean \pm SD, $n = 3$).

Fig. 3.16 The impact of **a)** the time of glutaraldehyde addition post-desolvation, **b)** addition rate of the organic solvent mixture, **c)** pre-treatment of the protein with heat and **d)** experimental temperature (inset: 4 ° C & 21 ° C) on the average particle size -■- and polydispersity index -□- of BSA nanoparticles (mean \pm SD, $n = 3$).

Fig. 3.17 a) The batch-to-batch variance in mean particle size of protein nanoparticles manufactured under various organic solvent compositions. **b)** Average particle size and PDI of nanoparticle preparations manufactured under identical conditions (Methanol: Ethanol, 70: 30) with each colour representing a new 10% BSA stock (mean \pm SD, $n = 3$).

Fig. 3.18 a) CD spectra for BSA, Desolvated BSA and BSA Nanoparticles. **b)** The relative proportions of secondary structure for the protein in its native and desolvated states, as well as the conformational change once formed into nanoparticles.

Fig. 3.19 BSA Nanoparticles images; **a)** A transmission electron micrograph imaged using a negative uranyl acetate stain and **b)** An atomic force microscopy image acquired via liquid tapping mode.

Fig. 3.20 A comparative study of BSA nanoparticles and Adenovirus type V (AdV); **a)** Nano-tracking analysis of the BSA nanoparticles with an average particle size of 75 nm compared to **b)** DLS & ζ -potential analysis (pH 8) of native AdV (Weng et al., 2014). **c)** & **d)** Transmission electron micrographs of BSA nanoparticles and AdV. **e)** Circular dichroism spectra for both the 75 nm BSA nanoparticle and that of the AdV hexon capsid protein (Day et al., 1972). **f)** Summary table highlighting the similarities in physiochemical properties between the protein nanoparticle mimic and that of the bona fide virus particle (Trilisky and Lenhoff, 2007).

3.1 Introduction

3.1.1 Viral Vectors

As discussed in Chapter II, the advent of gene therapy has caused a re-think in the bioprocessing sector in order to generate sufficient volumes of large-titre, clinical grade viral vectors. Novel methods of purification are required to handle more complex feedstocks, higher titres and more labile products. This chapter will focus on the human adenovirus and its potential in gene therapy. This adaptable vector has wide ranging applications, from tumour suppression using CRISPR-Cas 9 (Takayama and Mizuguchi, 2018) to the treatment of cystic fibrosis via transduction of airway basal cells (Cao *et al.*, 2018). The adenovirus (Ad) species have shown great efficacy as a targeted drug delivery vehicle, with high applicability in gene therapy and vaccine treatments. Ad and Ad-associated viruses are now the most commonly used vehicle for gene therapy, with 547 gene therapy clinical trials having been conducted to date (from 2600 globally), representing 20.5% of all vectors trialled (Ginn *et al.*, 2018b).

Whilst these vectors have huge implications for the bio-therapeutics market, issues often arise with their large scale manufacture, purification and quality/quantitation assays. Duffy *et al.* describe adenoviral production and purification as “labour intensive, costly and requiring specialised equipment” involving 120 hours of cell culture to observe cytopathic effects (CPE) and a further 36 hours for caesium chloride (CsCl) gradient ultracentrifugation to purify the vector. The cell culture alone can cost in the region of \$ 520 to produce a titre of $\sim 2 \times 10^{13}$ virus particles, with the risk of contamination and complications of safety, sampling and cell counting required, the process can be complex and costly to run (Isayeva *et al.* 2003; Duffy *et al.* 2005).

There are further complications downstream, such as the separation of empty capsids which can compete for cell-surface receptors and elicit a heightened immune response (Urabe *et al.*, 2006). Traditional methods of purification have an adverse effect on vector infectivity, variability and can lead to product aggregation (Fernandes *et al.*, 2015). Purification processes also need to consider the maturation cycle of the virus, as well as issues with assaying the vectors accurately.

The industry standard Maizel method (OD_{260}) runs into issues when titres are particularly low or contaminants cause any degree of interference. Infectivity assays are traditionally carried out by plaque (PFU) or tissue culture infectious dose ($TCID_{50}$) methods, which can take close to two weeks to observe any CPE traces. Reporter genes can also be used (GFP, Luciferase, β -galactosidase etc.) to track transduction efficiency, though again these methods can exhibit high variability, as well as being both labour and time consuming (Segura *et al.*, 2010).

There are also safety implications and issues with handling and storage of viral vectors. The UK requires a Biosafety Level 2 (BSL-2) to handle the vector, with stringent precautions to limit any risk of inhalation. Handling of the vector requires specialised material, such as Lo-Bind Eppendorf tubes to prevent loss of material and storage requirements need to consider the propensity for the virus to aggregate at high particle concentrations (Trilisky and Lenhoff, 2007).

In this chapter we explore the potential of protein nanoparticles and their ability to mimic the characteristics of real viral vectors, whilst circumventing many of the issues discussed above. Whilst protein nanoparticles have a multitude of applications across numerous fields, this thesis focusses on their application as a screening tool for present-day and emergent purifications systems, without the hassle of live viral feedstocks.

3.1.2 Virus Mimics

The desire to create mimics of viruses stems from a number of different areas, including biosensors, drug delivery, vaccines and water treatment. The methods employed have utilised a number of different starting materials, including gold, silica and polymeric nanoparticles, as well as the use of virus-like particles (Liu and Han, 2005; Ghosh *et al.*, 2008; Pang *et al.*, 2014; Hyun *et al.*, 2018).

In the case of gold and silica nanoparticles, a protein coat is often required to better represent a viral capsid and thus elicit a cell interaction or immune response (Pang *et al.*, 2014). Whilst gold nanoparticles have advantages of facile assaying due to their distinctive surface plasmon resonance (SPR) band and ease of coating (Schäffler *et al.*, 2014), there is a distinct issue with the high density of the nanoparticles and their propensity to aggregate, both as neat and coated nanoparticles (Zhao, Brook and Li, 2008; Meena Devi, 2014).

Silica nanoparticles have shown much promise, due to their relatively porous nature and ease of functionalisation with high impact applications such as the successful delivery of anti-cancer drugs such as camptothecin (Liu and Han, 2005; Lu *et al.*, 2007; Niu *et al.*, 2013). One of the main issues with functionalised silica nanoparticles is the uncertainty of their cytotoxic effects *in vivo*, particularly due to variations in particle size, which would need to be addressed prior to their widespread use as a drug delivery vector (DeForest, Polizzotti and Anseth, 2009; Nel *et al.*, 2009; Napierska *et al.*, 2010; Wu, Hung and Mou, 2011).

Polymeric-based nanoparticles such as poly(lactic-co-glycolic acid) (PLGA) and poly(lactic acid) (PLA) have been formulated for drug delivery due to the starting materials being approved by the FDA as biocompatible and their ability to biodegrade *in-vivo* (Bala, Hariharan and Kumar, 2004; Kim and Martin, 2006). However, their oil-in-water emulsion/solvent manufacturing technique can cause issues in manufacture and with reproducibility and the final nanoparticles also have issues with water solubility (Govender *et al.*, 1999).

The most promising viral mimic to date has been the use of virus-like particles (VLPs) which are essentially empty capsids devoid of any genetic material responsible for the infectivity potential of the viral vector. This feature circumvents many safety concerns such as reverse mutations or reverting back to pathogenic form, two issues commonly associated with attenuated vectors. VLPs are composed of all or part of the viral capsid and thus provide a representative surface of for antigen recognition to stimulate an appropriate immune response (Fuenmayor, Gòdia and Cervera, 2017).

One of the main disadvantages of VLPs is the arduous nature of manufacture, first requiring cloning of appropriate structural genes, followed by choice of a suitable expression system and finally purification and isolation of the vectors. The most common is *E. coli*, however many VLPs are insoluble in this expression system and require purification in the form of inclusion bodies, which require denaturing, re-folding and re-assembly (Zeltins 2013). In addition, *E. coli* culture requires monitoring and control systems and can take in excess of 48 hours, followed by cell lysis and capture steps which themselves are time consuming and require several man hours (Huo *et al.*, 2018).

3.1.3 Protein Nanoparticles

Rather than functionalise synthetic nanoparticles with proteins in order to mimic the physiochemical properties of viruses, there has been an alternative methodology of utilising protein(s) as starting materials for the formation of nanoparticles. There has been a lot of interest in protein nanoparticles, particularly for the purpose of drug delivery and vaccinations, due to their ease of manufacture, biocompatibility and low cytotoxicity (Lohcharoenkal *et al.*, 2014).

A significant advantage of using protein nanoparticles over synthetic particles is their ability to respond to environmental stimuli as a *bona fide* vector would, largely due to the fact that they are completely (and not partially) composed of similar polypeptide structures which make up the surface proteins of a typical viral capsid. This immediately puts them at an advantage as a surrogate virus mimic, whilst making their interaction behaviour (*in vivo* and *in vitro*) more predictable. This feature also allows proteins to self-assemble, changing conformation and forming inter- and intra-molecular bonds in response to their surroundings.

Another advantage of using protein nanoparticles is their strong avidity, possessing multiple potential binding sites for interaction as well as points for modification/conjugation to improve stability, biocompatibility and traceability. These include PEGylation to improve *in vivo* half-life of therapeutics, fluorescent functionalisation to aid in imaging and signalling peptides to facilitate cellular uptake and tumour targeting (Lin *et al.*, 1997; Langer *et al.*, 2000; Fahrländer *et al.*, 2015; X. Yu *et al.*, 2016).

It is this approach of protein nanoparticles that has been adopted in the chapter, aiming to create a mimic of the human adenovirus type V vector using a commonly available protein, Bovine Serum Albumin. This chapter will cover the manufacturing and characterisation of the protein nanoparticles for Bovine Serum Albumin and identify key processing parameters that impact the integrity of the final product. Also detailed are the important physiochemical characteristics of both the live vector and the surrogate mimic and how the two compare, with reference to their purification requirements. Subsequent chapters will look at building on the process knowledge developed and adapting the technique to target other virus particles of gene therapy interest.

It is envisaged that by optimising the manufacture and rigorous characterisation, the nanoparticles can be used for a novel application not yet applied in analytical chromatography; road testing purification media for their ability to isolate virus species, using sophisticated protein nanoparticles as surrogate virus mimics, thus removing the need for live viral feedstocks.

3.2 Materials & Methods

3.2.1 Materials & Reagents

Bovine Serum Albumin (fatty acid free, $\geq 96\%$), 8% Aqueous Glutaraldehyde, Methanol and Ethanol (both analytical grade, $\geq 99\%$), Sodium chloride (NaCl), Sodium phosphate monobasic (NaH_2PO_4) and dibasic (Na_2HPO_4), Sodium hydroxide (NaOH), Dimethyl Sulfoxide (DMSO) and all glassware and other reagents were obtained from Sigma Aldrich (Poole, Dorset) unless otherwise stated. Buffers and all aqueous solutions were based upon use of ultrapure water from a Sartorius Arium® Advanced EDI Pure Water System (Sartorius AG, Göttingen, Germany). Bicinchoninic Acid Assay Protein Kit (BCA) and Protein Concentrator Centrifugal Filters were obtained from Fisher Scientific (Loughborough, UK). Chromatography resins (Superdex 200 Prep Grade), PD-10 Desalting Columns and Tricorn empty glass columns were purchased from GE Healthcare (Uppsala, Sweden).

3.2.2 Preparation of Bovine Serum Albumin Nanoparticles

Protein Preparation Bovine Serum Albumin (BSA) nanoparticles were prepared using a desolvation technique as described by Weber *et al.* 2000; Jun *et al.* 2011 & von Storp *et al.* 2012. Briefly, a 10% BSA solution was prepared by dissolving lyophilised, lipid free Bovine Serum Albumin powder in 10 mM NaCl (hereafter referred to as aqueous solution, unless otherwise stated). The solution was then filtered through a 0.22 μm syringe filtration unit (Whatman, Maidstone, UK) to remove any aggregates or contaminants and subsequently adjusted to pH 8 using 1M NaOH and an Accumet® XL200 pH meter (Thermo Scientific, Stafford, UK).

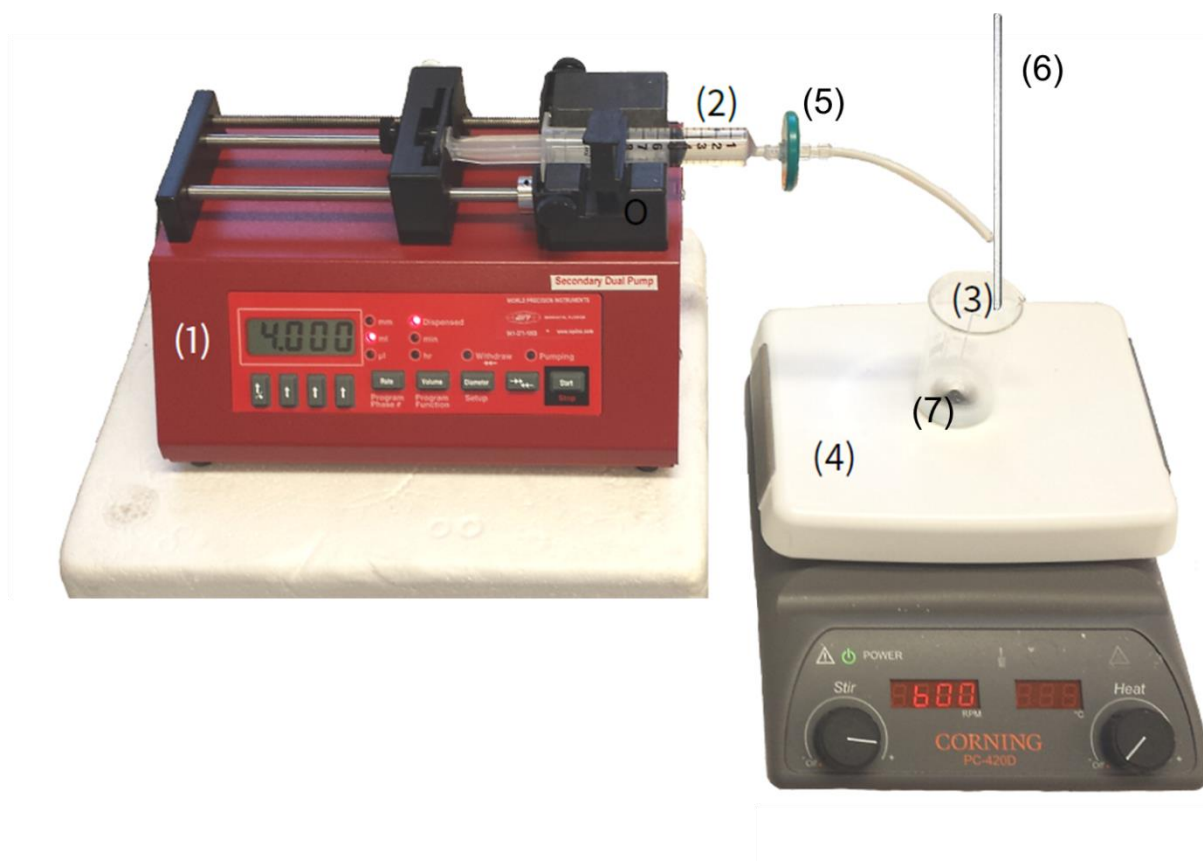


Fig. 3.1 *Experimental set up for the formation of protein nanoparticles using a syringe pump (1) to control the rate of addition of organic solvent contained within the syringe (2) before it enters the glass beaker (3). Stirring is controlled using a magnetic stirrer plate (4) and prior to addition the solvent is filtered using a 0.22 μm syringe filtration unit (5). The solvent flows through a PTFE tube before making physical contact with the glass rod (6), allowing the solvent to flow down the rod and allow uniform droplets to fall into the centre of the protein solution (7) to initiate protein unfolding.*

Desolvation Particle formation was achieved by controlled addition of an organic solvent mixture to 1 ml of protein solution aliquoted into a 50 ml beaker, diameter 35 mm (Simax Kavalierglass, Prague, Czech Republic) via a 0.22 μm syringe filtration unit connected with an adapter to a portion of PTFE tubing (VWR International, Radnor, PA, USA). Prior to addition of solvent, the beaker was placed on a magnetic stirrer plate (Corning PC-420D, Corning Inc., USA) with a rectangular Spinbar® magnetic flea (Sigma Aldrich, Poole, Dorset) of 25 mm in length used to maintain continuous stirring.

4 ml of desolvating organic solvent were added dropwise using a NE-1000 Programmable Syringe Pump (New Era Pump Systems, New York, USA) attached with either a 10 or 20 ml Luer-lock® syringe (BD, Franklin Lakes, USA) filled with the solvent mixture. A constant flow rate of 1.0 ml/min was maintained, under continuous stirring (600 rpm) at room temperature and such the solution became visibly turbid (Weber *et al.*, 2000) as the protein dehydrates and unfolds. Droplet size and placement was kept constant by placing the end of the syringe in direct contact with a glass rod held vertically above the centre of the glass beaker via a clamp stand. The organic solvent

would run axially down the glass rod and form droplets which fall from a set height into the centre of the glass beaker holding the protein solution. This is illustrated in the experimental set up in Fig. 3.1.

Cross-Linking After 4 minutes, 8% aqueous glutaraldehyde solution was added to induce particle cross-linking (Habeeb and Hiramoto, 1968), in an aliquot representative of 100% of the theoretic amount necessary for quantitative cross-linking of the sixty lysine residues present on each BSA molecule particle matrix in the 10% protein solution (Patterson and Geller, 1977; Weber *et al.*, 2000). The cross-linking process was left to complete under continuous stirring at 600 rpm for 12 hours at room temperature (von Storp *et al.*, 2012). The beaker was sealed with a sheet of Parafilm® (Sigma Aldrich, Poole, Dorset) to prevent contamination from airborne particulates, except during addition of protein and organic solvent.

Purification The nanoparticle suspension was purified from unused free protein and reagents by either three cycles of centrifugation and re-suspension in fresh buffer in 2 ml Eppendorfs at 15,000 x g for 30 mins (Sigma 3K30 refrigerated centrifuge, SciQuip, Shropshire, UK) at a constant temperature of 4 °C or four cycles of dialysis against a 300 000 MWCO protein concentrator polyethersulfone (PES) centrifugal filter (Thermo™ Scientific, Loughborough, UK) in an Eppendorf 5810 centrifuge (Eppendorf, Hamburg, Germany) at 2,500 rpm for 20 minutes. The retentate was re-suspended three times in the same buffer the initial protein was dissolved in before aliquoting into 15 ml Falcon tubes (Thermo Scientific, Stafford, UK) for subsequent analytical testing or for refrigerated storage at 4 °C.

3.2.3 Analysis

3.2.3.1 Dynamic Light Scattering

3.2.3.1.1 Particle Sizing

Determining the particle size distributions (PSD), average particle size (Z-Average) and polydispersity indices (PDI) of the nanoparticles were carried out using a Zeta Sizer Nano ZS (Malvern Instruments, Malvern, UK). Nanoparticle preparations were diluted 200-fold in aqueous solution, corresponding to a final concentration of ~ 0.1 mg/ml, providing sufficient light scatter intensity for the detector and correlator to generate a digital signal to be processed by the Zetasizer Nano ZS software (Malvern Instruments, Malvern, UK).

The diluted samples were then mixed by repeated gentle aspiration and then transferred, in aliquots of 0.8 ml, to disposable DTS0012 polystyrene semi-micro cuvettes (Thermo™ Scientific, Loughborough, UK) before placing into the cuvette chamber of the Zetasizer Nano ZS. The refractive indices for the sample were set at 1.45 and 1.33 for the sample (protein) and dispersant (aqueous solution), respectively (McMeekin, Groves and Hipp, 1964). Equilibration time was set to 120 seconds with conditions set at 25 °C, dispersant viscosity 0.8872 cp, with measurements performed at a backscattering angle of 173 °. This means that the detector is placed at an angle of 173 ° from the angle of incidence and is an example of a patented technique known as Non-Invasive Back Scatter (NIBS).

The use of NIBS is advantageous as the incidence beam does not traverse the entire sample and thus limits the effect of multiple scattering (scattered light from one particle scattered by other particles multiple times), facilitating the measurement of higher sample concentrations. Larger contaminant particles (e.g. dust) usually scatter in the forward direction, thus the use of NIBS greatly reduces the impact of contaminant interference (Malvern Instruments, 2004).

Data was evaluated for average particle diameter and polydispersity indices on the basis of scattering intensity data. Three separate measurements were then taken for each sample and subsequently averaged to determine a mean and standard deviation for each nanoparticle preparation.

3.2.3.1.2 Zeta Potential & Isoelectric Focussing

Zeta potential and isoelectric focussing measurements were both attained using the same Zetasizer Nano ZS. Samples of protein and protein nanoparticle were prepared by diluting stocks 200-fold in aqueous solution, equating to a final concentration of ~ 0.1 mg/ml to facilitate sufficient light scattering for optimum measurement conditions.

For single zeta potential measurements, samples were titrated to pH 8 by addition of small volumes of NaOH before transferring 1 ml aliquots into a re-useable DTS1061 folded capillary cell (Malvern Instruments, Malvern, UK). Isoelectric focussing data was accomplished with the aid of a MPT-2 auto-titrator and de-gasser connected to the Zetasizer Nano ZS (all Malvern Instruments, Malvern, UK). The refractive indices for the sample were set at 1.45 and 1.33 for the sample (protein) and dispersant (aqueous solution), respectively (McMeekin, Groves and Hipp, 1964). Equilibration time was set to 120 seconds with experimental temperature set at 25 °C, dispersant viscosity at 0.8872 cp and dielectric constant at 78.5.

For isoelectric focussing, 15 ml of protein or protein nanoparticle sample, prepared to the same concentrations as stipulated for sizing and single zeta potential measurements, were utilised for each isoelectric focussing curve, with 0.1 M NaOH and 0.1 M HCl used as titrants for pH adjustment. Starting at pH 8 or 9, the samples were titrated to pH 1.8 in increments of 0.5, applying a target pH tolerance of ± 0.05 . Three measurements were taken at each pH point with the sample re-circulated through the cuvette and magnetically stirred in the holding vessel between each measurement to ensure thorough mixing between samples and titrations of pH points.

Titration curves were fitted with a sigmoidal curve plotted using the Origin 2017 graphing package (OriginLab, MA, USA), with an isoelectric point determined for each curve ($y = 0$), resulting in a mean and standard deviation from three values for each sample.

3.2.3.2 Nano-Tracking Analysis

As a complimentary assay to dynamic light scattering and as a methodology for ascertaining particle concentration, purified nanoparticle preparations were analysed using Nano-tracking analysis (NTA). For this, nanoparticles were purified and prepared as with DLS, though diluted to a concentration such that a clear image of the scattering volume is obtained (usually between 10^6 to

10⁹ particles/ml). This involved an element of trial and error and was dependent on the sample type, though generally equated to a concentration of $\sim 2 \times 10^{-5}$ mg/ml of protein in the measurement sample.

Samples were measured using a NanoSight LM10 (NanoSight, Wiltshire, UK). Diluted samples were injected into the sample inlet of the flow cell, housed in a metal LM10 unit which was mounted onto a conventional microscope with an X20 objective attached. Here a focussed 635 nm laser passes through the LM10 unit into the 300 μ L sample chamber, causing the nanoparticle preparations to scatter light. The particles passing through the laser beam act as point scatterers and their random paths under Brownian motion are dynamically tracked and recorded (as a video) by a Marlin CCD camera (Allied Vision Technologies, Germany) operating at 30 frames per second (fps), to be analysed and de-convoluted by the NTA Software v. 1.5 (NanoSight, Wiltshire, UK).

Conditions were set and equilibrated at 25 °C, viscosity 0.8872 cp and gain and detection thresholds set at 1 and 10, respectively. The latter two are nominal values selected to increase signal below a certain limit and limit background noise, as well as removing any false centres where no clear particles were present and thus eliminate false positives. The first frame of the recorded video can be used to adjust parameters to remove blurring, threshold and smooth images. This ensures a better signal/noise ratio as well as tracking of appropriate particle size ranges for subsequent frames, facilitating better accuracy in generating a particle size distribution.

3.2.3.3 Protein Nanoparticle Quantification

3.2.3.3.1 Bicinchoninic Acid Assay

Protein and protein nanoparticle preparations were quantified using a bicinchoninic acid (BCA) assay, as described in Section 2.2.11.4. In the case of protein nanoparticle samples, the methodology follows that stipulated by Arroyo-Maya *et al.* 2014, whereby the protein content within the nanoparticles are measured via the same principles of a conventional BCA assay. This concept was validated by conducting a BCA assay with a stock nanoparticle preparation, developing a standard curve by serial dilution (in parallel to the customary protein standard curve) and observing a linear correlation between nanoparticle concentration and absorbance at 562 nm. On this basis, it was possible to use the protein standard curve to ascertain the concentration of BSA in any nanoparticle preparation.

3.2.3.3.2 Size Exclusion Chromatography

Superdex 200 Prep Grade chromatography media was flow-packed in a 5/100 Tricorn column using an ÄKTA Explorer 100 system (both GE Healthcare, Uppsala, Sweden) and tested prior for packing quality via a 2% Acetone pulse (As and h values of 1.11 and 0.04 cm, respectively).

The column was equilibrated with six column volumes (CV 3.54 ml) of phosphate buffered saline (20 mM phosphate, 150 mM NaCl, pH 8.0) before being subjected to a 0.1 ml isocratic load (via sample loop injection) of a crude nanoparticle preparation, previously diluted to a concentration of ~ 5 mg/ml. A variable wavelength UV-vis detector, set at 280 nm, alongside conductivity and

pH probes, were used to monitor species elution and buffer exchanges during packing and equilibration.

3.2.3.3.3 Native Polyacrylamide Gel Electrophoresis

Native Polyacrylamide Gel Electrophoresis (Native PAGE) was carried out on a range of unpurified nanoparticle samples to assess quality of nanoparticle preparation and degree of incorporation of protein within the nanoparticles. A Novex® NativePAGE™ Bis-Tris (3 – 12%) gel, with a resolution of 15 to 10,000 kDa under non-denaturing conditions, was procured from Life Technologies (Thermo™ Scientific, Loughborough, UK).

Sample Preparation Samples were prepared using the NativePAGE™ sample prep kit, diluting in sample buffer to yield a concentration of 0.1 mg/ml. Cathode (Bis-Tris 15 mM, Tricine 50 mM, Coomassie Brilliant Blue G-250 (0.002 %), pH 7) and anode (Bis-Tris 15 mM, pH 7) and sample (0.1 % PonceauS in 50% Glycerol) buffers were also prepared using the NativePAGE™ running buffer prep kit. 10 µL of sample were loaded into separate wells of the gel alongside a 10 µL aliquot of NativeMark™ unstained protein standard ladder.

Gel Electrophoresis The gel was secured in an Invitrogen™ Mini Gel Tank with an electrical field applied to the gel using a PowerEase™ 90W power supply (both Life Technologies, Thermo™ Scientific, Loughborough, UK). A constant voltage of 150 V was applied to the gel for a total run time of 115 minutes.

Gel Staining For enhanced visualisation of the protein bands, the gel was stained with Coomassie G-250; the gel was removed from the tank and submerged in a plastic container containing 100 ml of fixing solution (40% Methanol and 10% Acetic Acid) and microwaved at 900 W for 45 seconds. The gel was subsequently agitated on an orbital shaker for 30 minutes at room temperature. The fixing solution was then replaced by 100 ml of staining solution (0.02 % Coomassie Brilliant Blue G-250, 30% Methanol and 10% Acetic Acid) and the same process repeated. Finally, the staining solution was replaced by a de-staining solution (8% Acetic Acid) and the process repeated, except held on the orbital shaker for 3 hours until visual inspection of the contrast of the protein bands was deemed acceptable. The gel was then carefully placed in a plastic wallet before scanning on a CanoScan 9000F Mark II Flat Bed Scanner (Canon, Ota, Japan). Image processing was conducted using the image manipulation software ImageJ (NIH, MD, USA).

3.2.3.4 Circular Dichroism Spectroscopy

To observe the structural changes of BSA through the nanoparticle formation process, samples of BSA monomer, desolvated monomer and cross-linked nanoparticles were analysed using circular dichroism (CD) spectroscopy via a Jasco J-1500 instrument (Jasco, Tokyo, Japan). Protein samples, at a concentration of 0.1 mg/ml, were analysed in a quartz cuvette of 0.1 cm optical path length at room temperature. CD spectra were obtained between 190 -350 nm and a scanning speed of 100 nm/min was employed with four accumulations. Protein species were examined in the far UV range (190 – 250 nm) and de-convoluted using the SELCON3 algorithm (Sreerama and Woody, 1993) to assess changes in protein secondary structure.

3.2.3.5 *Transmission Electron Microscopy*

Investigation of the morphology of the nanoparticles was carried out through Transmission Electron Microscopy using a JEOL 1200EX (JEOL, Welwyn Garden City, UK). Briefly, a drop of nanoparticle sample, diluted 1: 100 in aqueous solution, was placed on a copper grid and subsequently dried in an exsiccator and a 1% uranyl acetate solution applied as a negative stain to enhance contrast before imaging.

3.2.3.6 *Atomic Force Microscopy*

To observe the nanoparticles in their aqueous state, Atomic Force Microscopy was employed. Sample preparation involved dropping a diluted sample of nanoparticle suspension onto a pre-coated poly-L-lysine glass slide (Sigma Aldrich, Poole, Dorset), leaving to settle for 30 mins before placing on the imaging stand of the JPK NanoWizard® II (JPK Instruments, Berlin, Germany). Phase and topographical images were acquired by fluid intermittent contact mode at room temperature and ambient conditions at a scan rate of 0.45 Hz. Gold/chromium reflex coated silicon nitride cantilevers (Budget Sensors-SiNi, NanoScience Instruments, Pheonix, AZ) with a resonant frequency between 20 – 40 kHz, a tip radius less than 15 nm and a spring constant of 0.27 N/m were used. Images were processed using the JPKSPM Data Processing software (JPK Instruments, Berlin, Germany).

3.3 Results & Discussion

3.3.1 Desolvation

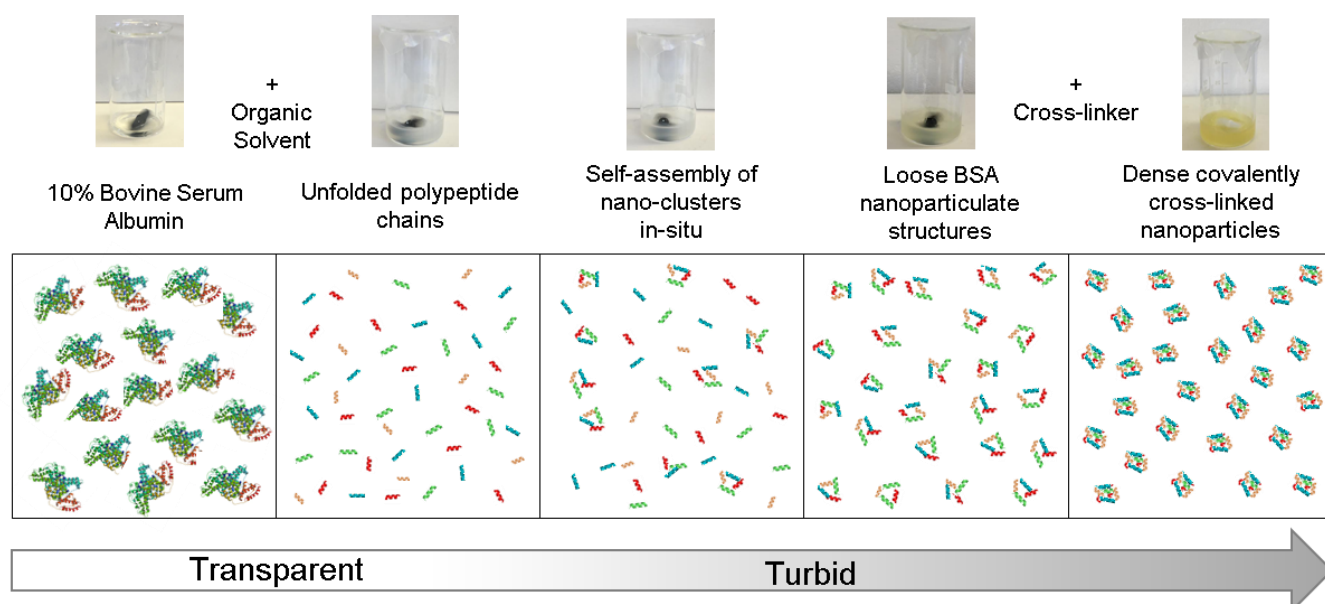


Fig. 3.2 The process of desolvation (adapted from Paik *et al.* 2013); a thermodynamically driven, self-assembling process to produce protein nanoparticles from their respective monomeric form (Holban, Grumezescu and Giri, 2016).

The technique involves an organic solvent replacing the water molecules that form a solvating shell around a protein macromolecule. Water molecules aid in stabilisation of the protein in its folded, hydrated state, facilitating a stable secondary and tertiary structure supported by hydrogen bonding and hydrophobic interaction resulting in a confirmation where the Gibbs free energy is at its lowest; hydrophobic, non-polar amino acid residues are buried in the core, whilst polar, hydrophilic residues exposed on the surface, aiding in solubilising the protein in aqueous solution (Raschke, 2006; Bellissent-Funel *et al.*, 2016). Consequently, addition of the organic solvent results in changes in the protein secondary structure (α -helices, β -sheets, turns and hairpins) as the protein begins to “re-shape” itself in response to its environment.

The use of Serum Albumin as a model protein for nanoparticulation has been widely documented in literature (Lin *et al.* 1997; Weber *et al.* 2000; Zhang *et al.* 2001; Jahanshahi & Najafpour 2006; Langer *et al.* 2008; Mehravar *et al.* 2009; Jun *et al.* 2011; von Storp *et al.* 2012; Yedomon *et al.* 2013; Yu *et al.* 2014; Galisteo-González & Molina-Bolívar 2014; Jahanban-Esfahlan *et al.* 2016; Deshapriya *et al.* 2015; Queiroz *et al.* 2016) for a variety of applications, including drug delivery and bio markers.

Bovine serum albumin in particular has been widely used as a model protein in separation science. Its physiochemical characteristics are well understood including its molecular weight, isoelectric point, crystal structure and amino acid sequence; thus making this protein a suitable protein for targeting specific residues for desolvation and cross-linking (Majorek *et al.*, 2012).

Desolvation, among other techniques, including emulsification, thermal gelation and nano-spray drying, have all been used to manufacture albumin nanoparticles (Elzoghby, Samy and Elgindy, 2012; Jahanban-Esfahlan, Dastmalchi and Davaran, 2016). Desolvation followed by coacervation and cross-linking has proved to be one of the more established and well characterised techniques and one which could be optimised and controllably adjusted to produce nanoparticulates within controlled size ranges.

As illustrated in Fig. 3.2, addition of organic solvent to a high concentration of an aqueous BSA solution results in unfolding of the quaternary, tertiary and secondary structure of the protein, which are held together by a balance of hydrophobic interactions, as well as hydrogen bonding, dipole-dipole interactions and van der Waals forces. This organic solvent-stimulated unfolding induces a conformational change whereby the polar and non-polar residues re-organise to its most thermodynamically favourable state, given its surrounding environment (Y. Yu *et al.*, 2016). As the protein becomes less hydrated *in situ*, the molecules begin to self-assemble into clusters due to electrostatic, hydrophobic and dipole-dipole interactions between the exposed residues.

3.3.2 Cross-Linking

Post-desolvation, cross-linking of the exposed ϵ -amino groups was induced using a bi-functional cross-linker, glutaraldehyde, to “lock” the self-assembled nanoparticulate structures into place. The un-protonated lysine residues behave as nucleophiles and form amide bonds through the carbonyl functional groups of the glutaraldehyde cross-linker.

The pH of the protein solution is adjusted to 8.0 as, despite glutaraldehyde being reactive with amines over pH ranges ≥ 3.0 , the reaction becomes irreversible between pH 7.0 – 9.0. Under acidic conditions, the aldehyde forms unstable Schiff's bases when the cross-linker undergoes nucleophilic attack from the ϵ -amino lysine residues, however at pH ≥ 7.0 , the reaction is shown to have exceptional stability (Migneault *et al.*, 2004).

3.3.3 Nanoparticle Purification

BSA nanoparticles were purified away from un-utilised cross-linker and protein and desolvating solvents and reconstituted into aqueous buffers by two methods, as highlighted in Fig. 3.3. The photograph in a) highlights the methodology as per Weber *et al.*, whereby the nanoparticles were centrifuged at high speed ($\geq 20,000$ g) directly onto the base of an Eppendorf tube, before removing the supernatant and re-suspending in deionised water via an ultrasonic bath.

The centrifugal g force and the spin time would vary slightly depending on the size of the nanoparticle required, with smaller nanoparticles requiring longer periods of time and higher g forces to pellet down. The work by K. Langer and his group allude to this purification requirement (Weber *et al.*, 2000) and this observation does fit with sedimentation rate theory; the sedimentation rate of a particle is proportional to the square of the particle radius, as determined by the Svedberg equation for the sedimentation coefficient (s) equation, below:

Equation 1:

$$s = \frac{2r^2(\rho_P - \rho_M)}{9\eta}$$

Where:

- ρ_P & ρ_M are the densities of the particle and liquid medium, respectively (kg/m^3)
- η is the viscosity of the liquid medium (kg/m.s)
- r is the particle radius (m)

Whilst this approach proved successful in some cases, it was often arduous to re-suspend the nanoparticles post centrifugation and the average particle size profile and polydispersity were not always preserved.

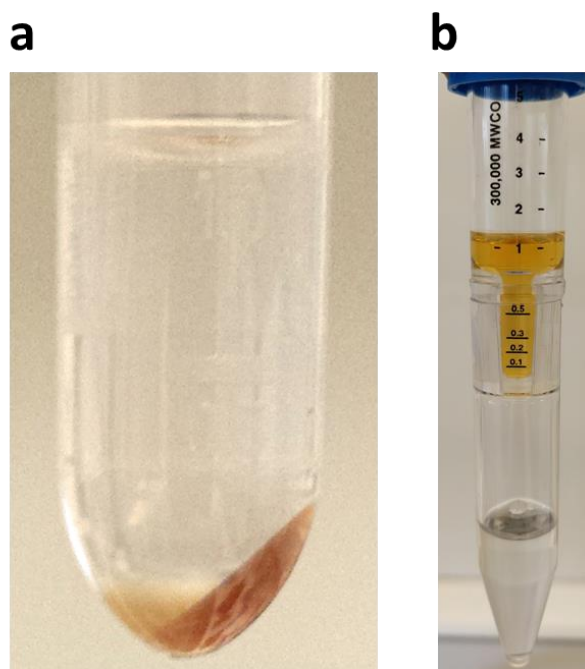


Fig. 3.3 a) The result of harsh centrifugation conditions on a nanoparticle preparation, whereby the nanoparticles would aggregate heavily onto the interior surface of the Eppendorf™ tube and could not be effectively re-dispersed using an L&R T-9 ultrasonic bath (L&R Ultrasonics, NJ, USA). **b)** An improved purification method (as stipulated in Section 3.2.2) whereby a centrifuge concentrator is used to dialyse the crude nanoparticle preparation against a 300 kDa membrane, allowing for removal of unreacted reagents, diafiltration and re-constitution of the nanoparticles into fresh buffer (3 times).

This technique does not require lengthy spells of incubation in an ultrasonic bath and avoids aggregation and adsorption of nanoparticles directly onto the polypropylene tube. The PES membrane filter is hydrophilic and commonly used for serum purification applications, resisting

the hydrophobic interaction driving forces which can contribute to protein adsorption onto filter surfaces (Goebel-Stengel et al., 2011; Murray et al., 2013).

For applications that require highly pure, undiluted sample (e.g. for chromatographic application and for morphological analysis) a gentler purification technique of centrifugation filtration was employed to avoid aggregation at the base of the round-bottom Eppendorf™ centrifuge tubes (Eppendorf, Cambridge, UK) as can be visualised in Fig. 3.3b.

In order to validate that the centrifugation filtration approach had removed any unincorporated BSA, samples were run on an SEC column pre- and post- centrifugation-filtration, as illustrated in Fig. 3.4. The figure illustrates the reproducibility of the purification technique across a variety of desolvating agent concentrations and average particle size ranges. Whilst the average particle size of the purified samples sees little compromise relative to its crude counterpart, interestingly 80% of the samples tested showed a slight decrease in size, post-purification.

It is stipulated that this may be attributed to a layer of BSA bound via weak electrostatic or hydrogen bond interaction to the surface of the nanoparticles, which is subsequently removed during the three cycles of washing in the centrifuge concentrator.

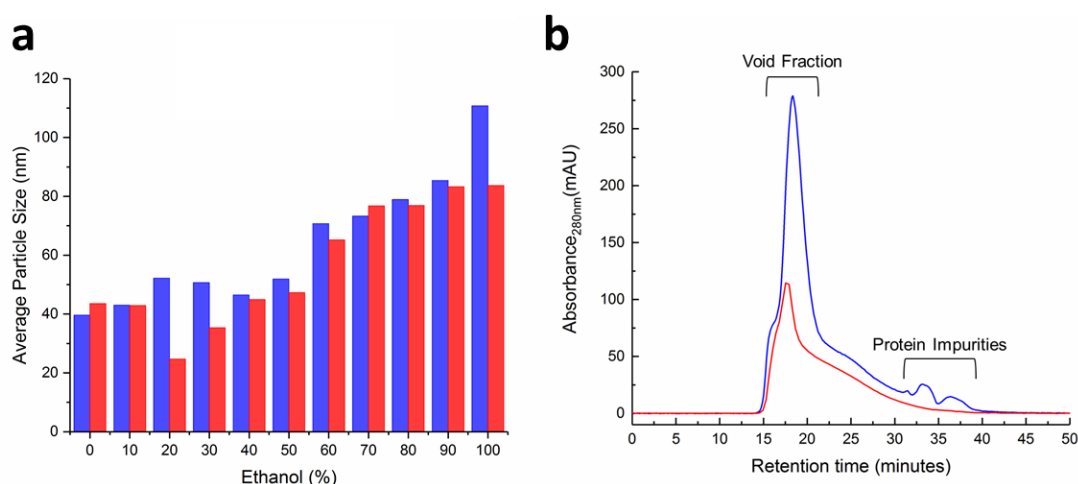


Fig. 3.4 Crude protein nanoparticles sampled direct from manufacture (bars & —) and purified nanoparticles after three cycles of dialysis against a 300,000 MWCO centrifugal concentrator membrane (bars & —). **a)** Changes in average particle size pre- and post- purification for BSA nanoparticles with respect to increasing Ethanol concentration in the desolvating “cocktail”. **b)** Size exclusion chromatograms illustrating the efficacy of purification in removing residual protein species from final nanoparticle preparations.

Importantly, the nanoparticles are fractionated in the void volume of the column as the Superdex 200 Prep Grade (fractionation range 10 kDa – 600 kDa for globular proteins) is unable to resolve particulates of this size (GE Life Sciences, 2000). Samples were run as an isocratic pulse with an injection volume of 100 μ L at a flow rate of 0.1 ml/min. Purified nanoparticles were more dilute than the un-purified samples due to the nature of the filtration technique, which accounts for the variation in peak absorbance between the two samples. Normalising (by nanoparticle peak height)

the spectra for the purified sample to the concentration of the un-purified sample illustrates that the protein impurities that elute later (32-40 minutes) still do not appear in the purified sample.

3.3.4 Particle Yield Analysis

In order to assess particle yield, a simple mass balance was applied and the protein content of the nanoparticles assayed after formation and purification using a BCA assay, with a standard curve of BSA used to determine concentration. It was found that, for a nanoparticle preparation with an average size of 73 nm, 76% of the original monomer solution was incorporated into the formed nanoparticles; a figure which corroborates well with similar yield quantitation (Arroyo-Maya *et al.*, 2014).

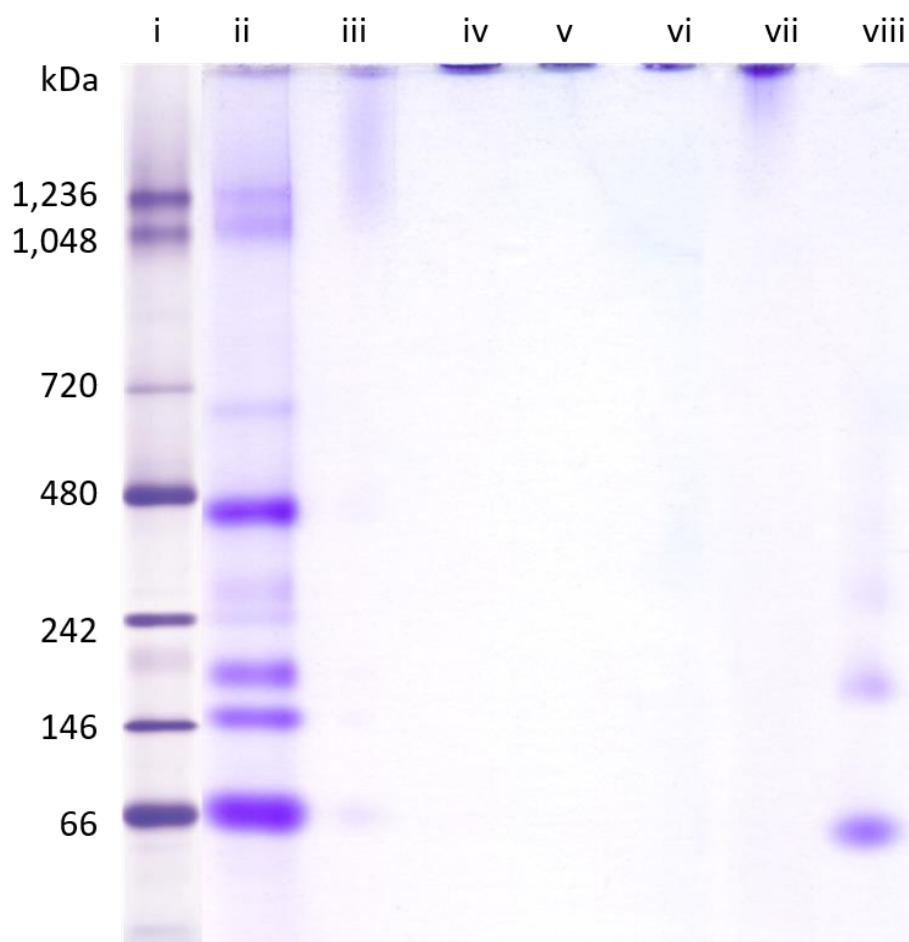


Fig. 3.5 NativePAGE™ Gel of Bovine Serum Albumin & Bovine Serum Albumin Nanoparticles of various sizes: **(i)** Invitrogen model protein ladder superimposed alongside the gel; **(ii)** NativeMark™ protein ladder utilised as a molecular weight standard; Nanoparticles of a variety of sizes: **(iii)** 49 nm; **(iv)** 75 nm; **(v)** 113 nm; **(vi)** 73 nm; **(vii)** 63 nm & **(viii)** Bovine Serum Albumin.

In addition to colorimetric determination of yield, the NativePAGE™ gel illustrated in Fig. 3.5 highlights migration of protein and nanoparticle species through a gel under non-denaturing conditions. The advantage of using a gel over the other respective orthogonal techniques is the increased sensitivity of the technique, as low as 30 ng of protein, compared to 20 µg for the BCA assay. The gel indicates that the bulk of the nanoparticle material experienced no migration through the gel and remained at the top. The smaller sized nanoparticle preparations ((iii) and (vii)) illustrate degrees of streaking which is indicative of a higher degree of polydispersity as the average size of the nanoparticle preparation decreases.

Worthy of note is the upper band in lane (viii) (BSA protein) which is likely trimeric BSA, though the bulk of the sample is monomeric BSA. This phenomenon is observed in similar experiments involving gel electrophoresis of BSA (Wise, 2000) and confirmed by HPLC (Shodex, 2018). Interestingly, a faint band at 66 kDa is evident for the smallest nanoparticle preparation [(iii) 49 nm], indicating the presence of some monomeric protein in the crude preparation. This evidence supports the fact that the yield is different depending on the organic solvent produced, which corroborates with the data in Fig. 3.6 and that smaller nanoparticles exhibit lower yields.

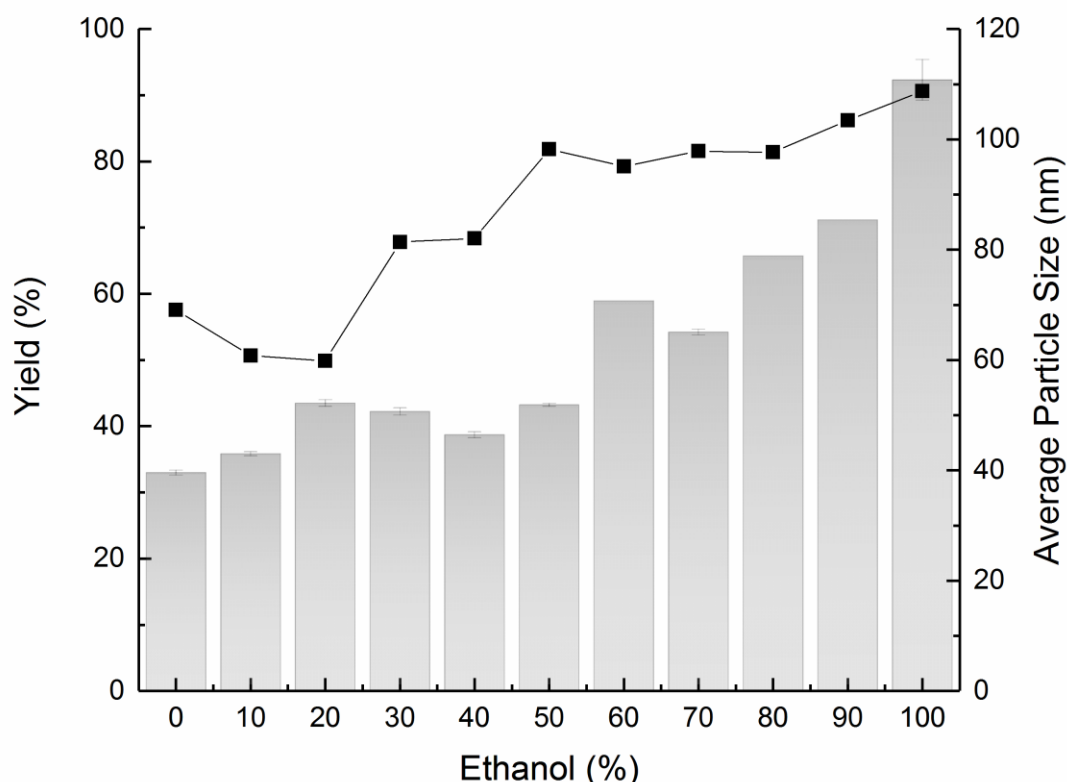


Fig. 3.6 Bovine Serum Albumin nanoparticles manufactured using varying ratios of Ethanol & Methanol (mean \pm SD, $n = 3$); the line & scatter plot represents protein yield whilst the bars represent the average particle size for each preparation. There is a positive correlation between particle size and yield and this conclusion supports the

hypothesis that the larger the nanoparticle produced, the more protein is incorporated and thus the higher the yield. The organic solvent composition will also play a role here, with more Ethanol comes higher degrees of hydrophobic interaction, “opening up” the protein molecules to reveal more lysine residues for incorporation with other proteins and nanoparticle nucleation sites.

This concept is discussed further in Section 3.3.8, but in essence the more polydisperse the preparation is, the more likely the inclusion of smaller mis-formed components existing in the crude nanoparticle preparation, as artefacts of the nanoparticle manufacturing methodology. These could be stray semi-cross linked polypeptide strands from the desolvated BSA, for instance, which could experience some, but limited migration into the gel.

3.3.5 Molecular Weight Analysis

Nanoparticle preparations were also analysed by size-exclusion chromatography using Sephacryl S-500 HR, a resin with a high M_R fractionation resin (up to a maximum of 100 MDa) but also with a range broad enough to also resolve BSA. In reality, for all nanoparticle preparations loaded onto the column, the nanoparticle fractions were isolated in the void volume of the column, illustrating that even the smallest nanoparticles formed were too large to be retained and fractionated by this matrix.

Based on work by Erickson in 2009, who determines a physically intuitive parameter for the size of protein species and assuming a spherical nanoparticle shape, a density of 1.37 g/cm^3 and a partial specific volume of $0.73 \text{ cm}^3/\text{g}$ (typical values for protein), the molecular weight can be derived using the following equations:

Equation 1:

$$V = \frac{(0.73 \text{ cm}^3/\text{g}) \times (10^{21} \text{ nm}^3/\text{cm}^3)}{6.023 \times 10^{23} \text{ Da/g}} \times M(\text{Da})$$

Equation 2:

$$R_{\min} = \left(\frac{3V}{4\pi}\right)^{\frac{1}{3}} = 0.066 M^{\frac{1}{3}}$$

Where:

- $V \text{ (nm}^3\text{)}$ is the volume occupied by a protein of mass M (Daltons)
- R_{\min} is the minimal radius of a sphere that could contain the given mass of protein

By rearranging Equation 2, it is possible to calculate the molecular weight of a given protein nanoparticle preparation. On this basis, the 75 nm nanoparticle preparation has a theoretical molecular weight of 147 MDa.

Nano-tracking analysis (further discussed in Section 3.3.6) reveals the concentration of nanoparticles per millilitre ($\sim 2.1 \times 10^{14}$ nanoparticles/ml) produced for the 75 nm nanoparticle preparation. Knowing the original starting concentration of the protein stock (10% solution), accounting for a 76% yield (revealed through the BCA assay) of BSA particles incorporated into nanoparticles (moles of BSA multiplied by Avogadro's constant) and the number of nanoparticles generated (through NTA analysis) the average molecular weight of the nanoparticle preparation is calculated to be ~ 218 MDa; a value in the same ball-park as the theoretical estimation as set out by Erickson.

To put this into context, the target virus of this chapter, Adenovirus type 5, has a molecular weight of ~ 170 MDa and a hydrodynamic size of ~ 80 to 100 nm (Horwitz *et al.* 1986; Klyushnichenko *et al.* 2000; Trilisky & Lenhoff 2007).

3.3.6 Dynamic Light Scattering vs. Nano-Tracking Analysis

Both dynamic light scattering (DLS) and Nano-tracking Analysis (NTA) were utilised as orthogonal techniques to assay protein nanoparticle preparations for their size distribution profiles. The two methods both work on similar principles, in that size distributions can be derived from the diffusion coefficient of the Stokes-Einstein equation, however their methodology varies slightly, as will be explained in the following sub-sections.

3.3.6.1 Dynamic Light Scattering

DLS functions by illuminating a nanoparticle suspension with a 633 nm He-Ne laser and analysing the fluctuations in intensity to relate the Brownian motion (the random collision of particles with surrounding liquid molecules) of the particles to their size. The Stokes-Einstein equation (see Chapter II, Equation 3) highlights an inverse relationship between particle size and its diffusional coefficient, i.e. the smaller the particle, the quicker its speed due to Brownian motion.

Note that this theory relies on a number of assumptions; the particles are perfectly or near-perfectly spherical in shape, monodisperse and homogeneous in solution (with equivalent density) and that the average particle size is significantly smaller than the wavelength of incidence light to avoid multiple scattering and such that the Rayleigh approximation remains valid.

A speckle pattern (see Fig. 3.7 b)), consisting of bright and dark patches, is created by the scattered light of the nanoparticles on a detector screen. Bright areas are created by particles in the same phase, constructively interfering to form a well-lit patch, whereas darker patches are formed where the phase additions are mutually destructive, cancelling one another out. This pattern of light and dark will be constantly changing as the particles randomly move under Brownian motion and scatter light differently. This causes an overall fluctuation in intensity with time and it is this rate of change in intensity that is used to calculate the size distribution of particles.

A digital correlator in the instrument measures the degree of similarity between the intensity signal of a spot on the speckle pattern a defined point in time (t) and a short (usually nanoseconds) time later ($t + \delta t$). As $t \rightarrow \infty$, the correlation function decays from one (perfect correlation) to zero (no

correlation). This rate of decay is much faster for smaller particles than for larger particles and thus the Malvern Zetasizer software utilises its proprietary algorithm to extract decay rates for various size classes to create a particle size distribution.

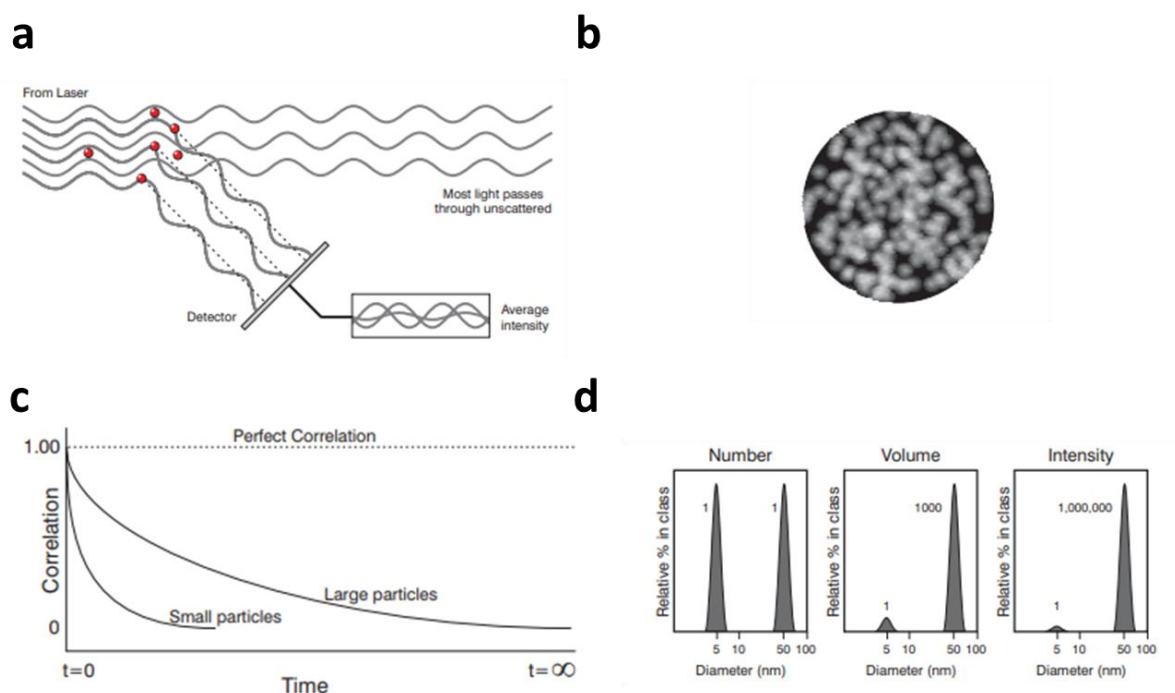


Fig. 3.7 Theoretical determination of particle size distributions using DLS. **a)** Particles causing a scattering of light creating **b)** a resultant speckle pattern on a detector screen. **c)** The relationship between particle size and correlation function decay rate and **d)** the three types of distribution achievable using the Zetasizer Nano ZS (Malvern Instruments, 2004).

Fig. 3.7 d) is an example of a bi-modal sample containing equal numbers of 5 nm & 50 nm nanoparticles. The first output from the Zetasizer is that of an intensity distribution, which can be subsequently manipulated into volume and number distributions. For the intensity distribution, the area of the 50 nm peak is 10^6 times larger than the 5 nm class due to the fact that larger particles scatter more light than smaller particles.

Equation 3:

$$I = I_0 \frac{1 + \cos^2 \theta}{2R^2} \left(\frac{2\pi}{\lambda} \right)^4 \left(\frac{n^2 - 1}{n^2 + 2} \right)^2 \left(\frac{d}{2} \right)^6$$

Where:

- **I** is the intensity of light scattered
- **I₀** is the intensity of the beam of unpolarised light from the laser and **λ** is its wavelength
- **R** is the distance to the particle
- **θ** is the scattering angle
- **d** is the diameter of the theoretical sphere with a refractive index **n**

According to Rayleigh's approximation (above), the intensity of light scattered is proportional to a sixth of the power of its diameter (Seinfeld and Pandis, 2006).

The volume distribution indicates a peak area 10³ times larger for the 50 nm particle class, relative to the 5 nm one. This is due to the fact that the volume of a sphere is proportional to a third of its radius (**Volume of a sphere** = $\frac{4}{3}\pi r^3$). Finally the number distribution displays both peaks with equal areas as both populations have an identical number of particles (Malvern Instruments, 2004).

It is possible to convert the basic intensity distribution output from the software to a number distribution (and subsequently volume distribution) using the following simplified relationship:

Equation 4:

$$I(x) = N(x)M(x, \tilde{n}_D, \tilde{n}_P)$$

Where:

- **I(x)** & **N(x)** represent the DLS intensity and number distributions, respectively
- **M(x, \tilde{n}_D , \tilde{n}_P)** is the Mie Scattering formula with D and P representing the dispersant and particle characteristics
- Volume distribution conversions can be derived using: **Volume of a sphere** = $\frac{4}{3}\pi\left(\frac{x}{2}\right)^3$

It is important to note that the converted distributions are sensitive to minute errors in correlation function data collection, which can be multiplied multi-fold in the conversion from intensity to number and volume distributions (Nobmann, 2016). For this reason, the DLS data displayed herein is that of the unedited and unconverted intensity data.

3.3.6.2 Nano-Tracking Analysis

Although based on the principle of the Stokes-Einstein equation and deriving the diffusion coefficient, NTA mechanistically operates quite differently. The technique still requires illumination of the particles, this time housed in a metal flow cell, using a focussed 80 μm 635 nm red laser.

Rather than interpreting their intensity fluctuations, the nanoparticles are visualised and tracked directly and in real time using NTA. The particles behave as Rayleigh scatterers which scatter light isotropically, provided they are ≤ 100 nm in size. Based on the Brownian motion of each particle and the path it takes, the NTA tracking analytical tool can determine the mean squared displacement (as well as predict statistically accurate trajectories of particles) and thus derive suitable displacement coefficients for each individual particle.

Given the temperature and viscosity of the sample, as well as an estimation of the Boltzmann constant, the software uses the Stokes-Einstein principle to calculate a hydrodynamic radius for each particle that is tracked. A particle size distribution can be generated from this data and as each and every particle is tracked (in a given volume – 400 μL) the distribution units can be given as particles per ml (NanoSight Ltd., 2007).

3.3.6.3 DLS vs. NTA

In deciding the optimal technique to characterise the protein nanoparticle distributions, both DLS and NTA have a lot to offer whilst also having significant drawbacks which require consideration. Fig. 3.5 highlights some important distinction between DLS and NTA; firstly it is evident that, for the same nanoparticle preparation, NTA has a much higher peak resolution than DLS, as the particle tracking technique is able to distinguish two peaks within the population distribution at 62 and 85 nm, which is not recognised by the DLS data, which presents a z-average particle mean size of 73 nm.

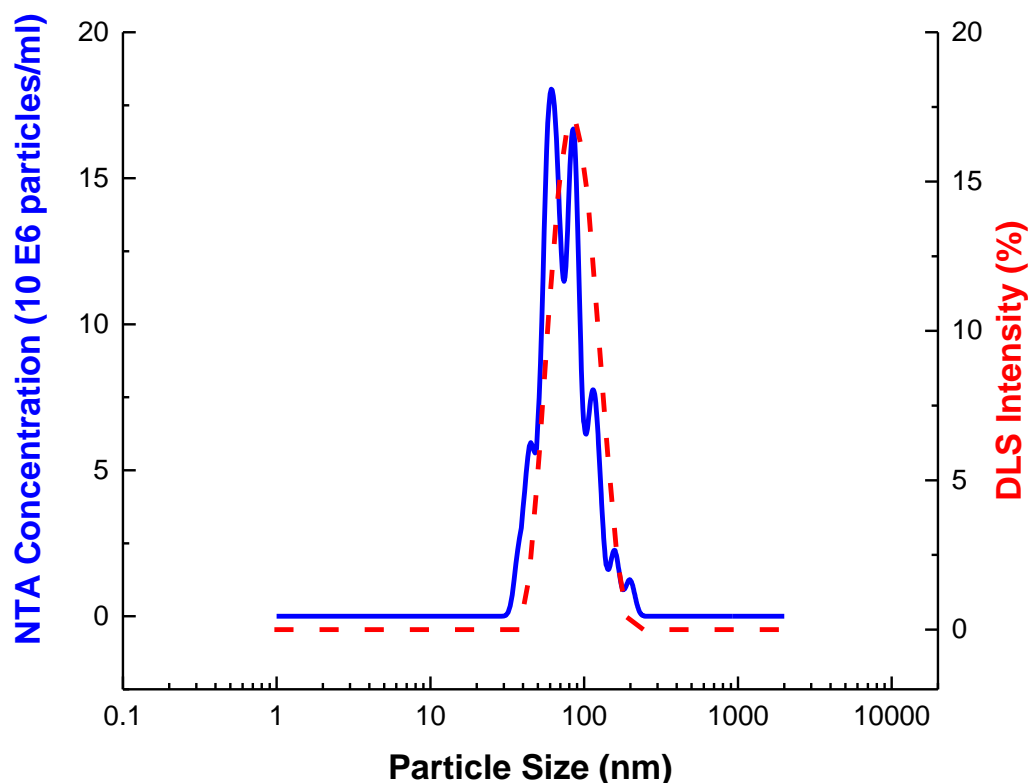


Fig. 3.8 Particle size distribution of a BSA nanoparticle preparation using DLS (- -) and NTA (—) analytical techniques.

A common issue encountered with DLS is that because all particles are assayed simultaneously, larger particles cause higher degrees of scattering and thus can skew the distribution, concealing the existence of smaller sub populations within the sample. This is a limitation of the intensity weighted z average correction factor used by DLS (Mehtala and Wei, 2014).

Generally DLS analysis produces much broader peak distributions as compared to NTA (Mehtala and Wei, 2014) with a peak resolution > 3 fold difference in diameter compared to NTA's < 0.5 and suffers from large errors between measurements due to changes in shape and position between measurements. In addition, NTA has little sensitivity to large contaminants such as dust and microorganisms, whereas this can heavily skew the intensity weighted z-average of DLS. (Filipe, Hawe and Jiskoot, 2010).

This phenomenon has been encountered and reported on numerous occasions in analysis of nanoparticles using these two orthogonal techniques and conclude that NTA produces narrower distributions and a much higher, unbiased peak resolution for samples which are not perfectly mono-disperse (Carr and Malloy, 2007; Filipe, Hawe and Jiskoot, 2010; Gercel-Taylor *et al.*, 2012; Mehtala and Wei, 2014; Nobbmann, 2016).

One significant advantage of DLS over NTA is the simplicity of the approach. Preparation for analysis is straightforward and only requires aliquoting sample into a disposable polystyrene cuvette and placing into the holder ready for measurement. Data input into the software prior to analysis is minimal, only requiring the user to set the temperature and viscosity conditions, as well as the refractive index of the sample. The built-in attenuator within the DLS system adjusts laser exposure to the sample automatically, which is both time saving but also accommodates a wider range of sample concentrations; $\sim 10^8$ - 10^{12} particles/ml compared to NTA's $\sim 10^7$ - 10^9 particles/ml (Filipe, Hawe and Jiskoot, 2010).

An interesting disadvantage of the NTA system is the exposure of sample to aggregate inducing surfaces such as stainless steel, nylon tubing and rubber O-rings as well as shear force as the sample is injected into the sample chamber, though this becomes more relevant when dealing with protein aggregates and antibody products; rather than protein nanoparticles as viral mimics which tend to be more stable and aggregation resistant (Bee *et al.* 2009; Bee *et al.* 2010; Remmele *et al.* 2015).

The NTA standard operating procedure is somewhat more complex, requiring a higher degree of operator skill and experience to be able to iteratively dilute the sample and judge the optimum conditions for video capture and analysis (e.g. low flaring, minimal blurring and appropriate thresholding) to achieve accurate PSDs. The dilution steps and temperature equilibration makes the NTA process much lengthier than DLS as well as having to ensure the sample chamber is clean before and after sampling. Filipe *et al.* 2010 estimate that NTA analysis can take up to 12 times longer per measurement compared with DLS, an approximation that corroborates with the experience in collecting the experimental data for this particular chapter.

The additional time consumed does derive benefits however, in that, as mentioned prior, the samples can be visualised and counted to give concentrations in particles/ml, which have facilitated molecular weight approximations as stipulated in Section 3.3.5. Furthermore, the peak resolutions are higher, distributions narrower and accuracy of the technique is much better for polydisperse samples.

Given the methodology and appraisal of both the techniques above, the speed of analysis for DLS was highlighted as the main factor in choosing between the techniques moving forward. Given the multitude of nanoparticle preparations that are analysed in this chapter and subsequent chapters, analytical throughput is a key factor. DLS evaluates each preparation in ≤ 5 minutes and sample conditions and methods can be pre-programmed to facilitate rapid set-up.

Whilst it was accepted that the technique displayed inferior peak resolution and was limited by intensity weighted averages, these factors were not deemed detrimental in identifying evident trends in our subsequent experimental analysis of nanoparticle preparations. A big contributor to this was the low polydispersity quotients that were achieved for the majority of the nanoparticle preparations made, which aided in reducing the errors caused by PSDs based on an intensity weighted average. Despite not being able to evaluate nanoparticle concentrations in particles/ml for all the preparations made, an alternative protein assay was utilised (see Section 3.2.3.3.1) to

provide quantitative data for the nanoparticles; an asset which was useful in both yield analysis and chromatographic media testing in Chapter V of this thesis.

One final advantage is the convenience of being able to run both sizing and zeta-potential measurements using the same Zetasizer Nano ZS equipment, with the same software and sample holder and only a change of cuvette type and method script necessary to carry out measurements.

3.3.7 DLS Validation

In evaluating nanoparticles by DLS, an appropriate degree of dilution is required in sample preparation to prevent excessive light scattering but also to achieve a sufficient level of laser obscuration to derive an accurate PSD.

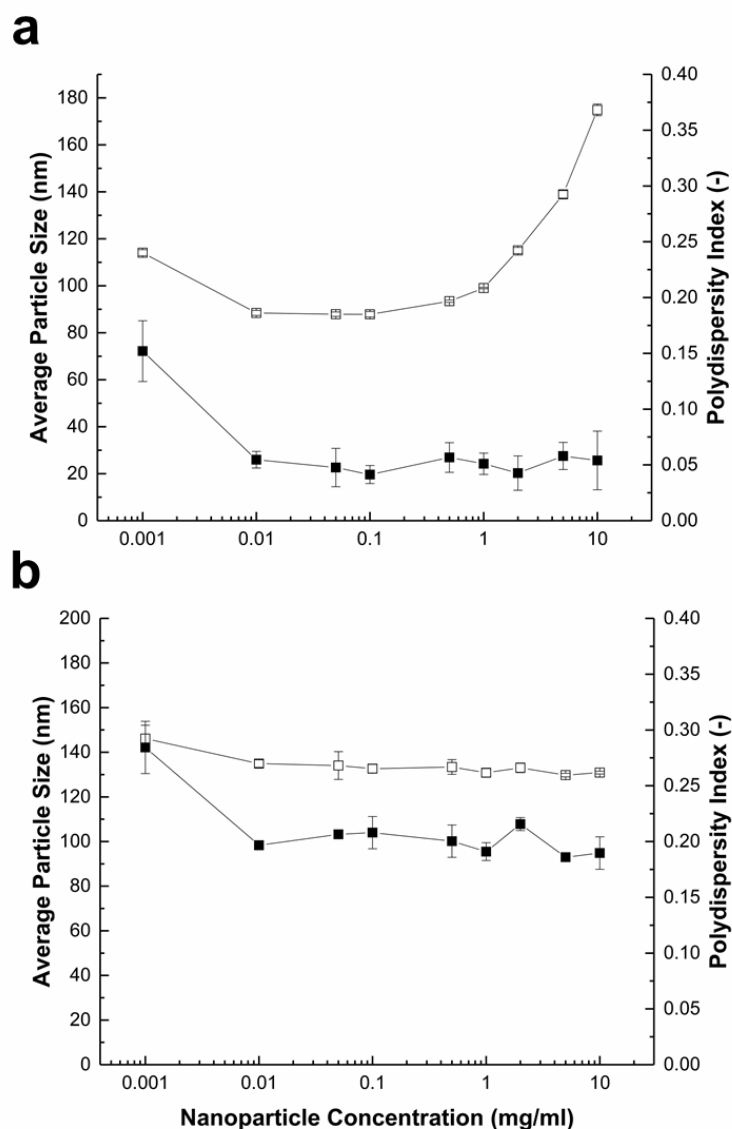


Fig. 3.9 Particle size -□- & polydispersity indices -■- for **a)** un-purified & **b)** purified nanoparticles as a function of nanoparticle concentration (mean \pm SD, $n = 3$). The data illustrates the importance of a correct dilution factor prior to analysis via DLS, to avoid issues of noise and contaminants skewing the average particle size and PDI data. At lower concentrations for both samples, insufficient levels of scattering occur and errors creep into the deconvolution of the speckle pattern to achieve a reliable PSD and PDI. This is further evidenced as, at lower nanoparticle concentrations, the Zetasizer attenuator index was set at value at 11, indicating no laser attenuation in an attempt to collect any available scattering signal. More pronounced increases in average particle size and polydispersity are observed at lower concentrations for un-purified samples, likely due to an increase in noise or contribution from contaminants in the sample. The lower the dilution, the higher the concentration of organic solvents in the sample, which can contribute to a change in the refractive index of the solution and again skew the particle

size distribution generated. In a similar vein, increased dilution improves the validity of the Smoluchowski approximation (aqueous solutions), thus improving the accuracy of the measurements; see Equation 6 for detail. For the purified samples in **b**), average particle size and PDI remain relatively constant across all dilutions greater than 0.01 mg/ml, likely due to removal of contaminants during the centrifugation/filtration process.

3.3.8 Impact of the Organic Solvent Composition on Nanoparticulation

In order to effectively adjust the size of the nanoparticles produced, the composition of the organic solvent “cocktail” used in the desolvation step was adjusted. Fig. 3.10a illustrates the impact of variation of concentrations of Methanol and Ethanol, both as mixtures and in aqueous solution, on the average particle size and polydispersity indices of the nanoparticle preparations. With respect to polydispersity, the general trend observed was that smaller nanoparticle preparations exhibited larger PDIs; this is discussed further in Section 3.3.9.

Observations from all nanoparticle preparations, both in method development and in producing nanoparticles for further characterisation, indicated that polydispersity varied batch to batch, dependent on a number of factors, including ambient conditions, stirrer speed, vessel size, flea size etc. and not just organic solvent-dependent. A polydispersity index < 0.2 was used as a general rule of thumb to categorise good nanoparticle preparations from poor ones. Once the method had been optimised, the majority of nanoparticles fell within these acceptability criteria.

To mimic the adenovirus type 5 viral vectors, the preparation used was a 70 : 30 MeOH : EtOH organic solvent mixture, which provided a relatively monodisperse preparation with an average particle size of 100 nm, approximately the same size as the vector itself (Trilisky and Lenhoff, 2007).

Three batches, produced using varying organic solvent conditions, were purified and stored at 4 °C in deionised water and re-analysed after a time period > 100 days to assess stability. Promisingly, little deviation in size (≤ 9 nm) and PDI (≤ 0.03) was observed on the stored samples indicating that the samples are stable for prolonged periods of time. This provides a significant advantage of these nanoparticles over *bona fide* viral vectors, as the latter have maturation life-cycles and will thus change their capsid composition and potentially their stability in solution, with respect to time (Rexroad *et al.*, 2003).

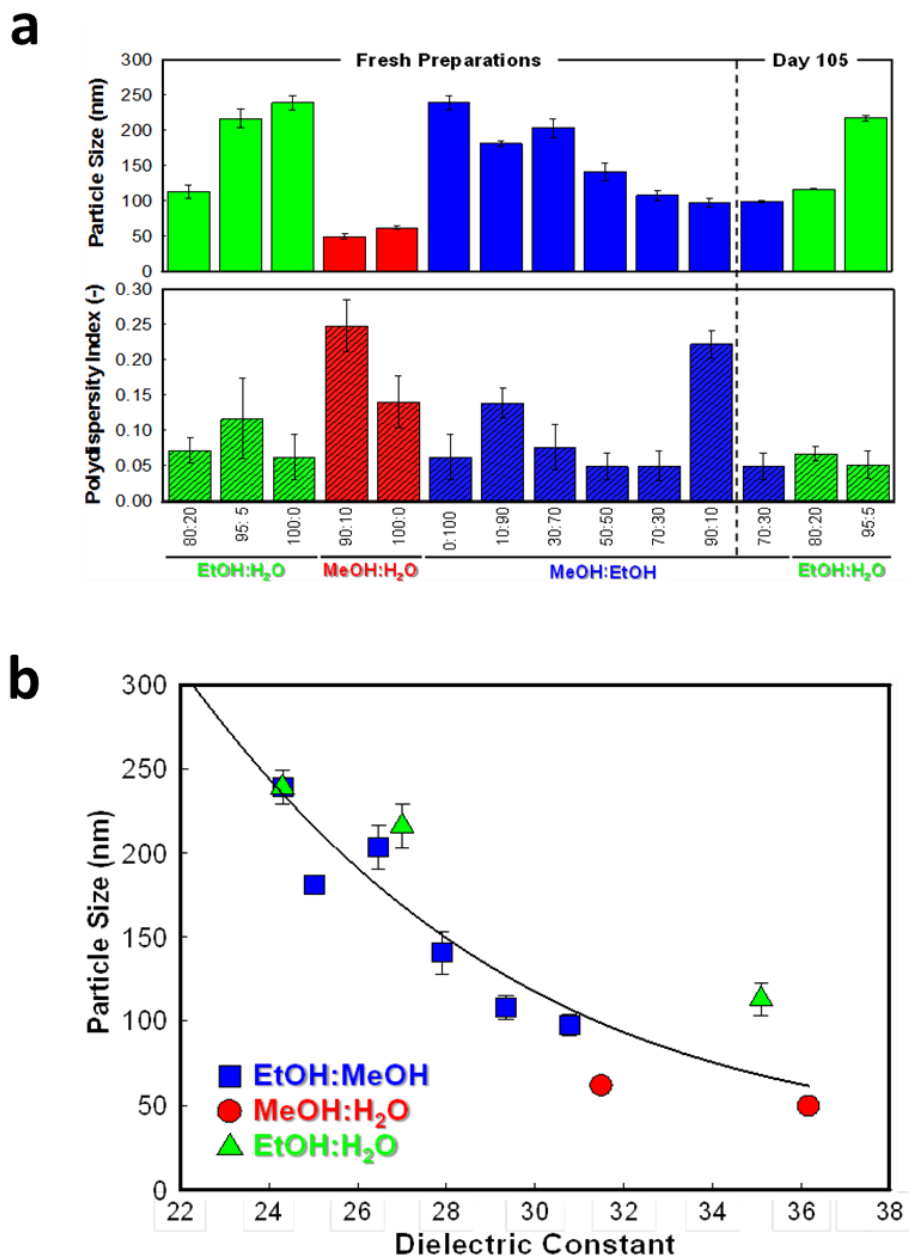


Fig. 3.10 The impact of variations in organic solvent on **a)** average BSA nanoparticle size and polydispersity index & **b)** the relationship between the dielectric constant of the organic solvent mixture and the eventual average particle size produced (mean \pm SD, $n = 3$) with a non-linear regression polynomial inverse first-order fit curve. Note that these protein solutions were initially dissolved in 10 mM NaCl, rather than in Deionised Water as with Fig. 3.4 & 3.6, though the trend holds true in both instances. See 3.3.10 for further discussion into the importance of ionic concentration on nanoparticle formation.

A trend was observed between particle size and an increase in the dielectric constant of the desolvating mixture, as per Fig. 3.9. b). As discussed in Chapter II, 2.3.3, the dielectric constant (or real permittivity) is a measure of the polarisability of the molecules in the sample and their

ability to store electrical energy. The dielectric constant of each organic solvent mixture is calculated by totalling the dielectric constants of each constituent component of the desolvating “cocktail”, as per the Silberstein Equation, below (Arnold *et al.*, 1985):

Equation 5:

$$D_{\epsilon} = \frac{(P_1 \times \epsilon_1) + (P_2 \times \epsilon_2) + \dots (P_n \times \epsilon_n)}{100}$$

Where:

- D_{ϵ} is the dielectric constant of the mixture (kg m/ (V /s))
- P is the volume fraction for each solvent fraction, 1 to n
- ϵ is the dielectric constant for each pure organic solvent (kg m/ (V /s)) (Ethanol: 24.6, Methanol: 32.6 & Deionised Water: 78.54) (Furniss *et al.*, 1989)

A solvent mixture with a higher dielectric constant creates a higher electrical flux and also better protein hydration *in situ* (von Storp *et al.*, 2012; Mohammad-Beigi *et al.*, 2016). Henry’s equation, below, describes the inversely proportional relationship between the zeta potential (ζ (V)) of the protein molecule and the dielectric constant of the suspending medium.

Equation 6:

$$\zeta = \frac{U_e 3\eta}{2\epsilon f(\kappa\alpha)}$$

Where:

- U_e is the electrophoretic mobility of the protein (m²/V.s)
- η is the absolute zero-shear viscosity of the surrounding medium (kg/ m.s)
- ϵ is the dielectric constant of the surrounding medium (kg m/ (V /s))
- $f(\kappa\alpha)$ is the Henry function (dimensionless), the ratio of a particle’s radius (a) to its Debye length ($(1/\kappa)$ - the radius of a spherical, charge-carrying particle and its net electrostatic effect). The Smoluchowski approximation states $f(\kappa\alpha) = 1.5$ for particles > 20 nm in diameter in aqueous (or ionic) media (Lowry *et al.*, 2014).

Thus at high dielectric constants, the protein molecules exhibit less charge repulsion and thus smaller, more compact and tightly-cross linked nanoparticles are formed.

With respect to particle size, as evidenced in both Fig. 3.4 and Fig. 3.10 a), particle size is correlated to the composition of organic solvents used for desolvation. During desolvation, the aqueous

protein is thermodynamically destabilised upon addition of the organic solvents due to increase in the protein's chemical potential and depending on the type of solvent. Depending on the solvent composition, varying degree of denaturation may occur due to hydrophobic interaction with non-polar side chains, increasing the chemical state of the protein.

Both solvents have the ability to behave as proton donors and can form strong intermolecular (hydrogen bonding, dipole-dipole, hydrophobic and van der Waals) interactions with the protein. This causes disruption to the protein's alpha helical and beta sheet/turn/coil and un-ordered 2^0 structures occur. This ultimately causes denaturation and the formation of un-ordered aggregates, which are subsequently cross linked into nanoparticles.

The solvents themselves also play a role; a higher proportion of Ethanol in the purely organic solvent mixtures results in the average particle size increasing. This is due to the fact that Ethanol allows for better disruption of the protein's hydrophilic layer, causing higher disruption to the protein's 2^0 structure, ultimately causing more pronounced denaturation and the formation of larger clusters or "building blocks", which are ultimately cross linked into larger nanoparticles. Systematic studies on the denaturation transitions of proteins found that "the effectiveness of alcohols as protein denaturants increases with increasing chain length and hydrocarbon content, in conformance (with) the disorganisation of the hydrophobic interior of proteins revealed by 3D X-ray structures" (Herskovits, Gadegbeku and Jaillet, 1970).

High Ethanol concentrations are better than Methanol-dominant "cocktails" at solubilising the non-polar residues that form the albumin core (mainly due to the additional methyl group), as confirmed by more drastic changes in secondary structure, seen through CD spectral data; see Section 0 and Mohammad-Beigi *et al.* 2016.

This corroborates well with experimental observations, whereby desolvating cocktails high in Methanol took significantly longer to exhibit solution turbidity (compared to Ethanol), indicating that Methanol is less effective at disrupting the albumin's structure.

By applying a more water-miscible, protic, polar solvent (such as Methanol, rather than Ethanol)⁹ to an aqueous protein solution, a retarded decrease of the mixture's polarity occurs and the protein molecules experience a slower and more ordered dehydration. In addition to this, Methanol has a slightly lower high dipole moment, relative to Ethanol (1.6 and 1.7, respectively) which limit the formation of large hydrogen bond lattices and larger nanoparticulate structures (Pagni 2005, Mohammad-Beigi *et al.* 2016).

As Methanol has a higher dielectric constant, higher addition volumes can have an impact on the interfacial tension and enthalpy of the proteins, creating a larger protein surface area to volume ratio for the zero-length glutaraldehyde cross-linker to interact with the exposed lysine residues which in turn forms tighter cross-linked and eventually smaller nanoparticles. This coupled with

⁹ The Hildebrand solubility parameters for Water, Ethanol and Methanol are 48, 26.2 and 26.9, respectively (von Storp *et al.*, 2012; Mohammad-Beigi *et al.*, 2016). The parameter is a numerical indication of solvency characteristics and can be used as a measure of interaction between molecules (Burke, 1984).

the fact that higher volumes of Methanol will reduce the overall viscosity of the solution (Methanol: 0.55, Ethanol 1.10 & Water 1.00, all centipoise) (Sigma Aldrich, 2018a) and thus promote better mixing and cross-linking reactivity due to elevated diffusion coefficients, as determined by the Stokes-Einstein equation, as discussed in Chapter II (Equation 3).

3.3.9 Relationship between Size & PDI

Adjusting the composition of desolvating agent invariably causes changes in the particle size and polydispersity of the preparations. It was found that there is a distinct inverse relationship between increasing Ethanol concentration (and particle size) with the polydispersity indices of said preparations, as illustrated in Fig. 3.11.

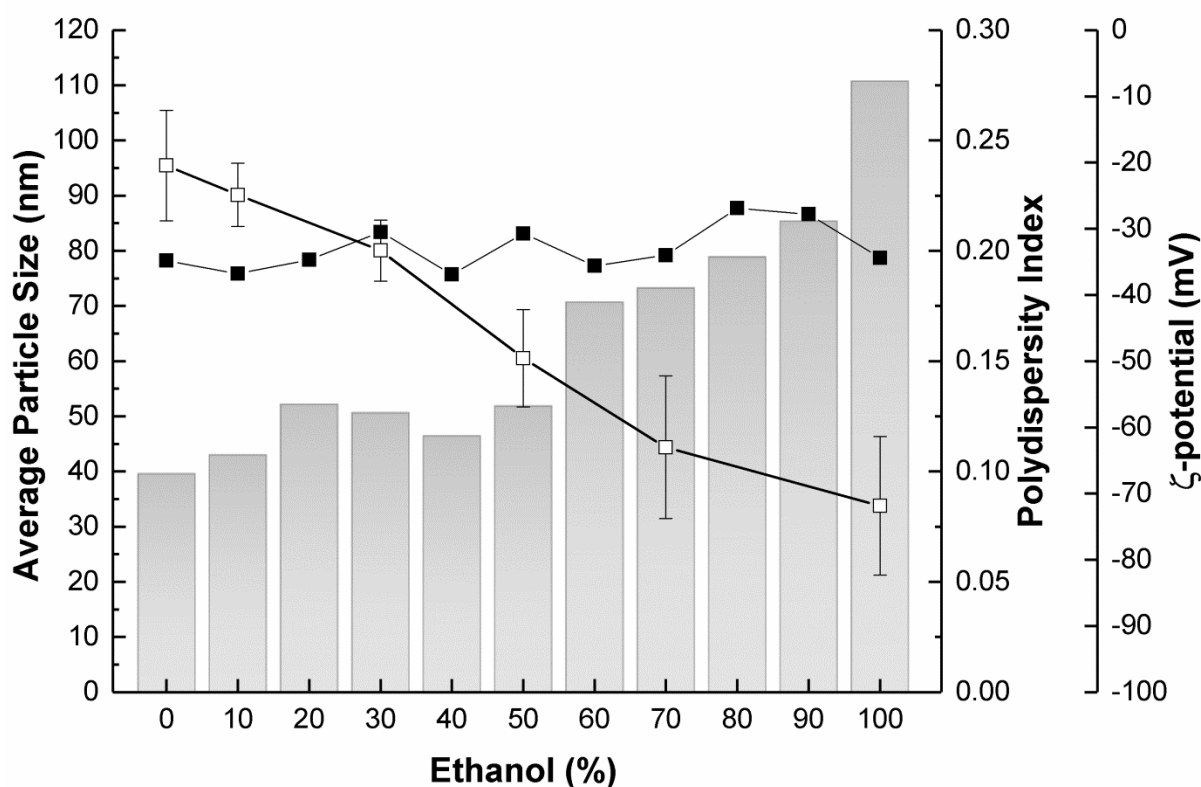


Fig. 3.11 The relationship between increasing Ethanol concentration (in an Ethanol-Methanol desolvating mixture) on the average particle size (grey columns) with respect to polydispersity indices \square - and ζ -potential (at pH 8) \blacksquare - of the BSA nanoparticles (mean \pm SD, $n = 3$).

The relationship between solvent ratios and size has been discussed earlier in the chapter; however, Fig. 3.11 highlights an important trend between solvent concentration and PDI. It is hypothesised that as the proportion of Ethanol decreases (and thus Methanol increases), the polar groups on the surface of the protein, as well as the solvation layer surrounding the protein, are more strongly disrupted when the organic solvent makes contact with the aqueous protein solution.

Additionally, the lower hydrophobic potential that comes with higher Methanol concentrations may result in more disordered unfolding and aggregation mechanisms, disrupting the self-assembly process of the nanoparticles. This is further corroborated by the increased time span required to observe solution turbidity with desolvating cocktails of higher Methanol concentration, indicating

that the time window to form disordered aggregates is longer, which could lead to higher polydispersities for the nanoparticle preparation.

A colloidal suspension with predominantly smaller nanoparticles will have stronger gap interactions due to an increased surface area: volume ratio, resulting in increased van der Waals and depletion interaction (and subsequent decrease in the height of the potential barrier), which can cause the nanoparticles to flocculate together; an entropic-driven process to reduce the surface energy of the particles (Kovalchuk and Starov, 2012). This effect may cause an increased deviation in average particle size due to the existence of multi-particle agglomerates in suspension, resulting in an apparent increase in polydispersity index for the preparation. This should be balanced against the increase in repulsive forces that should theoretically occur with smaller nanoparticles; though Fig. 3.11 suggests that there is no significant relationship between smaller particle sizes and ζ -potential, rather that the surface charge is more a reflection of the re-ordering of amino acids on the surface of the nanoparticles during desolvation. This further supports the hypothesis of more significant attractive forces contributing to higher polydispersities.

It should also be mentioned that the degree of impact on PDI could be a result of the impact of a few large particles in a suspension of smaller nanoparticles, as discussed prior in Section 3.3.6.3. Common contaminants, such as gas bubbles, can appear as artefacts in light scattering measurements and will scatter more intensely than smaller particles. This will cause a higher degree of polydispersity in smaller nanoparticle preparations relative to larger nanoparticles, where the contaminants will fit closer to the mean of the particle size distribution (~ 100 nm).

3.3.10 Relationship between Size & Ionic Strength

An important factor which plays an influential role in the average particle size of the nanoparticles is the ionic concentration of the starting 10% protein solution. Based on previous work, Langer *et al.* in 2003 stated the requirement of a small amount of NaCl in order to reliably adjust the pH of the solution, especially at high protein concentrations, as per Westcott 1978 & Salis *et al.* 2006, who conclude that a background electrolyte is required to improve the reliability of a pH reading using a glass electrode.

A buffered solution was also attempted by Langer *et al.*, however these experiments were thwarted due to interference with the desolvation, resulting in large aggregates, salt precipitation and non-uniform nanoparticles. The cross-linking process was also affected, particularly with TRIS buffer due to its primary amino group competing for substrate with the lysyl residues on the protein (Langer *et al.*, 2003). For this reason, 10 mM NaCl was adopted as a background electrolyte for accurate pH readings, achieving predictable and reproducible nanoparticle characteristics.

However, it was found that the presence of 10 mM NaCl had an impact on the average particle size produced after cross-linking, as illustrated in Fig. 3.12. Despite the issue of pH measurement reliability, consistent nanoparticles were produced using deionised water as a diluent which followed the same trend as with 10 mM NaCl over a range of desolvating conditions, with a 50 – 70% reduction in average particle size.

It is hypothesised that the salt behaves as a surfactant and the Na^+ ions shield charges on the protein / nanoparticle surface (see Fig. 3.13a)), thus reducing protein charge repulsion and enhancing hydrophobic interaction mechanisms between protein molecules and intermediate nanoparticulate structures, causing them to flocculate and increase the overall average particle size, for a given desolvating condition. These findings corroborate well with those of other research groups, namely Jun *et al.* 2011 and Galisteo-González & Molina-Bolívar 2014, who also indicate a drop in the zeta potential with increasing ionic strength.

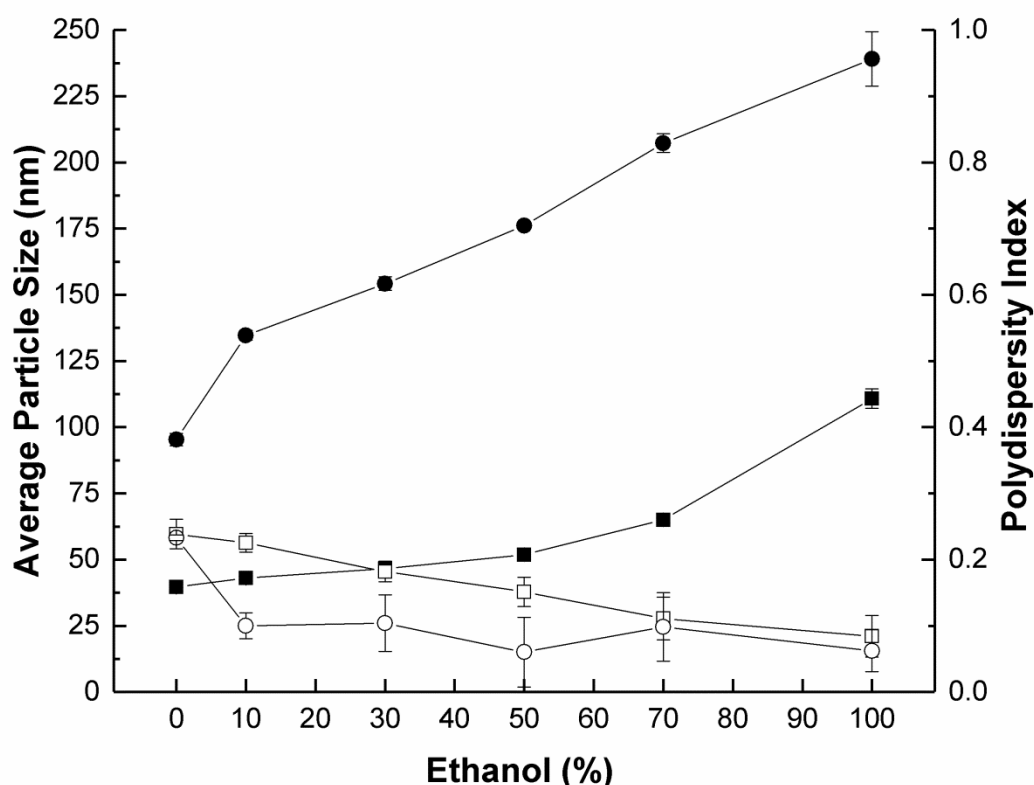


Fig. 3.12 The impact of 10 mM NaCl (circles -○-/●-) vs. deionised water (squares -■-/□-) on the average particle size (filled symbols) and polydispersity indices (open symbols) of the BSA nanoparticles, with respect to increasing Ethanol concentration (in an Ethanol / Methanol mixture (mean \pm SD, $n = 3$)).

Interestingly, the polydispersity indices are overall slightly better for the 10 mM NaCl samples compared to those produced in water, though this may more likely be due to the relationship between size and PDI, as discussed in 3.3.9.

3.3.11 Zeta Potential & Isoelectric Focussing

In order to evaluate the surface charge of the nanoparticles produced under various manufacturing conditions (as illustrated in Fig. 3.11), zeta potential analysis was employed. With the dielectric constant and viscosity of the suspending medium is known and by using the Smoluchowski approximation it is possible to measure the electrophoretic mobility of the nanoparticle suspension

and thus derive the zeta potential using the Henry Equation (Equation 6). The zeta potential of a colloid in suspension is explained in more detail in Fig. 3.13a.

The sample is placed in a micro-electrophoresis cell with +ve and -ve charged electrodes at either end (see Fig. 3.13b) and electric field is applied across the electrolyte solution, causing migration of the particles towards the electrode with opposing charge. Equilibrium is reached between this attractive force and resistive viscous forces in the medium, such that the particles then move with constant velocity which is measured and termed the particle's electrophoretic mobility.

In order to calculate the zeta potential for a nanoparticle preparation, the velocity of the particles is measured using Laser Doppler Velocimetry (see Fig. 3.13c). Here an incident beam is applied to the capillary cell and the scattered light from the migrating particles are collected. Nanoparticles that move through the measurement volume will result in fluctuations in the intensity of light with a frequency which is proportional to the velocity of the particles.

The beam is first run through compensation optics, to correct for cell wall thickness and dispersant refraction as well as to maintain alignment, and combining optics, to relate and combine the received beam to a reference beam from the laser source (via a beam splitter placed behind the measurement cell). An optical modulator with an oscillating mirror is also used to determine the positive or negative sign of the zeta potential. The combined beam is then run through a digital signal processor to determine the signature frequencies from the scattered light and translated via the Malvern Zetasizer Nano ZS software; here a frequency spectrum is generated and the rate of fluctuation used to calculate the velocity of the migrating nanoparticles and thus the electrophoretic mobility and zeta potential.

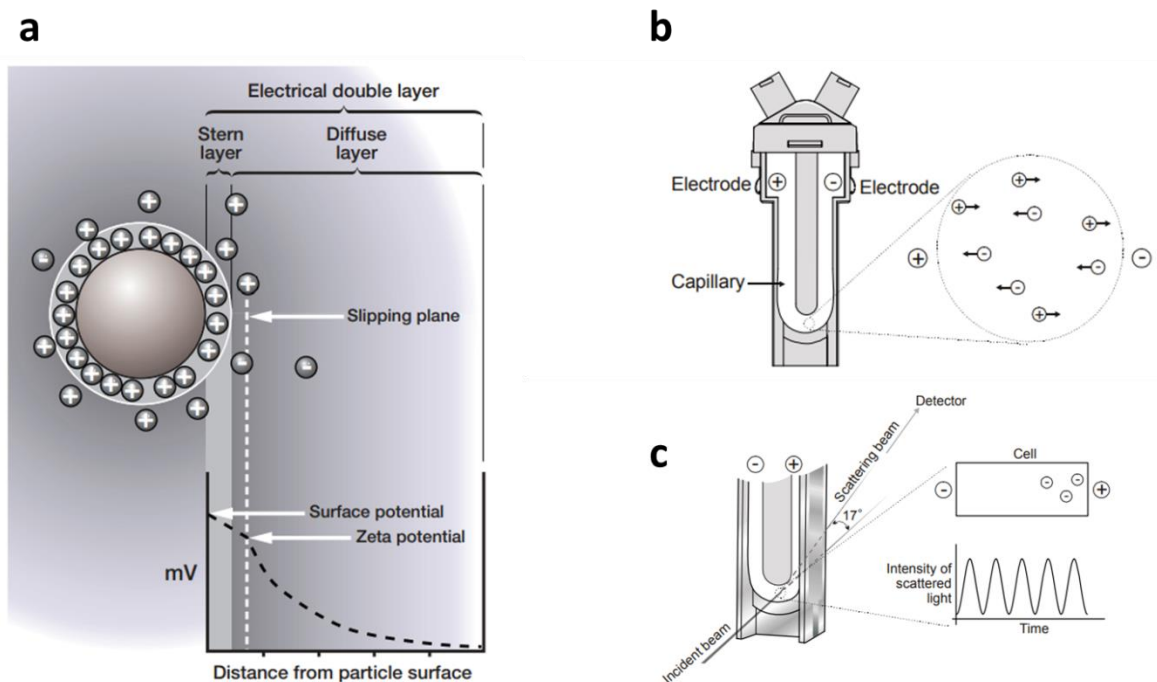


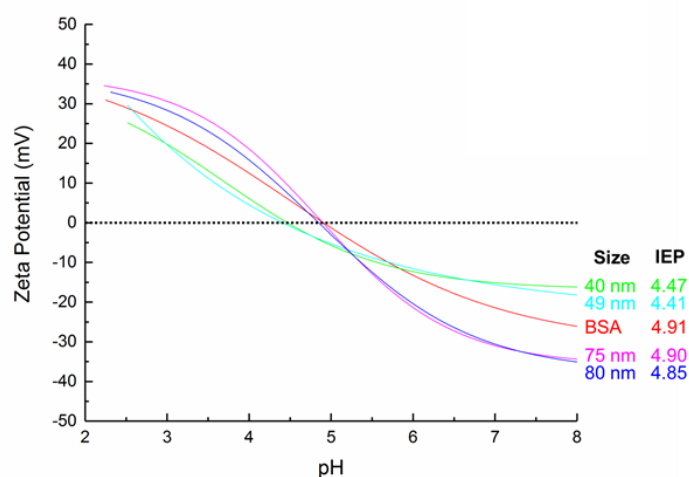
Fig. 3.13 a) An illustration of the electrical double layer that surrounds each protein nanoparticle in a suspension. A two-part liquid layer surrounds each particle, the inner layer is known as the Stern layer, where counter-ions are strongly attached and an outer, more diffuse layer where there is a significantly weaker interaction between the ions and the particle. A boundary exists within the diffuse layer where the ions and particle are stable, whereby when the particle moves the ions within the boundary move with the particle; this boundary is termed the slipping plane, or the surface of hydrodynamic shear. It is the potential at this boundary that is the zeta potential. **b)** The folded capillary cell used to carry out micro-electrophoresis to determine the electrophoretic mobility of the particles. **c)** Laser Doppler Velocimetry measuring fluctuations in intensity signals from scattered light to determine the velocity of the migrating particles. Images and theory courtesy of Malvern Instruments 2004.

An important characteristic to determine is how the surface charge of a species changes in different pH environments, especially in the context of purification systems, which is discussed in subsequent chapters. In order to assess this, isoelectric focussing was carried out whereby the zeta potential of the BSA nanoparticles was measured through incremental changes in pH buffer conditions. Using this technique it is also possible to determine the isoelectric point of the nanoparticles, which has significance both for colloidal stability and in tailoring its purification strategy.

Figure 3.14 highlights changes in the isoelectric point dependent on the size of the nanoparticles (a), as well as how the size of the nanoparticle changes as the pH of the suspension approaches and diverges from the isoelectric point (b). Interestingly, the larger nanoparticle preparations present an IEF curve shape and pI similar to that of the native protein, whilst the smaller nanoparticles have more acidic pI values, with less overall charge at both extremes of the curve.

With respect to isoelectric point deviations, as discussed in 3.3.8, increased Methanol concentrations have the potential to increase the efficiency of cross-linking reactions by “opening up” the protein structure, creating a larger surface area for cross linking of the lysine residues, producing smaller, tighter cross-linked nanoparticles. As lysine is a basic residue, with a pI of 9.7 (Carey, 2000), logically a higher level of cross-linking would result in more lysine residues being used for cross-linking and thus an acidic shift in the pI, compared to larger nanoparticles manufactured using less Methanol.

a



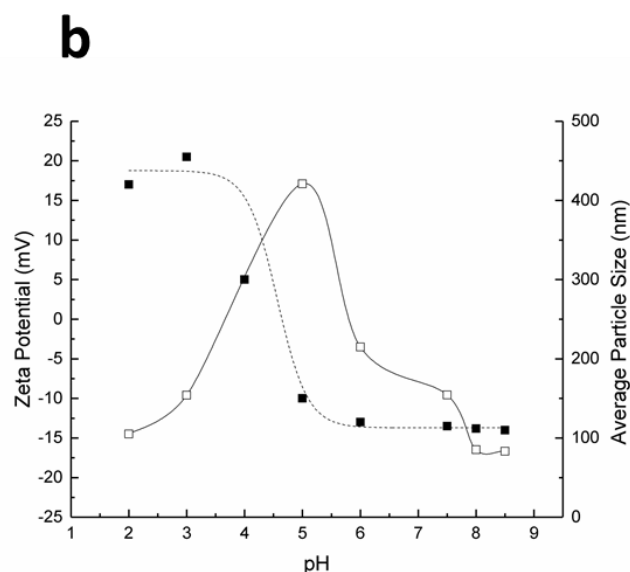


Fig. 3.14 a) Isoelectric focussing curves of BSA & BSA Nanoparticles of various sizes and **b)** changes in ζ -potential -■- and average particle size -□- of an 85 nm BSA nanoparticle as a function of varying pH.

Referring to Fig. 3.6, the yield (and thus, degree of incorporation of starting protein) increases as a function of average particle size. As more BSA molecules are incorporated into each nanoparticle (for a constant cross-linker concentration), the efficiency of glutaraldehyde in cross-linking proteins drops, resulting in larger, more loosely bonded nanoparticulates. It is therefore reasonable to assume that the larger nanoparticles experience less amino acid structural change as a result of cross linking and so will exhibit a similar isoelectric point to that of the native protein.

When considering the magnitude of ζ -potential at pH's away from the pI, the IEF curves suggest that the smaller nanoparticles internalise their polar residues (and present hydrophobic patches onto the surface of the nanoparticle) to a higher degree than the larger nanoparticles. It is hypothesised that this may be due to the method of manufacture of the nanoparticles, as the higher methanol concentrations required in the desolvation process to create smaller nanoparticles cause a higher degree of disruption to the solvation layer around the protein, allowing for better exposure and re-ordering of hydrophobic residues on the surface of the particles.

Considering that lysine is a charged, basic residue, one would expect that better cross-linked, smaller nanoparticles would have a more acidic pI and lower magnitudes of charge away from the pI compared to larger nanoparticles and native BSA. This is largely down to more efficient cross-linking removing free positively charged amino groups, thus whilst titrating toward basic conditions, fewer hydroxyl ions are required to reduce the colloidal surface charge to zero (or to reach pI), as confirmed by the work of Weber *et al.* in 2000 and Langer *et al.* in 2003.

It should also be mentioned that, as indicated by Fig. 3.14, the ζ -potential of the colloids at operating pH is independent of size or solvent preparation. BSA has 26 arginine ($pK_a = 12.48$), 17 histidine ($pK_a = 6.04$) and 60 lysine ($pK_a = 10.75$) (all positively charged at pH 8.0) and 59 glutamic acid ($pK_a = 4.10$) and 40 aspartic acid ($pK_a = 3.66$) (both negatively charged at pH 8.0) residues (Henchoz *et al.*, 2007). It is the ordering of these respective residues at the surface of the nanoparticle which will ultimately determine the nanoparticle species' overall surface charge.

When considering Fig. 3.14 b), as the suspending medium experiences a basic-shift away from the colloidal pI, for instance at pH 8.0, the solution counter-ions, in this case Na^+ , develop a stable coating around the colloid; the Stern layer, as illustrated in Fig. 3.14 a). In these conditions, charge repulsion prevents any flocculation of the nanoparticles together and keeps the colloids in suspension, with a stable particle size of ~ 80 nm.

Moving towards the isoelectric point through hydrochloric acid titration, the diffuse layer is built up with Cl^- ions, causing charge neutralisation at the surface of hydrodynamic shear, or the slipping plane. In this scenario, the charge repulsion effect is lost, causing the nanoparticles to aggregate together and eventually crash out of solution; this can be seen as at \sim pH 5, the average particle size is at its highest (421 nm – a 5 fold increase) with the nanoparticles visually aggregating and falling out of solution in the capillary cell. As the suspension transitions to acidic pHs beyond the pI of the nanoparticles, the effect is reversed and charge repulsion is restored (with opposite charges), preventing aggregation and a restoration of the average particle size.

3.3.11 Scale Down of Nanoparticle Fabrication

An ultra-scale down (USD) approach was adopted to facilitate the expeditious screening of multiple process parameters in order to determine the key variables which affect the quality of the nanoparticles produced. In addition to this, this approach allowed for lower volumes of expensive materials (solvent and protein) to be used as well as adopting a single-use approach of disposable Eppendorf tubes rather than having to clean 50 ml glass beakers; this would also reduce the risk of cross-contamination across batches as well as improve the batch-to-batch reproducibility whilst also saving time that would otherwise go into cleaning the glass vessels.

Figure 3.15 describes how this scale down was carried out and the associated key geometric parameters. The scale down was based on a 10 fold volumetric reduction in working volume, adding 100 μ L of 10% protein and 400 μ L of desolvating agent, before addition of 6 μ L of cross-linker. An important parameter to maintain was the stirrer: vessel diameter ratio, within commercially available constraints, thus a micro-flea was used and placed within an Eppendorf clamped directly above a magnetic stirrer plate.

To assess the efficacy and reproducibility of the scale down approach, a direct comparison was carried out at both scales under the same desolvating conditions, as illustrated in Fig. 3.14 d). It became apparent that although the overall trend in the reduction of particle size with increasing dielectric constant was preserved, the average particle size was on average 20-30% larger at the 0.1 ml working volume scale.

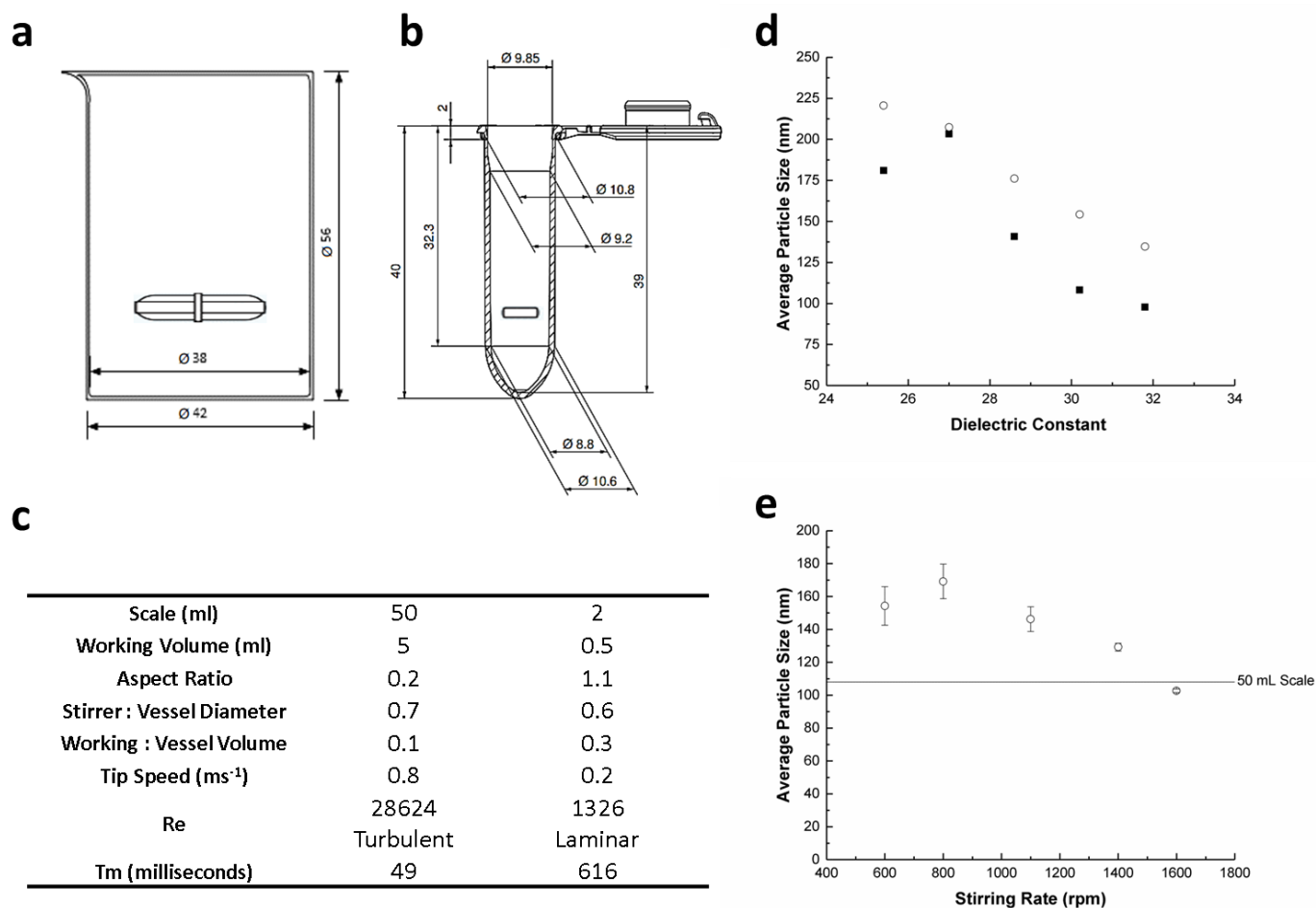


Fig. 3.15 Scale down approach for the manufacture of protein nanoparticles; **a)** large scale Simax 50 ml beaker utilising a 25 × 6 Spinbar® polygon stirrer, **b)** 2 ml Safe-Lock Eppendorf tube with a 5 × 2 Spinbar® microflea for stirring. Note that all dimensions are in mm and drawings are not to scale. **c)** key dimensions and metrics for both scales. The Reynolds number (Re) was calculated based on a 10% BSA solution desolvated by a 70: 30 MeOH: EtOH solvent mixture at a volumetric ratio of 1: 4, resulting in $\rho = 836.32 \text{ kg/m}^3$ & $\mu = 0.000872 \text{ N.s/m}^2$ (Chick and Lubrzynska, 1913; Doran, 1995). This dimensionless value would increase proportionally with additional Methanol in the mixture. **d)** The impact on scale down on average particle size over a range of dielectric constants for 50 ml scale -■- and 0.5 ml scale -○-. The native protein was dissolved in 10 mM NaCl prior to desolvation, in order to stabilise the high concentrations of protein at lower working volumes. **e)** The effect of increasing stirring rate on a 10% BSA solution desolvated by a 70: 30 MeOH: EtOH solvent mixture at 0.5 ml scale and the equivalent size for the same conditions at 50 ml scale (mean ± SD, n = 3).

The disparity in particle size as shown in Fig. 3.15 d) can be attributed to a number of factors and is likely a consequence of poor mixing patterns within the Eppendorf. Naturally poorer mixing conditions would limit the cross-linking reaction and result in looser, more open-structured and ultimately larger nanoparticles forming. In addition, the larger the stirrer: vessel diameter for a given power input or rpm, the lower the mixing time and thus the quicker the suspension reaches homogeneity and thus at smaller scale (for the same rotational speed) the mixing will be poorer (Nienow, 1997).

Furthermore, the aspect ratio of the vessel plays a very important role in mixing conditions; the ratio is 6 times larger at smaller scale and thus with a single agitator system, mixing is worse and time to homogeneity is longer (Afshar-Ghotli *et al.* 2013). This is due to the fact that the liquid level is much higher above the moving mixer component in the vessel and as such axial mixing becomes more difficult to achieve.

Calculation of tip speed, Reynolds number (Re) and mixing time (T_m) are shown below:

Equation 7:

$$Tip\ Speed = \pi \cdot D_s \cdot N_i$$

Where:

D_s is the diameter of the stirrer (m)

N_i is the rotational speed of the stirrer (s^{-1})

Equation 8:

$$Re = \frac{\rho u D}{\mu}$$

Where:

ρ is the density of the liquid (kg/m^3)

u is the velocity of the solution, in this case the tip speed of the stirrer (m/s)

D is the characteristic length of flow, in this case the internal diameter of the vessel (m)

μ is the dynamic viscosity of the liquid ($N \cdot sm^{-2}$)

To calculate the mixing the following equation was used:

Equation 9:

$$Tm = \frac{1.54 \cdot V}{D_s \cdot N_i}$$

Where:

V is the volume of the liquid (m³)

D_s is the diameter of the stirrer (m)

N_i is the rotational speed of the stirrer (s⁻¹)

Note that the approximation is determined for a Rushton turbine, however this is deemed to be the closest estimation available and is kept constant across both scales for the sake of comparison (Doran, 1995).

A further characteristic which is disparate between the two scales is that of the tip speed of the stirrer. Fig. 3.14 c) highlights that the tip speed is four times lower at small scale (for the same rpm) and thus mixing at the edge of the stirrer is severely limited. In addition to this, the power input per unit volume is much lower at the smaller scale ($P/V \propto u^2$) and thus mixing and circulation time will be lengthier, resulting in poorer cross-linking.

The Reynolds number (Re), which is the relationship between inertial and viscous forces in the solution and describes the fluid flow and thus the mixing conditions within the vessel, is used here to describe the degree of turbulence in the two systems (Doran, 1995). There is a stark difference in the flow patterns; at large scale the flow is turbulent and thus good mixing is achieved, whilst in the Eppendorf the mixing is much poorer, characterised by a laminar flow, with smoother fluid paths and low momentum convection.

The final parameter to calculate is, of course, the mixing time, which is based on a relationship between the system volume and the diameter of the stirrer (Equation 9). Evidently, the mixing time is significantly (12.5 times) longer at small scale indicating that it takes much longer for the suspension to reach homogeneity. This can result in an inefficient desolvation and will severely limit cross-linking reaction times, resulting in larger nanoparticles forming, as seen in Fig. 3.15 d).

In order to remediate the inconsistencies in particle size at smaller scale, the stirrer speed was systematically increased and average particle size recorded, as illustrated in Fig. 3.15 e). Theoretically, to reach the tip speed and mixing time needed to match large scale would require rotational speeds of 3000 rpm and 7000 rpm, respectively, which would be experimentally unfeasible.

However, by increasing the rotational speed above 1500 rpm in the Eppendorf vessels, the average particle size of the nanoparticles matched that of the 50 ml scale, for the same desolvating conditions. For these specific conditions, the tip speed and mixing time are 0.42 m/s and 230 milliseconds, respectively; not quite the same conditions but a significant improvement. The crucial

parameter here is the Re, which for these conditions is 3535, which represents a change from laminar flow to transient, verging on turbulent. This indicates that the fluid flow in the vessel has changed significantly, resulting in better mixing.

The justification for not requiring rotational speeds as dictated by identical tip speeds or mixing times may be down to the geometry of the vessel; the Eppendorf is round bottomed and thus there is less chance of mixing dead-spots due to improved radial mixing and circulation fluid dynamics, relative to a rectangular-bottomed vessel like the 50 ml glass beaker. For subsequent screening of process conditions, a stirrer speed of 1500-1600 rpm was adopted.

3.3.12 Influence of Process Parameters

In order to produce nanoparticles reproducibly and within a controlled size range, it is important to understand the impact of variations in manufacturing parameters and how this affects the characteristics of the nanoparticle suspension formed. Being able to predict and adjust these parameters to target specific sized nanoparticles becomes relevant when attempting to manufacture nanoparticles as surrogates of viral vectors. A summary of the experimental factors tested are detailed in Fig. 3.16.

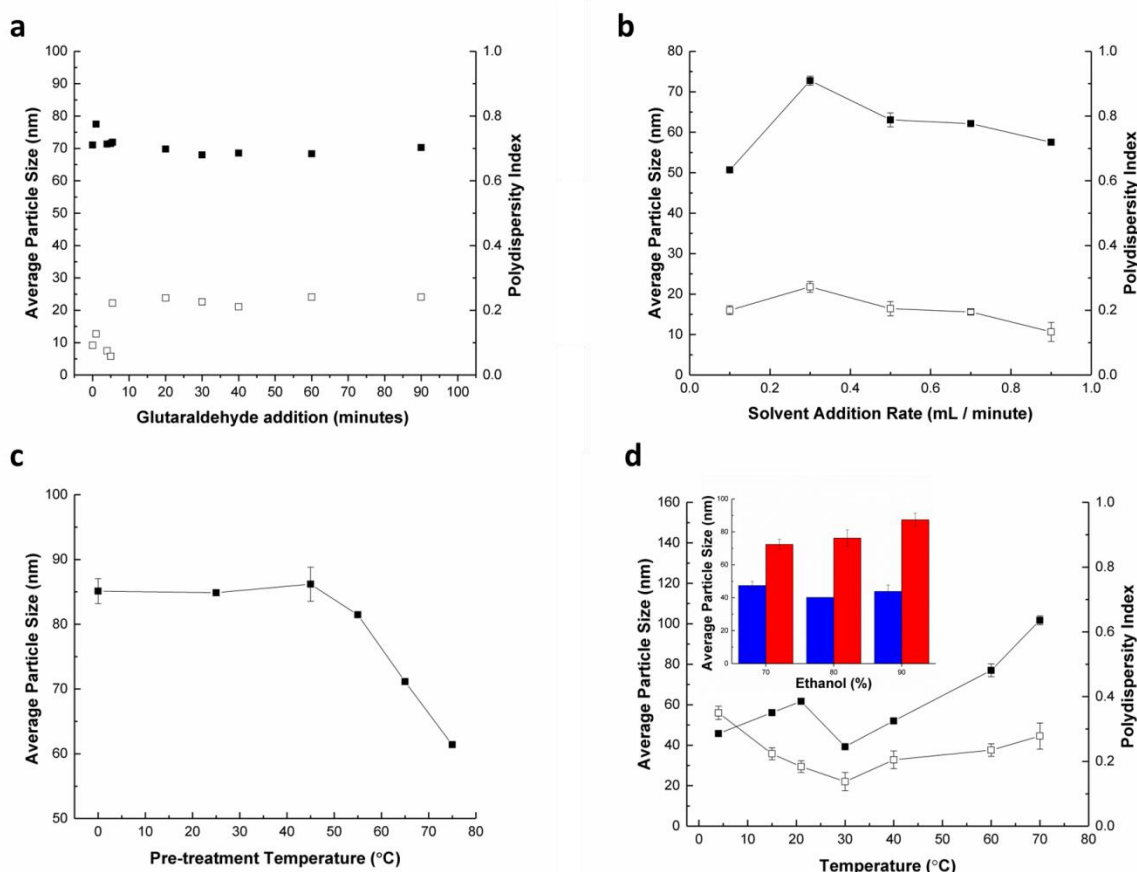


Fig. 3.16 The impact of **a)** the time of glutaraldehyde addition post-desolvation, **b)** addition rate of the organic solvent mixture, **c)** pre-treatment of the protein with heat and **d)** experimental temperature (inset: 4°C & 21°C) on the average particle size -■- and polydispersity index -□- of BSA nanoparticles (mean \pm SD, $n = 3$).

It is important to note here that some operating parameters were not considered for assessment based on prior optimisation detailed in literature; the fact that stirring rate should be ≥ 500 rpm in order to preserve both particle size and low polydispersity was demonstrated by von Storp *et al.* in 2012. The use of 60 μL of cross-linker is to theoretically cross-linker 100% of the available lysyl groups on BSA, though cross-linker amount was systematically varied and found to have little impact on particle size ranging from 40% to 200% of the theoretical required amount (Langer *et al.*, 2003).

The same group varied the concentration of serum albumin from 2.5% to 10%; the increase to 10%, whilst causing a slight increase in the eventual particle size, derived the lowest polydispersity, relative to lower starting concentrations of protein. These findings were confirmed by both Mehravar *et al.* in 2009 and Galisteo-González & Molina-Bolívar in 2014; the latter related the observations to nucleation rate theory, see Equations 10 and 11 below:

Equation 10:

$$J = c \cdot e^{\left(\frac{-B}{(\ln S)^2}\right)}$$

Equation 11:

$$B = \frac{16\pi\sigma^3V_s^2}{3k_B^3T^3}$$

Where:

J is the nucleation rate (per unit volume & unit time)

c is a constant of proportionality

B is the free energy at the pinnacle of the nucleation barrier

S is the degree of supersaturation ($S = C/C_0$; Solute concentration (C), Equilibrium solute solubility (C_0))

σ is the interfacial tension at the solid-liquid interface

V_s is the solute molecule volume

k_B is the Boltzmann constant (1.381×10^{-23} J/K) ($k_B = R \div N_A$, where N_A is the Avogadro constant, 6.022×10^{23}) (Reeks, 2011)

T is the absolute temperature (K)

(Genck, 1969)

A higher concentration of starting BSA results in higher viscosities, which limits the frequency of molecular transport of protein from the aqueous solution to organic solvent (as well as the rate of cross-linking), slowing the nucleation rate, allowing fewer and larger nucleation sites to form, facilitating the self-assembly of larger nanoparticles in more ordered structures, reducing the polydispersity too. However, higher protein concentrations also improve the degree of supersaturation (S), increasing the rate of nucleation, which could result in smaller nanoparticles forming (Langer *et al.*, 2003; Galisteo-González and Molina-Bolívar, 2014). These counter-acting influences may account for the only slight increase in particle size.

A protein: solvent ratio of 1: 4 was chosen based on literature and experimental observation. In all desolvating conditions, 4 ml of organic solvent was sufficient to observe turbidity in the solution, indicating appropriate unfolding of the protein and the beginning of the self-assembly process. These observations were confirmed by Weber *et al.*, who found little compromise to particle size also assessed the yield of protein and found that the degree of incorporation into the nanoparticles drastically improved as the ratio increased from 1: 0.5 to 1: 4 (Weber *et al.* 2000).

With respect to cross-linking incubation time, once again both literature and experimental trial and error were used to inform a reliable protocol. A number of groups (Weber *et al.* 2000; von Storp *et al.* 2012; Galisteo-González & Molina-Bolívar 2014; Jahanban-Esfahlan *et al.* 2016) quote overnight, 18 or 12 hours as appropriate time for cross-linking, however running sacrificial batches and sampling at 12, 18, 24, and 48 hours revealed little differences in the average particle size and polydispersity of the nanoparticles. For this reason, we have adopted a protocol of 12 hours to improve the throughput of our screening tests.

Finally, both Mehravar *et al.* and Galisteo-González & Molina-Bolívar optimised the pH of the protein solution, finding that titrating the pH of the solution above pH 8 resulted in consistent average particle sizes and low polydispersity of the nanoparticles (Mehravar, Jahanshahi and Saghatoleslami, 2009; Galisteo-González and Molina-Bolívar, 2014). Although glutaraldehyde can react with amino residues over a broad pH range (\geq pH 3) (Migneault *et al.*, 2004), this reaction is irreversible only between pH 7 to 9 (Okuda *et al.*, 1991) and thus sheds some light on optimal nanoparticles being formed at pH 8. Furthermore, at this pH, the protein and intermediate nanoparticles possess a strong net negative charge (see Fig. 3.14) and thus will exhibit strong electrostatic repulsion which limits coagulation of proteins during the cross-linking process and aids in keeping polydispersity down.

3.3.12.1 Cross-linker Addition

As detailed in Fig. 3.2, the process of re-folding of BSA post-desolvation into nanoclusters is one of self-assembly. The cross-linker is subsequently used to “lock” the structures into place via covalent cross-linkages and to maintain rigidity and stability.

In order to optimise the manufacturing process it is important to define an appropriate addition point to add the cross-linker and this was assessed systematically, as described in Fig. 3.16. It was promising to see that average particle size and polydispersity remain relatively constant after a delay of five minutes, which appears to be sufficient time for the nanoparticles to self-assemble into stable nanoparticles.

There does appear to be a window between instantaneous addition and five minutes where a polydispersity < 0.1 can be attained, without compromising the average particle size, which should be ~ 70 nm given the 70:30 Ethanol : Methanol desolvating ratio used. If this window is missed, the PDI appears to increase and then stabilise to ~ 0.2 (which is still acceptable) indicating that given more than five minutes, the self-assembly process becomes more disordered as the nanoparticles already formed have more time to interact and are subsequently cross-linked into di, tri or even poly-clusters, increasing the value of the polydispersity index.

3.3.12.2 Addition Rate of Organic Solvent

Whilst the majority of protocols opt for the use of a 1 ml / min addition rate of organic solvent (Weber *et al.* 2000; Langer *et al.* 2003; Langer *et al.* 2008; von Storp *et al.* 2012), an investigation into the rate of addition was carried out. The work by Langer *et al.* in 2003, Meharavar *et al.* and Galisteo-González & Molina-Bolívar, detail a decrease in particle diameter with increasing addition rate and conflicting results with respect to PDI (some proportional and others inversely proportional to addition rate). This data was collected over a broad range of addition rates, extending up to 10 ml/min in some cases.

These optimisation experiments were aimed at investigating the effects on particle size at much lower addition rates and in this range (0.1 – 1 ml / min) a similar trend was found, with decreasing particle sizes and improvement in PDI at higher rates. Interestingly, at very low rates of addition (0.1 ml / min) the average particle size doesn't fit the trend and is much lower than expected; the desolvating conditions were 80: 20, Ethanol : Water in this scenario (BSA in water), with an expected size of ~ 55 -60 nm at an addition rate of 1 ml/min.

It is hypothesised that this phenomenon can be explained by a change in the organic solvent mixture with respect to time. Despite stringent attempts to maintain a closed system, there is a portion of the manufacturing process where the system is open; the solvent runs along a glass rod to form uniform droplets into the protein solution and there is headspace in the vessel once the organic solvent has dropped into solution. Both aspects provide room for evaporation of solvent, especially at a flow rate of 0.1 ml / min, where it takes 40 minutes to complete the desolvation step. In this time, the composition of the organic solvent mixture is changing due to the higher volatility of Ethanol, relative to water, at room temperature (Pagni, 2005). As the Ethanol evaporates, the ratio is driven in favour of water, thus increasing the dielectric constant of the solution and, as per Fig. 3.10, the average particle size is reduced.

The polydispersity follows a similar trend to average particle size, with better preparations being formed with higher addition rates. This is likely due to more rapid desolvation taking place, with the protein in solution unfolding simultaneously leaving little solvated protein left in solution to

disrupt the self-assembly process of nanoparticles, helping to improve the polydispersity index. These findings justify the use of a 1 ml/min addition rate in good agreement with similar work, especially that of Mehravar *et al.* who demonstrate a parabolic relationship between addition rate and PDI, with a minima at 1 ml/min (Mehravar, Jahanshahi and Saghatoleslami, 2009).

3.3.12.3 Temperature

Another important factor to take into account is the influence of temperature, which can have a profound effect both on the structure of the protein, but also on the rate of reaction of unfolding and cross-linking. It was therefore important to investigate the impact of temperature on the formation of nanoparticles; first through heat pre-treatment of the monomer and secondly adjusting the temperature of the coacervation reaction.

3.3.12.3.1 Pre-heat Treatment

A systematic heat treatment study was carried out on the 10% BSA solution prior to desolvation. The solution was heated to a set temperature and held for five minutes under identical mixing conditions as the desolvation/cross-linking process. The solution and apparatus were subsequently allowed to cool to room temperature; all temperatures were checked with aid of an infrared thermometer (Extech IR400, Extech Instruments, NH, USA).

The study highlights little change between 0 °C (protein solution stored in an ice bath) to room temperature through to 45 °C. Beyond this temperature, an evident decrease in size is observed. This can be attributed to a permanent change in the secondary structure of the protein. Takeda *et al.* looked at the conformational changes of BSA during thermal denaturation and found that the ratio of α -helices to β -sheets decreased (characteristic of mild aggregation) with increasing temperature, though this conformational change was reversible below 45 °C., with some partial reversibility even up to 65 °C (Takeda *et al.*, 1989).

Whilst theoretically BSA has 59 lysyl groups available for cross-linking, Weber *et al.* demonstrate that in reality only ~ 9 amino groups per serum albumin molecules (HSA) are available for cross-linking. This is largely due to the secondary structure of BSA, ~ 55 -60% alpha-helical (Baler *et al.*, 2014) stabilised by 17 disulphide linkages (Wang and Chen, 2010), most of which are buried within the core of the protein and inaccessible to the surrounding solution (Carter and Ho, 1994).

Weber *et al.* illustrated an increase in available amino groups upon heating serum albumin to 70 °C, rising from 9 to 14; this was strongly supported by the work of Rombouts *et al.*, who demonstrated a re-ordering of the disulphide linkages upon heating BSA to 90 °C (Weber *et al.* 2000 and Rombouts *et al.* 2015). Their findings corroborate well with the concept that the native BSA conformation becomes more flexible (Borzova *et al.*, 2016) and the secondary structure distorts to various degrees under heat, unravelling to reveal more lysyl sites for potential cross-linking, facilitating stronger, tighter nanoparticle formation and a smaller average particle size.

A competing hypothesis is that the heat treatment, particularly at higher temperatures, leads to the formation of small, stable aggregates, which are subsequently cross-linked and fixed and thus

contribute to driving the average particle size down. No observable trend could be determined for PDI with respect to temperature increase (range between 0.18-0.22) however similar work by Borzova *et al.* document the precipitation of small particulates ($\sim 10\text{-}30\text{ nm}$) upon heating of BSA above 70°C (Borzova *et al.*, 2016), which support this hypothesis.

Heating beyond 75°C led to visible aggregation of the protein in solution, even after cooling to room temperature, thus nanoparticles could not be formed. A study by Murayama *et al.* found that above 74°C , the FTIR amide I band fingerprint at 1645 cm^{-1} for BSA broadens significantly as well as the appearance of strong bands at 1615 cm^{-1} and 1685 cm^{-1} , illustrating a disintegration of secondary disordered moieties and formation of strongly hydrogen-bonded β -sheet structures, respectively. Both indicate significant loss of native structure and for the latter, irreversible aggregation of the protein (Murayama and Tomida, 2004).

3.3.12.3.2 Experimental Temperature

Temperature also plays a role on the formation of nanoparticles during desolvation and cross-linking and impacts the process in a number of ways. The trend in Fig. 3.16d suggests a proportional relationship between temperature and average particle size, with a dip between $30\text{-}40^\circ\text{C}$ and polydispersities generally constant with a small dip over the same temperature range. The column graph, inset, illustrates the reduction in particle size at lower temperatures is reflected across a range of desolvating conditions.

The general trend of increasing temperature and average particle size is supported by both Rahimnejad *et al.* in 2002 and Galisteo-González *et al.* in 2014, who also demonstrate larger sized protein nanoparticles with respect to increasing temperatures. Initially, an increase in temperature will have an impact on the native protein, as discussed in the previous section, though in this scenario the protein is held at set temperature for a significant time period (12 hours) which can impact the intermolecular electrostatic, hydrophobic interactions and particularly the hydrogen bonding, all of which aid in stabilising the protein in its native state.

As we have seen with pre-treatment, higher temperatures ($\geq 45^\circ\text{C}$) lead to decreases in particle size, however the inverse is true in this instance. This suggests that, whilst protein structural change is integral here, the impact of temperature on other factors during desolvation/cross-linking are playing a more influential role on the overall trend here.

Temperature plays a pivotal role in the nucleation rate (Equations 10 & 11) and thus the final particle size; a slower nucleation rate creates fewer nuclei per unit volume, which will promote growth of the nanoparticles and lead to a larger average particle size (Zhang *et al.*, 2006; Park and Yeo, 2010; Galisteo-González and Molina-Bolívar, 2014). Equations 10 & 11 highlight the fact that an increase in temperature (T) reduces the free energy for the formation of a nucleus (B), thus subsequently reducing the rate of nucleation (J). To support this theory, the equations to derive the frequency factor (A), which describes the regularity of particle collisions, from the Arrhenius equation, are described below:

Equation 12:

$$A = N_0 v$$

Equation 13:

$$v = \frac{k_B T}{3\pi\alpha^3\eta}$$

Where:

N_0 is the initial number of molecules per unit volume

v is the frequency of molecular transport to the solid-liquid interface

α is the mean effective diameter of the solute (m)

η is the viscosity of the suspending liquid viscosity (kg/m.s)

k_B is the Boltzmann constant (1.381×10^{-23} J/K) ($k_B = R \div N_A$, where N_A is the Avogadro constant, 6.022×10^{23}) (Reeks, 2011)

T is the absolute temperature (K)

(Cao, 2004)

As temperature increases, the supersaturation reduces by enhancing the solubility of protein in the desolvating solvent, which reduces the rate of nucleation, creating fewer and larger nucleation sites, increasing the average particle size (see Equation 10). In addition, an increased temperature will lower the viscosity of the solution (see the Arrhenius-Guzman equation, Chapter II, Equation 2), and so the frequency of molecular transport and consequently the frequency of collisions will increase, facilitating an agglomeration effect in creating larger nanoparticles. Furthermore, the diffusional coefficient (Stokes-Einstein equation) will increase at higher temperatures (see Chapter II, Equation 3) which will again improve the accumulation of unfolded protein at nucleation sites, further contributing to the creation of larger particle sizes.

Considering the decrease in average particle size at $\sim 30-40^\circ \text{C}$, there are two possible hypotheses as to why this phenomenon occurs. The first is that globular proteins exhibit a parabolic temperature profile with respect to the free energy of stabilisation, with a minimum at $\sim 20^\circ \text{C}$ (for the protein chymotrypsinogen) (Jaenicke, 1990); it is feasible that BSA would have a similar profile with a minimum shift to higher temperatures due to its larger molecular weight. This parabolic relationship indicates the protein structure (and the intermolecular forces holding it together) is sensitive to disruption at both high and low temperatures.

At low temperatures, hydrogen bonding improves due to low bond energy requirements whilst concurrently the entropic-favoured hydrophobic interactions within the protein are weakened (Jaenicke, 1990). Thus smaller nanoparticles may be formed at low extremes of temperature due to a higher susceptibility of disruption from the organic solvent during desolvation and thus better exposure of buried lysine residues. The change in balance between these interactions during the transition from each extreme of temperature may contribute to changes in protein structure and the eventual formation of nanoparticles post-desolvation and cross-linking.

Alternatively, the decrease in particle size in this range may be due to a change in desolvating agent composition (Ethanol / Water mixture) as discussed in 3.3.12.2, with evaporation of the Ethanol accelerated at higher temperatures (the flash point of absolute Ethanol is 17 ° C (Pagni, 2005)), thus increasing the dielectric constant of the solution and driving the average particle size further down. The fact that the trend does not continue at higher temperatures may be due to competing impacts of temperature superseding that of higher rates of evaporating solvent and impacts on protein structure.

3.3.13 Nanoparticle Reproducibility

In order to optimise the manufacture of protein nanoparticles, production needs to be both reproducible and robust such that a defined experimental set up will produce predictable results. Fig. 3.17 demonstrates variance between batches and from different protein stocks.

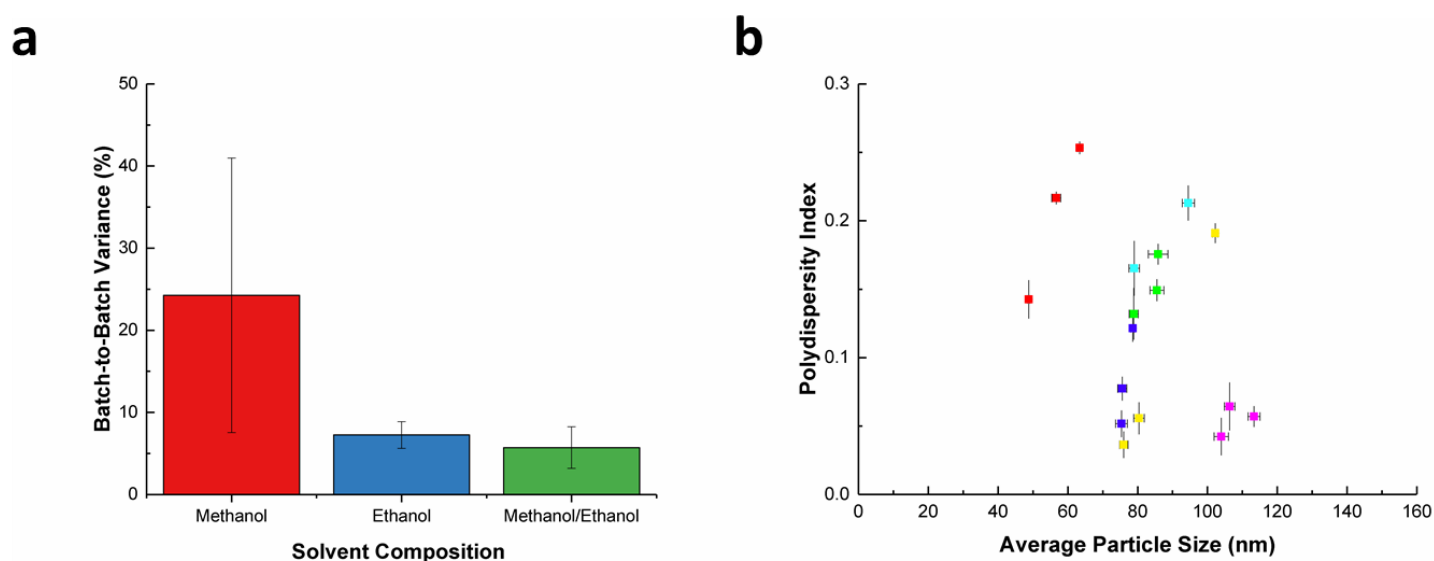


Fig. 3.17 a) The batch-to-batch variance in mean particle size of protein nanoparticles manufactured under various organic solvent compositions. **b)** Average particle size and PDI of nanoparticle preparations manufactured under identical conditions (Methanol: Ethanol, 70: 30) with each colour representing a new 10% BSA stock (mean \pm SD, $n = 3$).

Equation 14:

$$\text{Variance} = \frac{\text{Standard Deviation}}{\text{Mean Particle Size}}$$

Methanolic desolvating agents appear to produce nanoparticles with the highest batch-to-batch variance. This may be attributed to the smaller average particle size produced using Methanol; its absolute size deviation appearing more significant when compared relatively to the other conditions. On the other hand, the solvent itself may play a role in the batch variance; absolute Methanol has the highest volatility of the three organic solvent conditions tested, thus will be the most susceptible to evaporation during manufacture. It is feasible that variations in room temperature on any given day could contribute to the rate of evaporation of the solvent and thus result in disparities in average particle size from batch-to-batch.

Mixtures of ethanol/methanol appear to show the least variation, likely due to the influence of both solvents limiting evaporation through inter-molecular forces such as hydrophobic interaction and hydrogen bonding, which aid in keeping the Methanol in solution.

Fig. 3.17b highlights the importance of the starting BSA stock solution used to manufacture the nanoparticles. Lyophilised BSA powder dissolved in aqueous solution can contain a mixture of monomeric, dimeric and trimeric BSA in varying ratios. In order to maintain reproducibility in the manufacturing process, the monomeric protein should be purified via size-exclusion chromatography step prior to protein nanoparticle manufacture (Murayama and Tomida, 2004).

3.3.14 Protein 2° Structure Analysis

In order to probe the secondary structure characteristics of the various protein species and track changes through the nanoparticle manufacturing process, a circular dichroism approach was adopted. The spectral data was analysed for structural composition using a self-consistent method, whereby the secondary structure of the protein species is estimated via a deconvolution algorithm, SELCON3 (Sreerama and Woody, 1993).

Inspection of the raw spectra indicates secondary structural changes do occur upon desolvation. BSA is predominantly α -helical, with classical minima at both 208 and 222 nm, with a maximum at 190 nm. The spectra also highlight very little change in the 250-300 nm region, which suggests a preservation of the protein tertiary structure and the environment surrounding phenylalanine, tyrosine, cysteine and tryptophan residues (Greenfield, 2006).

During unfolding and re-folding, increases in β -sheet/turn formation and subsequent reduction in α -helical structure, with little change to the unordered secondary structures occur. This is symptomatic of protein aggregation, where the formation of β -sheet fibres occurs. These findings correlate well with that of the coacervation of α -lactalbumin nanoparticles (Arroyo-Maya *et al.*, 2014). This fibrillation/amyloidation process derives stability for partially folded or unfolded states as the protein residues re-orientate to the new organic solvent conditions (Holm *et al.*, 2007). Upon addition of a cross-linker, it appears this conformational change is locked in place, coinciding with the formation of stable protein nanoparticles.

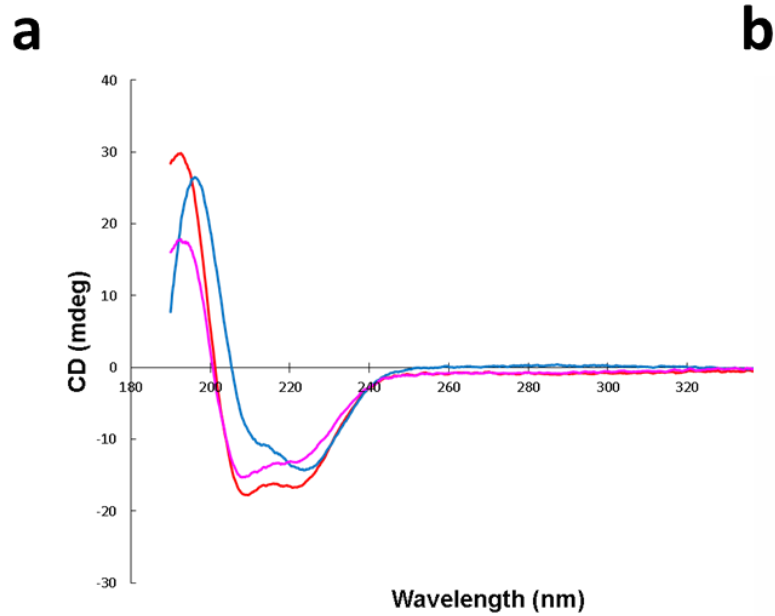


Fig. 3.18 a) CD spectra for *BSA*, *Desolvated BSA* and *BSA Nanoparticles*. **b)** The relative proportions of secondary structure for the protein in its native and desolvated states, as well as the conformational change once formed into nanoparticles.

3.3.15 Nanoparticle Morphology

Two orthogonal techniques were utilised to image the protein nanoparticles to assess their morphology and homogeneity, as demonstrated in Fig. 3.19.

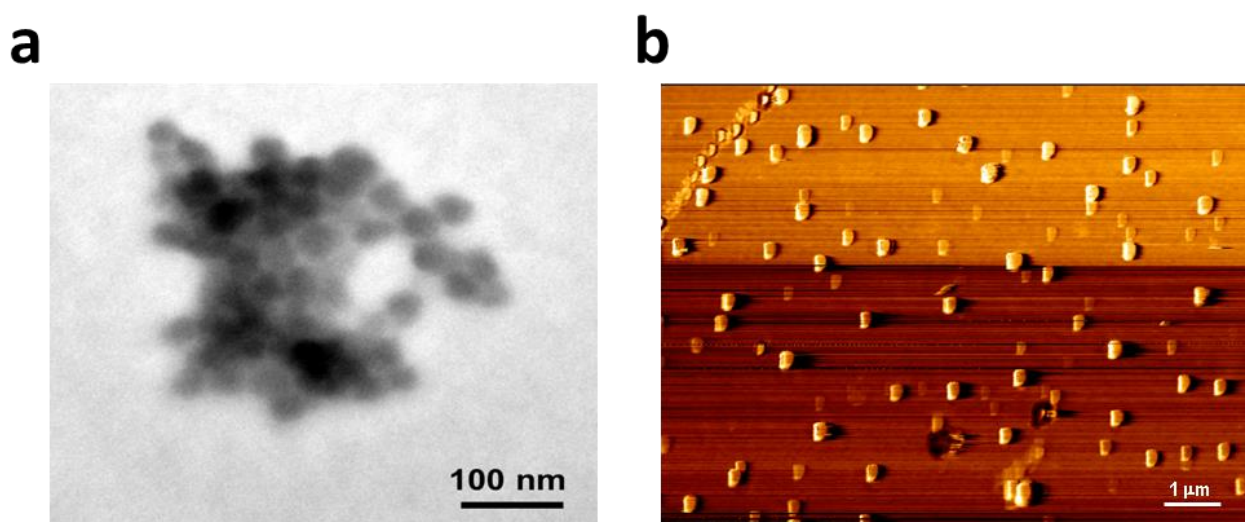


Fig. 3.19 BSA Nanoparticles images; **a)** A transmission electron micrograph imaged using a negative uranyl acetate stain and **b)** An atomic force microscopy image acquired via liquid tapping mode.

3.3.15.1 Transmission Electron Microscopy

Transmission Emission Microscopy images illustrate the formation of nanoparticle aggregates, pertinent to the sample preparation involved in BIO-TEM. The sample is critical point dried, removing, to trace, water, before being negatively stained with uranyl acetate, in order to enhance imaging contrast. Images reveal smooth, rounded nanoparticles aggregated in clumps during dehydration. The comparative sizes of the nanoparticles from the TEM images, as processed by ImageJ, were approximately 50% smaller than the Stokes diameter indicated by DLS. This is as a result of shrinking during dehydration and corroborates well with other similar studies (Yu *et al.*, 2014).

3.3.15.2 Atomic Force Microscopy

Atomic Force Microscopy facilitated the imaging of the nanoparticle species in their hydrated state, immersed in an aqueous-based buffer. The phase image illustrates relatively monodisperse, uniform nanoparticles anchored onto the poly-L-lysine slide, with a size distribution corroborating well to the 80 nm average size attained from DLS analysis.

3.3.16 Adenovirus Type V Mimic

In order to create suitable viral mimics which are applicable to the characterisation of chromatography media, the protein nanoparticles should exhibit similar physiochemical properties such that they interact with the purification resin in an analogous fashion. Given the optimisation of manufacture of nanoparticles, it is possible to target specific nanoparticle sizes within narrow distribution ranges, in order to mimic viral particles. Fig 3.20 illustrates the similarity in average particle size, whilst the TEM images reveal similarities in the morphology of both species.

The CD spectra demonstrate that both species have α -helical character; the hexon protein is mostly random coil, with close to equal amounts of both α -helical (27%) and β -sheet/turn (26%) structure. Important to note here is that the AdV capsid is composed of multiple proteins; mostly hexon proteins (60%), followed by varying amounts of minor proteins (IIIa, VI, VIII & IX), penton bases and fibres (Rexroad *et al.*, 2003). This is therefore a rudimentary estimation of the composition of the viral capsid, but nonetheless a good starting point for comparison. Crucially, ζ -potential values for both species (and the isoelectric point) are similar, indicating they will behave in a similar fashion when interacting with a chromatography resin.

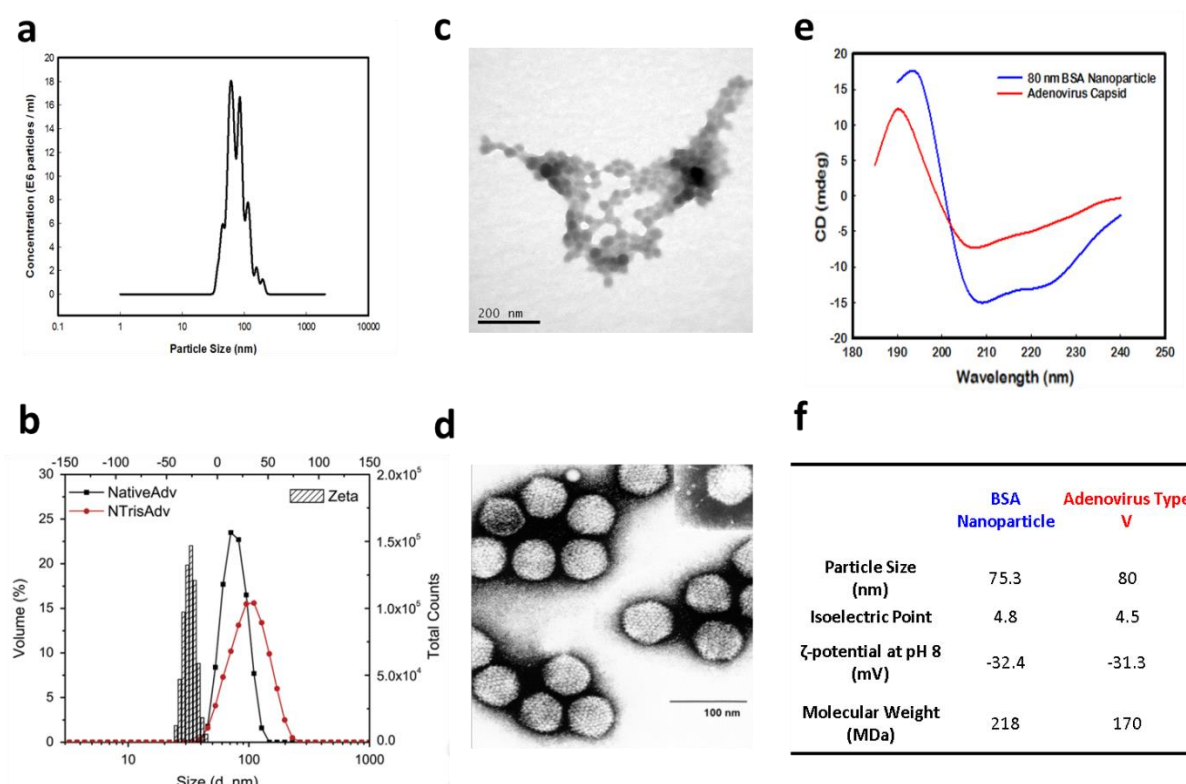


Fig. 3.20 A comparative study of BSA nanoparticles and Adenovirus type V (AdV); **a**) Nano-tracking analysis of the BSA nanoparticles with an average particle size of 75 nm compared to **b**) DLS & ζ-potential analysis (pH 8) of native AdV (Weng et al., 2014). **c**) & **d**) Transmission electron micrographs of BSA nanoparticles and AdV¹⁰. **e**) Circular dichroism spectra for both the 75 nm BSA nanoparticle and that of the AdV hexon capsid protein (Day et al., 1972). **f**) Summary table highlighting the similarities in physiochemical properties between the protein nanoparticle mimic and that of the bona fide virus particle (Trilisky and Lenhoff, 2007).

3.4 Conclusions

This chapter demonstrates the reproducible and robust manufacture of Bovine Serum Albumin nanoparticles from native protein using a desolvation and cross-linking technique. The work details both the influence of a variety of process parameters as well as the effective scale down of the technique to improve throughput of analytical testing.

Characterisation of the nanoparticles has also been described herein, using numerous complimentary techniques to understand the physiochemical properties of the nanoparticles produced. The work highlights the ability to create protein nanoparticles as appropriate surrogate mimics of a virus species with gene therapy applicability.

The ability to generate these synthetic protein nanoparticles in high volume and in a relatively short time span has the potential to create a pathway for screening and characterising new and already commercial chromatography and alternative purification media via the analytical tools shown

¹⁰ Image sourced from http://www.virology.net/Big_Virology/EM/Adeno-FD.jpg

herein. This holds promise for rapid development and optimisation of the downstream process chain of high value gene therapy products in the near future.

3.5 References

- Afshar Ghotli, R. et al., 2013. LIQUID-LIQUID MIXING IN STIRRED VESSELS: A REVIEW. *Chemical Engineering Communications*, 200(5), pp.595–627. Available at: <http://www.tandfonline.com/doi/abs/10.1080/00986445.2012.717313> [Accessed September 23, 2018].
- Arnold, K. et al., 1985. The dielectric properties of aqueous solutions of poly(ethylene glycol) and their influence on membrane structure. *Biochimica et biophysica acta*, 815(3), pp.515–8. Available at: <http://www.ncbi.nlm.nih.gov/pubmed/3995041> [Accessed July 20, 2018].
- Arroyo-Maya, I.J. et al., 2014. α -Lactalbumin nanoparticles prepared by desolvation and cross-linking: Structure and stability of the assembled protein. *Biophysical Chemistry*, 193–194, pp.27–34. Available at: <http://linkinghub.elsevier.com/retrieve/pii/S0301462214000878> [Accessed March 8, 2017].
- Bala, I., Hariharan, S. & Kumar, M.R., 2004. PLGA Nanoparticles in Drug Delivery: The State of the Art; *Critical Reviews in Therapeutic Drug Carrier Systems*, 21(5), pp.387–422. Available at: <http://www.dl.begellhouse.com/journals/3667c4ae6e8fd136,3531fe42318c587e,108d6b8570af47da.html> [Accessed October 3, 2018].
- Baler, K. et al., 2014. Electrostatic Unfolding and Interactions of Albumin Driven by pH Changes: A Molecular Dynamics Study. Available at: <https://pubs.acs.org/sharingguidelines> [Accessed September 29, 2018].
- Bee, J.S. et al., 2010. Aggregation of a monoclonal antibody induced by adsorption to stainless steel. *Biotechnology and Bioengineering*, 105(1), pp.121–129. Available at: <http://www.ncbi.nlm.nih.gov/pubmed/19725039> [Accessed April 24, 2018].
- Bee, J.S. et al., 2009. Response of a concentrated monoclonal antibody formulation to high shear. *Biotechnology and Bioengineering*, 103(5), pp.936–943. Available at: <http://www.ncbi.nlm.nih.gov/pubmed/19370772> [Accessed April 24, 2018].
- Bellissent-Funel, M.-C. et al., 2016. Water Determines the Structure and Dynamics of Proteins. *Chemical Reviews*, 116(13), pp.7673–7697. Available at: <http://pubs.acs.org/doi/10.1021/acs.chemrev.5b00664> [Accessed July 24, 2018].
- Borzova, V.A. et al., 2016. Kinetics of Thermal Denaturation and Aggregation of Bovine Serum Albumin. *PloS one*, 11(4), p.e0153495. Available at: <http://www.ncbi.nlm.nih.gov/pubmed/27101281> [Accessed September 29, 2018].
- Burke, J., 1984. Solubility Parameters: Theory and Application. *The American Institute for Conservation*, 3. Available at: <https://cool.conservation-us.org/coolaic/sg/bpg/annual/v03/bp03-04.html> [Accessed August 13, 2018].
- Cao, G., 2004. *Nanostructures and Nanomaterials*, Imperial College Press. Available at: <https://www.worldscientific.com/worldscibooks/10.1142/p305> [Accessed September 30, 2018].

- Cao, H. et al., 2018. Transducing Airway Basal Cells with a Helper-Dependent Adenoviral Vector for Lung Gene Therapy. *Human Gene Therapy*, 29(6), pp.643–652. Available at: <http://www.ncbi.nlm.nih.gov/pubmed/29320887> [Accessed October 2, 2018].
- Carey, F.A., 2000. *ORGANIC CHEMISTRY* 4th ed., James M. Smith. Available at: <https://peralta18.files.wordpress.com/2011/12/francis-a-carey-organic-chemistry-4th-ed.pdf> [Accessed September 18, 2018].
- Carr, B. & Malloy, A., 2007. *NanoParticle Tracking Analysis – The NANOSIGHT system*, Available at: <http://www.me.umn.edu/centers/cdr/reports/NanoSightPaper.pdf> [Accessed April 24, 2018].
- Carter, D.C. & Ho, J.X., 1994. Structure of serum albumin. *Advances in protein chemistry*, 45, pp.153–203. Available at: <http://www.ncbi.nlm.nih.gov/pubmed/8154369> [Accessed September 29, 2018].
- Chick, H. & Lubrzynska, E., 1913. *VII. THE VISCOSITY OF SOME PROTEIN SOLUTIONS*, London. Available at: <https://www.ncbi.nlm.nih.gov/pmc/articles/PMC1276544/pdf/biochemj01209-0068.pdf> [Accessed September 23, 2018].
- Day, L.A. et al., 1972. Optical Properties of the Hexon of Adenovirus. *European Journal of Biochemistry*, 29(3), pp.537–541. Available at: <http://doi.wiley.com/10.1111/j.1432-1033.1972.tb02019.x> [Accessed April 21, 2017].
- DeForest, C.A., Polizzotti, B.D. & Anseth, K.S., 2009. Sequential click reactions for synthesizing and patterning three-dimensional cell microenvironments. *Nature Materials*, 8(8), pp.659–664. Available at: <http://www.ncbi.nlm.nih.gov/pubmed/19543279> [Accessed October 3, 2018].
- Deshapriya, I.K. et al., 2015. Fluorescent, Bioactive Protein Nanoparticles (Prodots) for Rapid, Improved Cellular Uptake. *Bioconjugate chemistry*, 26(3), pp.396–404.
- Doran, P.M., 1995. *Bioprocess engineering principles*, Academic Press. Available at: https://books.google.co.uk/books?id=GoOqw3hKIyIC&pg=PA149&clpg=PA149&dq=mixing+time+1.54&source=bl&ots=ZM_elA8ji_&sig=qVX25OoV01TqBEzpLal87XzcV1A&hl=en&sa=X&ved=2ahUKEwi4hLmSrtPdAhVROBoKHQV4DUMQ6AEwBHoECAYQAQ#v=onepage&q=tip speed&f=false [Accessed September 24, 2018].
- Duffy, A.M. et al., 2005. Purification of adenovirus and adeno-associated virus: comparison of novel membrane-based technology to conventional techniques. *Gene Therapy*, 12(S1), pp.S62–S72. Available at: <http://www.nature.com/articles/3302616> [Accessed October 2, 2018].
- Elzoghby, A.O., Samy, W.M. & Elgindy, N.A., 2012. Albumin-based nanoparticles as potential controlled release drug delivery systems. Available at: https://ac.els-cdn.com/S016836591100558X/1-s2.0-S016836591100558X-main.pdf?_tid=15dda475-6b1e-4fb8-856b-58db850becb8&acdnat=1534177126_fae4bc6f36207bb91c84e1a739dc1015 [Accessed August 13, 2018].

- Erickson, H.P., 2009. Size and Shape of Protein Molecules at the Nanometer Level Determined by Sedimentation, Gel Filtration, and Electron Microscopy. *Biological Procedures Online*, 11(1), pp.32–52.
- Fahlränder, E. et al., 2015. PEGylated human serum albumin (HSA) nanoparticles: preparation, characterization and quantification of the PEGylation extent. *Nanotechnology*, 26(14), p.145103. Available at: <http://www.ncbi.nlm.nih.gov/pubmed/25789544> [Accessed October 3, 2018].
- Fernandes, C.S.M. et al., 2015. Biobased Monoliths for Adenovirus Purification. Available at: www.acsami.org [Accessed October 3, 2018].
- Filipe, V., Hawe, A. & Jiskoot, W., 2010. Critical Evaluation of Nanoparticle Tracking Analysis (NTA) by NanoSight for the Measurement of Nanoparticles and Protein Aggregates. *Pharmaceutical Research*, 27(5), pp.796–810. Available at: <http://www.ncbi.nlm.nih.gov/pubmed/20204471> [Accessed April 24, 2018].
- Fuenmayor, J., Gòdia, F. & Cervera, L., 2017. Production of virus-like particles for vaccines. *New Biotechnology*, 39, pp.174–180. Available at: <https://www.sciencedirect.com/science/article/pii/S1871678416325511?via%3Dihub> [Accessed October 3, 2018].
- Furniss, B.S. et al., 1989. *Vogel's Textbook of Practical Organic Chemistry* 5th ed., Longman Scientific & Technical. Available at: https://fac.ksu.edu.sa/sites/default/files/vogel_-_practical_organic_chemistry_5th_edition.pdf [Accessed July 20, 2018].
- Galisteo-González, F. & Molina-Bolívar, J.A., 2014. Systematic study on the preparation of BSA nanoparticles. *Colloids and Surfaces B: Biointerfaces*, 123, pp.286–292.
- GE Life Sciences, 2000. *BioProcess™ Media-Made for bioprocessing Secure Supply • Large capacity production integrated with clear ordering and delivery routines-means availability in the*, Available at: www.gelifesciences.com/protein-purification [Accessed July 21, 2018].
- Genck, W.J., 1969. *Temperature effects on growth and nucleation rates in mixed suspension crystallization*, Available at: <https://lib.dr.iastate.edu/rtd/4105> [Accessed September 30, 2018].
- Gercel-Taylor, C. et al., 2012. Nanoparticle analysis of circulating cell-derived vesicles in ovarian cancer patients. *Analytical Biochemistry*, 428(1), pp.44–53. Available at: <https://www.sciencedirect.com/science/article/pii/S0003269712003089?via%3Dihub> [Accessed April 24, 2018].
- Ghosh, P. et al., 2008. Gold nanoparticles in delivery applications☆. *Advanced Drug Delivery Reviews*, 60(11), pp.1307–1315. Available at: <http://linkinghub.elsevier.com/retrieve/pii/S0169409X08000999>.
- Ginn, S.L. et al., 2018. Gene therapy clinical trials worldwide to 2017: An update. *The Journal of Gene Medicine*, (January), p.e3015.
- Goebel-Stengel, M. et al., 2011. The importance of using the optimal plasticware and glassware in

- studies involving peptides. *Analytical biochemistry*, 414(1), pp.38–46. Available at: <http://www.ncbi.nlm.nih.gov/pubmed/21315060> [Accessed April 26, 2018].
- Govender, T. et al., 1999. PLGA nanoparticles prepared by nanoprecipitation: drug loading and release studies of a water soluble drug. *Journal of Controlled Release*, 57(2), pp.171–185. Available at: <https://www.sciencedirect.com/science/article/pii/S0168365998001163> [Accessed October 3, 2018].
- Greenfield, N.J., 2006. Using circular dichroism spectra to estimate protein secondary structure. *Nature protocols*, 1(6), pp.2876–90. Available at: <http://www.ncbi.nlm.nih.gov/pubmed/17406547> [Accessed October 2, 2018].
- Henchoz, Y. et al., 2007. Rapid determination of pK_a values of 20 amino acids by CZE with UV and capacitively coupled contactless conductivity detections. *Analytical and Bioanalytical Chemistry*, 389(6), pp.1869–1878. Available at: <http://link.springer.com/10.1007/s00216-007-1568-5> [Accessed October 28, 2018].
- Herskovits, T.T., Gadegbeku, B. & Jaillet, H., 1970. On the Structural Stability and Solvent Denaturation of Proteins. *THE JOURNAL OF BIOLOGICAL CHEMISTRY*, 245(10), pp.2588–2598. Available at: <http://www.jbc.org/> [Accessed October 23, 2018].
- Holban, A.M., Grumezescu, A.M. & Giri, T.K., 2016. Alginate Containing Nanoarchitectonics for Improved Cancer Therapy. *Nanoarchitectonics for Smart Delivery and Drug Targeting*, pp.565–588. Available at: <https://www.sciencedirect.com/science/article/pii/B9780323473477000203> [Accessed July 24, 2018].
- Holm, N.K. et al., 2007. Aggregation and fibrillation of bovine serum albumin. *Biochimica et Biophysica Acta (BBA) - Proteins and Proteomics*, 1774(9), pp.1128–1138. Available at: <http://www.sciencedirect.com/science/article/pii/S1570963907001501> [Accessed April 21, 2017].
- Horwitz, M., Fields, B.N. & Knipe, D.M., 1986. *Fundamental virology*, Raven Press.
- Huo, Y. et al., 2018. Expression and purification of norovirus virus like particles in Escherichia coli and their immunogenicity in mice. *Molecular Immunology*, 93, pp.278–284. Available at: <https://linkinghub.elsevier.com/retrieve/pii/S0161589017304443> [Accessed October 3, 2018].
- Hyun, H. et al., 2018. Surface modification of polymer nanoparticles with native albumin for enhancing drug delivery to solid tumors. *Biomaterials*, 180, pp.206–224. Available at: <http://www.ncbi.nlm.nih.gov/pubmed/30048910> [Accessed September 3, 2018].
- Isayeva, T. et al., 2003. Advanced methods of adenovirus vector production for human gene therapy: roller bottles, microcarriers, and hollow fibers. *BioProcess J*, 2(5), pp.75–81.
- Jaenicke, R., 1990. Protein structure and function at low temperatures. *Philosophical transactions of the Royal Society of London. Series B, Biological sciences*, 326(1237), pp.535–51–3. Available at: <http://www.ncbi.nlm.nih.gov/pubmed/1969647> [Accessed September 30, 2018].

- Jahanban-Esfahlan, A., Dastmalchi, S. & Davaran, S., 2016. A simple improved desolvation method for the rapid preparation of albumin nanoparticles. *International Journal of Biological Macromolecules*, 91, pp.703–709. Available at: <https://www.sciencedirect.com/science/article/pii/S0141813016304433?via%3Dihub> [Accessed August 9, 2018].
- Jahanshahi, M. & Najafpour, G.D., 2006. Production of biological nanoparticles from bovine serum albumin for drug delivery. *African Journal of Biotechnology*, 5(20), pp.1918–1923.
- Jun, J.Y., Nguyen, H.H., Paik, S.-Y.-R., et al., 2011. Preparation of size-controlled bovine serum albumin (BSA) nanoparticles by a modified desolvation method. *Food Chemistry*, 127(4), pp.1892–1898. Available at: <http://www.sciencedirect.com/science/article/pii/S0308814611002986> [Accessed August 18, 2015].
- Jun, J.Y., Nguyen, H.H., Paik, S.Y.R., et al., 2011. Preparation of size-controlled bovine serum albumin (BSA) nanoparticles by a modified desolvation method. *Food Chemistry*, 127(4), pp.1892–1898. Available at: <http://dx.doi.org/10.1016/j.foodchem.2011.02.040>.
- Kim, D.-H. & Martin, D.C., 2006. Sustained release of dexamethasone from hydrophilic matrices using PLGA nanoparticles for neural drug delivery. *Biomaterials*, 27(15), pp.3031–3037. Available at: <https://www.sciencedirect.com/science/article/pii/S0142961206000044> [Accessed October 3, 2018].
- Klyushnichenko, V. et al., 2001. Improved high-performance liquid chromatographic method in the analysis of adenovirus particles. *Journal of chromatography. B, Biomedical sciences and applications*, 755(1–2), pp.27–36. Available at: <http://www.ncbi.nlm.nih.gov/pubmed/11393714> [Accessed March 13, 2018].
- Kovalchuk, N.M. & Starov, V.M., 2012. Aggregation in colloidal suspensions: Effect of colloidal forces and hydrodynamic interactions. *Advances in Colloid and Interface Science*, 179–182, pp.99–106. Available at: <https://www.sciencedirect.com/science/article/pii/S0001868611001187> [Accessed September 5, 2018].
- Langer, K. et al., 2008. Human serum albumin (HSA) nanoparticles: reproducibility of preparation process and kinetics of enzymatic degradation. *International journal of pharmaceutics*, 347(1–2), pp.109–17. Available at: <http://www.ncbi.nlm.nih.gov/pubmed/17681686> [Accessed November 9, 2015].
- Langer, K. et al., 2003. Optimization of the preparation process for human serum albumin (HSA) nanoparticles. *International Journal of Pharmaceutics*, 257(1–2), pp.169–180.
- Langer, K. et al., 2000. Preparation of avidin-labeled protein nanoparticles as carriers for biotinylated peptide nucleic acid. *European Journal of Pharmaceutics and Biopharmaceutics*, 49(3), pp.303–307. Available at: <https://www.sciencedirect.com/science/article/pii/S0939641100000680> [Accessed October 3, 2018].
- Lin, W. et al., 1997. Preparation of surface-modified albumin nanospheres. *Biomaterials*, 18(7),

- pp.559–565. Available at: <https://www.sciencedirect.com/science/article/pii/S0142961296001767> [Accessed April 30, 2018].
- Liu, S.H. & Han, M.Y., 2005. Synthesis, Functionalization, and Bioconjugation of Monodisperse, Silica-Coated Gold Nanoparticles: Robust Bioprobes. *Advanced Functional Materials*, 15(6), pp.961–967. Available at: <http://doi.wiley.com/10.1002/adfm.200400427>.
- Lohcharoenkal, W. et al., 2014. Protein nanoparticles as drug delivery carriers for cancer therapy. *BioMed research international*, 2014, p.180549. Available at: <http://www.ncbi.nlm.nih.gov/pubmed/24772414> [Accessed October 3, 2018].
- Lowry, G. V et al., 2014. Guidance to improve the scientific value of zeta potential measurements in nanoEHS. Available at: <https://pubs.rsc.org/en/content/articlepdf/2016/en/c6en00136j> [Accessed July 24, 2018].
- Lu, J. et al., 2007. Mesoporous Silica Nanoparticles as a Delivery System for Hydrophobic Anticancer Drugs. *Small*, 3(8), pp.1341–1346. Available at: <http://doi.wiley.com/10.1002/smll.200700005> [Accessed October 3, 2018].
- Majorek, K.A. et al., 2012. Structural and immunologic characterization of bovine, horse, and rabbit serum albumins. *Mol.Immunol.*, 52, pp.174–182. Available at: <https://www.rcsb.org/structure/3V03> [Accessed August 9, 2018].
- Malvern Instruments, 2004. Zetasizer Nano Series User Manual. , 1.1, pp.1–270. Available at: http://www.biophysics.bioc.cam.ac.uk/files/Zetasizer_Nano_user_manual_Man0317-1.1.pdf [Accessed April 23, 2018].
- McMeekin, T.L., Groves, M.L. & Hipp, N.J., 1964. Refractive Indices of Amino Acids, Proteins, and Related Substances. In pp. 54–66. Available at: <http://pubs.acs.org/doi/abs/10.1021/ba-1964-0044.ch004> [Accessed March 7, 2018].
- Meena Devi, J., 2014. Aggregation of thiol coated gold nanoparticles: A simulation study on the effect of polymer coverage density and solvent. *Computational Materials Science*, 86, pp.174–179. Available at: <https://www.sciencedirect.com/science/article/pii/S0927025614000603> [Accessed October 3, 2018].
- Mehravar, R., Jahanshahi, M. & Saghatoleslami, @bullet Naser, 2009. (HSA) Nanoparticles as Drug Delivery System: Preparation, Optimization and Characterization Study. *Dynamic Biochemistry, Process Biotechnology and Molecular Biology*, 51. Available at: <https://pdfs.semanticscholar.org/1841/a789b5dbfdbc2b3523cd3ddb4d1e2949821d.pdf> [Accessed April 30, 2018].
- Mehtala, J.G. & Wei, A., 2014. Nanometric Resolution in the Hydrodynamic Size Analysis of Ligand-Stabilized Gold Nanorods. *Langmuir*, 30(46), pp.13737–13743. Available at: <http://pubs.acs.org/doi/10.1021/la502955h> [Accessed April 24, 2018].
- Migneault, I. et al., 2004. Glutaraldehyde: behavior in aqueous solution, reaction with proteins, and application to enzyme crosslinking. *BioTechniques*, 37(5), pp.790–802. Available at:

- <http://www.ncbi.nlm.nih.gov/pubmed/15560135> [Accessed August 13, 2018].
- Mohammad-Beigi, H. et al., 2016. The Effects of Organic Solvents on the Physicochemical Properties of Human Serum Albumin Nanoparticles. *Iranian journal of biotechnology*, 14(1), pp.45–50. Available at: <http://www.ncbi.nlm.nih.gov/pubmed/28959317> [Accessed July 20, 2018].
- Murayama, K. & Tomida, M., 2004. Heat-Induced Secondary Structure and Conformation Change of Bovine Serum Albumin Investigated by Fourier Transform Infrared Spectroscopy. Available at: <https://pubs.acs.org/sharingguidelines> [Accessed September 29, 2018].
- Murray, A.N. et al., 2013. Surface adsorption considerations when working with amyloid fibrils in multiwell plates and Eppendorf tubes. *Protein Science*, 22(11), pp.1531–1541. Available at: <http://doi.wiley.com/10.1002/pro.2339> [Accessed April 26, 2018].
- NanoSight Ltd., 2007. *NanoSight LM10 Nanoparticle Analysis System & NTA 1.5 Analytical Software Operating Manual*, Salisbury. Available at: www.nanosight.co.uk [Accessed April 24, 2018].
- Napierska, D. et al., 2010. The nanosilica hazard: another variable entity. *Particle and Fibre Toxicology*, 7(1), p.39. Available at: <http://www.ncbi.nlm.nih.gov/pubmed/21126379> [Accessed October 3, 2018].
- Nel, A.E. et al., 2009. Understanding biophysicochemical interactions at the nano–bio interface. *Nature Materials*, 8(7), pp.543–557. Available at: <http://www.ncbi.nlm.nih.gov/pubmed/19525947> [Accessed October 3, 2018].
- Nienow, A.W., 1997. On impeller circulation and mixing effectiveness in the turbulent flow regime. *Chemical Engineering Science*, 52(15), pp.2557–2565. Available at: https://ac.els-cdn.com/S0009250997000729/1-s2.0-S0009250997000729-main.pdf?_tid=d71bb136-8793-4c51-b739-104d9facab73&acdnat=1537710882_7759cba351521567b539e93da1430fe1 [Accessed September 23, 2018].
- Niu, Y. et al., 2013. Nanoparticles Mimicking Viral Surface Topography for Enhanced Cellular Delivery. *Advanced Materials*, 25(43), pp.6233–6237. Available at: <http://doi.wiley.com/10.1002/adma.201302737> [Accessed October 3, 2018].
- Nobbmann, U., 2016. *NTA or DLS?*, Available at: <http://www.materials-talks.com/blog/2016/09/15/nta-or-dls/> [Accessed April 23, 2018].
- Okuda, K. et al., 1991. Reaction of glutaraldehyde with amino and thiol compounds. *Journal of Fermentation and Bioengineering*, 71(2), pp.100–105. Available at: <https://www.sciencedirect.com/science/article/pii/0922338X91902315> [Accessed September 27, 2018].
- Pagni, R., 2005. Solvents and Solvent Effects in Organic Chemistry, Third Edition (Christian Reichardt). *Journal of Chemical Education*, 82(3), p.382. Available at: <http://pubs.acs.org/doi/abs/10.1021/ed082p382.2> [Accessed August 13, 2018].

- Paik, S.-Y.-R. et al., 2013. Robust size control of bovine serum albumin (BSA) nanoparticles by intermittent addition of a desolvating agent and the particle formation mechanism. *Food Chemistry*, 141(2), pp.695–701. Available at: <http://www.ncbi.nlm.nih.gov/pubmed/23790836> [Accessed July 30, 2018].
- Pang, L. et al., 2014. Mimicking filtration and transport of rotavirus and adenovirus in sand media using DNA-labeled, protein-coated silica nanoparticles. *Water Research*, 62, pp.167–179. Available at: <https://www.sciencedirect.com/science/article/pii/S0043135414004278?via%3Dihub> [Accessed May 11, 2018].
- Park, M.-W. & Yeo, S.-D., 2010. Antisolvent Crystallization of Roxithromycin and the Effect of Ultrasound. *Separation Science and Technology*, 45(10), pp.1402–1410. Available at: <http://www.tandfonline.com/doi/abs/10.1080/01496391003689538> [Accessed September 30, 2018].
- Patterson, J.E. & Geller, D.M., 1977. Bovine microsomal albumin: Amino terminal sequence of bovine proalbumin. *Biochemical and Biophysical Research Communications*, 74(3), pp.1220–1226. Available at: <http://linkinghub.elsevier.com/retrieve/pii/0006291X77916485> [Accessed March 7, 2018].
- Queiroz, R.G. et al., 2016. Radiation-synthesized protein-based drug carriers: Size-controlled BSA nanoparticles. *International Journal of Biological Macromolecules*, 85, pp.82–91.
- Rahimnejad, M., Jahanshahi, M. & Najafpour, G., 2002. *Production of biological nanoparticles from bovine serum albumin for drug delivery*, Academic Journals. Available at: <https://www.ajol.info/index.php/ajb/article/view/55912/44371> [Accessed September 30, 2018].
- Raschke, T.M., 2006. Water structure and interactions with protein surfaces. *Current Opinion in Structural Biology*, 16(2), pp.152–159. Available at: <https://www.sciencedirect.com/science/article/pii/S09594440X06000406> [Accessed July 24, 2018].
- Reeks, M.W., 2011. STOKES-EINSTEIN EQUATION. In *A-to-Z Guide to Thermodynamics, Heat and Mass Transfer, and Fluids Engineering*. Begellhouse. Available at: <http://www.thermopedia.com/content/1156/> [Accessed January 29, 2018].
- Remmele, R.L. et al., 2015. Characterization of Monoclonal Antibody Aggregates and Emerging Technologies. In pp. 113–158. Available at: <http://pubs.acs.org/doi/10.1021/bk-2015-1202.ch005> [Accessed April 24, 2018].
- Rexroad, J. et al., 2003. Structural Stability of Adenovirus Type 5. *Journal of Pharmaceutical Sciences*, 92(3), pp.665–678. Available at: <http://linkinghub.elsevier.com/retrieve/pii/S0022354916311923> [Accessed April 21, 2017].
- Rombouts, I. et al., 2015. Formation and reshuffling of disulfide bonds in bovine serum albumin demonstrated using tandem mass spectrometry with collision-induced and electron-transfer dissociation. *Scientific Reports*, 5(1), p.12210. Available at:

- <http://www.ncbi.nlm.nih.gov/pubmed/26193081> [Accessed September 29, 2018].
- Salis, A. et al., 2006. Specific Anion Effects on Glass Electrode pH Measurements of Buffer Solutions: Bulk and Surface Phenomena. Available at: <https://pubs.acs.org/sharingguidelines> [Accessed September 26, 2018].
- Schäffler, M. et al., 2014. Blood protein coating of gold nanoparticles as potential tool for organ targeting. *Biomaterials*, 35(10), pp.3455–3466.
- Segura, M.M. et al., 2010. A real-time PCR assay for quantification of canine adenoviral vectors. *Journal of Virological Methods*, 163(1), pp.129–136. Available at: <https://www.sciencedirect.com/science/article/pii/S0166093409004108?via%3Dihub> [Accessed October 3, 2018].
- Seinfeld, J.H. & Pandis, S.N., 2006. *Atmospheric chemistry and physics : from air pollution to climate change* 3rd ed., New Jersey: John Wiley & Sons. Available at: <https://www.wiley.com/en-us/Atmospheric+Chemistry+and+Physics%3A+From+Air+Pollution+to+Climate+Change%2C+3rd+Edition-p-9781118947401> [Accessed April 23, 2018].
- Shodex, 2018. Dimer and Trimer of BSA. *ShodexHPLC.com*. Available at: <https://shodexhplc.com/applications/dimer-and-trimer-of-bsa/> [Accessed March 13, 2018].
- Sigma Aldrich, 2018. *Physical properties of solvents*, Available at: https://www.sigmaaldrich.com/content/dam/sigma-aldrich/docs/Aldrich/General_Information/labbasics_pg144.pdf [Accessed September 23, 2018].
- Sreerama, N. & Woody, R.W., 1993. A Self-Consistent Method for the Analysis of Protein Secondary Structure from Circular Dichroism. *Analytical Biochemistry*, 209(1), pp.32–44. Available at: <http://linkinghub.elsevier.com/retrieve/pii/S0003269783710791> [Accessed March 27, 2017].
- von Storp, B. et al., 2012. Albumin nanoparticles with predictable size by desolvation procedure. *Journal of microencapsulation*, 29(2), pp.138–46. Available at: <http://www.ncbi.nlm.nih.gov/pubmed/22329480>.
- Takayama, K. & Mizuguchi, H., 2018. Generation of Optogenetically Modified Adenovirus Vector for Spatiotemporally Controllable Gene Therapy. *ACS Chemical Biology*, 13(2), pp.449–454. Available at: <http://www.ncbi.nlm.nih.gov/pubmed/29327920> [Accessed October 2, 2018].
- Takeda, K. et al., 1989. Conformational change of bovine serum albumin by heat treatment. *Journal of protein chemistry*, 8(5), pp.653–9. Available at: <http://www.ncbi.nlm.nih.gov/pubmed/2610859> [Accessed February 5, 2018].
- Trilisky, E.I. & Lenhoff, A.M., 2007. Sorption processes in ion-exchange chromatography of viruses. *Journal of Chromatography A*, 1142(1), pp.2–12.
- Urabe, M. et al., 2006. Removal of Empty Capsids from Type 1 Adeno-Associated Virus Vector

- Stocks by Anion-Exchange Chromatography Potentiates Transgene Expression. *Molecular Therapy*, 13(4), pp.823–828. Available at: <https://www.sciencedirect.com/science/article/pii/S1525001606000074> [Accessed October 3, 2018].
- Wang, C.-H. & Chen, W., 2010. Raman Characterizing Disulfide Bonds and Secondary Structure of Bovine Serum Albumin. *AIP Conference Proceedings*, 1267, p.346. Available at: <http://aip.scitation.org/toc/apc/1267/1> [Accessed September 29, 2018].
- Weber, C., Coester, C., et al., 2000. Desolvation process and surface characterisation of protein nanoparticles. *International journal of pharmaceutics*, 194(1), pp.91–102. Available at: <http://www.ncbi.nlm.nih.gov/pubmed/10601688>.
- Weber, C., Kreuter, J. & Langer, K., 2000. Desolvation process and surface characteristics of HSA-nanoparticles. *International Journal of Pharmaceutics*, 196, pp.197–200.
- Weng, D. et al., 2014. Enhanced structural stability of adenovirus nanocapsule. *Progress in Natural Science: Materials International*, 24(2), pp.171–174. Available at: <https://www.sciencedirect.com/science/article/pii/S1002007114000240> [Accessed October 2, 2018].
- Westcott, C.C., 1978. *pH measurements*, Academic Press.
- Wise, D.L. (Donald L., 2000. *Handbook of pharmaceutical controlled release technology*, Marcel Dekker. Available at: https://books.google.co.uk/books?id=paEzHRHlXE4C&pg=PA405&lp=PA405&dq=trimeric+bsa&source=bl&ots=oyGE8-o9tU&sig=mPc_yrCbBGXL46SILNRQbSpCDU&hl=en&sa=X&ved=0ahUKEwjNoLDv6enZAhXSCewKHQwUCU0Q6AEISDAF#v=onepage&q=trimeric+bsa&f=false [Accessed March 13, 2018].
- Wu, S.-H., Hung, Y. & Mou, C.-Y., 2011. Mesoporous silica nanoparticles as nanocarriers. *Chemical Communications*, 47(36), p.9972. Available at: <http://xlink.rsc.org/?DOI=c1cc11760b> [Accessed October 3, 2018].
- Yedomon, B., Fessi, H. & Charcosset, C., 2013. Preparation of Bovine Serum Albumin (BSA) nanoparticles by desolvation using a membrane contactor: A new tool for large scale production. *European Journal of Pharmaceutics and Biopharmaceutics*, 85(3), pp.398–405.
- Yu, X. et al., 2016. Enhanced tumor targeting of cRGD peptide-conjugated albumin nanoparticles in the BxPC-3 cell line. *Scientific Reports*, 6(1), p.31539. Available at: <http://www.nature.com/articles/srep31539> [Accessed October 3, 2018].
- Yu, Y. et al., 2016. The effects of organic solvents on the folding pathway and associated thermodynamics of proteins: a microscopic view. *Scientific Reports*, 6(1), p.19500. Available at: <http://www.nature.com/articles/srep19500> [Accessed August 9, 2018].
- Yu, Z. et al., 2014. Bovine serum albumin nanoparticles as controlled release carrier for local drug delivery to the inner ear. *Nanoscale Research Letters*, 9(1), p.343. Available at: <http://www.nanoscalereslett.com/content/9/1/343> [Accessed April 13, 2016].

- Zeltins, A., 2013. Construction and characterization of virus-like particles: A review. *Molecular Biotechnology*, 53(1), pp.92–107.
- Zhang, J.-Y. et al., 2006. Preparation of amorphous cefuroxime axetil nanoparticles by controlled nanoprecipitation method without surfactants. *International Journal of Pharmaceutics*, 323, pp.153–160. Available at: https://ac.els-cdn.com/S0378517306004315/1-s2.0-S0378517306004315-main.pdf?_tid=9d717c6a-4311-4123-91d8-dc8d356ff81a&acdnat=1538332883_5b369a31b245f145210c27563822d64e [Accessed September 30, 2018].
- Zhang, Z. et al., 2001. Design and assembly of solid-phases for the effective recovery of nanoparticulate bioproducts in fluidised bed contactors. *Bioseparation*, 10(1–3), pp.113–32. Available at: <http://www.ncbi.nlm.nih.gov/pubmed/11787793> [Accessed April 27, 2015].
- Zhao, W., Brook, M.A. & Li, Y., 2008. Design of Gold Nanoparticle-Based Colorimetric Biosensing Assays. *ChemBioChem*, 9(15), pp.2363–2371. Available at: <http://doi.wiley.com/10.1002/cbic.200800282> [Accessed October 3, 2018].

CHAPTER IV

BUILDING & CHARACTERISING A LIBRARY OF VIRAL MIMICS VIA A TOOLBOX APPROACH

Abstract

The utility of viral vectors in the application of gene therapy and vaccine treatments has been a topic of great interest in the bioprocessing industry. However, their labour intensive and downstream processing complications have posed new challenges to process development scientists in optimising the throughput of viral vectors to clinic.

The previous chapter demonstrated the potential of protein nanoparticles as promising surrogates of viruses, particularly Bovine Serum Albumin nanoparticles as surrogates of the adenoviral vector. This work will detail how we have incorporated the process knowledge surrounding this technique into a “toolbox approach” for targeting other virus types which have relevance in the gene therapy field. These include adeno-associated, human papilloma and polio viruses, transitioning towards nanoparticles which mimic the physiochemical characteristics of these *bona fide* vectors without the cost and safety implications of the true viral vectors.

The chapter also explores the use of different cross-linking mechanisms and targeting different functional groups to create multi-component, “2nd generation” nanoparticles to move towards the creation of more accurate viral mimics. The aspiration is that this approach will facilitate the construction of “custom-built” viral mimics to suit the requirements of the end user.

Abbreviations

AAV: Adeno-associated Virus	Cys: Cysteine	His: Histidine
AdV: Adenovirus Type V	DLS: Dynamic Light Scattering	HPV: Human Papilloma Virus
AEX: Anion Exchange Chromatography	DTME: Dithio-bis-maleimidoethane	LYS: Lysozyme
Arg: Arginine	DTT: Dithiothreitol	OVA: Ovalbumin
Asp: Aspartic Acid	EDC: N-(3-Dimethylaminopropyl)-N'-ethylcarbodiimide	PES: Polyethersulfone
BHB: Bovine Haemoglobin	Glu: Glutamic Acid	pI: Isoelectric point
BSA: Bovine Serum Albumin	HCl: Hydrochloric Acid	SEC: Size-Exclusion Chromatograph

Table of Contents

CHAPTER IV	224
Abstract.....	224
Abbreviations.....	224
List of Figures.....	226
4.1 Introduction	228
4.1.1 Viral Vectors in Gene Therapy	228
4.1.2 Protein Characteristics	229
4.1.3 Functional Groups & Cross-Linkers	230
4.2 Materials & Methods	232
4.2.1 Materials & Reagents	232
4.2.2 Preparation of Protein Nanoparticles	232
4.2.3 Analysis.....	234
4.3 Results & Discussion	235
4.3.1 Protein Building Blocks	235
4.3.2 Bovine Haemoglobin Nanoparticles.....	236
4.3.3 Lysozyme Nanoparticles.....	238
4.3.4 Multi-Component 2 nd Generation Nanoparticles	239
4.4 Conclusions	250
4.5 References	252

List of Figures

Fig. 4.1 The proportions of viral vectors used in gene therapy to date (Ginn *et al.*, 2018b).

Fig. 4.2 The physiochemical characteristics of common non-enveloped viral vectors employed in gene therapy applications (Wu, Asokan and Samulski, 2006; Arbyn *et al.*, 2007; Regenmortel, 2009; Michen and Graule, 2010; Thomassen *et al.*, 2013; Zhou, 2013; Ghebremedhin, 2014; Potter *et al.*, 2014).

Fig. 4.3 Characteristics of common proteins as potential building blocks of protein nanoparticles (Stein *et al.*, 1991; Shoichet *et al.*, 1995; Aranda *et al.*, 2008; Majorek *et al.*, 2012).

Fig. 4.4 Mechanisms for cross-linking amino acid residues (1 & 2) via the **a)** EDC or **b)** DTME route. Note that the reduction of the disulphide bonds is required prior to cross-linking using DTME to liberate the thiol groups for reaction with DTME. Schematics were adapted from the ThermoFisher Scientific cross-linker selection guide.

Fig. 4.5 Nanoparticle formation characteristics from novel protein building blocks; **a)** Particle Size Distributions & **b)** Isoelectric focussing curves for Ovalbumin (- / -■-) and Bovine Haemoglobin (- / -□-) formed using a 90 : 10 Methanol : Water desolvating mixture. The isoelectric points for Ovalbumin & Bovine Haemoglobin were 4.41 and 6.61, respectively and each fitted with a sigmoidal fit curve.

Fig. 4.6 The impact of variations in organic solvent on **a)** average BSA (filled) and BHB (gradient filled) nanoparticle size and polydispersity index (dashed fill). The relationship between the dielectric constant of the organic solvent mixture and the eventual average particle size for **b)** BSA & **c)** BHB nanoparticles produced (mean \pm SD, $n = 3$) with non-linear regression polynomial inverse first-order fit curves.

Fig. 4.7 a) DLS size distribution for LYS nanoparticles formed using the conventional desolvation/ cross-linking manufacturing strategy as used for BSA & **b)** Isoelectric focussing curve for native LYS with non-linear regression polynomial inverse fifth-order fit curve.

Fig. 4.8 a) Average particle size (columns) & polydispersity indices (line & scatter) of purified, blended BSA-LYS with respect to increasing LYS dosing concentrations by percentage volume. Inset data values above the bars indicate the molar percentage of LYS relative to BSA. **b)** Isoelectric focussing curve for native BSA (-) and LYS (- -) with non-linear regression sigmoidal and polynomial inverse fifth-order fit curves, respectively. The isoelectric points of BSA & LYS are 4.78 & 11.12, respectively.

Fig. 4.9 Scouting studies to optimise the coating method for formation of core-shell nanoparticles. **a)** SEC purification chromatograms for LYS-coated BSA nanoparticles of different starting scaffold sizes (with identical starting concentrations of both protein species); 65.18 nm (-) & 44.92 nm (- -). **b)** Photograph of centrifugal concentrators used to purify LYS-coated (EDC) BSA nanoparticles with varying molar ratios of nanoparticle to coat protein. The average particle size for the scaffold nanoparticle was 41 nm in each case and the centrifugal filters were run under identical conditions (2,500 \times g for 20 minutes).

Fig. 4.10 a) Isoelectric focussing curves for native BSA (-) & LYS (- -) alongside a control BSA nanoparticle sample and LYS-coated BSA nanoparticles via two cross-linking methods. Non-linear regression sigmoidal and

polynomial inverse fifth-order (LYS only) fit curves were used to create the IEF curves respectively. **b)** Changes in average particle size upon coating of LYS onto the BSA nanoparticle scaffold (columns) as well as modification of isoelectric point (-■-) & % loss of nanoparticulate bulk when incubated with a Sepharose 6 Fast Flow SEC matrix (-□-). Isoelectric points for BSA-NPs, EDC LYS-BSA NPs & DTME LYS-BSA NPs were 4.61, 5.07 & 4.82, respectively.

Fig. 4.11 Relative binding capacities for the BSA nanoparticle scaffold and the two cross-linking strategies when challenged at the same starting concentration onto a strong anion-exchange resin (Q-Sepharose Fast Flow) and the binding capacity determined through colorimetric assay of the supernatant and subsequent mass balance.

Fig. 4.12 Confocal Laser Scanning Micrographs of fluorescent core-shell LYS-coated BSA nanoparticles bound to the surface of the anion exchanger Q-Sepharose Fast Flow. **a)** BSA nanoparticles tagged with Texas-Red X. Lysozyme, pre-tagged with Cy5, coated onto un-tagged BSA nanoparticles via **b)** EDC cross-linking & **c)** DTME cross-linking. BSA NPs and Lysozyme, both pre-tagged separately with Fluorescamine & Cy5, respectively, then formed into core-shell nanoparticles; **d) Detecting BSA NPs:** sample excited with a 405 nm laser and detected at 465 nm ($\lambda_{\text{EXC}} = 390 \text{ nm}$, $\lambda_{\text{Emi}} = 465 \text{ nm}$ for fluorescamine), **e) Detecting incorporated LYS:** sample excited with a 635 nm laser and detected at 666 nm ($\lambda_{\text{EXC}} = 646 \text{ nm}$, $\lambda_{\text{Emi}} = 666 \text{ nm}$ for Cy5). **f)** Laser lines from **d)** & **e)** run sequentially over the same focal plane suggesting co-localisation of both BSA-NPs & Lysozyme in the same locality.

4.1 Introduction

4.1.1 Viral Vectors in Gene Therapy

Viral vectors represent a promising vehicle for delivery of therapeutic payloads to treat genetic disorders and in the implementation of DNA vaccines. There are a number of viral vectors which are suitable for this application, depending on their individual features and requirements of the therapy. These include retroviral and adenoviral vectors, two of the most common genetic vehicles used in the industry, amongst a number of others, as illustrated in Fig. 4.1 (Ginn *et al.*, 2018b).

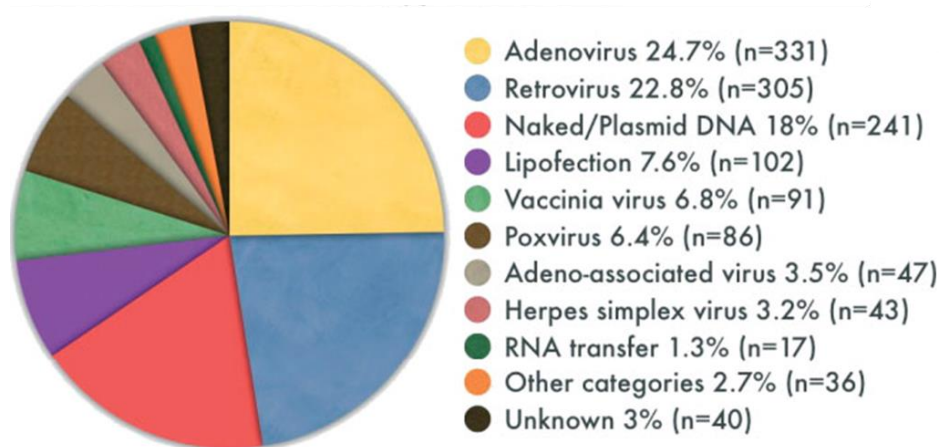


Fig. 4.1 The proportions of viral vectors used in gene therapy to date (Ginn *et al.*, 2018b).

As discussed in Chapter III, one of the main aims of the work is to demonstrate the use of protein nanoparticles as mimics of viral vectors, aiming to imitate the surface characteristics of viral capsids. In this way, it is hoped that the virus analogues interact with purification media as a virus would and thus provide a useful simulation tool for optimisation of purification unit operations, without the hassle of working with infectious, expensive viral material.

Naturally, in attempting to mimic protein capsids, enveloped vectors were not considered for mimicking, as the lipid envelope that surrounds vectors such as the *retroviridae*, *poxviridae* and *herpesviridae* families will play an important role in their surface interactions and physiochemical properties. This can complicate their purification strategies, as the biophysical properties of this envelope are not completely known (Steppert *et al.*, 2016) and thus hard to re-create within a mimic.

For this reason, the library of viral mimics developed in this chapter is restricted to non-enveloped viruses, which are highlighted in Fig. 4.2. Whilst the applicability of the adenoviral vector has been detailed in Chapter III, there have also been strong cases made for the use of alternative viral vectors, including the human papilloma virus (HPV) (Storey *et al.*, 1991; Chen *et al.*, 1995, 1996;

Hung *et al.*, 2012), polio virus (Morrow, Ansardi and Porter, 1997; Mandl *et al.*, 1998; van Kuppeveld *et al.*, 2002; Ylä-Pelto, Tripathi and Susi, 2016) and adeno-associated virus (AAV) (Flotte and Carter, 1995; Gao *et al.*, 2002; Hauswirth *et al.*, 2008; Konishi *et al.*, 2008; Naso *et al.*, 2017) as suitable vectors for targeted gene therapy.

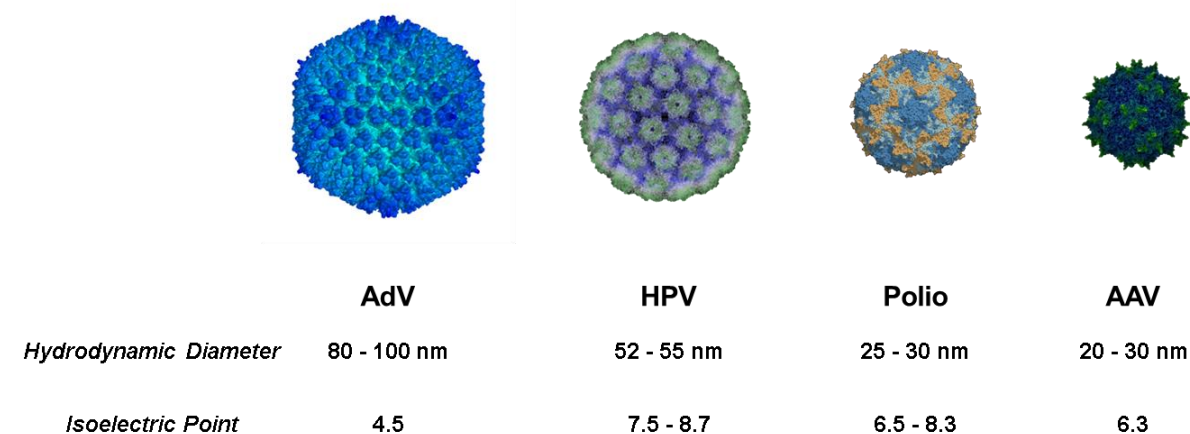
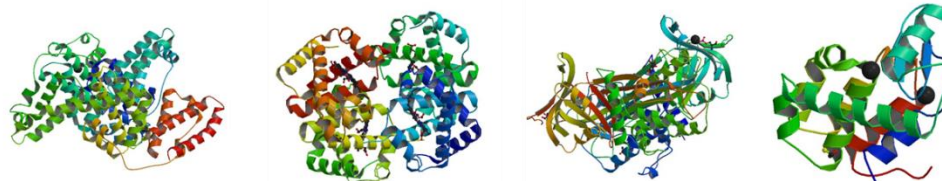


Fig. 4.2 The physicochemical characteristics of common non-enveloped viral vectors employed in gene therapy applications (Wu, Asokan and Samulski, 2006; Arbyn *et al.*, 2007; Regenmortel, 2009; Michen and Graule, 2010; Thomassen *et al.*, 2013; Zhou, 2013; Ghebremedhin, 2014; Potter *et al.*, 2014).

As such, it becomes important to develop “second generation” protein nanoparticles which can mimic the characteristics of these vectors. Each viral vector has its own distinct features and thus the conventional approach of forming nanoparticles using serum albumin will have to be modified (via a “toolbox approach”) in order to successfully represent these species with respect to their size and surface characteristics.

4.1.2 Protein Characteristics

The first strategy will be replacing the starting protein molecule and observing how different proteins perform under coacervation and cross-linking manufacture. Fig. 4.3 demonstrates a range of commonly available, relatively inexpensive proteins which have potential use as starter building blocks for the formation of nanoparticle viral mimics.



	BSA	BHG	OVA	LYS	
Molecular Weight (kDa)	66.4	64.5	44.3	14.3	
Isoelectric Point	4.8	6.8	4.3	11.0	
Hydrophobic Index	1	0.66	0.98	0.89	
Amino Acid Content	Lysine	60	12	20	11
	Aspartic Acid	40	8	14	7
	Glutamic Acid	59	4	33	8
	Cysteine	35	1	6	4

Fig. 4.3 Characteristics of common proteins as potential building blocks of protein nanoparticles (Stein *et al.*, 1991; Shoichet *et al.*, 1995; Aranda *et al.*, 2008; Majorek *et al.*, 2012).

Evidently, each protein has its own individual characteristics and thus will respond differently when manipulated to form nanoparticles, partially due to their molecular weights, hydrodynamic radius, surface charge and hydrophobicity index. It is therefore hypothesised that these proteins could have potential in developing protein nanoparticles that mimic the characteristics of the gene therapy vectors illustrated in Fig. 4.2.

4.1.3 Functional Groups & Cross-Linkers

With the single protein experiments, glutaraldehyde was maintained as the cross-linker of choice such that the only influential variable was the characteristics of the protein. As lysine residues are present on all four of the proteins under experimentation, glutaraldehyde should theoretically be able to stabilise the formed nanoparticles via the formation of imines (or Schiff bases) through nucleophilic attack from the ϵ -amino group of the lysine residue.

With respect to the second generation nanoparticles, more sophisticated cross-linking approaches were adopted to capitalise upon the availability of available reactive residues on the proteins. These include carboxylic acids (usually aspartic or glutamic acid residues) and thiols (cysteine residues).

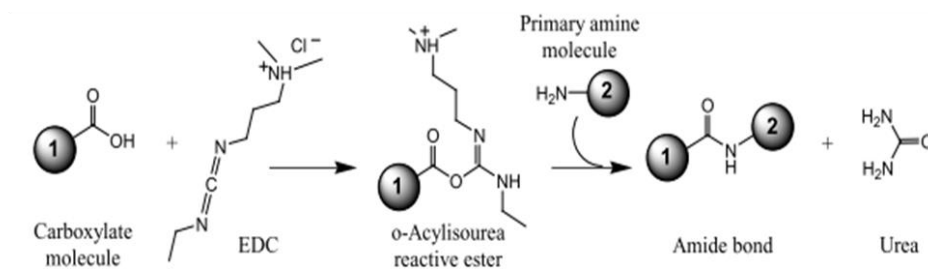
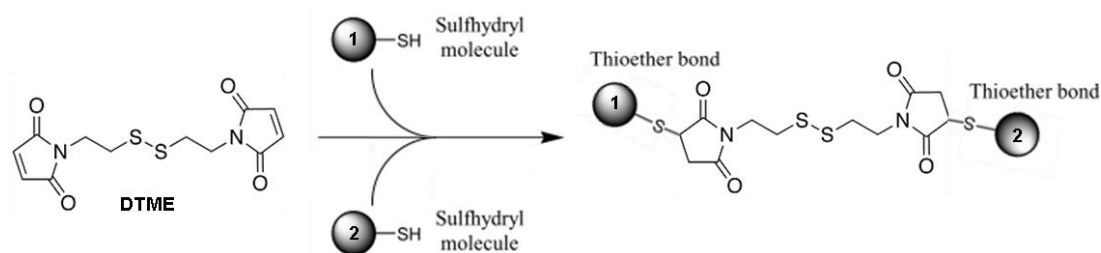
a**b**

Fig. 4.4 Mechanisms for cross-linking amino acid residues (1 & 2) via the **a)** EDC or **b)** DTME route. Note that the reduction of the disulphide bonds is required prior to cross-linking using DTME to liberate the thiol groups for reaction with DTME. Schematics were adapted from the ThermoFisher Scientific cross-linker selection guide.

4.1.3.1 EDC Cross-Linking

N-(3-Dimethylaminopropyl)-N'-ethylcarbodiimide (EDC) is a water soluble, heterobifunctional cross-linker that achieves cross-linking via a two-step process. Initially, the carbodiimide group within the cross-linker reacts with an available carboxyl residue on the protein to create an o-acylisourea ester intermediate, followed by a substitution reaction with a primary amine from a second amino acid residue to form a peptide bond, with urea as a bi-product. One advantage of EDC is that it is, by definition, zero length as it does not remain within the final cross-linked product (Nakajima and Ikada, 1995).

4.1.3.2 DTME Cross-Linking

Dithio-bis-maleimidoethane (DTME) is a water soluble, homobifunctional cross-linker that reacts with sulfhydryl reactive groups on cysteine residues of proteins. A significant advantage of DTME is that the cross-linking process is reversible due to a disulphide group in the middle of the molecule, which can be cleaved under reducing conditions (Green, Reisler and Houk, 2008). A detailed schematic for both cross-linking mechanisms is provided in Fig. 4.4.

4.2 Materials & Methods

4.2.1 Materials & Reagents

Bovine Serum Albumin (fatty acid free, $\geq 96\%$), Albumin from chicken egg white (Ovalbumin) ($\geq 98\%$), Haemoglobin from bovine blood, Lysozyme from chicken egg white ($\geq 90\%$), N-(3-Dimethylaminopropyl)-N'-ethylcarbodiimide hydrochloride (EDC), dithio-bis-maleimidoethane (DTME), Fluorescamine, 8% Aqueous Glutaraldehyde, Methanol and Ethanol (both analytical grade, $\geq 99\%$), Sodium chloride (NaCl), Sodium phosphate monobasic (NaH_2PO_4) and dibasic (Na_2HPO_4), Sodium hydroxide (NaOH), Dimethyl sulfoxide (DMSO) and all glassware and other reagents were obtained from Sigma Aldrich (Poole, Dorset) unless otherwise stated.

Texas Red-X Succinimidyl Ester and Cyanine 5 Succinimidyl Ester (Cy5TM) were obtained from Fisher Scientific (Loughborough, UK). Buffers and all aqueous solutions were based upon use of ultrapure water from a Sartorius Arium® Advanced EDI Pure Water System (Sartorius AG, Göttingen, Germany). Chromatography resins (Q-Sepharose Fast Flow & Sepharose 6 Fast Flow) and PD-10 Desalting columns were purchased from GE Healthcare (Uppsala, Sweden).

4.2.2 Preparation of Protein Nanoparticles

Protein nanoparticles were prepared using the desolvation technique as described in Chapter III (3.2.2). Slight deviations are reported to accommodate for different protein characteristics or cross-linking strategies, which are detailed on a case by case basis in the discussion.

Various cross-linking strategies were employed in the work detailed in this chapter. With respect to Ovalbumin (OVA), Bovine Haemoglobin (BHB) and the initial Lysozyme (LYS) nanoparticle formation experiments, the 8% glutaraldehyde protocol used for conventional BSA nanoparticles was conducted, as detailed in Chapter III. In the development of 2nd generation nanoparticles, two novel strategies were employed.

4.2.2.1 Blended Nanoparticles

BSA-LYS blended nanoparticles were manufactured in a similar fashion to that of conventional BSA nanoparticles. 10% BSA and 10% LYS solutions were prepared separately in ultrapure water, before mixing a working solution of varying ratios of BSA: LYS to a total volume of 1 ml. This solution was then used for desolvation, cross-linking and subsequent purification, as detailed previously.

4.2.2.2 Core-Shell Nanoparticles

BSA nanoparticles were initially formulated, purified and analysed via DLS to determine particle size and polydispersity characteristics. These preparations were subsequently used as scaffolds for the preparation of core-shell nanoparticles, using LYS as a coating protein.

4.2.2.2.1 EDC Cross-Linking

A 10% LYS aqueous solution was prepared and aliquots were added to 1 ml of purified BSA nanoparticles (~ 14 mg/ml) in molar ratios of 1: 2, 1: 5 and 1:10, LYS: BSA (194 μ L, 78 μ L and 39 μ L of LYS starting solution, respectively). The native LYS in solution was desolvated using 1 ml of organic solvent (identical conditions to that of the original BSA nanoparticles) and allowed to self-assemble in-situ around the BSA nanoparticles.

After five minutes, aqueous EDC was added in a 10 fold molar excess (relative to total protein content in solution) and left for three hours to complete the cross-linking reaction (Jahanban-Esfahlan, Dastmalchi and Davaran, 2016).

4.2.2.2.2 DTME Cross-Linking

A 0.2 ml working solution of aqueous LYS was prepared to a concentration of 1.475 mg/ml before being aliquoted into 1 ml of a purified BSA-NP solution at an approximate concentration of 14 mg/ml (representing a 1 : 10 molar ratio LYS : BSA). As with EDC cross-linking, 1 ml of desolvating agent (identical ratios used in the formation of the BSA-NP scaffold) was added at a controlled addition rate of 1 ml/min under continuous stirring to induce unfolding of the added LYS.

To initiate reduction of the disulphide bonds in both protein species, a molar excess of (74 μ g) NaBH_4 (4: 1 molar ratio NaBH_4 : LYS) was dissolved in 80 μ L of 0.6 M NaOH before being aliquoted into the desolvating mix (Ashraf *et al.*, 2014). The NaOH in this case is required to create a basic environment to stabilise the intermediate thiolate which forms prior to cross-linking (Duane Brown, 1960). After ten minutes, a molar excess of DTME cross-linker (1.22 mg dissolved in 60 μ L DMSO) was added (2: 1 DTME: NaBH_4) to favour the formation of covalent cross-linkages and limit interference from un-reacted NaBH_4 . The cross-linking process was left in an oxygen-free environment for three hours under continuous stirring to run to completion.

Purification of all the formed nanoparticles was carried out either by size-exclusion chromatography using disposable PD-10 Desalting Columns or via six wash cycles of centrifugation/filtration (2,500 $\times g$, 20 minutes), with re-dispersion in 1 M NaCl (3X) and subsequently in aqueous buffer (3X) using a 300 000 MWCO protein concentrator polyethersulfone (PES) centrifugal filter (ThermoTM Scientific, Loughborough, UK), prior to storing at 4 °C, as detailed in Chapter III (3.2.2). The high salt washes were required to eliminate any electrostatically bound protein and to ensure any coated protein was linked covalently via the cross-linker chosen.

4.2.3 Analysis

4.2.3.1 *Dynamic Light Scattering, Zeta Potential & Isoelectric Focussing*

Determination of particle size, ζ -potential and isoelectric focussing studies were carried out as described in Chapter III, 3.2.3.1.1 & 3.2.3.1.2.

4.2.3.2 *Protein Nanoparticle Quantification*

Protein and protein nanoparticle preparations were quantified using a bicinchoninic acid (BCA) assay, as described in Chapter III, 3.2.3.3.

4.2.3.3 *Static Binding Studies*

Nanoparticle challenges onto anion-exchange (Q-Sepharose Fast Flow) & control size-exclusion matrices (Sephacrose 6 Fast Flow) were conducted as described in Chapter II, 2.2.11.3. The buffer system in this instance was 0.01 M Tris-HCl (pH 8.0) and the settled bed volume 20 μ L.

4.2.3.4 *Confocal Laser Scanning Microscopy*

CLSM analysis of the beads conjugated with protein nanoparticles (through static binding studies) were conducted via the same methodology as detailed in Chapter II 2.2.11.6. In these experiments, LYS was tagged with Cy5 (λ_{exc} =646 nm, λ_{emi} =666 nm) and purified via gel filtration prior to coating BSA nanoparticles (for both EDC and DTME approaches). BSA Nanoparticles were conjugated with either Texas Red-X (λ_{exc} =596 nm, λ_{emi} =615 nm) or Fluorescamine (λ_{exc} =390 nm, λ_{emi} =465 nm) prior to coating with LYS (Life Technologies, 1996). The only deviation from the original protocol is that Fluorescamine was incubated with the protein species for 10 minutes as opposed to an hour due to its rapid reaction with amino groups on the protein (Funk *et al.*, 1986).

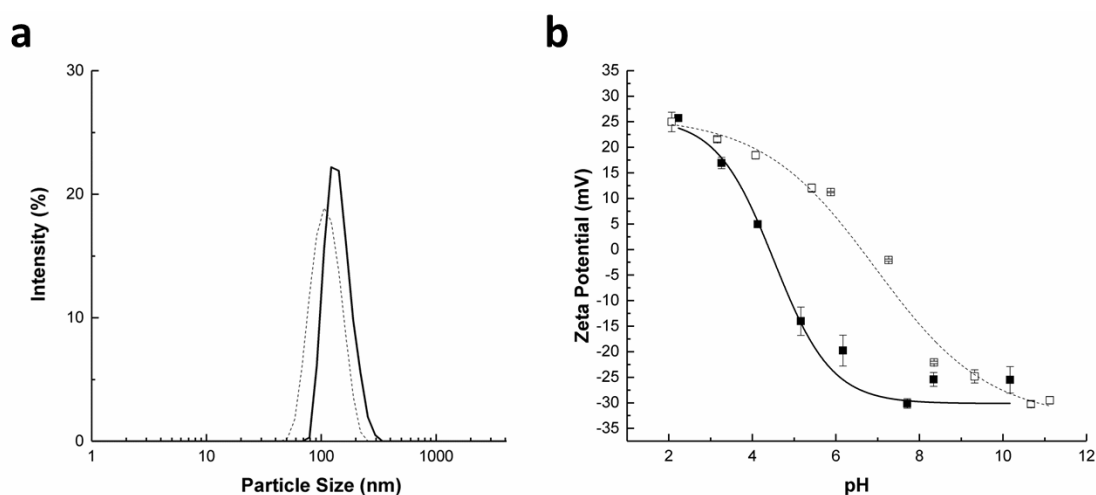
4.3 Results & Discussion

The approach adopted was to target specific viral vectors based on their size and surface characteristics using different starting proteins with varying proportions of amino acids and thus surface properties and isoelectric points. In the first instance, proteins were substituted in for BSA and carried through the original desolvation/cross-linking process to observe how the new proteins responded and the characteristics of the nanoparticles that formed as a result. Similar systematic variations in organic solvent ratios were also assessed to determine if trends could be observed independent of starting protein.

4.3.1 Protein Building Blocks

Two proteins, Ovalbumin (OVA) & Bovine Haemoglobin (BHB), were initially assessed for their feasibility as starting materials in the formation of self-assembling nanoparticles, as per BSA as previously outlined. Fig. 4.5a) illustrates that both proteins are amenable to the desolvation/cross-linking method and formed nanoparticles with a relatively tight size distribution.

Fig. 4.5 Nanoparticle formation characteristics from novel protein building blocks; **a)** Particle Size Distributions



b) Isoelectric focussing curves for Ovalbumin (- / -■-) and Bovine Haemoglobin (- - / -□-) formed using a 90 : 10 Methanol : Water desolvating mixture. The isoelectric points for Ovalbumin & Bovine Haemoglobin were 4.41 and 6.61, respectively and each fitted with a sigmoidal fit curve.

Rationally, this result is plausible given that both proteins have a significant amount of lysine residues available for cross-linking and will unfold when exposed to organic solvent and hydrophobic environments. Indeed, there have been numerous accounts of the formation of protein nanoparticles (including ovalbumin and haemoglobin) using a plethora of starting proteins including α -lactalbumin, β -lactoglobulin and gelatin (Gunasekaran, Ko and Xiao, 2006; Arroyo-Maya *et al.*, 2014; Wang *et al.*, 2015; Etorki *et al.*, 2016; Ahsan and Rao, 2017).

As the ultimate aim of the work is to create protein nanoparticles with a more basic isoelectric point (to target and mimic a wider range of viral vectors), BHB was carried forward for more

systematic assessment. One adjustment was made to the manufacturing process and that was the titration of dissolved BHB to pH 9.0 (rather than 8.0 for BSA); thus the surface charge of BHB is as close as possible to that of BSA in the original experiments detailed in Chapter III, though still within the pH range in which glutaraldehyde cross-links irreversibly.

4.3.2 Bovine Haemoglobin Nanoparticles

As with BSA, BHB was methodically evaluated to identify possible trends in nanoparticle formation such that specific sizes could be targeted where relevant. Fig. 4.6 demonstrates a comparative study between the two proteins and the resultant nanoparticle characteristics as the organic solvent ratios are varied.

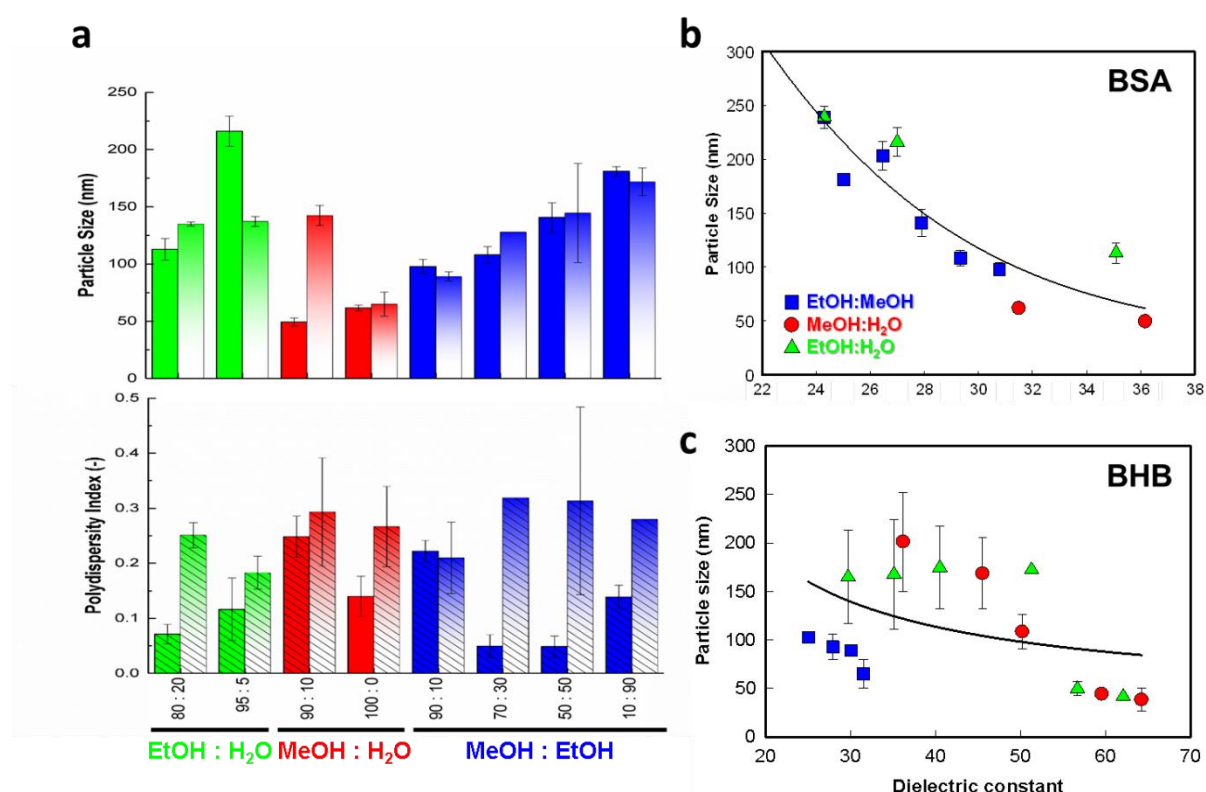


Fig. 4.6 The impact of variations in organic solvent on **a)** average BSA (filled) and BHB (gradient filled) nanoparticle size and polydispersity index (dashed fill). The relationship between the dielectric constant of the organic solvent mixture and the eventual average particle size for **b)** BSA & **c)** BHB nanoparticles produced (mean \pm SD, $n = 3$) with non-linear regression polynomial inverse first-order fit curves.

Generally, BHB nanoparticles could be formed across a range of organic solvent conditions, though in most cases producing nanoparticles of larger sizes than BSA. A second important characteristic of BHB nanoparticle formation was the increased batch-to-batch variation, reflected in higher standard deviations for BHB nanoparticle samples.

These differences may be attributed to the structure of BHB; a largely spherical protein, built on four subunits (2 identical α & β globin chains, each) ordered as a tetrahedral with non-polar

residues buried to facilitate water solubility. Each subunit houses a porphyrin ring coordinated around a ferrous atom (known as a haem molecule) within a hydrophobic cleft creviced between two helices (the haem pocket) to protect the Fe atom against oxidation (Dickerson and Geis, 1983; Perutz *et al.*, 1993).

As with BSA, the mechanisms of unfolding are governed by the disruption of the inter- and intra-molecular interactions which give BHB its native conformation; these are composed of hydrogen bonding, van der Waals, ionic and hydrophobic interactions which stabilise the polypeptides chains to maintain the secondary, tertiary and quaternary tetra sub-unit structure (Dickerson and Geis, 1983).

It is a combination of solvent-protein side chain hydrophobic interaction and disruption of inter-chain hydrogen bonding which cause BHB to dissociate into its subunits and subsequently un-fold into its secondary structure (Herskovits, Gadegbeku and Jaillet, 1970; Asakura, Adachi and Schwartz, 1978; Frantzen *et al.*, 1997; Wang, Wang and Li, 2000).

An important observation was a greater deal of aggregation within the glass vessel after the cross-linking reaction (compared to BSA desolvations) and this is reflected in the elevated polydispersities for BHB as the formed aggregates are cross-linked together to form larger complexes. This may be attributed to incomplete unfolding of protein and potential cross-linking of either whole tetrameric structures or α & β subunits to form un-ordered nanoparticulate assemblies. This is corroborated by the work of MacDonald & Pepper, who studied the stabilisation of native haemoglobin through inter- and intra- molecular cross-linkages using glutaraldehyde and found a heterogeneous mixture of products was formed including cross-linked tetramers, oligomers and “a wide range of higher molecular weight species” (MacDonald and Pepper, 1994).

This hypothesis can be supported by a second experimental observation; that desolvating mixtures with higher percentages of water (relative to organic solvent) could not form measurable nanoparticles due to a high degree of aggregation occurred in the vessel. This indicates that higher percentages of solvent are required to completely unfold BHB subunits in order to form uniform nanoparticles and that lower concentrations of solvent can in fact have a stabilising effect on BHB, as demonstrated by Asakura *et al.* in 1978.

To support this further, the surface charge of BHB also needs to be taken into account. Despite titrating to pH 9.0, BHB has a ζ -potential of -14.7 mV whereas at pH 8.0 BSA has a surface charge of -24.0 mV. This difference may contribute to the aggregation observed in the formation of BHB nanoparticles due to lower surface charge repulsion and thus less resistance to inter-particle aggregation.

A third observation was a distinct change in colour prior to and post-addition of solvent, with the 10% protein solution presenting as a dark red and upon addition of organic solvent, the mixture transitioned to a dark brown. This colour change indicates oxidation of the ferrous haem (Fe^{2+} to Fe^{3+}) to produce haematin and thus a conversion of BHB to methaemoglobin, which is

symptomatic of a change in the hydrophobic environment of the prosthetic group and potential disruption of structure due to the organic solvent addition (Blanco and Blanco, 2017).

Circular dichroism studies have shown tertiary structural disruption of haemoglobin to release the prosthetic haem group when exposed to only 30% Methanol (Wang *et al.*, 2010); a completely dissociated free haem group can instigate protein aggregation through catalysis of oxidation and cross-linking reactions between peptides (Kumar and Bandyopadhyay, 2005) which may be a contributing factor to both batch-to-batch variation through random aggregation and higher polydispersities within batches.

Work by Asakura *et al.* has also revealed the shear sensitivity of haemoglobin and observed that under mechanical shaking the protein denatures and irreversible precipitation occurs rapidly (Asakura *et al.*, 1974, 1977; Ohnishi and Asakura, 1976). Given the high rotational speeds used to form nanoparticles in this set up, it is feasible that BHB also undergoes shear stress and denatures to form irreversible aggregates, contributing to the variations illustrated in Fig. 4.6.

Percentage incorporation of BHB into BHB nanoparticles ranged between 80 – 90% and increased with increasing Ethanol concentration, as with BSA nanoparticles (see Chapter III, Fig 3.6) (3 samples, $n = 1$). The reason for the low sample number was a significant issue with purifying BHB nanoparticles to determine yield and for subsequent analytical studies. The crude nanoparticles were purified using centrifugal concentrators but for most manufacturing conditions the nanoparticles would aggregate on the surface of the membrane and blind the pores of the filter rendering them impossible to be re-solubilised and diafiltered into fresh buffer.

This observation corroborates with adsorption studies carried out between BHB and BSA onto hydrophilic and hydrophobic polymer surfaces, whereby at pH 8.0 a higher mass of BHB adsorbed onto the surface of both surface types, relative to BSA. This is likely due to hydrophobic patches on the surface of BHB providing hydrophobic interaction sites with the concentrator membrane (Shirahama, Suzuki and Suzawa, 1989). These issues with purification prevented subsequent analytical methods such as isoelectric focussing studies to be carried out on the BHB nanoparticles.

4.3.3 Lysozyme Nanoparticles

Whilst BHB nanoparticles could be formed with some degree of predictability, issues with purification for further characterisation justified investigation of a new protein; in this case, lysozyme. A much smaller protein with a far more basic pI (11), it was hypothesised that lysozyme would be a suitable candidate as a starting “building block” protein to form nanoparticles which would mimic viruses such as HPV, Polio & AAVs.

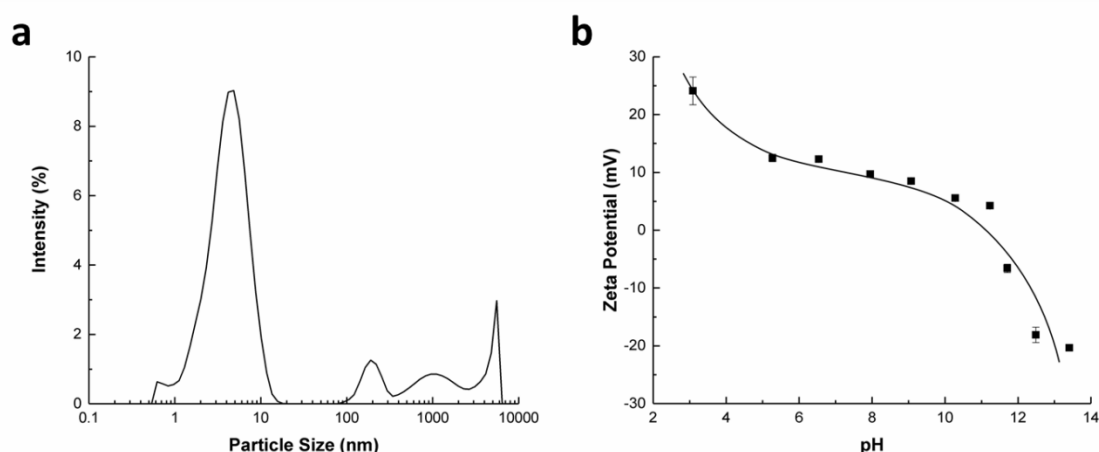


Fig. 4.7 a) DLS size distribution for LYS nanoparticles formed using the conventional desolvation/cross-linking manufacturing strategy as used for BSA & **b)** Isoelectric focussing curve for native LYS with non-linear regression polynomial inverse fifth-order fit curve.

LYS desolvation & cross-linking was attempted at pH 8.0 and the resultant PSD is shown in Fig. 4.7. Evidently, little-to-no nanoparticles were formed using this technique, with a high percentage of monomeric LYS dominating the distribution with a peak at 5 nm. Visually, aggregates formed at the base of the vessel almost instantaneously as the organic solvent was added. This is likely due to a very weak positive surface charge (10.2 mV) on LYS which would do little to prevent aggregation between the lysozyme molecules in solution. Indeed, prior work on human serum albumin nanoparticles recommends a surface charge of ± 20 mV to successfully produce protein nanoparticles (Langer *et al.*, 2003).

With this in mind, identical desolvations were carried out at pH 3.2 (ζ -potential = 22.8 mV) and pH 13.5 (ζ -potential = -23.8 mV) in order to replicate the required surface charge as defined by Langer *et al.* However, PSD data similar to that of Fig. 4.7a) were produced, with the same aggregation visible and no nanoparticles formed. This is likely due to the inefficiency of glutaraldehyde at these two extremes of pH conditions, thus the nanoparticles could not be stabilised through covalent cross-linkage (Migneault *et al.*, 2004).

4.3.4 Multi-Component 2nd Generation Nanoparticles

Given the issues documented with BHB and LYS nanoparticles, a multi-component approach was adopted, whereby the well characterised BSA nanoparticle manufacture would be utilised and then spiked with a second protein, LYS, in order to elevate the resulting isoelectric point of the nanoparticle preparation and begin to move towards the surface characteristics of different viral vectors. As most viral capsids are composed of multiple protein subunits (Stewart and Burnett, 1995; Wu, Asokan and Samulski, 2006; Glasgow and Tullman-Ercek, 2014), which contribute to its overall surface charge, it is plausible that a multifarious protein approach would represent a more accurate nanoparticle mimic.

4.3.4.1 Blended Nanoparticles

The first approach was to “blend in” varying molar ratios of LYS into the starting BSA solution (to a final concentration of 10%) such that LYS could be cross-linked with BSA through available amino groups on both proteins and form structured and stable nanoparticles.

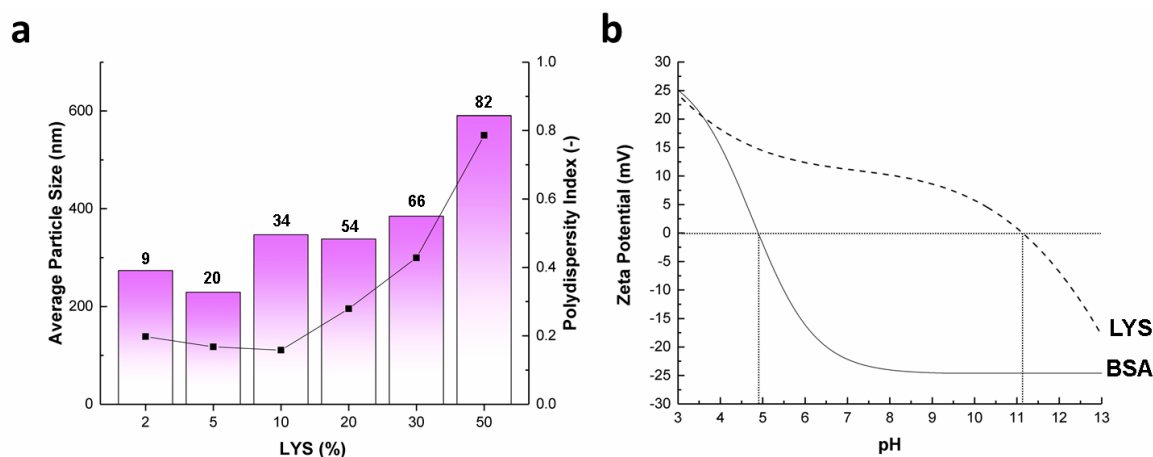


Fig. 4.8 a) Average particle size (columns) & polydispersity indices (line & scatter) of purified, blended BSA-LYS with respect to increasing LYS dosing concentrations by percentage volume. Inset data values above the bars indicate the molar percentage of LYS relative to BSA. **b)** Isoelectric focussing curve for native BSA (-) and LYS (- -) with non-linear regression sigmoidal and polynomial inverse fifth-order fit curves, respectively. The isoelectric points of BSA & LYS are 4.78 & 11.12, respectively.

Fig 4.8a) illustrates the resultant nanoparticle characteristics with respect to the volume proportion of LYS included in the initial 10% protein mixture. Interestingly, even as low as a 9% molar percentage inclusion of LYS resulted in an ~ 5-fold increase in average particle size, relative to just BSA prepared under the same desolvating conditions (70 : 30, Methanol : Ethanol), though the polydispersity indices remained at ~ 0.2, indicating a relatively homogenous nanoparticle suspension had formed.

As the percentage of LYS increases, so too does the average particle size and polydispersity of the produced nanoparticles, whereby when the two proteins are in equal volume proportion, the average particle size and polydispersity of the resultant nanoparticles are 10-fold and 4-fold larger, respectively, relative to just BSA under the same conditions.

The increase in particle size with increasing starting LYS concentration may suggest incorporation of LYS into the nanoparticle structures, though during the manufacture, aggregation of protein was visible and became more extreme as the percentage of LYS increased. This is not particularly surprising given that, at pH 8.0, BSA has a net negative charge of -24.0 mV and LYS has a net positive charge of 10.2 mV; thus when mixed in solution, the proteins will attract due to electrostatic interaction.

Similar work on albumin-lysozyme mixtures have indicated the formation of structure-less aggregates or precipitates (Yu *et al.*, 2006) as well as hetero-protein complexes in the order of micrometres in diameter (Diarrassouba *et al.*, 2015; Santos, de Carvalho and Garcia-Rojas, 2018). One would expect this effect to be exacerbated further when both proteins are desolvated and thus also prone to hydrophobic interaction-led aggregation.

Importantly, as the volume percentage of LYS in the mixture increases, so too do the total moles of protein in the 1 ml starting mixture, whilst the number of available lysine residues available for cross-linking decreases. Thus the number of available sites for cross-linking per unit protein molecule diminishes with increasing LYS %, so the potential to create smaller, tightly cross-linked nanoparticles via numerous covalent intermolecular linkages is significantly reduced.

4.3.4.2 Core-Shell Nanoparticles

As with BHB, the blended nanoparticles were particularly difficult to purify, largely due to their large particle sizes and being interspersed in a polydisperse solution of aggregates of various sizes. For this reason, an alternative core-shell approach was adopted to incorporate LYS onto the surface of pre-fabricated BSA nanoparticles.

This methodology was based on the creation of a suspension of core BSA nanoparticles, exploiting the well characterised manufacturing technique documented in Chapter III and subsequently coating them with a shell of LYS to achieve a core-shell nanoparticle architecture. The technique plays on the concept of electrostatic attraction between the BSA nanoparticles, which display a strong negative charge at pH 8.0 (ζ -potential = -43.9 mV), and LYS, which exhibits a mild positive charge (ζ -potential = 10.2 mV) and to subsequently cross-link the two proteins to form the desired core-shell structure.

Furthermore, it was hypothesised that a core-shell approach would improve the issues of excessive particle size and aggregation during manufacture. Firstly, the core BSA nanoparticle can be tightly controlled and unlike with the blending approach using native BSA, the BSA nanoparticles are structured and highly ordered and would provide a rigid scaffold for the coat LYS to envelope and interlock around.

In order to maximise the number of cross-linking sites available on LYS, the protein is desolvated with the nanoparticles *in situ*, prior to addition of an appropriate cross-linker depending on the coupling strategy and the specific functional groups being targeted.

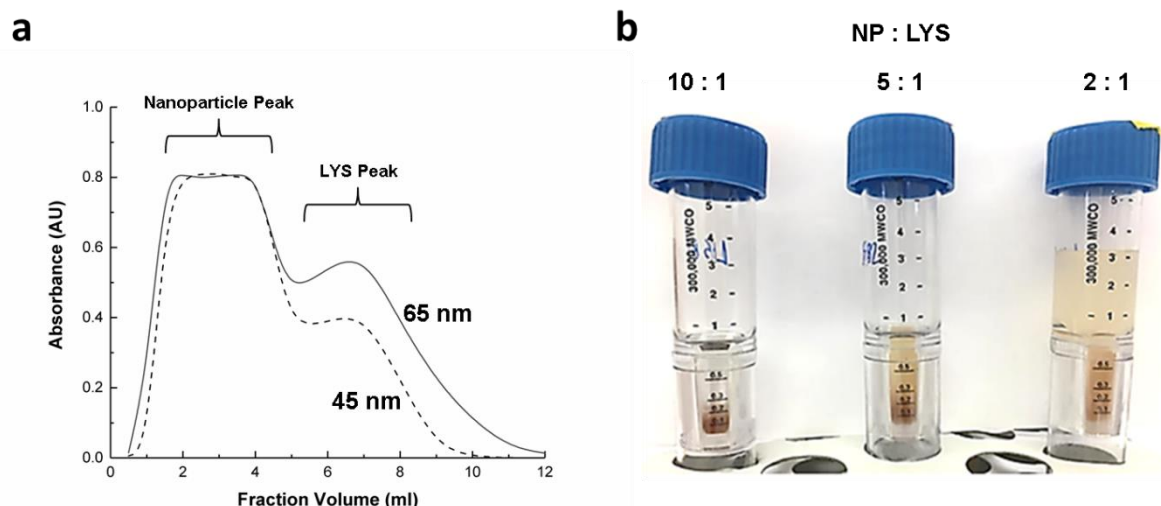


Fig. 4.9 Scouting studies to optimise the coating method for formation of core-shell nanoparticles. **a)** SEC purification chromatograms for LYS-coated BSA nanoparticles of different starting scaffold sizes (with identical starting concentrations of both protein species); 65.18 nm (—) & 44.92 nm (---). **b)** Photograph of centrifugal concentrators used to purify LYS-coated (EDC) BSA nanoparticles with varying molar ratios of nanoparticle to coat protein. The average particle size for the scaffold nanoparticle was 41 nm in each case and the centrifugal filters were run under identical conditions ($2,500 \times g$ for 20 minutes).

Initial scouting experiments were carried out to determine the optimal starting BSA nanoparticle scaffold size as well as an appropriate concentration of LYS to spike into the nanoparticle solution. From a logical perspective, starting with smaller nanoparticles would provide a higher surface area to volume ratio to maximise LYS surface attachment. Indeed, Fig. 4.9a) corroborates with this reasoning; given an identical starting concentration of LYS and scaffold NP, the second free protein peak is lower for the smaller nanoparticle scaffold, indicating a higher percentage of LYS has been incorporated onto the surface of the nanoparticles.

An important side note here; the nanoparticle peak does not directly relate to concentration (as you would otherwise expect the nanoparticle peak for the 45 nm sample to be higher). This is as a result of a distortion of the UV absorbance reading due to scattering by the nanoparticles and as such determination of concentration cannot be ascertained by direct UV measurement (Mamane, Ducoste and Linden, 2006; Porterfield and Zlotnick, 2010).

A second important factor to consider is the concentration of the coat protein to spike into scaffold nanoparticle solution. As with blended nanoparticles, lower molar ratios of LYS proved to be the most effective for coating. Ratios greater than 10: 1 of NP: LYS produced a heterogeneous population of nanoparticles dispersed between aggregates, which formed a thick cake on the surface of the centrifugal filters, rendering purification unviable, as illustrated in Fig. 4.9b).

Whilst glutaraldehyde has proven to be an effective cross-linker for the formation of nanoparticles thus far, its reactivity is limited to coupling primary amine groups and as such can only target lysine

residues on each respective protein species. As per Fig. 4.3, LYS has only 11 lysine residues available for coupling and one would expect that the lysine content for the glutaraldehyde cross-linked BSA nanoparticles scaffolds would be significantly exhausted.

For this reason, novel cross-linking strategies were employed to capitalise on other available amino acid residues on both BSA and LYS (see Fig. 4.3), thus boosting the probability that LYS could successfully assimilate into the scaffold particles.

4.3.4.2.1 EDC Coupling

The first approach was to use N-(3-Dimethylaminopropyl)-N'-ethylcarbodiimide (EDC) as a cross-linker to couple available primary amines (lysine) to carboxyl groups (glutamate & aspartate), forming stable amide bonds between both LYS and the scaffold BSA nanoparticles (Nakajima and Ikada, 1995).

Given the particle sizes of the *bona fide* virus species this methodology aims to mimic, EDC as a zero-length cross-linker should facilitate a thin coat of LYS on the surface of the nanoparticles. As such, a 10 fold molar excess of EDC to total protein concentration was added to maximise the opportunity for LYS incorporation. The only by-product, urea (see Fig. 4.4), can subsequently be removed via the centrifugal-filter purification step.

4.3.4.2.2 DTME Coupling

The second approach was to exploit the availability of reactive thiol groups on both BSA nanoparticles and free LYS cysteine residues using dithio-bis-maleimidoethane (DTME) as a coupling agent. As the functional groups form disulphide bonds in both native species, which are integral to the structure of both proteins, a reduction step (using NaBH₄) is required to liberate free thiol groups prior to cross-linking (Guez *et al.*, 2002; Rombouts *et al.*, 2015).

As such, the DTME coupling approach is a little more complex and time consuming than glutaraldehyde and EDC as pre-treatment of the protein species is required, as well as the requirement of a vacuum to prevent oxidation of the free sulfhydryls and re-formation of disulphide bonds, prior to the cross-linking reaction taking place (Brinkley, 1992).

The core-shell nanoparticles were characterised with respect to their particle size and isoelectric point, as well as how they interact with size-exclusion and anion exchange chromatography media, the results of which are illustrated in Fig. 4.10.

The starting BSA nanoparticle scaffold control provides a point of comparison to observe the impact of a LYS coat on the surface of the nanoparticles. It should be stated here that any electrostatically, non-covalently attached LYS is assumed to be removed by three high salt wash steps prior to characterisation.

The first indication of LYS incorporation is the increase in average particle size relative to the control (12% and 49% increase for EDC and DTME cross-linked strategies, respectively). When

incubated with the SEC media Sepharose 6 Fast Flow (pore size of 50 nm) in a finite bath experiment, an initial mass balance of the supernatant revealed a correlation between the average particle size and a decrease in the species lost within the porous structure of the beads. This indicates that a lower percentage of the coated nanoparticles were able to penetrate into the porous structure of the beads and confirms an increase in size, relative to the control.

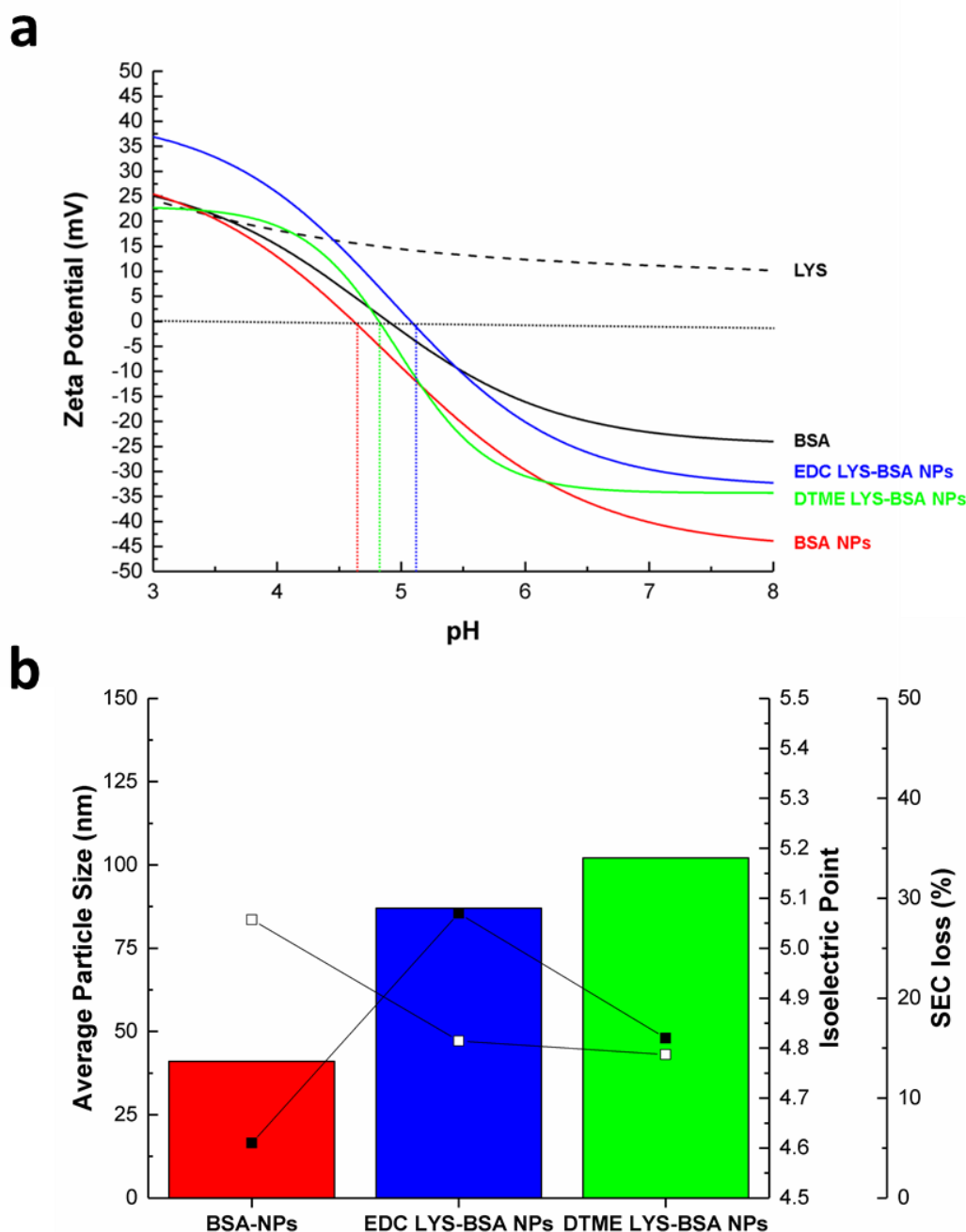


Fig. 4.10 a) Isoelectric focussing curves for native BSA (-) & LYS (- -) alongside a control BSA nanoparticle sample and LYS-coated BSA nanoparticles via two cross-linking methods. Non-linear regression sigmoidal and polynomial inverse fifth-order (LYS only) fit curves were used to create the IEF curves respectively. **b)** Changes in average particle size upon coating of LYS onto the BSA nanoparticle scaffold (columns) as well as modification of

isoelectric point (-■-) & % loss of nanoparticulate bulk when incubated with a Sepharose 6 Fast Flow SEC matrix (-□-). Isoelectric points for BSA-NPs, EDC LYS-BSA NPs & DTME LYS-BSA NPs were 4.61, 5.07 & 4.82, respectively.

Interestingly, despite the limited number of available cysteine residues available for cross-linking on both species, DTME coated nanoparticles exhibited the larger increase in average particle size. This may potentially be due to the relatively long 13.3 Å⁰ spacer arm within the DTME molecule (Green, Reisler and Houk, 2008) which will contribute to an extended hydrodynamic radius.

A second plausible explanation is that the presence of NaOH in creating a basic environment for stabilising the reduced intermediate thiolate would adjust the electrostatic interaction dynamic between the desolvated LYS on the surface of the nanoparticles. In these basic conditions (pH of 13.5) LYS and BSA nanoparticles have a net negative surface charge of -23.8 mV and -45.33 mV, respectively and as such one would expect a degree of electrostatic repulsion between amino acid residues on both species. It is therefore hypothesised that this effect would change the orientation of the desolvated LYS on the surface of the nanoparticles and as such limited cross-linking could take place to form a strongly interlocked, tight shell around the scaffold BSA nanoparticle.

The amino acid residues which contribute to the overall charge of the protein species are arginine (Arg), histidine (His), lysine (Lys) (all positively charged at pH 8.0) and glutamic (Glu) and aspartic (Asp) acid (both negatively charged at pH 8.0). Simple BSA nanoparticles are likely to exhibit a stronger negative charge at pH 8.0 than native BSA due to positively charged lysine residues being exhausted through the glutaraldehyde cross-linkages and as such the proportion of negatively charged amino acids increases. This does vary, likely due to the orientation of the other charged residues when the nanoparticle forms and is independent of the size of the nanoparticles formed (see Chapter III, Section 3.3.1.1).

Both coated nanoparticles exhibit a basic shift in isoelectric point due to the additional arginine, histidine and lysine residues introduced through the LYS coat. EDC cross-linked nanoparticles exhibit a more exaggerated shift due to a significant change in the ratio of positive and negatively charged amino acids on both proteins during the coating. There is a significantly higher availability of carboxyl functional groups for cross-linking via EDC on both BSA (59 Glu, 40 Asp) and LYS (8 Glu, 7 Asp) and 11 lysine residues on LYS to contribute reactive amino groups. Compare this to the DTME approach; 35 and 4 cysteine residues on each BSA and LYS molecule, respectively, are available for thiol cross-linking and as such LYS incorporation is relatively limited.

Glu and Asp residues are negatively charged and are depleted during EDC cross-linking, increasing the proportion of positively charged residues within the nanoparticle species. Titrating towards acidic conditions with HCl, fewer H⁺ ions are required to reduce the colloid surface charge to zero (i.e. reach the isoelectric point) due to a lower proportion of negatively charged amino acid residues on the nanoparticle surface. As such, the isoelectric point shifts to the right and is more basic, compared to the BSA NP control sample.

In a similar vein, the surface charge of the EDC coated nanoparticles is less negative at pH 8.0 and more positive at pH 3.0, relative to the control BSA NP scaffold. Occupying the acidic residues via EDC cross-linking allows a greater contribution to the overall net colloid surface charge from the basic, positively charged Arg, His and Lys side chains from both BSA and the introduced LYS at both extremes of pH.

Conversely, the surface charge for the DTME cross-linked nanoparticles are similar to the BSA nanoparticle control at pH 3.0, as cysteine has a limited contribution to the overall protein charge. As Glu and Asp residues remain un-conjugated in both the DTME and BSA NP control samples and as both residues have a $pK_a \sim 4.0$, at pH conditions of 4.0 and above, the side chains become deprotonated and increasingly negatively charged. This drives the surface charge down and causes the sharp declining slope in ζ -potential observed at this point in Fig. 4.10a).

This same decline is shallower and begins at more basic pH conditions for the EDC sample due to a lower net negative charge contribution stemming from Glu and Asp residues utilised for cross-linking. At pH 8.0, DTME samples are significantly less negative than the BSA NP control; as with EDC this likely due to the contribution of the additional positively charged Arg, His and (limited) Lys residues from a successfully integrated LYS shell.

The isoelectric point shift and the shape of the isoelectric focussing curves for the respective nanoparticle species provide interesting insights into the degree of LYS incorporation. For both coated nanoparticle preparations, the isoelectric point shifted to a more basic pI (4% increase for DTME & 9% for EDC), relative to the scaffold; a strong indication that whilst the entire scaffold nanoparticle has not been coated, an appreciable amount of the surface has been enriched with LYS protein.

4.3.4.3 Finite Bath & CLSM Analysis

As an orthogonal characterisation study, finite bath studies were carried out to assess the binding characteristics of the two nanoparticle samples and the control BSA NP scaffolds on the anion exchange chromatography resin, Q-Sepharose Fast Flow. As all three species exhibit some degree of negative charge at pH 8.0, this buffer condition was employed when challenging the resin with the three sample types, with each nanoparticle suspension loaded at the same concentration.

EDC cross-linked LYS coated samples demonstrated a 51.3% reduction in anion-exchange binding, relative to the scaffold control. This is indicative of both a shielding effect of the coat LYS, limiting electrostatic interaction between the predominantly negatively charged surface residues on the original BSA nanoparticle structure and the anion exchanger surface. The removal of Glu and Asp residues for cross-linking will also contribute to this effect. This reduction in binding capacity corroborates well with the isoelectric focussing data and indicates the surface charge of the species plays an important part in its binding characteristics to ion exchangers.

Interestingly, DTME cross-linked core-shell nanoparticles finite bath mass balance data did not corroborate with its isoelectric focussing, as the binding capacity to the anion-exchanger in fact increased by 22.8%, relative to the scaffold control. Despite the apparent increase (less negative)

in ζ -potential for the DTME sample, the significantly large size of the formed nanoparticles may play a role in the elevated binding capacity.

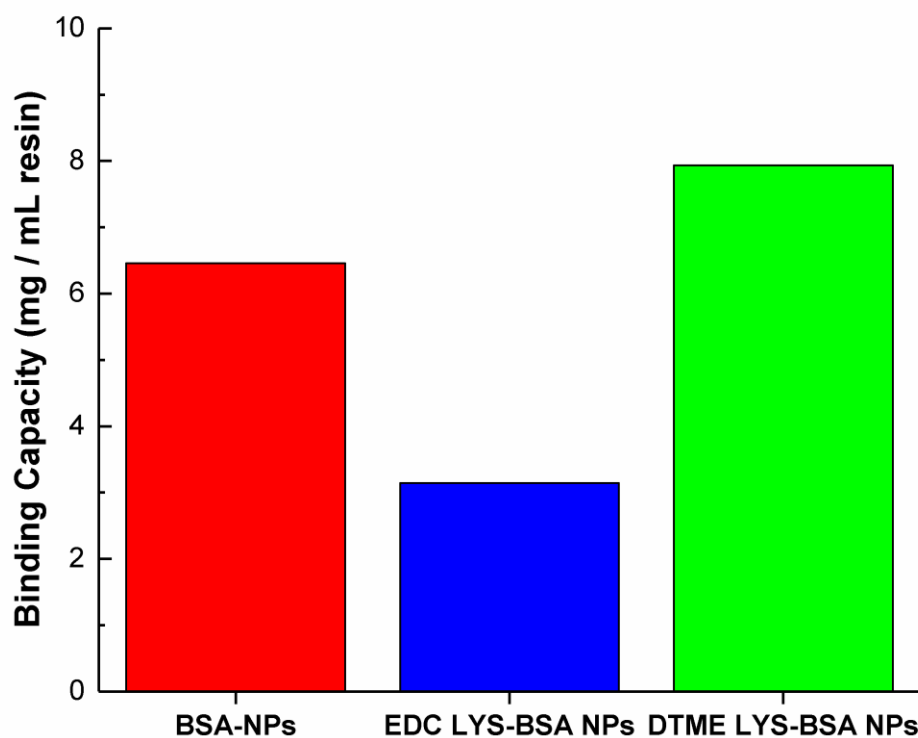


Fig. 4.11 Relative binding capacities for the BSA nanoparticle scaffold and the two cross-linking strategies when challenged at the same starting concentration onto a strong anion-exchange resin (*Q-Sepharose Fast Flow*) and the binding capacity determined through colorimetric assay of the supernatant and subsequent mass balance.

Due to a limited number of available functional cysteine residues to cross-link on both protein species, it was hypothesised that the alteration to the surface chemistry of the BSA nanoparticles through DTME would be less significant than EDC. As DTME has a relatively long spacer arm and the conditions for cross-linking could impact the intra-particle electrostatic environment, it could be envisaged that a tentacular-type nanoparticle morphology is achieved; whilst the LYS is locked through covalent linkages between the sulfhydryl groups at specific points on the nanoparticle surface, the bulk of the coat LYS extends away from the nanoparticle scaffold.

This can create a higher surface area for electrostatic interaction between the anion-exchange ligand and the negatively charged residues on the nanoparticle species. It appears that this effect supersedes the impact of coating the nanoparticles with a basic protein and the apparent adjustment of surface charge and as such results in a slight increase in binding, relative to the control.

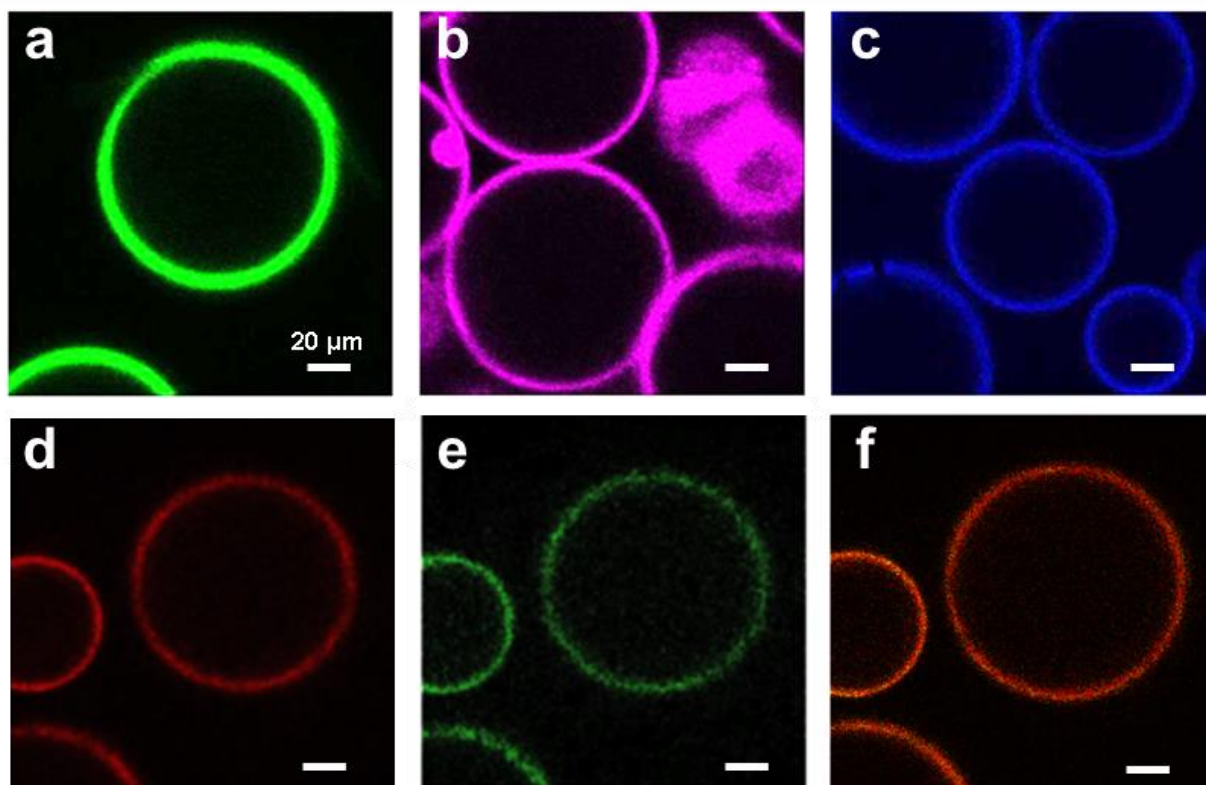


Fig. 4.12 Confocal Laser Scanning Micrographs of fluorescent core-shell LYS-coated BSA nanoparticles bound to the surface of the anion exchanger *Q*-Sepharose Fast Flow. **a)** BSA nanoparticles tagged with Texas-Red X. Lysozyme, pre-tagged with Cy5, coated onto un-tagged BSA nanoparticles via **b)** EDC cross-linking & **c)** DTME cross-linking. BSA NPs and Lysozyme, both pre-tagged separately with Fluorescamine & Cy5, respectively, then formed into core-shell nanoparticles; **d)** **Detecting BSA NPs:** sample excited with a 405 nm laser and detected at 465 nm ($\lambda_{\text{EXC}} = 390 \text{ nm}$, $\lambda_{\text{EMI}} = 465 \text{ nm}$ for fluorescamine), **e)** **Detecting incorporated LYS:** sample excited with a 635 nm laser and detected at 666 nm ($\lambda_{\text{EXC}} = 646 \text{ nm}$, $\lambda_{\text{EMI}} = 666 \text{ nm}$ for Cy5). **f)** Laser lines from **d)** & **e)** run sequentially over the same focal plane suggesting co-localisation of both BSA-NPs & Lysozyme in the same locality.

Fluorescent tags were conjugated onto each respective protein species to facilitate visual confirmation of LYS integration into the nanoparticles, as illustrated in Fig. 4.12. The fluorescent micrographs reveal interaction of the nanoparticles solely on the surface of the resin, forming a bright fluorescent corona around the beads. This is due to a size-exclusion effect as the size of the nanoparticles are too large to penetrate into the porous structure and can only interact with the anion-exchange ligands on the surface of the beads. Fig. 4.12b) and c) reveal the presence of LYS as native LYS was pre-tagged prior to coating on the surface of the nanoparticles. The lack of interaction with the centre of the bead suggests that the LYS is localised to the nanoparticulate species, with a similar corona formed to that of the control BSA NP scaffolds highlighted in a).

To confirm the assimilation of LYS within the BSA nanoparticles, the scaffold nanoparticles and LYS were separately pre-tagged with fluorescent dyes (with no overlap of emission spectra) that could be excited with two separate laser lines. The DTME cross-linking strategy was employed

rather than EDC to avoid interference of the amine reactive fluorescent probe limiting any potential sites for cross-linking (see Chapter V for further discussion on impact of labelling).

Fig 4.12d) and e) highlight the existence of both fluorescent species on the same bead through excitation with each separate laser line and finally f) confirms co-localisation of the two protein species by exciting both fluorescent species sequentially. As both protein species were conjugated using the same dye: protein molar ratio when tagged, the intensity provides some indication as to the degree of incorporation of the coat protein. The fluorescent intensity is significantly higher for the BSA NP with a rather weaker signal for LYS; indicative of some degree of integration of LYS, though not a complete envelopment over the scaffold, understandable given the molar ratio of LYS spiked into the nanoparticle solution.

4.4 Conclusions

The work detailed in this chapter has detailed the development of novel approaches to forming more sophisticated protein nanoparticles based on the platform established manufacturing BSA nanoparticles detailed in the previous chapter. The main aim of this chapter has been to adopt a “tool-box approach” whereby the knowledge ascertained from previous work can be used to inform the development of better viral mimics. A key example of this is the manufacture of very small BSA nanoparticles as a starting scaffold structure to incorporate a significant amount of LYS onto the surface without causing significant aggregation. Through an understanding of dielectric constants of the desolvating agents and its impact on the average nanoparticle size, this was made possible.

Pleasingly, the work carried out on BHB revealed similar trends with respect to dielectric constant and particle size, though the complexity of the starting protein led to batch to batch variability and significantly high polydispersities. As such, despite its relatively high isoelectric point, the difficulties in purification and its lack of sufficient reproducibility made further characterisation impractical.

Whilst other proteins were also tested for formation of protein nanoparticles, the most promising and arguably most interesting aspect of the work is the formation of multi-component nanoparticles with a core-shell architecture. Whilst EDC appeared to be the more successful cross-linker with respect to LYS incorporation, DTME provides a useful alternative approach as the cross-linker is “reversible” i.e. it contains a disulphide in the spacer arm that can be disrupted by a reducing agent such as DTT or β -mercaptoethanol. This would allow quantitative assessment of the degree of incorporation of LYS onto the scaffold nanoparticles by a cleaving reaction and quantitative analysis of free LYS produced; thus providing a useful tool in optimising the manufacturing technique further.

Whilst the technique requires further optimisation to better replicate the surface characteristics of a *bona fide* virus such as Polio or AAV, the work illustrates the potential to tailor specific loading concentrations of a coat protein to “titrate” onto the surface of a scaffold, dependent on the mimic requirements. There is even scope to titrate specific amino acid residues or oligopeptides onto the surface for more specific modification of the colloid’s surface properties.

As an aside, work by Yu *et al.* report a technique for the formation of stable OVA-LYS “nanogels” with particle sizes < 100 nm, PDI values < 0.2 and an isoelectric point of approximately 7.0. The technique involves careful addition and titration of both proteins (in equal molar ratios) to modulate surface charge and prevent aggregation. The mixture is then heated to 80 °C to achieve thermal stabilisation through inter-protein hydrogen bonding, disulphide linkages and hydrophobic interaction (Yu *et al.*, 2006). It is important to note that the total protein concentration used to form the nanogels was significantly lower (86 μ M, compared to 1.5 mM for these experiments) which aids in limiting aggregation during the manufacture of the nanogels, though may impact the concentration of protein nanoparticles produced.

This electrostatically-driven self-assembly of two proteins with opposite charge into a nanogels may be an alternative avenue to explore in the future in the creation of accurate viral mimics, though due consideration should be given to particle stability and response to environmental changes such as pH, temperature and ionic strength adjustments.

4.5 References

- Ahsan, S.M. & Rao, C.M., 2017. The role of surface charge in the desolvation process of gelatin: implications in nanoparticle synthesis and modulation of drug release. *International Journal of Nanomedicine*, Volume 12, pp.795–808. Available at: <https://www.dovepress.com/the-role-of-surface-charge-in-the-desolvation-process-of-gelatin-impli-peer-reviewed-article-IJN> [Accessed October 1, 2018].
- Aranda, R. et al., 2008. Structural analysis of fish versus mammalian hemoglobins: Effect of the heme pocket environment on autooxidation and heme loss. *Proteins*, 75, pp.217–230. Available at: <http://www.rcsb.org/structure/2QSS> [Accessed October 10, 2018].
- Arbyn, M. et al., 2007. *IARC Monographs on the Evaluation of Carcinogenic Risks to Humans Human Papillomaviruses* 90th ed., Lyon: International Agency for Research on Cancer. Available at: <http://monographs.> [Accessed October 10, 2018].
- Arroyo-Maya, I.J. et al., 2014. α -Lactalbumin nanoparticles prepared by desolvation and cross-linking: Structure and stability of the assembled protein. *Biophysical Chemistry*, 193–194, pp.27–34. Available at: <http://linkinghub.elsevier.com/retrieve/pii/S0301462214000878> [Accessed March 8, 2017].
- Asakura, T. et al., 1974. Abnormal precipitation of oxyhemoglobin S by mechanical shaking. *Proceedings of the National Academy of Sciences of the United States of America*, 71(5), pp.1594–8. Available at: <http://www.ncbi.nlm.nih.gov/pubmed/4525907> [Accessed October 26, 2018].
- Asakura, T. et al., 1977. Denatured hemoglobin in sickle erythrocytes. *The Journal of clinical investigation*, 59(4), pp.633–40. Available at: <http://www.ncbi.nlm.nih.gov/pubmed/845254> [Accessed October 26, 2018].
- Asakura, T., Adachi, K. & Schwartz, E., 1978. Stabilizing Effect of Various Organic Solvents on Protein*. *The Journal of Biological Chemistry*, 253(18), pp.6423–6425. Available at: <http://www.jbc.org/> [Accessed October 23, 2018].
- Ashraf, S. et al., 2014. Lysozyme-coated silver nanoparticles for differentiating bacterial strains on the basis of antibacterial activity. *Nanoscale research letters*, 9(1), p.565. Available at: <http://www.ncbi.nlm.nih.gov/pubmed/25435831> [Accessed September 3, 2018].
- Blanco, G. & Blanco, A., 2017. *Medical biochemistry* 1st ed., Academic Press.
- Brinkley, M., 1992. A Brief Survey of Methods for Preparing Protein Conjugates with Dyes, Haptens, and Cross-Linking Reagents. *Bioconjugate Chem*, 3, pp.2–13. Available at: <https://pubs.acs.org/sharingguidelines> [Accessed October 28, 2018].
- Chen, Z. et al., 1995. Effectiveness of three ribozymes for cleavage of an RNA transcript from human papillomavirus type 18. *Cancer gene therapy*, 2(4), pp.263–71. Available at: <http://www.ncbi.nlm.nih.gov/pubmed/8548580> [Accessed October 10, 2018].
- Chen, Z. et al., 1996. Effects on tumor cells of ribozymes that cleave the RNA transcripts of human papillomavirus type 18. *Cancer gene therapy*, 3(1), pp.18–23. Available at: <http://www.ncbi.nlm.nih.gov/pubmed/8785706> [Accessed October 10, 2018].
- Diarrassouba, F. et al., 2015. Self-assembly of β -lactoglobulin and egg white lysozyme as a potential carrier for nutraceuticals. *Food Chemistry*, 173, pp.203–209. Available at: <https://www.sciencedirect.com/science/article/pii/S0308814614015660> [Accessed October 26, 2018].

- Dickerson, R.E. & Geis, I., 1983. *Hemoglobin: structure, function, evolution, and pathology*, Benjamin/Cummings Pub. Co.
- Duane Brown, W., 1960. Reduction of protein disulfide bonds by sodium borohydride. *Biochimica et Biophysica Acta*, 44, pp.365–367. Available at: <https://www.sciencedirect.com/science/article/pii/0006300260915791> [Accessed October 9, 2018].
- Etorki, A.M. et al., 2016. Effects of Desolvating Agent Types, Ratios, and Temperature on Size and Nanostructure of Nanoparticles from α -Lactalbumin and Ovalbumin. *Journal of Food Science*, 81(10), pp.E2511–E2520. Available at: <http://doi.wiley.com/10.1111/1750-3841.13447> [Accessed April 30, 2018].
- Flotte, T.R. & Carter, B.J., 1995. Adeno-associated virus vectors for gene therapy. *Gene therapy*, 2(6), pp.357–62. Available at: <http://www.ncbi.nlm.nih.gov/pubmed/7584109> [Accessed October 10, 2018].
- Frantzen, F. et al., 1997. Selective Precipitation of Human Hemoglobin by Organic Solvents and Metal Cations. *Hemoglobin*, 21(2), pp.155–172. Available at: <http://www.tandfonline.com/doi/full/10.3109/03630269708997519> [Accessed October 25, 2018].
- Funk, G.M. et al., 1986. Use of a rapid and highly sensitive fluorescamine-based procedure for the assay of plasma lipoproteins. *Journal of lipid research*, 27(7), pp.792–5. Available at: <http://www.ncbi.nlm.nih.gov/pubmed/3760715> [Accessed October 9, 2018].
- Gao, G.-P. et al., 2002. Novel adeno-associated viruses from rhesus monkeys as vectors for human gene therapy. *Proceedings of the National Academy of Sciences of the United States of America*, 99(18), pp.11854–9. Available at: <http://www.ncbi.nlm.nih.gov/pubmed/12192090> [Accessed October 10, 2018].
- Ghebremedhin, B., 2014. Human adenovirus: Viral pathogen with increasing importance. *European Journal of Microbiology and Immunology*, 4(1), pp.26–33. Available at: <http://www.ncbi.nlm.nih.gov/pubmed/24678403> [Accessed October 10, 2018].
- Ginn, S.L. et al., 2018. Gene therapy clinical trials worldwide to 2017: An update. *The Journal of Gene Medicine*, (January), p.e3015.
- Glasgow, J. & Tullman-Ercek, D., 2014. Production and applications of engineered viral capsids. *Applied Microbiology and Biotechnology*, 98(13), pp.5847–5858.
- Green, N.S., Reisler, E. & Houk, K.N., 2008. Quantitative evaluation of the lengths of homobifunctional protein cross-linking reagents used as molecular rulers. *Protein Science*, 10(7), pp.1293–1304. Available at: <http://doi.wiley.com/10.1110/ps.51201> [Accessed October 10, 2018].
- Guez, V. et al., 2002. Role of individual disulfide bonds in hen lysozyme early folding steps. *Protein Science*, 11(5), pp.1136–1151. Available at: <http://www.ncbi.nlm.nih.gov/pubmed/11967370> [Accessed October 28, 2018].
- Gunasekaran, S., Ko, S. & Xiao, L., 2006. Use of whey proteins for encapsulation and controlled delivery applications. Available at: <https://pdfs.semanticscholar.org/a39e/835484e4a4d35b30a8c64fcc2502afe1eb67.pdf> [Accessed April 30, 2018].

- Hauswirth, W.W. et al., 2008. Treatment of Leber Congenital Amaurosis Due to *RPE65* Mutations by Ocular Subretinal Injection of Adeno-Associated Virus Gene Vector: Short-Term Results of a Phase I Trial. *Human Gene Therapy*, 19(10), pp.979–990. Available at: <http://www.liebertpub.com/doi/10.1089/hum.2008.107> [Accessed October 10, 2018].
- Herskovits, T.T., Gadegbeku, B. & Jaillet, H., 1970. On the Structural Stability and Solvent Denaturation of Proteins. *THE JOURNAL OF BIOLOGICAL CHEMISTRY*, 245(10), pp.2588–2598. Available at: <http://www.jbc.org/> [Accessed October 23, 2018].
- Hung, C.-F. et al., 2012. Ovarian Cancer Gene Therapy Using HPV-16 Pseudovirion Carrying the HSV-tk Gene J. Najbauer, ed. *PLoS ONE*, 7(7), p.e40983. Available at: <http://dx.plos.org/10.1371/journal.pone.0040983> [Accessed October 10, 2018].
- Jahanban-Esfahlan, A., Dastmalchi, S. & Davaran, S., 2016. A simple improved desolvation method for the rapid preparation of albumin nanoparticles. *International Journal of Biological Macromolecules*, 91, pp.703–709. Available at: <https://www.sciencedirect.com/science/article/pii/S0141813016304433?via%3Dihub> [Accessed August 9, 2018].
- Konishi, M. et al., 2008. Gene transfer into guinea pig cochlea using adeno-associated virus vectors. *The journal of gene medicine*, 10(6), pp.610–618.
- Kumar, S. & Bandyopadhyay, U., 2005. Free heme toxicity and its detoxification systems in human. *Toxicology Letters*, 157(3), pp.175–188. Available at: <https://www.sciencedirect.com/science/article/pii/S0378427405000883> [Accessed October 26, 2018].
- van Kuppeveld, F.J.M. et al., 2002. Studies towards the potential of poliovirus as a vector for the expression of HPV 16 virus-like-particles. *FEMS Immunology & Medical Microbiology*, 34(3), pp.201–208. Available at: <https://academic.oup.com/femspd/article-lookup/doi/10.1111/j.1574-695X.2002.tb00625.x> [Accessed October 10, 2018].
- Langer, K. et al., 2003. Optimization of the preparation process for human serum albumin (HSA) nanoparticles. *International Journal of Pharmaceutics*, 257(1–2), pp.169–180.
- Life Technologies, 1996. Amine-Reactive Probes | 2 Labeling Proteins. , 1996, pp.1–11.
- MacDonald, S.L. & Pepper, D.S., 1994. Hemoglobin polymerization. *Methods in Enzymology*, 231, pp.287–308. Available at: <https://www.sciencedirect.com/science/article/pii/0076687994310211> [Accessed October 25, 2018].
- Majorek, K.A. et al., 2012. Structural and immunologic characterization of bovine, horse, and rabbit serum albumins. *Mol.Immunol.*, 52, pp.174–182. Available at: <https://www.rcsb.org/structure/3V03> [Accessed August 9, 2018].
- Mamane, H., Ducoste, J.J. & Linden, K.G., 2006. *Effect of particles on ultraviolet light penetration in natural and engineered systems*, Available at: <https://pdfs.semanticscholar.org/d755/0f667568923475807f2cd623a4eaac1f217b.pdf> [Accessed October 27, 2018].
- Mandl, S. et al., 1998. Poliovirus vaccine vectors elicit antigen-specific cytotoxic T cells and protect mice against lethal challenge with malignant melanoma cells expressing a model antigen. *Proceedings of the National Academy of Sciences of the United States of America*, 95(14), pp.8216–21.

- Available at: <http://www.ncbi.nlm.nih.gov/pubmed/9653167> [Accessed October 10, 2018].
- Michen, B. & Graule, T., 2010. Isoelectric points of viruses. *Journal of Applied Microbiology*, 109(2), pp.388–397. Available at: <http://doi.wiley.com/10.1111/j.1365-2672.2010.04663.x> [Accessed June 13, 2016].
- Migneault, I. et al., 2004. Glutaraldehyde: behavior in aqueous solution, reaction with proteins, and application to enzyme crosslinking. *BioTechniques*, 37(5), pp.790–802. Available at: <http://www.ncbi.nlm.nih.gov/pubmed/15560135> [Accessed August 13, 2018].
- Morrow, C.D., Ansardi, D.C. & Porter, D.C., 1997. Methods for the Use of Poliovirus Vectors for Gene Delivery. In *Gene Therapy Protocols*. New Jersey: Humana Press, pp. 103–116. Available at: <http://link.springer.com/10.1385/0-89603-484-4:103> [Accessed October 10, 2018].
- Nakajima, N. & Ikada, Y., 1995. Mechanism of amide formation by carbodiimide for bioconjugation in aqueous media. *Bioconjugate chemistry*, 6(1), pp.123–30. Available at: <http://www.ncbi.nlm.nih.gov/pubmed/7711098> [Accessed October 10, 2018].
- Naso, M.F. et al., 2017. Adeno-Associated Virus (AAV) as a Vector for Gene Therapy. *BioDrugs : clinical immunotherapeutics, biopharmaceuticals and gene therapy*, 31(4), pp.317–334. Available at: <http://www.ncbi.nlm.nih.gov/pubmed/28669112> [Accessed October 10, 2018].
- Ohnishi, T. & Asakura, T., 1976. Denaturation of oxyhemoglobin S by mechanical shaking. *Biochimica et Biophysica Acta (BBA) - Protein Structure*, 453(1), pp.93–100. Available at: <https://www.sciencedirect.com/science/article/pii/0005279576902531> [Accessed October 26, 2018].
- Perutz, M.F. et al., 1993. A Novel Allosteric Mechanism in Haemoglobin: Structure of Bovine Deoxyhaemoglobin, Absence of Specific Chloride-binding Sites and Origin of the Chloride-linked Bohr Effect in Bovine and Human Haemoglobin. *Journal of Molecular Biology*, 233(3), pp.536–545. Available at: <https://www.sciencedirect.com/science/article/pii/S0022283683715305?via%3Dihub> [Accessed October 23, 2018].
- Porterfield, J.Z. & Zlotnick, A., 2010. A simple and general method for determining the protein and nucleic acid content of viruses by UV absorbance. *Virology*, 407(2), pp.281–288. Available at: <https://www.sciencedirect.com/science/article/pii/S0042682210005453> [Accessed October 27, 2018].
- Potter, M. et al., 2014. A simplified purification protocol for recombinant adeno-associated virus vectors. *Molecular therapy. Methods & clinical development*, 1, p.14034. Available at: <http://www.ncbi.nlm.nih.gov/pubmed/26015974> [Accessed October 10, 2018].
- Regenmortel, M.H. V., 2009. *Synthetic Peptide Vaccines and the Search for Neutralization B Cell Epitopes*, Available at: <http://www.biacore.com/lifesciences/events/vaccine2008/home/index.html> [Accessed October 10, 2018].
- Rombouts, I. et al., 2015. Formation and reshuffling of disulfide bonds in bovine serum albumin demonstrated using tandem mass spectrometry with collision-induced and electron-transfer dissociation. *Scientific Reports*, 5(1), p.12210. Available at: <http://www.ncbi.nlm.nih.gov/pubmed/26193081> [Accessed September 29, 2018].
- Santos, M.B., de Carvalho, C.W.P. & Garcia-Rojas, E.E., 2018. Heteroprotein complex formation of bovine serum albumin and lysozyme: Structure and thermal stability. *Food Hydrocolloids*, 74,

- pp.267–274. Available at: <https://linkinghub.elsevier.com/retrieve/pii/S0268005X17307002> [Accessed October 26, 2018].
- Shirahama, H., Suzuki, K. & Suzawa, T., 1989. Bovine hemoglobin adsorption onto polymer lattices. *Journal of Colloid and Interface Science*, 129(2), pp.483–490. Available at: <https://www.sciencedirect.com/science/article/pii/0021979789904621> [Accessed October 26, 2018].
- Shoichet, B.K. et al., 1995. A relationship between protein stability and protein function. *Proc.Natl.Acad.Sci.U.S.A.*, 92, pp.452–456. Available at: <http://www.rcsb.org/structure/253L> [Accessed October 10, 2018].
- Stein, P.E. et al., 1991. Crystal structure of uncleaved ovalbumin at 1.95 Å resolution. *J.Mol.Biol.*, 221, pp.941–959. Available at: <http://www.rcsb.org/structure/1OVA> [Accessed October 10, 2018].
- Steppert, P. et al., 2016. Purification of HIV-1 gag virus-like particles and separation of other extracellular particles. *Journal of Chromatography A*, 1455, pp.93–101. Available at: <https://www.sciencedirect.com/science/article/pii/S0021967316306446> [Accessed October 9, 2018].
- Stewart, P.L. & Burnett, R.M., 1995. Adenovirus Structure by X-ray Crystallography and Electron Microscopy. In Springer Berlin Heidelberg, pp. 25–38. Available at: http://www.springerlink.com/index/10.1007/978-3-642-79496-4_2 [Accessed June 20, 2017].
- Storey, A. et al., 1991. Anti-sense phosphorothioate oligonucleotides have both specific and non-specific effects on cells containing human papillomavirus type 16. *Nucleic acids research*, 19(15), pp.4109–14. Available at: <http://www.ncbi.nlm.nih.gov/pubmed/1651476> [Accessed October 10, 2018].
- Thomassen, Y.E. et al., 2013. Isoelectric Point Determination of Live Polioviruses by Capillary Isoelectric Focusing with Whole Column Imaging Detection. *Analytical Chemistry*, 85(12), pp.6089–6094. Available at: <http://www.ncbi.nlm.nih.gov/pubmed/23672432> [Accessed October 10, 2018].
- Wang, E., Wang, H. & Li, Z., 2000. *Protein Structural Characterization by Scanning Tunneling Microscopy with Electrochemistry*, Available at: https://www.jstage.jst.go.jp/article/analsci/16/2/16_2_205/_pdf [Accessed October 23, 2018].
- Wang, K. et al., 2015. Acid Denaturation Inducing Self-Assembly of Curcumin-Loaded Hemoglobin Nanoparticles. Available at: www.mdpi.com/journal/materials [Accessed October 23, 2018].
- Wang, X. et al., 2010. Observation of symmetric denaturation of hemoglobin subunits by electrospray ionization mass spectrometry. *Journal of mass spectrometry: JMS*, 45(11), pp.1306–11. Available at: <http://www.ncbi.nlm.nih.gov/pubmed/20963788> [Accessed October 26, 2018].
- Wu, Z., Asokan, A. & Samulski, R.J., 2006. Adeno-associated Virus Serotypes: Vector Toolkit for Human Gene Therapy. *Molecular Therapy*, 14(3), pp.316–327. Available at: <https://www.sciencedirect.com/science/article/pii/S1525001606002048> [Accessed

October 10, 2018].

- Ylä-Pelto, J., Tripathi, L. & Susi, P., 2016. Therapeutic Use of Native and Recombinant Enteroviruses. *Viruses*, 8(3), p.57. Available at: <http://www.ncbi.nlm.nih.gov/pubmed/26907330> [Accessed October 10, 2018].
- Yu, S. et al., 2006. Nanogels prepared by self-assembly of oppositely charged globular proteins. *Biopolymers*, 83(2), pp.148–158. Available at: <http://www.ncbi.nlm.nih.gov/pubmed/16718679> [Accessed September 3, 2018].
- Zhou, C.-M., 2013. Characterization of human papillomavirus by capillary isoelectric focusing with whole-column imaging detection. *ELECTROPHORESIS*, 34(20–21), p.n/a-n/a. Available at: <http://www.ncbi.nlm.nih.gov/pubmed/23925949> [Accessed October 10, 2018].

CHAPTER V

SYNTHETIC PROTEIN NANOPARTICLES AS TOOLS INFORMING THE CHROMATOGRAPHY OF VIRUS PARTICLE PRODUCTS

Abstract

The acquisition of representative virus feedstock, sufficient in quantity and particle concentration, as well as the methods for monitoring these species during chromatography, poses several practical issues in the realm of virus particle purification. This chapter follows on from that described in Chapter II and aims to characterise the bi-functional materials, as well as two commercial resins, using the BSA nanoparticles described in Chapter III. Specific modifications, including conjugation with fluorophores, allow for the nanoparticles to be tracked in both the mobile and porous stationary phases of chromatographic media to facilitate an in-depth study of protein species/matrix interaction. To optimise chromatography performance and assess binding kinetics, the use of protein assays and confocal laser scanning microscopy have been employed.

Using monomer and nanoparticles to mimic a crude virus feedstock has enabled the characterisation and optimisation of both commercial chromatography media and resins manufactured in-house. The results highlight the utility of both commercial resins, Q-Sepharose Fast Flow and Capto™ Core 700, in purifying the surrogate mimics. Of the bi-layered materials, Superose 6 Prep Grade generally outperformed both Sepharose 6 Fast Flow and Superose 12 Prep Grade, revealing differences between the media not shown by the plasmid DNA binding studies. This was generally supported by the complimentary confocal data, which provided an insight into the spatial location and binding kinetics when challenged onto the beads.

This information can be used to inform scale-up of viral purification columns in a cost-effective and efficient manner, excluding the need for contact with real virus species and their associated complications. These sophisticated nanoparticles serve to broaden the scope of virus chromatography and enable the collection of effective and novel data to improve recovery and purification of viruses, tailoring the selection of media and operating conditions to a specific target nanoplex. It is envisioned that the manufacture of reproducible, well characterised and multi-functional nanoparticles will provide a platform for assessment of established and novel viral purification media in the near future.

Abbreviations

Ad: Adenovirus

AU: Absorbance Units

BCA: Bicinchoninic Acid

BSA NP: Bovine Serum Albumin
Nanoparticles

BSA: Bovine Serum Albumin

CD: Circular Dichroism

CLSM: Confocal Laser Scanning Microscopy

DMSO: Dimethyl Sulfoxide

DNA: Deoxyribonucleic Acid

IEF: Isoelectric Focussing

LM: Light Microscopy

pDNA: Plasmid DNA

Q: Trimethylamine Chloride

SBC: Static Binding Capacity

SI: Selectivity Index

TRIS-HCl: Trisaminomethane
hydrochloride

TRX: Texas Red-X

UV: Ultraviolet

Table of Contents

CHAPTER V	258
Abstract.....	258
Abbreviations.....	259
List of Figures.....	261
List of Tables.....	262
5.1 Introduction.....	263
5.2 Materials & Methods	265
5.2.1 Materials & Reagents	265
5.2.2 Preparation of Bovine Serum Albumin Nanoparticles.....	265
5.2.3 Analysis	265
5.3 Results & Discussion	268
5.3.1 Fluorophore Conjugation	268
5.3.2 Challenging Nanoparticles on Commercial Resins	271
5.3.3 Challenging Nanoparticles on Resins Manufactured In-House.....	275
5.4 Conclusions.....	281
5.5 References	282

List of Figures

Fig. 5.1 **a)** Isoelectric focussing curves for blank and fluorescent protein and protein nanoparticles, with species tagged prior to and post formation. **b)** Summary table detailing the particle size distribution (PSD) average particle size and the isoelectric point (IEP) of each species. **c)** The particle size distribution of the blank adenovirus mimic. **d)** Chromatogram illustrating the retention times of blank (-) & fluorescently conjugated (-) BSA on a cation exchange resin.

Fig. 5.2 **a)** CD spectra of BSA in native, tagged, unfolded and nanoparticulate forms. **b)** Changes in the secondary structure of BSA upon conjugation of the fluorophore, in its unfolded state and finally once cross-linked into nanoparticles.

Fig. 5.3 Timed finite bath binding characteristics for **BSA** and **BSA Nanoparticles** on the commercial anion-exchanger *Q*-Sepharose Fast Flow (GE Healthcare) supplemented with the associated fluorescent images below.

Fig. 5.4 Timed finite bath binding characteristics for **BSA** and **BSA Nanoparticles** on the commercial bi-layered media *Capto*TM Core 700 (GE Healthcare) supplemented with the associated fluorescent images below and inset.

Fig. 5.5 Small scale column runs for **BSA** and **BSA Nanoparticles** on **a)** *Q*-Sepharose Fast Flow and **b)** *Capto*TM Core 700. All four runs underwent gradient elution using 1 M NaCl, 1 M NaOH and 30% Isopropanol.

Fig. 5.6 **a)** Static binding capacities for the three bi-layered materials with respect to challenges of **BSA** and **BSA Nanoparticles** of **38 nm** average size with selectivity indices detailed on the lower x-axis. **b)** Reduction in binding capacities for both species with respect to the fully functionalised control resin.

Fig. 5.7 **a)** Static binding capacities for the three bi-layered materials with respect to challenges of **BSA** and **BSA Nanoparticles** of **94 nm** average size with selectivity indices detailed on the lower x-axis. **b)** Reduction in binding capacities for both species with respect to the fully functionalised control resin.

Fig. 5.8 Light microscopy (LM) and confocal laser scanning (CLSM) images of fluorescent **BSA** and **BSA Nanoparticles** of **38 nm** average size challenged onto manufactured control and bi-layered resins.

Fig. 5.9 Light microscopy (LM) and confocal laser scanning (CLSM) images of fluorescent **BSA** and **BSA Nanoparticles** of **94 nm** average size challenged onto manufactured control and bi-layered resins.

List of Tables

Table 5.1 *Comparison of equilibrium binding capacities across the two purification resins and challenge species. All values are quoted as mg of species / ml of chromatographic resin.*

5.1 Introduction

Biological nanoplexes are a fast growing and diverse product group in the current biopharmaceutical environment. They generally consist of plasmid DNA, viral vectors, virus-like particles (VLPs), mega-molecular vaccines, mega protein complexes and IgMs. They are characterised by their large physical size, fragility, complex surfaces and chemical similarity to smaller contaminating macromolecular components (Arpanaei *et al.*, 2010; Olszewski *et al.*, 2013).

The adenovirus (Ad) species have shown great efficacy as a targeted drug delivery vehicle, with high applicability in gene therapy and vaccine treatments. Ad and Ad-associated viruses are now the most commonly used vehicle for gene therapy, with > 500 gene therapy clinical trials having been conducted to date, representing 20.5% of all vectors trialled (Ginn *et al.*, 2018a). Despite its potential, the current purification of nanoplexes (such as Ad) for clinical work leaves much room for improvement. Routine purification of therapeutic Ad products rely on sucrose, iodixanol or caesium chloride density gradients, in combination with ultracentrifugation, with vector yields typically in the order of 70% (Blom *et al.*, 2014).

Although conferring an efficient separation of recombinant viral particles from cell debris and defective virions, there has been a recent trend in using chromatography for purification of such nanoplexes (Burova and Ioffe, 2005). As opposed to density based separation, which present labour and time intensive issues as well as limited scalability, chromatographic purification exploits retention and affinity characteristics to isolate viral units, whilst also providing a gentler method of purification; appropriate for a shear-sensitive product of interest.

Higher throughput times in chromatography are also beneficial in safeguarding the lability and infectivity of the virus particles, whilst also boasting better selectivity, facilitating purer isolation of particles of interest from physically similar contaminants such as host cell proteins and DNA (Morenweiser, 2005 & McGrath *et al.*, 1978).

Chromatography based techniques have also displayed comparable yields when processing crude viral feedstocks, reaching yields of 80% and purities as high as 99% when using two-step chromatography purification trains (Blanche *et al.*, 2000). These figures are based on the use of Q-Sepharose XL media, a chromatography resin traditionally associated with purification of much smaller protein products; a resin, one could argue, that is not suited to purifying large macromolecules such as Ads.

This has fuelled a trend in the production of chromatography media more suited to large nanoplex purification. An example of this is the multifunctional matrix, Capto™ Core 700, a product of GE Healthcare released in 2012. Purification works in flow-through mode, where the large targets of interest are excluded by a size-exclusion matrix shell, whilst the core, functionalised with a potent octylamine ligand, binds target-similar yet smaller protein impurities through anion and hydrophobic interaction.

In this study we develop a platform for assessing chromatography resins such as these by manufacturing protein nanoparticles which, from the perspective of downstream purification, mimic *bona fide* viruses of therapeutic interest. The nanoparticles are first characterised using dynamic light scattering for their size distributions and polydispersity. Isoelectric focussing & circular dichroism spectroscopy are employed to assess surface characteristics and 2° structure, whilst atomic force and transmission electron microscopy are utilised to visualise surface shape and morphology.

In this study, we employ two commercial chromatography media; Q-Sepharose Fast Flow and Capto™ Core 700 to compare performance in purifying nanoparticle and protein solutions, as well as the bi-layered materials manufactured and detailed in Chapter II, to demonstrate the value of using the surrogate mimics to thoroughly characterise viral chromatography media.

5.2 Materials & Methods

5.2.1 Materials & Reagents

Bovine Serum Albumin (fatty acid free, $\geq 96\%$), 8% Aqueous Glutaraldehyde, Methanol and Ethanol (both analytical grade, $\geq 99\%$), Sodium chloride, Sodium phosphate monobasic and dibasic, Sodium hydroxide, Dimethyl sulfoxide and all glassware and other reagents were obtained from Sigma Aldrich (Poole, Dorset) unless otherwise stated. Buffers and all aqueous solutions were based upon use of ultrapure water from a Sartorius Arium® Advanced EDI Pure Water System (Sartorius AG, Göttingen, Germany).

Chromatography equipment and media; Q-Sepharose Fast Flow, Sepharose 6 Fast Flow, Capto™ Core 700 and PD-10 pre-packed columns, as well as 5/50 Tricorn columns were obtained from GE Healthcare Life Sciences (Uppsala, Sweden). Texas Red-X succinimidyl ester for tagging of the protein was purchased from Thermo™ Scientific (Loughborough, UK).

5.2.2 Preparation of Bovine Serum Albumin Nanoparticles

Bovine serum albumin nanoparticles were prepared as described in Chapter III, Section 3.2.2, with specific average nanoparticle sizes targeted by modulating the organic solvent composition during desolvation. The nanoparticles were prepared, purified and re-buffered into sodium phosphate buffer (20 mM, pH 8.0, 150 mM NaCl) prior to contact with the chromatography resins.

5.2.3 Analysis

5.2.3.1 *Dynamic Light Scattering, ζ -potential & IEF*

BSA nanoparticle preparations were characterised with for average particle size and surface charge using dynamic light scattering and ζ -potential analysis, as described in Chapter III, Section 3.3.2.

5.2.3.2 *Protein Quantification*

Quantification of protein content for BSA and BSA nanoparticle samples was carried out via BCA assay as detailed in Chapter II, Section 2.2.11.4.

5.2.3.3 *Cation Exchange Chromatography*

Effects of dye labelling on protein retention behaviour were assessed using cation exchange chromatography. SP Sepharose Fast Flow (GE Healthcare, Uppsala, Sweden) media was manually packed into a 5/100 Tricorn column. 1: 100 dilutions in a running buffer containing 0.2 M NaCl was carried out before sample injection via sample loop under isocratic conditions using an ÄKTA Explorer 100 system (GE Healthcare, Uppsala, Sweden).

5.2.3.4 Circular Dichroism Spectroscopy

Secondary structural analysis was carried out using CD spectroscopy as detailed in Chapter III, Section 3.2.3.4.

5.2.3.5 Static Binding Studies

Commercial Resins: For analysis on commercial resins, 10% slurry of each chromatography resin was prepared by gravity settling before buffer exchange from storage buffer with sodium phosphate buffer (20 mM, pH 7.8, 0.15 M NaCl). The settled bed volume was set at 100 μ L and aliquoted into 2 ml Eppendorf tubes (Eppendorf, Cambridge, UK). Adsorption was initiated by addition of 2 ml of either BSA nanoparticles or BSA (protein concentrations of 2.5 mg/ml and 10 mg/ml respectively). Finite baths were carried out in triplicate to assess binding kinetics whilst a fourth vessel used tagged protein species for subsequent confocal analysis.

Bi-layered Resins: For analysis of bi-layered beads, a weaker ionic concentration buffer system was chosen (10 mM Tris-HCl, pH 8.0) to highlight any small binding differences between samples which could be masked by salt shielding effects, as well as to mirror the conditions run for the bi-layered samples in Chapter II. The settled bed volume chosen was 20 μ L (due to scarcity of manufactured matrix material) and a nanoparticle load of 0.4 mg/ml for each nanoparticle size (38 nm & 94 nm) was chosen; this was based on the static binding capacities of all three control resins (see Figs. 5.6 & 5.7) being between 5 – 10 mg / ml resin, thus a load of 0.4 mg on 20 μ L of beads was deemed sufficient to observe binding behaviour, if any.

A Stuart Scientific SB1 rotator carousel mixer (Bibby Scientific, Stone, United Kingdom) was used to maintain end-over-end agitation, except before sampling, where the Eppendorf tube was briefly centrifuged using a micro-centrifuge (VWR MiniStar Silverline, VWR International, Radnor, USA) for 20 seconds at 2000 g before a 20 μ L sample was taken from the supernatant for subsequent BCA analysis to determine protein concentration. The resin particles were re-suspended by inversion and confirmed by visual inspection, before resumption of carousel mixing. This was repeated for time points from one minute through to two hours.

5.2.3.6 Commercial Resin Column Studies

Capto™ Core 700 and Q-Sepharose Fast Flow resins were manually flow-packed into separate 5/100 Tricorn columns (GE Healthcare, Uppsala, Sweden) using an ÄKTA Explorer 100 system and tested prior for packing quality (As values of 1.04 and 1.19 and h values of 0.07 and 0.06 for Capto™ Core 700 and Q-Sepharose Fast Flow, respectively) .

The columns were subjected to sample loop loading of BSA at concentrations of 10 mg/ml and 35 mg/ml for Capto™ Core 700 and Q-Sepharose Fast Flow respectively and also 80 nm BSA nanoparticles at a concentration of 2 mg/ml for both resins. Sodium phosphate (20 mM, pH 7.8, 0.15 M NaCl) was used as a running buffer and gradient elution was carried out using a buffer of 1 M NaOH, 1 M NaCl and 30% (v/v) Isopropanol.

5.2.3.7 Confocal Laser Scanning Microscopy

In order to measure batch uptake with respect to time, a similar approach to Linden *et al.*, 1999's finite bath experiments was adopted. The samples from the timed finite bath experiments were washed and re-suspended in sodium phosphate buffer and after brief mixing and subsequent centrifugation under the same conditions, fixed volumes of the washed adsorbent particles were prepared as samples for CLSM.

For sample preparation, resin, in 5 μL aliquots, were pipetted onto microscope slides, with a cover slip carefully placed on top to hold the samples in place. Precautions were taken to minimise fluorophore bleaching; the use of low laser powers, minimised exposure times and use of aluminium foil to cover all samples during manufacture, transition and storage.

5.3 Results & Discussion

5.3.1 Fluorophore Conjugation

5.3.1.1 Physiochemical Characteristics

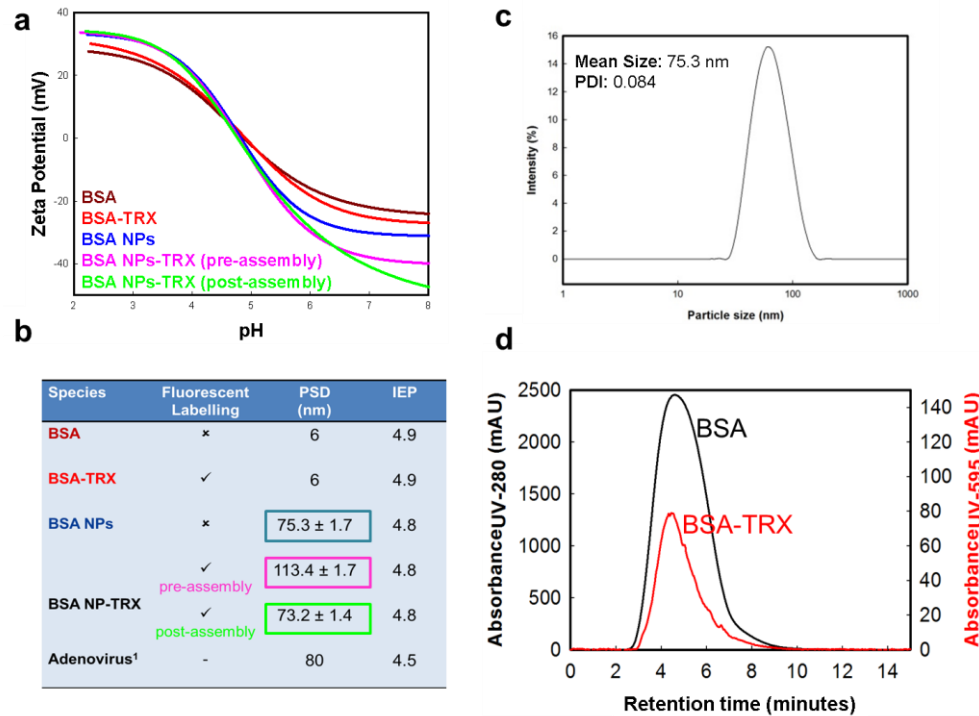


Fig. 5.1 a) Isoelectric focussing curves for blank and fluorescent protein and protein nanoparticles, with species tagged prior to and post formation. **b)** Summary table detailing the particle size distribution (PSD) average particle size and the isoelectric point (IEP) of each species. **c)** The particle size distribution of the blank adenovirus mimic. **d)** Chromatogram illustrating the retention times of blank (-) & fluorescently conjugated (-) BSA on a cation exchange resin.

To observe spatial adsorption of protein species within specific chromatography resins using confocal laser scanning microscopy, detection requires BSA to be labelled by a suitable fluorescent dye molecule (Ljunglöf and Hjorth, 1996; Ljunglöf and Thömmes, 1998; Hubbuch *et al.*, 2002). It was imperative that the attachment of the dye molecule was carried out in a controlled fashion and the impact of labelling on the protein species assessed.

Selection of appropriate dye molecules was based on the works of Teske, Hubbuch and Susanto, who have shown that dye molecule attachment changes the adsorption behaviour of proteins.

¹¹ (Trilisky and Lenhoff, 2007)

Their work demonstrated that screening tests on Texas Red-X-conjugated BSA created the least effect on retention behaviour and therefore it was chosen to tag both free BSA and BSA nanoparticles. The fluorophore was coupled to protein using Texas Red-X succinimidyl ester which conjugates to available lysine residues on the protein species, via a simple click-chemistry conjugation reaction (Life Technologies, 1996; Ljunglöf and Thömmes, 1998; Teske *et al.*, 2007; Hubbuch and Kula, 2008). To confirm the effect, if any, of fluorophore conjugation on the surface characteristics of the free protein and protein nanoparticles, two complimentary analytical techniques were employed. Initially, comparisons were drawn between BSA, BSA-NPs and Texas-Red (TRX) BSA-NPs using DLS and isoelectric focussing to determine changes in zeta potential and isoelectric points of the species, respectively.

In addition, species of tagged and untagged protein were run as an isocratic pulse on an SP Sepharose cation exchange column to observe changes in retention time. It was observed that retention time varied negligibly, indicating little change to the overall binding characteristics of BSA, confirming the work of previous authors. It was, therefore, with a degree of confidence that we could assess locational and kinetic binding of fluorescent BSA and BSA nanoparticles on chromatography resins.

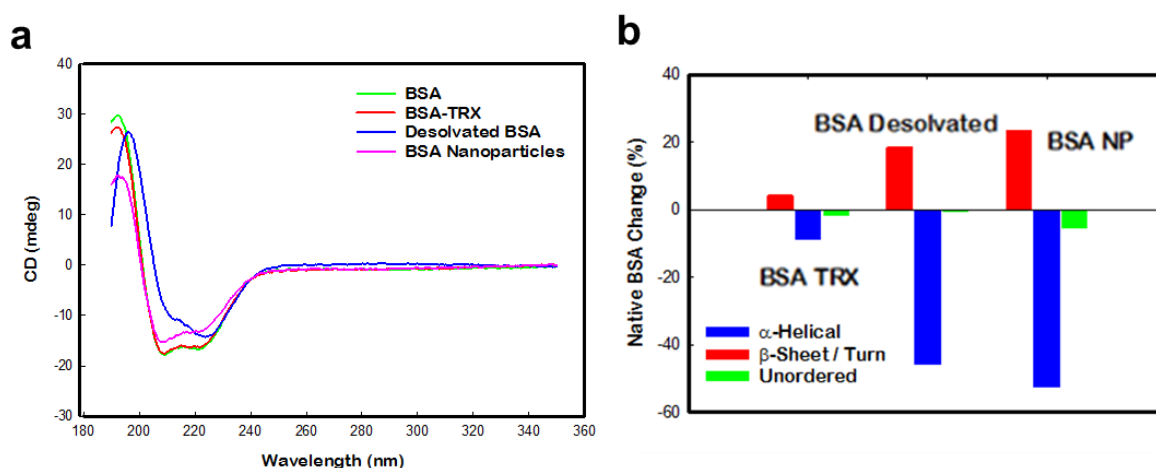


Fig. 5.2 a) CD spectra of BSA in native, tagged, unfolded and nanoparticulate forms. **b)** Changes in the secondary structure of BSA upon conjugation of the fluorophore, in its unfolded state and finally once cross-linked into nanoparticles.

It is important, however to determine any changes or impact the conjugated fluorophore has on the physiochemical properties of the protein species, such that its binding properties to chromatography media are not compromised. The isoelectric point of the free protein and nanoparticle species, both tagged and untagged, had little variance.

A more negative zeta potential for the bare nanoparticle relative to the monomer is suggestive of an internalisation of the hydrophobic residues of the protein monomers within the nanoparticle and therefore a presentation of more negatively charged residues on the surface. An interesting observation was made regarding two potential fluorescent conjugation strategies; the first being to

tag the monomer (pre-assembly) and the second to conjugate a fluorophore after nanoparticulation (post-assembly).

Pre-assembly formed larger nanoparticles under identical desolvating conditions as the fluorophore conjugates to lysine residues that would have been used up in the cross-linking process used in nanoparticulation. This leads to a drop in cross-linking efficiency, leading to a looser, more open nanoparticle structure with a greater Stokes' diameter.

5.3.1.2 2^o Structural Analysis

In order to probe the secondary structure characteristics of the various protein species and track changes through the nanoparticle manufacturing process, a circular dichroism approach was adopted. The spectral data was deconvoluted using Sreerama & Woody's self-consistent method, whereby the secondary structure of the protein species is estimated (Sreerama and Woody, 1993). Inspection of the raw spectra indicates secondary structural changes do occur upon unfolding. Promisingly, little change is observed upon conjugation of the fluorophore to the protein monomer, further fortifying the argument that Texas Red-X addition has little impact to the protein's overall characteristics.

During unfolding and re-folding, increases in β -sheet/turn formation and subsequent reduction in α -helical structure, with little change to the unordered secondary structures occur. This is symptomatic of protein aggregation, where the formation of β -sheet fibres occurs. This fibrillation/amyloidation process derives stability for partially folded or unfolded states as the protein residues re-orientate to the new organic solvent conditions (Holm *et al.*, 2007). Upon addition of a cross-linker, it appears this conformational change is locked in place, coinciding with the formation of stable protein nanoparticles.

5.3.2 Challenging Nanoparticles on Commercial Resins

5.3.2.1 Finite Bath Experiments

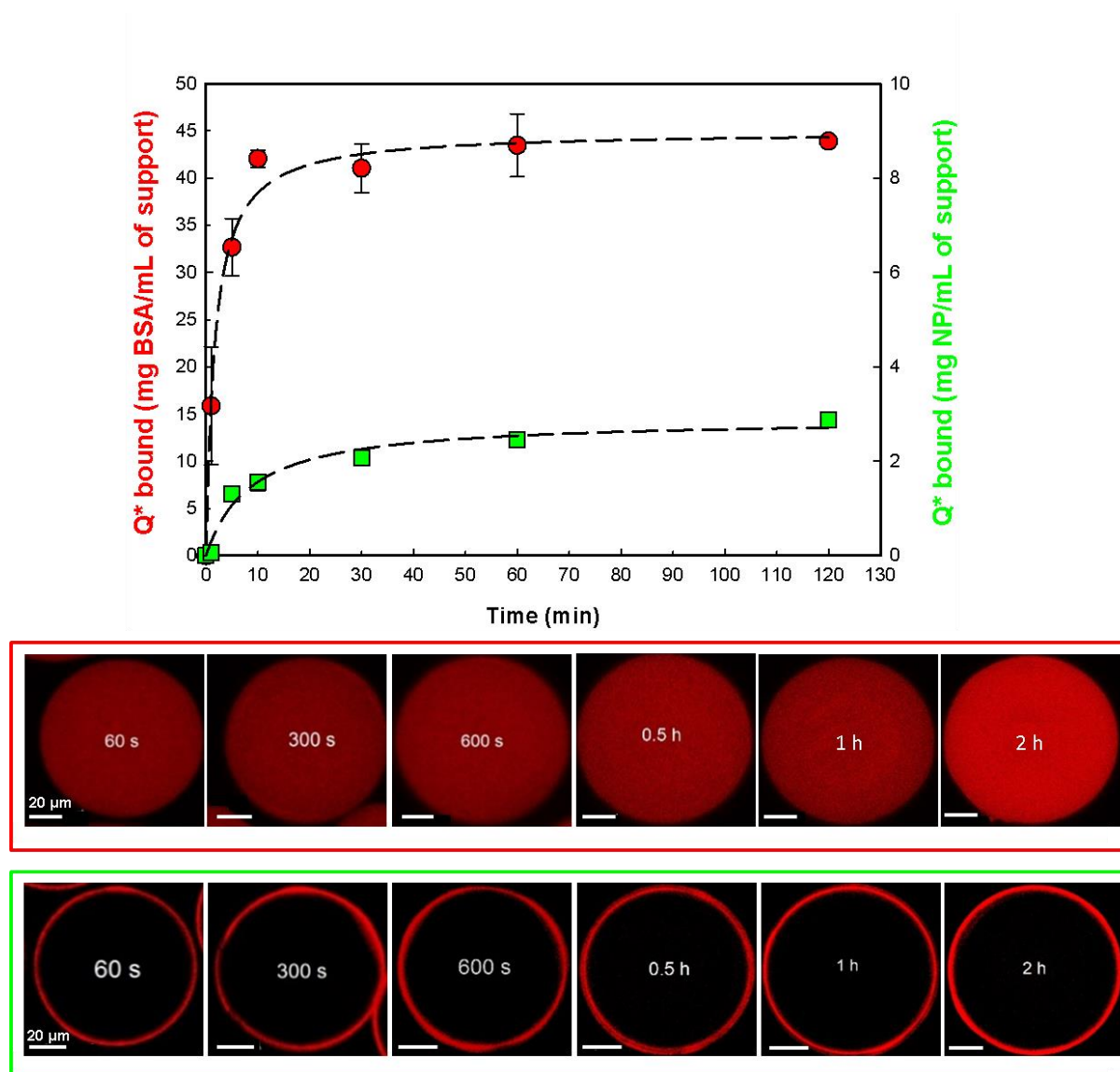


Fig. 5.3 Timed finite bath binding characteristics for *BSA* and *BSA Nanoparticles (80 nm)* on the commercial anion-exchanger *Q-Sepharose Fast Flow* (GE Healthcare) supplemented with the associated fluorescent images below.

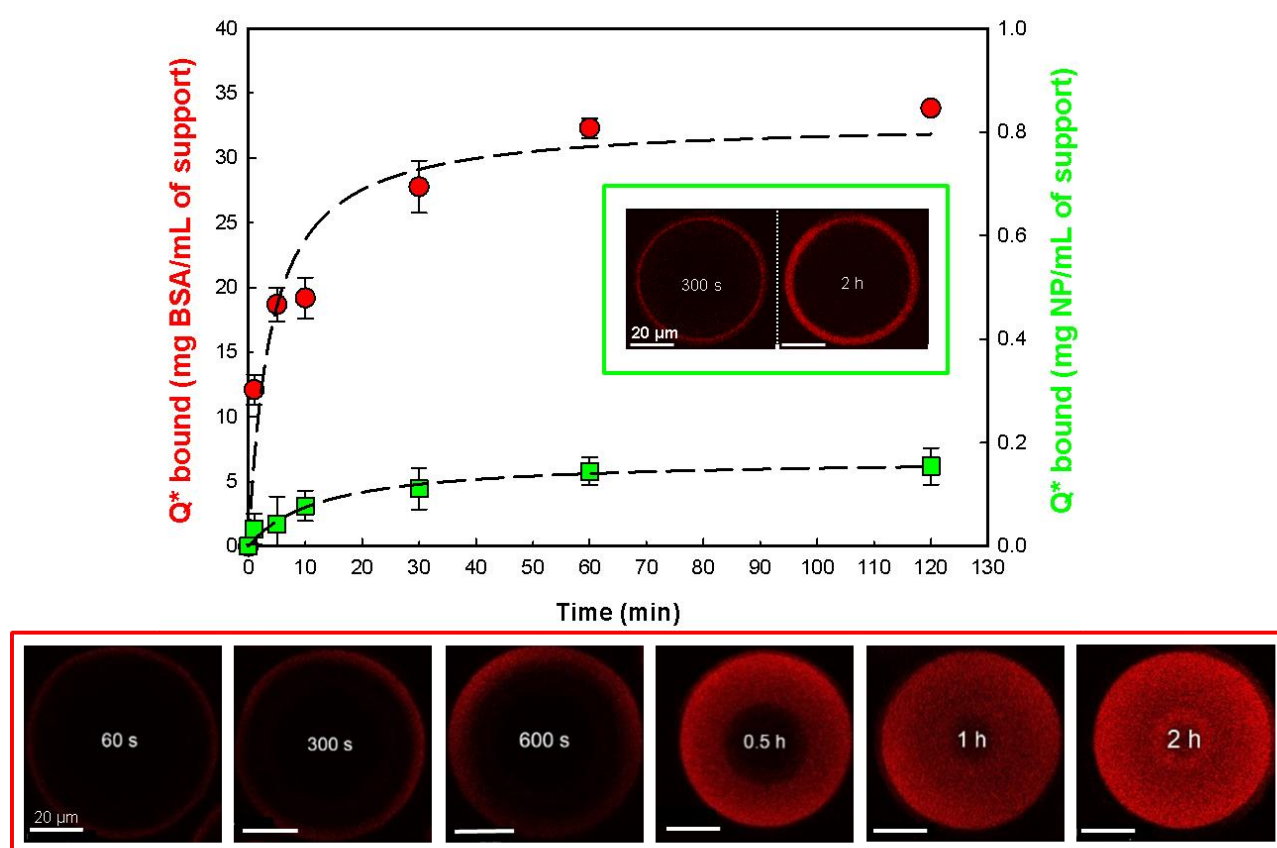


Fig. 5.4 Timed finite bath binding characteristics for *BSA* and *BSA Nanoparticles (80 nm)* on the commercial bi-layered media Capto™ Core 700 (GE Healthcare) supplemented with the associated fluorescent images below and inset.

BCA analysis of supernatant concentrations from finite bath studies revealed varied adsorption kinetics for the two protein species challenged to the bi-layered and conventional anion-exchange matrices. Q Sepharose Fast Flow demonstrated a relatively rapid uptake of bovine serum albumin with a higher equilibrium static binding capacity than the Capto™ Core 700 media. The shrinking core effect of BSA uptake into the a bead can be visualised in the Capto™ Core 700 bead, however the effect is too rapid in the instance of Q Sepharose Fast Flow. This can be attributed to the ionic capacities of the two media, 0.21 and 0.066 mmol Cl-/ml resin, respectively (GE Healthcare, 2018).

Despite Capto™ Core 700 being functionalised with a more potent octylamine ligand, which posits both anion and hydrophobic interaction with the protein challenge, the concentration of the ligand, as well as reduction in capacity due to the bi-layering architecture (for a similar bead size), contribute to the disparities in binding kinetics and overall static binding capacity.

Adsorption of the nanoparticle species also followed similar binding, with Qmax plateauing over time, though the time to reach equilibrium is longer and the static binding capacity an order of magnitude lower. The assay for measuring protein nanoparticle concentration is based on the conventional BCA assay used to measure monomeric protein concentration, against a BSA

standard curve. In reality, the technique measures the amount of BSA protein in the nanoparticles as a method of quantification as it remains linear across a range of nanoparticle solution concentrations and can therefore be applied to the finite bath studies.

The 80 nm nanoparticle species can only access and interact with the surface ligands of the Q Sepharose Fast Flow support due to their inability to penetrate the small pore openings, unlike the ~ 6 nm BSA. This rationalises the lower rate of binding and equilibrium binding capacity for the nanoparticle species relative to the protein monomer. The static binding capacity of Capto™ Core 700 is similar to that of a size exclusion matrix with a similar pore size (Sepharose 6 Fast Flow), as shown in Table 5.1. Confocal laser scanning microscopy imaging captures some interaction between the viral mimics at the surface, perhaps due to a low concentration of octylamine ligands on the surface of the beads, non-specific interaction between the nanoparticles and the agarose-backbone of the matrix or precipitation of the nanoparticle species on the surface of the beads.

Table 5.1 Comparison of equilibrium binding capacities across the two purification resins and challenge species. All values are quoted as mg of species / ml of chromatographic resin.

Capto™ Core 700		Q-Sepharose Fast Flow		Sepharose 6 Fast Flow	
BSA	Nanoparticles	BSA	Nanoparticles	BSA	Nanoparticles
33.8	0.15	43.9	2.8	2.4	0.11

Despite this interaction, the static binding capacity is comparatively low and the majority of the nanoparticle load remains in the supernatant. As Capto™ Core 700's derives its value from being an isolation-by-flow-through matrix, the low static binding capacity for the virus mimic corroborates well with a high level of purification. This, in combination with a competitive binding capacity for smaller protein contaminants (simulated by BSA in this instance), makes it a highly effective purification tool for crude viral feedstocks.

In order to supplement the colorimetric assays from the finite bath studies, parallel studies using fluorescent protein species were provided as a challenge to the functionalised matrices. The time series' images provide qualitative support to the colorimetric assay data with the shrinking core clearly visible for the Capto™ Core 700 media. In the case of Q Sepharose Fast Flow, the shrinking-core effect is not visible; the lack of this phenomenon could be attributed to rapid adsorption of the protein species, as corroborated by the BCA assay data, such that the effect's window cannot be captured in the initial 60 seconds. Due to pore size restriction, the nanoparticle species is only able to interact with the exterior ligands of the Q Sepharose matrices, with an observed increase in intensity from the corona with respect to time. This fits with the adsorption kinetics observed for the nanoparticle challenge on Q Sepharose, with a relatively low concentration of probe bound at a slower rate to the smaller protein species.

5.3.2.2 On-Column Analysis

Scaling up the finite bath studies to column scale under similar, yet dynamic, adsorption conditions reveal similar trends in mobile/stationary phase interaction. Comparing absorbance values at 280 nm for BSA challenged to the two media, it would appear that Q-Sepharose Fast Flow has a significantly higher dynamic binding capacity, though this would need to be confirmed via systematic breakthrough studies.

It is interesting to note that a small amount of nanoparticle material binds and is subsequently eluted from the Capto™ Core 700 column. As demonstrated in the finite bath studies, there is a small amount of the mimic material interacting with the media. Confocal imaging from the finite bath studies confirms there is a weak interaction on the resin surface as well as a downward flux through the porous media, potentially facilitating bead-nanoparticle interaction. Absorbance at 280 nm, along with assay data and normalised intensity values from the radial plots confirm that a very low amount of nanoparticle material does interact, with the majority (~ 90%) of the target viral mimic isolated in the flow-through fraction.

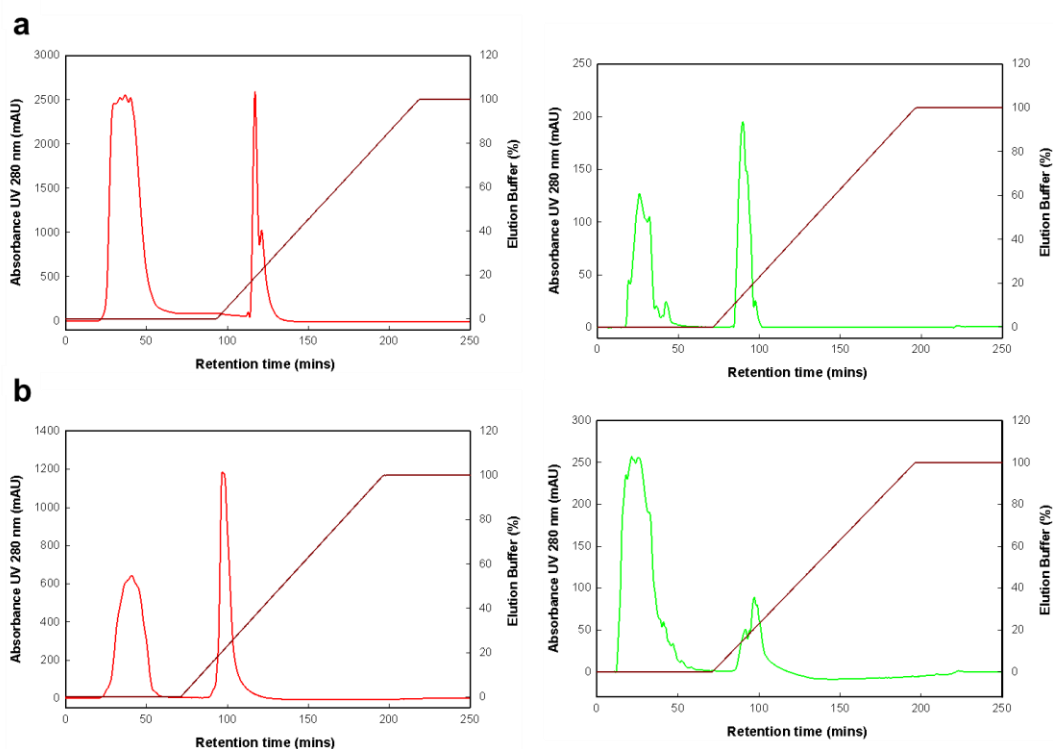


Fig. 5.5 Small scale column runs for *BSA* and *BSA Nanoparticles* on **a)** *Q-Sepharose Fast Flow* and **b)** *Capto™ Core 700*. All four runs underwent gradient elution using 1 M NaCl, 1 M NaOH and 30% Isopropanol.

5.3.3 Challenging Nanoparticles on Resins Manufactured In-House

5.3.3.1 Binding Data

Using a similar methodology as applied to the commercial resins, two nanoparticle preparations with average particle sizes of 38 nm and 94 nm were challenged onto the bi-layered media. As in Chapter II, a selectivity index was used to characterise the media in this instance, as described by Equations 1 & 2.

In essence, the selectivity index (SI) quantifies how well the bi-layered sample retains core-binding (Bovine Serum Albumin binding capacity) and how well it excludes shell-binding (BSA nanoparticles binding capacity) compared to the fully functionalised control made from the same base matrix. The lower the value of the selectivity index, the better performing the resin, as the ratio $\rightarrow 0$ as the core binding is maximised to the level of the control and the shell binding reduces to zero. It should be noted here that for direct comparison of performance between probes (i.e. pDNA & BSA nanoparticles), % reductions against a control should be used rather than comparing absolute SI values.

Equation 1:

$$\% \text{ Reduction in probe SBC} = \frac{\text{Probe SBC}_{\text{Control}} - \text{Probe SBC}_{\text{Sample}}}{\text{Probe SBC}_{\text{Control}}}$$

Equation 2:

$$\text{Selectivity Index (mg BSA NPs / mg BSA)} = \frac{\text{SBC BSA NPs}}{\text{SBC BSA}}$$

Where:

- The probe refers to either BSA or BSA Nanoparticles
- SBC is the static binding capacity for a matrix (mg species / ml resin)
- The control sample is one which has been fully functionalised without any bi-layering
- Sample refers to any material which has been partially brominated to create a bi-layered matrix

Addressing the control samples first (i.e. no bi-layering, behaving as conventional anion exchangers), Superose 6 PG exhibited the highest binding capacity for the smaller nanoparticle preparation, whilst for the 94 nm challenge, Superose 12 PG displayed the highest binding capacity. The latter follows the same pattern as observed for pDNA in Chapter II, which follows given both are relatively large colloidal species and as such will have more sites for interaction, particularly with a heavily functionalised Superose 12 media given its higher percentage of cross-linked agarose.

Interestingly, the 6% cross-linked agarose exhibited a higher static binding capacity for the smaller nanoparticle preparation; one would posit that this may be due the nanoparticles accessing a higher percentage of the bead volume (due to further pore penetration) as 39 nm is below the exclusion limit for both resins (see Chapter II Table 2.1). However, the confocal images in Figs 5.8 and 5.9 reveal this binding to be solely on the surface of the resin, with a corona forming around the beads, as seen with Q-Sepharose Fast Flow.

Despite a lack of deep pore access, it may be hypothesised that the smaller nanoparticles have a higher degree of access to the immediate surface pores of Sepharose and Superose 6 media which are of course “wider” than their Superose 12 counterparts. As the nanoparticles are smaller, there is less steric hindrance and thus access to available Q ligands within these pores is more readily available, though outside the resolution capabilities of confocal microscopy for this phenomenon to be observed. As discussed previously, Superose 6 resins are markedly smaller in size than Sepharose 6 and so have a larger surface area to volume ratio available for nanoparticle interaction.

With respect to the bi-layered binding data, the first observation to note is that the binding reductions are not as marked for the BSA nanoparticles as they were for the plasmid DNA, with maximum reductions capping out at ~ 75%, compared to close to 100% for plasmid DNA. One possible explanation for this is that the surface charge of the protein nanoparticles (~ - 30 mV) is somewhat more strongly negative than plasmid DNA (-17.6 mV) and although plasmid DNA may be larger in terms of hydrodynamic diameter (~ 200 – 400 nm) (Liaw, Chang and Hsiao, 2001), a lower nanoplex surface charge may account for an “easier” reduction in binding.

Whilst the Superose 6 media performed well for both plasmid DNA and BSA nanoparticle challenges, the Superose 12 performed unexpectedly poorly when incubated with both nanoparticle preparations. As stipulated prior, the stronger negative charge of the nanoparticles and the higher percentage of cross-linked agarose of Superose 12 (and thus more available sites for ligand conjugation) gives the nanoplex more opportunity to interact with any residual surface ligands. Sepharose 6 samples generally performed better with the larger nanoparticle challenge, partially due to a lower surface area to volume ratio on account of the larger bead size but perhaps also due to steric hindrance and charge repulsion effects of larger nanoparticles inhibiting binding.

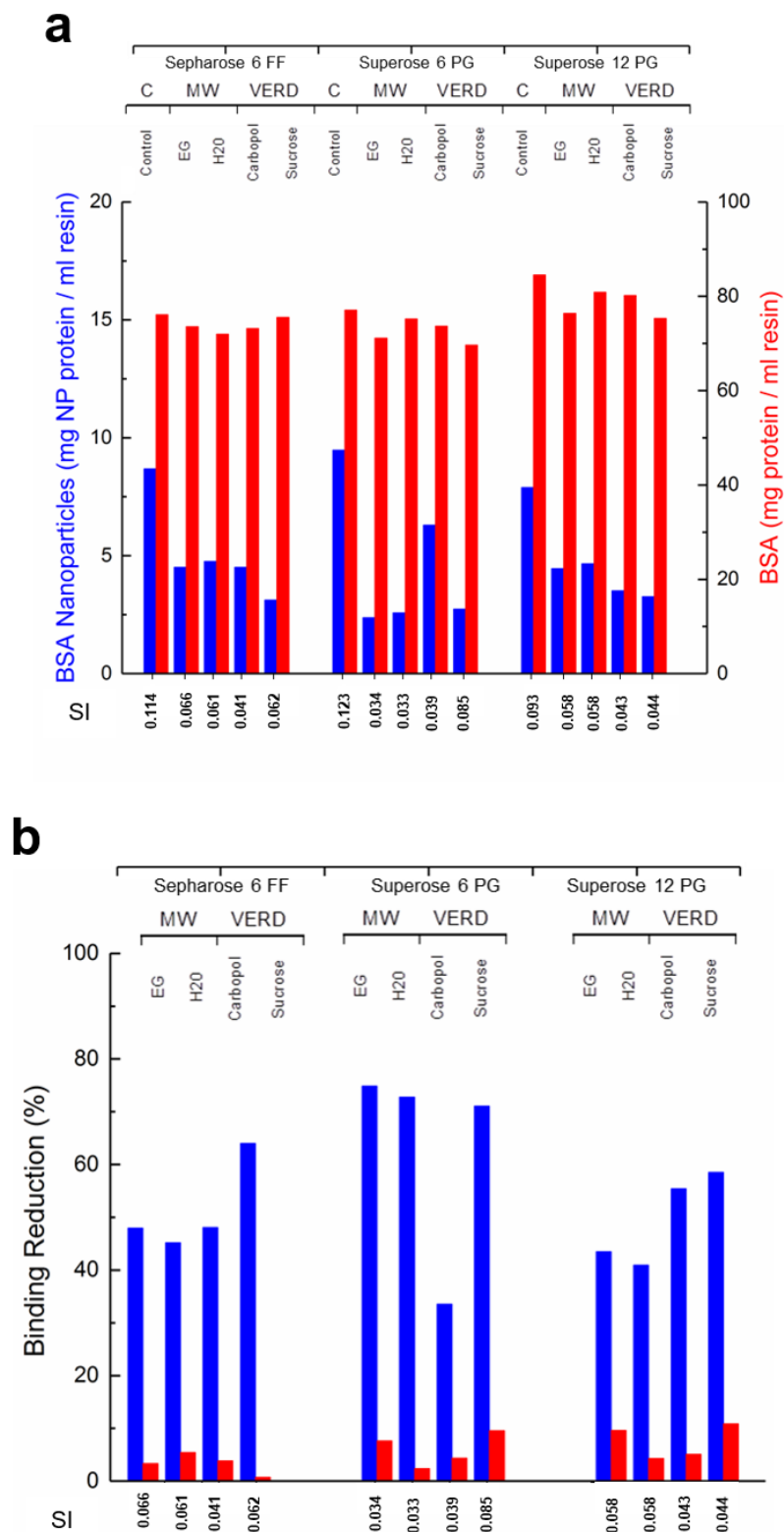


Fig. 5.6 a) Static binding capacities for the three bi-layered materials with respect to challenges of **BSA** and **BSA Nanoparticles** of **38 nm** average size with selectivity indices detailed on the lower x-axis. **b)** Reduction in binding capacities for both species with respect to the fully functionalised control resin.

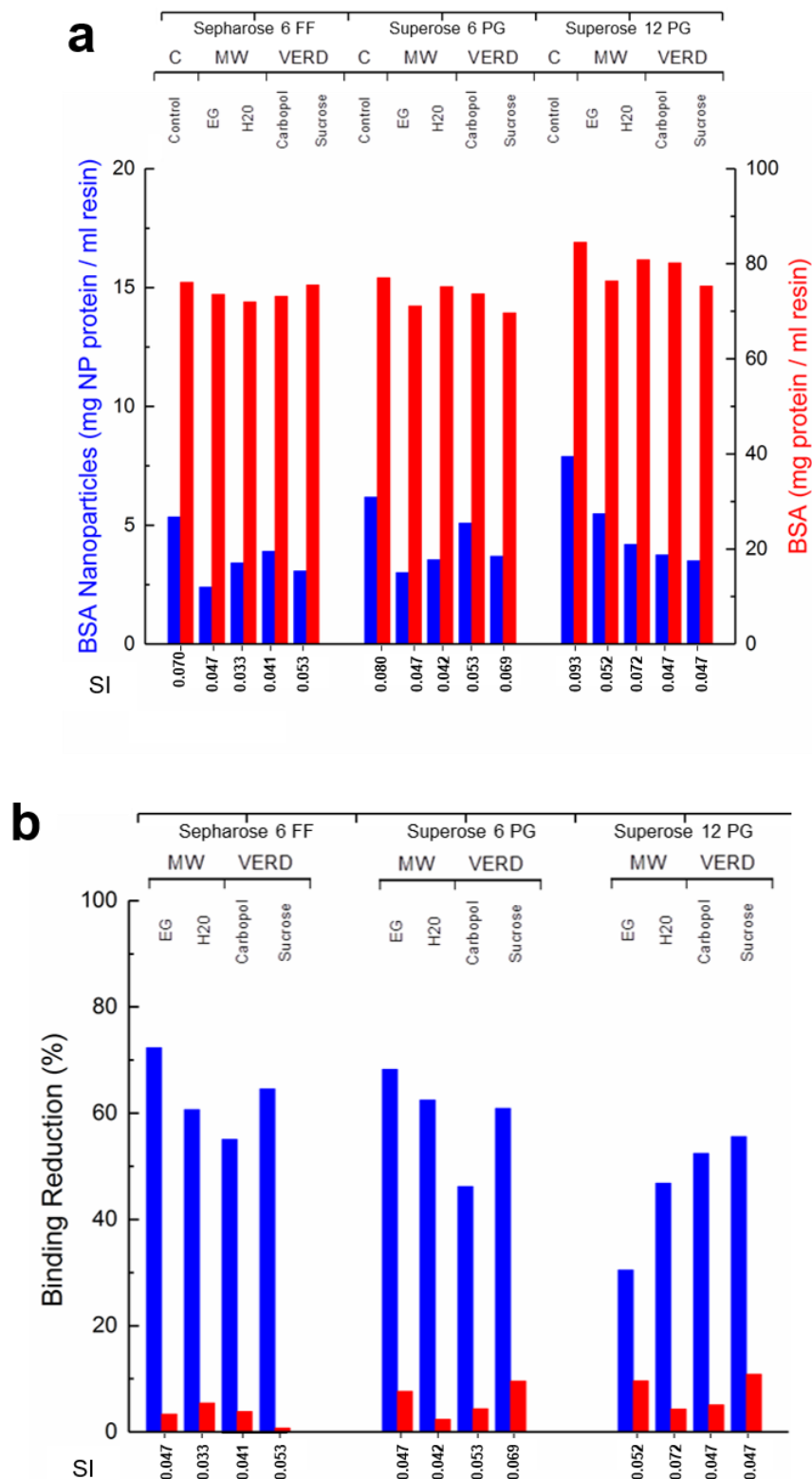


Fig. 5.7 a) Static binding capacities for the three bi-layered materials with respect to challenges of *BSA* and *BSA Nanoparticles* of **94 nm** average size with selectivity indices detailed on the lower x-axis. **b)** Reduction in binding capacities for both species with respect to the fully functionalised control resin.

5.3.3.2 Fluorescent Imaging

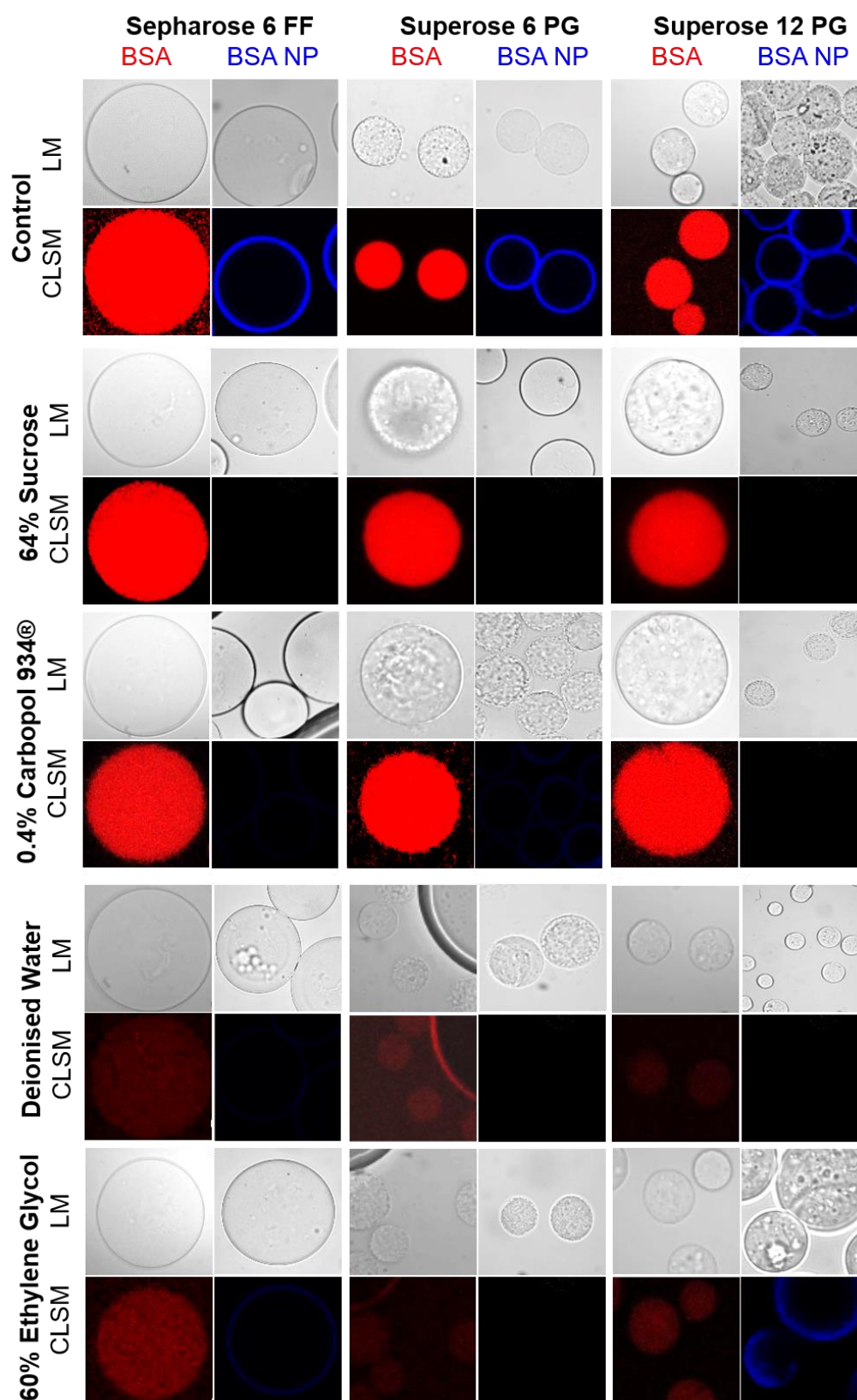


Fig. 5.8 Light microscopy (LM) and confocal laser scanning (CLSM) images of fluorescent *BSA* and *BSA Nanoparticles* of **38 nm** average size challenged onto manufactured control and bi-layered resins.

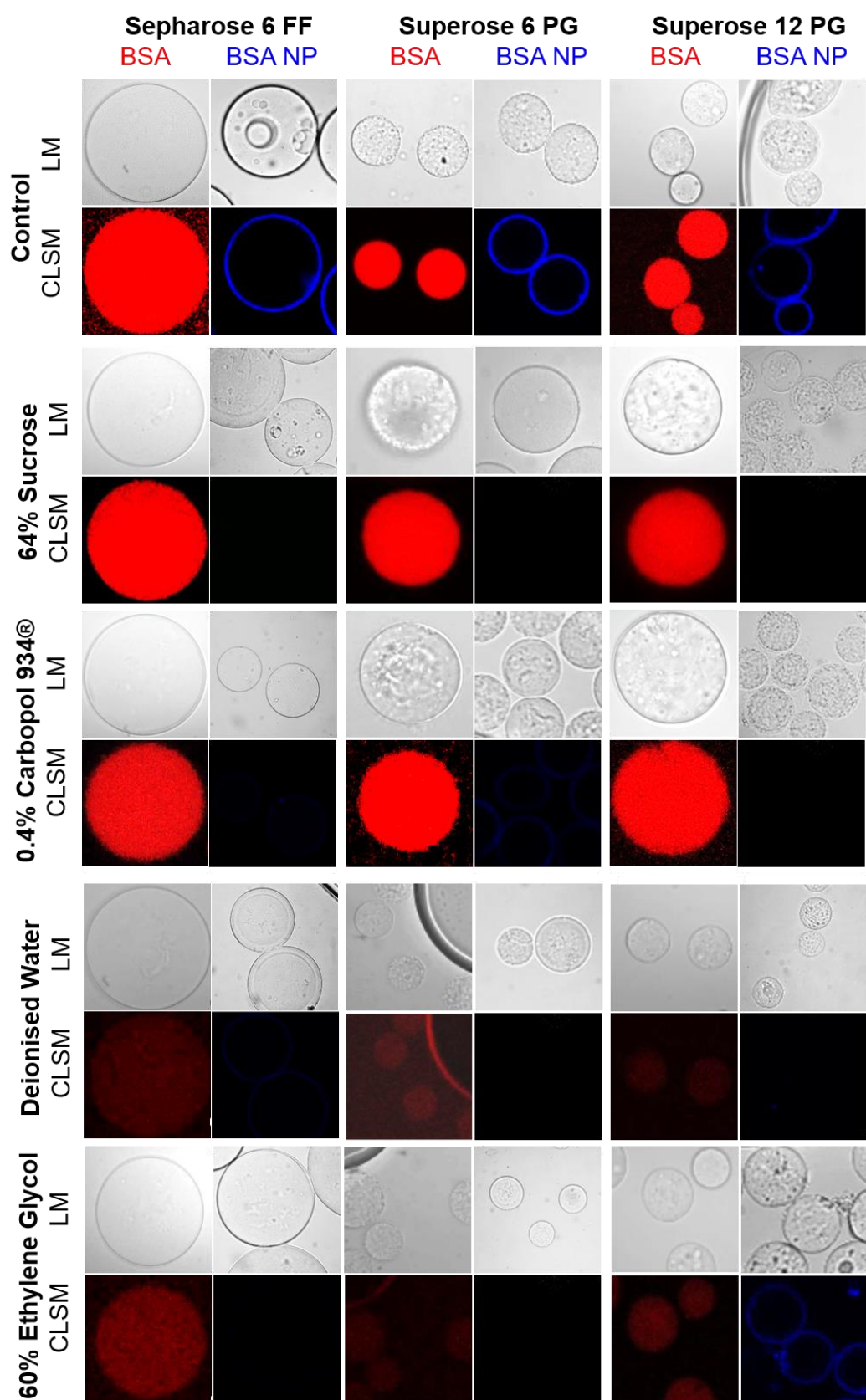


Fig. 5.9 Light microscopy (LM) and confocal laser scanning (CLSM) images of fluorescent *BSA* and *BSA Nanoparticles* of 94 nm average size challenged onto manufactured control and bi-layered resins.

The confocal images tend to agree well with the binding data, for instance one of the worst performing samples, Superose 12 bi-layered manufactured using 60% ethylene glycol (microwave), exhibits clear rings of BSA nanoparticle binding when challenged with both 38 nm (SI 0.058) and 94 nm (SI 0.052) nanoparticles.

Interestingly, worse performing beads tended to be completely coated by a corona of nanoparticles, rather than patches as observed with plasmid DNA binding images. This may point to a nanoparticle-nanoparticle interaction, perhaps driven by hydrophobic interactions of amino acid residue forming non-polar patches on the surface of the nanoparticles, or perhaps a non-specific interaction whereby nanoparticles nucleate at an interface (i.e. the surface of a chromatography bead) and begin to aggregate with each other, resulting in a pseudo-binding effect.

5.4 Conclusions

In summary, the research here continues from that illustrated in Chapter II and reinforces the promise of the bi-layered resins in purifying not only plasmid DNA, but an array of gene therapy-relevant nanoplexes. Interestingly, the data highlights that resins perform with varying degrees of success depending on the size and type of vector being purified and as such small scale optimisation studies are required to identify the best resin for the target species.

The work also demonstrates the utility of protein nanoparticles as informative tools for the chromatography of virus particle products. Behaving as virus surrogates, these nanoparticles offer a safer and cheaper method of screening purification media and can be produced in large volume in a relatively short period of time. This methodology holds promise as a useful tool in the rapid development and optimisation of the downstream process chain of high value gene therapy products in the near future.

5.5 References

- Arpanaei, A. *et al.* (2010) 'Surface modification of chromatography adsorbents by low temperature low pressure plasma', *Journal of Chromatography A*. Elsevier B.V., 1217(44), pp. 6905–6916. doi: 10.1016/j.chroma.2010.08.069.
- Blom, H. *et al.* (2014) *Efficient chromatographic reduction of ovalbumin for egg-based influenza virus purification, Vaccine*. doi: 10.1016/j.vaccine.2014.04.033.
- GE Healthcare (2018) *Q Sepharose High Performance SP Sepharose High Performance*. Available at: <https://www.gelifesciences.co.jp/catalog/pdf/18117288.pdf> (Accessed: 8 February 2018).
- Ginn, S. L. *et al.* (2018) 'Gene therapy clinical trials worldwide to 2017: An update', *The Journal of Gene Medicine*, 20(5), p. e3015. doi: 10.1002/jgm.3015.
- Holm, N. K. *et al.* (2007) 'Aggregation and fibrillation of bovine serum albumin', *Biochimica et Biophysica Acta (BBA) - Proteins and Proteomics*, 1774(9), pp. 1128–1138. doi: 10.1016/j.bbapap.2007.06.008.
- Hubburch, J. *et al.* (2002) 'Dynamics of protein uptake within the adsorbent particle during packed bed chromatography', *Biotechnology and Bioengineering*, 80(4), pp. 359–368. doi: 10.1002/bit.10500.
- Hubburch, J. and Kula, M. R. (2008) 'Confocal laser scanning microscopy as an analytical tool in chromatographic research', *Bioprocess and Biosystems Engineering*, 31(3), pp. 241–259. doi: 10.1007/s00449-008-0197-5.
- Liaw, J., Chang, S.-F. and Hsiao, F.-C. (2001) 'In vivo gene delivery into ocular tissues by eye drops of poly(ethylene oxide)-poly(propylene oxide)-poly(ethylene oxide) (PEO-PPO-PEO) polymeric micelles', *Gene Therapy*. Nature Publishing Group, 8(13), pp. 999–1004. doi: 10.1038/sj.gt.3301485.
- Life Technologies (1996) 'Amine-Reactive Probes | 2 Labeling Proteins', pp. 1–11. doi: MAN0001774.
- Ljunglöf, A. and Hjorth, R. (1996) 'Confocal microscopy as a tool for studying protein adsorption to chromatographic matrices', *Journal of Chromatography A*, 743(1), pp. 75–83. doi: 10.1016/0021-9673(96)00290-7.
- Ljunglöf, A. and Thömmes, J. (1998) 'Visualising intraparticle protein transport in porous adsorbents by confocal microscopy', *Journal of Chromatography A*, 813(2), pp. 387–395. doi: 10.1016/S0021-9673(98)00378-1.
- McGrath, M. *et al.* (1978) 'Retrovirus purification: Method that conserves envelope glycoprotein and maximizes infectivity', 25(3), pp. 923–927.
- Morenweiser, R. (2005) 'Downstream processing of viral vectors and vaccines', *Gene Therapy*, 12, pp. S103–S110. doi: 10.1038/sj.gt.3302624.
- Olszewski, P. *et al.* (2013) 'In situ modification of chromatography adsorbents using cold atmospheric pressure plasmas', *Applied Physics Letters*, 102(20), p. 204104. doi: 10.1063/1.4807391.
- Sreerama, N. and Woody, R. W. (1993) 'A Self-Consistent Method for the Analysis of Protein Secondary Structure from Circular Dichroism', *Analytical Biochemistry*, 209(1), pp. 32–44. doi: 10.1006/abio.1993.1079.
- Teske, C. A. *et al.* (2007) 'Changes in retention behavior of fluorescently labeled proteins during

ion-exchange chromatography caused by different protein surface labeling positions.', *Biotechnology and bioengineering*, 98(1), pp. 193–200. doi: 10.1002/bit.21374.

Trilisky, E. I. and Lenhoff, A. M. (2007) 'Sorption processes in ion-exchange chromatography of viruses', *Journal of Chromatography A*, 1142(1), pp. 2–12. doi: 10.1016/j.chroma.2006.12.094.

CHAPTER VI

CONCLUDING REMARKS & FURTHER RECOMMENDATIONS

Table of Contents

CHAPTER VI.....	284
Abbreviations.....	284
6.1 Bi-Layered Chromatography Materials	285
6.2 BSA Nanoparticles.....	285
6.3 Viral Mimic Library.....	286
6.4 Nanoparticles Informing Viral Purification	287
6.5 References	287

Abbreviations

AFM: Atomic Force Microscopy

AGE: Allyl Glycidyl Ether

ATPS: Aqueous Two Phase Systems

BSA: Bovine Serum Albumin

HIC: Hydrophobic Interaction Chromatography

pDNA: Plasmid DNA

Q ligand: Trimethylamine Chloride

TEM: Transmission Electron Microscopy

6.1 Bi-Layered Chromatography Materials

The manufacture of bi-layered materials was based on an AGE activation / partial bromination functionalisation technique on blank size exclusion media. I chose Sepharose 6 Fast Flow, Superose 6 and Superose 12 Prep Grade to vary the starting bead size and porosity and to observe the impact this would have when applied under the same manufacturing technique and the eventual binding characteristics.

One important factor moving forward would be to use a wider selection of media, with different cross-linking chemistries and structural components; it would be interesting to see how different cross-linkers impact the AGE activation step. In a similar vein, assaying a wider range of viscosity enhancing and/or microwave-assisting buffers, depending on their bromine stability data could perhaps yield better results. One of the fundamental experimental points is to ensure that the resin suspension is well mixed upon addition of the bromine solution during the partial bromination step; this may avoid the patchy binding visualised in the pDNA static binding studies.

Future work would certainly consist of scaling up the manufacturing process (~ 5 fold) such that the bi-layered resins can be packed into columns for dynamic assessment, which will provide a real insight into how the resins perform under flow.

With respect to the Arrhenius-Stokes equation, it would also be interesting to see if lowering temperature significantly below ambient would limit the rate of diffusion such that the bromine only reacts with the initial surface layer of the support, to create a thin shell. In this case, a suitable buffer would need to be selected to avoid loss of bromine through side-reactions.

Orthogonal analytical techniques may be applied to the manufactured chromatography resins in the future to assess how successful the layering reaction was. I attempted to use Confocal Raman microscopy to map the location of Q ligand during this work, however ran into resolution issues in locating a definitive bi-layered structure. The technique has been used with success for other chromatographic adsorbents (Ljunglöf *et al.*, 2000; Larsson and Lindgren, 2005) and consequently would need some optimisation to have utility in this application too.

6.2 BSA Nanoparticles

The BSA nanoparticles were systematically assessed across a range of operating parameters to a point that a specific average target size (within ~ 10 nm) could be manufactured through prior knowledge of the conditions required, whether that be organic solvent conditions, temperature, pH, ionic strength etc.

In terms of characterisation, it would be interesting to have done more morphological analysis on the nanoparticles; perhaps looking at how different mixing patterns impacted the shape of the nanoparticles as well as how nanoparticles composed of different starting proteins / mixtures eventually looked under a TEM or AFM microscope. I believe it would also be important to carry out a systematic CD study, looking at how different concentrations of organic solvent impact

secondary structural changes in the protein, which would cement our understanding of the unfolding characteristics of the protein and hopefully corroborate with the findings in Chapter III.

During this research project, I managed to acquire a small aliquot of un-purified adenoviral vector material from our collaborators at UCL. However, during my experimental design, I found that to properly purify and to yield sufficient viral particles, as well as the specialist equipment required to handle and assay the material, would cost in excess of £2000. In a sense, this justifies the rationale for creating surrogates for virus material in order to assay chromatography materials, however real adenovirus is the gold standard for comparison and future work would certainly entail a head-to-head binding assay between the adenovirus mimic and the true *bona fide* virus.

6.3 Viral Mimic Library

The viral mimic library is a concept that is in its infancy; the idea being that given the process knowledge gained from systematically testing BSA in forming nanoparticles, a “toolbox approach” could be applied to other proteins and protein mixtures to custom build virus mimics according to the basic physiochemical properties. The bovine haemoglobin work was promising as it took a non-albumin based protein and showed it was possible to form nanoparticles and pleasingly, some of the trend observed, such as the influence of dielectric constant on particle size, was similar to BSA.

Future studies would encompass a range of proteins with different initial starting properties; one of the main reasons for doing the scale down work was to facilitate low volume screening tests to be carried out on more expensive proteins with attractive characteristics for virus mimics, such as conalbumin (pI 6.6, MW: 77 kDa).

Going forward, I believe it would be important to include an assay for hydrophobicity into the suite of analytics for the nanoparticles as this will also play an important role in virus mimic customisation. I did purchase a HIC 1 ml Hi-Trap Selection Kit (GE Healthcare, Uppsala, Sweden) with the intention of running this assay, which would have involved looking at the retention / elution profiles of the nanoparticles and native protein species through various HIC columns as a measure of their surface hydrophobicity. Crucially, this would also provide an insight into the ordering of amino acid residues on the surface of the nanoparticle upon formation.

With regard to the multi-component nanoparticle work, both blending and core-shell nanoparticles have potential to form interesting virus surrogates. Future work would look to make this approach more systematic and to use SDS-PAGE gels, ion-exchange chromatography and reducing conditions to reverse the thiol cross-linkage to quantify the amount of incorporated second protein. It may also be worth considering other scaffold/coat protein combinations, depending on the type of virus being targeted. Finally, it may also be interesting to conjugated single amino acid residues or short peptide sequences (Look *et al.*, 2015) to the surface of the nanoparticles as opposed to whole, globular proteins such as lysozyme. This may remove some of the steric and electrostatic interferences from other amino acids within the protein and allow for a tighter control of surface charge modification.

6.4 Nanoparticles Informing Viral Purification

The utility of these virus surrogates is not limited to the chromatography materials tested here, but could also be applied to a range of chromatography resins and purification methods such as filtration, centrifugation and ATPS. As the nanoparticles can be easily assayed using colorimetric methods, quantitative data can easily be attained to inform optimised protocols for each of these units operations too. Much of their promise stems from their ability to be functionalised with fluorophores, as well as the ability to tailor their manufacture to mimic a range of different viral vectors.

6.5 References

- Larsson, M. & Lindgren, J., 2005. Analysis of glutathione and immunoglobulin G inside chromatographic beads using surface-enhanced Raman scattering spectroscopy. *Journal of Raman Spectroscopy*, 36(5), pp.394–399. Available at: <http://doi.wiley.com/10.1002/jrs.1304> [Accessed January 3, 2019].
- Ljunglöf, A. et al., 2000. Measurement of ligand distribution in individual adsorbent particles using confocal scanning laser microscopy and confocal micro-Raman spectroscopy. *Journal of Chromatography A*, 893(2), pp.235–244. Available at: <https://www.sciencedirect.com/science/article/pii/S0021967300006841> [Accessed January 3, 2019].
- Look, J. et al., 2015. Ligand-Modified Human Serum Albumin Nanoparticles for Enhanced Gene Delivery. *Molecular Pharmaceutics*, 12(9), pp.3202–3213. Available at: <http://www.ncbi.nlm.nih.gov/pubmed/26218774> [Accessed January 3, 2019].

CHAPTER VII

APPENDICES

7.1 The Art of Bioprocessing

Since Genentech & Eli Lilly developed the first Food & Drug Agency (FDA) approved biotherapeutic product, Humulin® (insulin), in 1982, the biopharmaceutical industry has progressed significantly to sustain a plethora of therapeutic products ranging in size, complexity and culture platforms (Cooke 2001). It was the development of recombinant-DNA and hybridoma technologies that acted as a springboard for the development of an array of different biotherapeutic products. Humulin was the first recombinant plasmid DNA therapeutic approved, though the door has since been opened for a host of new biotherapeutic product types, including recombinant proteins, nucleic acids, vaccines and antibody based therapies.

In the 18 years since the launch of Humulin to the turn of millennium, 84 biotherapeutics had been approved in Europe and the USA, treating a variety of indications including autoimmune disorders, cancers, blood disorders and heart disease (Walsh, 2003). To date, more than 200 biopharmaceutical products have been approved for therapeutic use (Pohlscheidt, Kiss and Gottschalk, 2018) and the market is expected to grow in value to \$213.97 billion by 2021 (Challener, 2018).

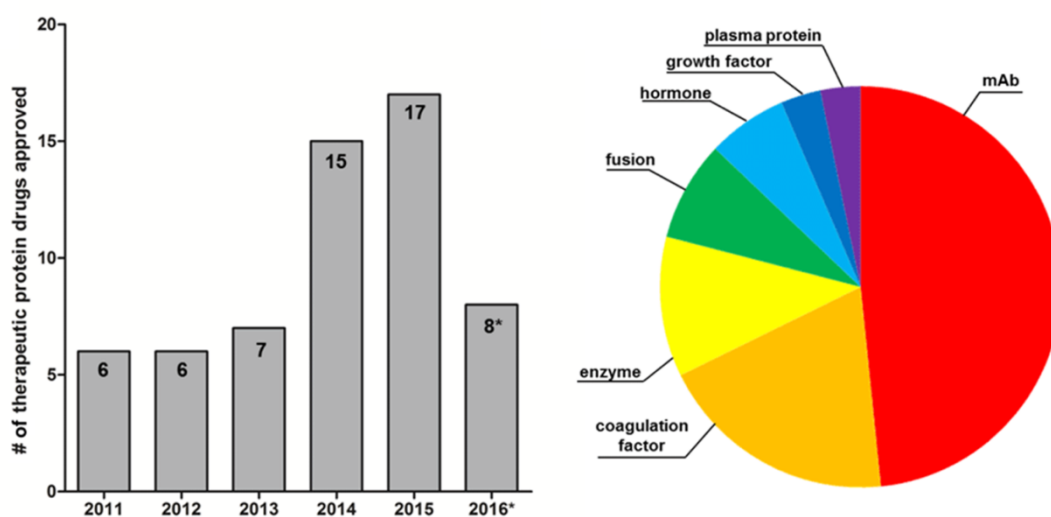


Fig. 7.1 The rise of therapeutic protein-based therapeutics to *August 31st 2016 and the distribution of therapeutic classes which make up the total protein therapeutics market (Lagassé *et al.*, 2017).

Monoclonal antibodies (mAbs) dominate the biopharmaceutical market with approximately 1500 potential drugs in the pipeline in 2016 (Sun Hong *et al.*, 2017). This is somewhat unsurprising due to their affinity to a plethora of biomolecules as well as their high specificity, making them

amenable to a wide range of clinical applications. Emerging onto the market in 1986 with Orthoclone OKT3 (muromonab) to prevent kidney transplant rejection, mAb-based therapeutics have since developed to treat a range of disorders including macular degeneration, asthma and multiple sclerosis (Kennedy *et al.*, 2018). There are currently ~ 300 mAb products in the pipeline and with an approval rate of ~ 4 products/ year and a projected 70 mAb products by 2020, there is little to suggest that the growth in the mAb market will be kerbed in the mid-to-long term (Ecker, Jones and Levine, 2015).

There are, of course, a multitude of other protein therapeutic classes on the market, including but not limited to growth and blood factors, receptor proteins, cytokines, enzymes and hormones. A high proportion of these are recombinant products, produced in expression systems including bacteria (Baneyx, 1999; Sørensen and Mortensen, 2005), yeast (Sanchis *et al.*, 1998; Cregg *et al.*, 2000; Cereghino *et al.*, 2002), insect (Maiorella *et al.*, 1988; Altmann *et al.*, 1999), mammalian (Wurm and Bernard, 1999; Wurm, 2004; Geisse and Henke, 2005) and even transgenic plant systems (Kusnadi, Nikolov and Howard, 1997; Ma, Drake and Christou, 2003).

Table 7.1 Characteristics of therapeutic protein expression systems (adapted from Dingermann 2008).

Expression System	Classification	Disulphide Bonds	Glycosylation	Secretion	Fermentation Costs	Safety Costs	Scale
<i>E. coli</i>	Gram Negative Bacterium	✓ (Periplasm)	✗	Periplasmic	↓ to moderate, though promoter dependent	↓	Industrial
<i>Saccharomyces cerevisiae</i>	Budding Yeast	✓	✓ (↑ mannose)	Possible	↓	↓	Industrial
<i>Pichia pastoris</i>	Methylotrophic Yeast	✓	✓ (no terminal α 1,3 mannose)	Possible	↓	↓	Industrial

Expression System	Classification	Disulphide Bonds	Glycosylation	Secretion	Fermentation Costs	Safety Costs	Scale
<i>Hansenula polymorpha</i>	Methylotrophic Yeast	✓	✓ (no terminal α 1,3 mannose)	Possible	↓	↓	Industrial
<i>Plant Cells</i>	Higher Eukaryote	✓	✓ (terminal fucose)	Possible though with size restrictions	↓ to moderate	↓	Pilot to production
<i>Mammalian Cells</i>	Higher Eukaryote	✓	✓ (typically human-compliant)	Usually	↑	↑	Industrial
<i>Animal</i>	Mammals	✓	✓ (typically human-compliant)	Usually	Moderate to ↑, usually farming costs	↑	Industrial

Bacterial expression systems offer numerous advantages for recombinant protein expression, largely due to their well characterised genetic manipulation strategies and established and comparatively low cost and scalable culture platforms. However, bacterial expression systems often fall short in the folding and secretion of eukaryotic proteins, particularly those rich in cysteine residues which form disulphide linkages. The proteins are often expressed as insoluble inclusion bodies which require a re-folding step which can complicate the downstream processing train whilst also compromising the yield of active protein (Verma, Boleti and George, 1998).

As a result, immunoglobulins are usually expressed in mammalian systems, which facilitate appropriate folding and glycosylation patterns to form through the sophisticated endoplasmic reticulum available in mammalian cells. With the rise of antibody-based products, mammalian expression systems have come to the fore as the most popular expression system in the biotherapeutics field (see Fig. 1.2) as the two go hand-in-hand.

There are a number of popular mammalian cell lines used for recombinant protein production, including Chinese Hamster Ovary (CHO), Mouse Myeloma (NSO, SP2/0), Mouse Kidney (COS), Human Embryonic Kidney (HEK) and Baby Hamster Kidney (BHK), which are utilised for their stable expression systems and high specific production rate. In addition to this, their glycosylation patterns are close to that of human and some are amenable to amplification systems such as glutamine synthetase (GS) which facilitates stable and high-yielding cell lines (Brown *et al.*, 1992; Barnes, Bentley and Dickson, 2000; Dempsey *et al.*, 2003; Yu, Lee and Lee, 2018).

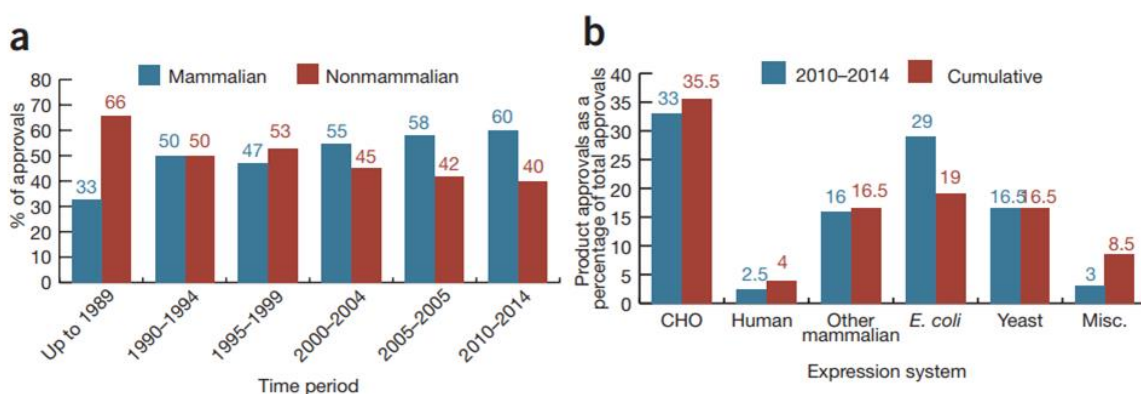


Fig. 7.2 The increasing popularity of mammalian cell culture platforms for the production of biopharmaceutical products **a)** from 1989 – 2014 and **b)** with respect to competing cell culture systems (Walsh, 2014).

There are, however, a number of issues associated mammalian cell cultures which need to be addressed, namely scalability, low product titres, process complexity (including shear sensitivity, high media/serum complexity, oxygenation requirements and costs and also the need for viral inactivation/removal (Palomares, Estrada-Mondaca and Ramírez, 2004).

In light of this, there have been significant improvements in recombinant protein production over the last twenty years through significant research and development (e.g. host cell line engineering and clone development), process control including, but not limited to; metabolic engineering, process analytical technology, improvement in on-line, offline sensors and improvements in media composition. There has also been a drive to integrate product quality by process design to facilitate better product characterisation, monitoring tools and ease of validation to ensure regulatory requirements are met. This has been supplemented by more focussed process intensification, including better bioreactor design (e.g. to improve dissolved oxygen content, mixing patterns etc.) and operation (such as perfusion reactors, micro-carriers etc.) (O’Callaghan *et al.*, 2010; Butler and Meneses-Acosta, 2012; Gronemeyer, Ditz and Strube, 2014).

Since the 1980s, recombinant protein productivity in mammalian cells has increased 100-fold with specific cell productivities of ~ 90 pg/cell/day and product titres in excess of 10 g/L when run in fed-batch operation; mAb titres can be as high as 25 g/L in some perfusion systems, whilst improvements in bioreactor engineering has resulted in the processing of volumes in the order of

20, 000 L and thus yields of 15 – 100 kg of mAb /batch (Wurm, 2004; Sommerfeld and Strube, 2005; Kelley, 2009; F. Li *et al.*, 2010; Gronemeyer, Ditz and Strube, 2014; Legastelois *et al.*, 2017).

Other expression systems have also seen growing popularity in recent times, including yeast, insect and plants which exploit their ease of manipulation (particularly yeast) whilst also being scalable, having a high throughput and are relatively inexpensive (especially insect and plant systems) compared to mammalian expression (Verma, Boleti and George, 1998; Dingermann, 2008; Walsh, 2014).

There is no “one-size-fits-all” for protein expression systems and as such one platform will never become the gold standard for all future therapeutic protein manufacture. As each protein has its own unique amino acid sequence, it will be more amenable to one expression system over another as well as a number of other factors. These include post-translational modification requirements (including but not restricted to glycosylation patterns), expression pathway, protein sequence, immunogenicity, viral and endotoxin considerations as well as bioprocess considerations including scale of production (quantity and purity of product) , throughput requirement and also the associated cost of capital, ancillary and support systems (Verma, Boleti and George, 1998; Leader, Baca and Golan, 2008).

Whilst antibody-based therapeutics in mammalian cell culture systems have been the staple of therapeutic production in recent times, there have been a number of other interesting trends developing the field of biotherapeutics. New, experimental therapies are being developed, transitioning away from the *au fait* antibody therapeutics and adopting novel approaches such as regenerative medicine, including tissue engineering and/or complimentary gene therapy. This opens the door for the treatment of a wide range of patient issues, including inherited diseases, infections, autoimmune diseases and certain cancer types (Cotrim and Baum, 2008; Muñoz Ruiz and Regueiro, 2012).

7.2 How does Gene Editing Work?

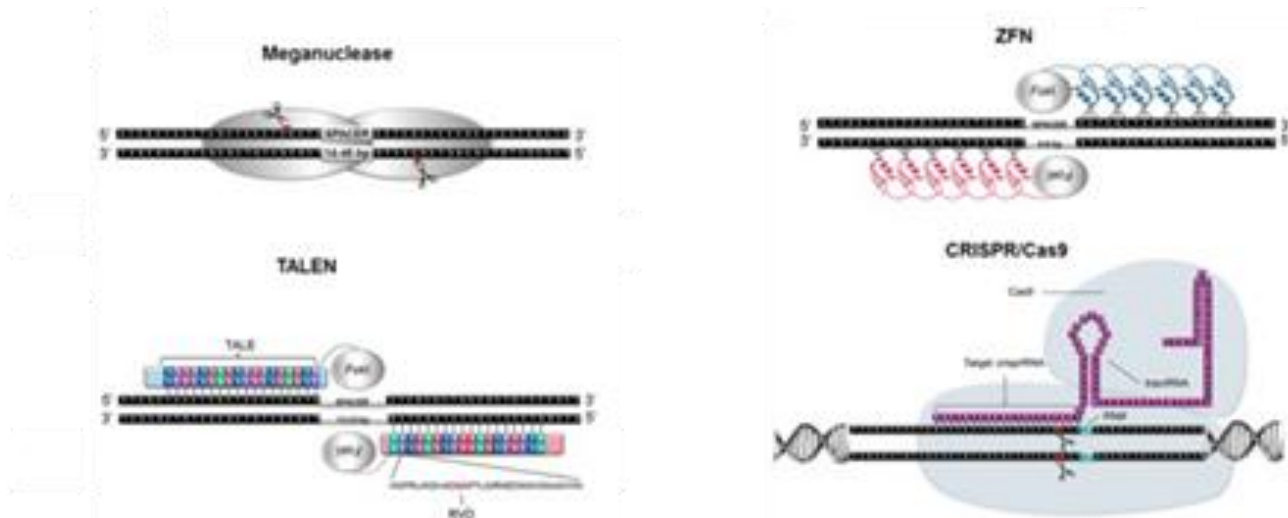


Fig. 7.3 Four mechanisms of gene editing (Image & detail were sourced from Delhove & Qasim 2017)

Gene editing is based on the concept of introducing a double-stranded break into a sequence of genomic DNA, resulting in a knockout of gene function. Four main approaches currently exist, acting as “molecular scissors” to achieve gene editing:

1. Meganucleases are essentially molecular scissors with adjustable recognition sequences to allow modification of a variety of target sequences.
2. TALENs are engineered restriction enzymes which contain 34 amino acid repeat sequences in the DNA binding domain with two divergent amino acids, termed the repeat variable di-residue (RVD), which have a high specificity for nucleotide recognition and can target a single base on the target sequence.
3. ZFNs are also engineered restriction enzymes made up of a zinc finger binding domain with three nucleotides of the target sequence and a DNA cleavage domain which requires dimerization of two *FokI* domains for cleavage to occur.
4. CRISPR-Cas9 uses the endonuclease enzyme Cas9 and requires RNA guidance to achieve cleavage of the target sequence. A protospacer adjacent motif (PAM) sequence flanks the target site three bases downstream to ensure successful cleavage.